TURBULENCE MODELS FOR PREDICTING WALL SHEAR FLOWS WITH HEAT TRANSFER IN ENGINEERING APPLICATIONS

by

Hirofumi Hattori

B.S., Nagoya Institute of Technology, 1989

Doctoral Dissertation

Submitted to
Nagoya Institute of Technology
in partial fulfillment of
the requirements for the degree of
Doctor of Engineering

January 2002

Acknowledgments

First of all, the author would like to express his gratitude to the Examining Committee members, Professor Y. Nagano, Professor N. Ohiwa, Professor O. Kitoh and Professor A. Tominaga for carefully reviewing the manuscript and for making appropriate suggestions.

The author wishes to express his sincere gratitude to his supervisor, Professor Y. Nagano, for his encouragement, guidance, and many helpful suggestions in the course of this investigation, and for suggesting the subject of this research.

During the author's research program at the Nagoya Institute of Technology (NIT), he received much assistance from the members of the Heat Transfer Laboratory in the Department of Mechanical Engineering. Special thanks are due to Dr. T. Kondoh (Toyota Central Research and Development Laboratories, Inc.), Dr. H. Sato (Denso Corporation), Dr. K. Abe (Kyushu University), Dr. Y. Suzuki (The University of Tokyo), Dr. M. Shimada (Software Cradle Co., Ltd.), Dr. M. Kondoh (Fuji Denki Kagaku Co., Ltd.), Dr. Y. Hattori (Central Research Institute of Electric Power Industry) and Dr. T. Houra for their valuable discussions and helpful comments both in and outside the Laboratory. The author wishes to thank the graduate students in the Heat Transfer Laboratory for their generous assistance and discussions.

The author wishes to thank Dr. M. Tagawa for his valuable suggestions and helpful comments. The author obtained fundamental approach to research from him.

Thanks are also due to Professor N. Kasagi of the University of Tokyo, Professor H. Kawamura of the Science University of Tokyo and to A. Yoshizawa of the Institute of Industrial Science, the University of Tokyo for their helpful discussions and incisive comments.

Part of this research program has been supported through the research project on "Micro Gas Turbine/Solid Oxide Fuel Cell Hybrid Cycle for Distributed Energy System" by the Department of Core Research for Evolutional Science and Technology (CREST) of the Japan Science and Technology Corporation (JST).

Finally, on a personal note, my heartfelt thanks to my family, Mio Hattori who is my wife, Kouhei Hattori who is my son, Fuko Hattori who is my daughter and my parents, for their unfailing encouragement and support.

Abstract

In order to apply the low-Reynolds-number two-equation heat-transfer models to an engineering calculation of turbulent heat and mass transfer and fluid flows, several turbulence models are improved.

First, the modified low-Reynolds-number (LRN) k–ε model is proposed for applying a turbulent boundary layer flow with pressure gradient. In particular, the turbulent boundary layer flow with adverse pressure gradient (APG) does not maintain the standard log-law profile, i.e., $\bar{U}^+ = 2.44 \ln y^+ + 5.0$, in which the mean more rapidly reaches the log-law region than a zero-pressure gradient (ZPG) flow. Since almost all low-Reynolds-number k–ε models adopt the nondimensional distance y^+ in the wall-reflection function, these models must give the velocity profile along the standard log-law. The proposed model includes the nondimensional pressure-gradient parameter P^+ in the wall-reflection function. Therefore, the proposed model improves the prediction of turbulent quantities in the APG flow. The model adopts the quasi-dissipation rate, $\widetilde{\varepsilon}$, for the calculation stability, the so-called k–$\widetilde{\varepsilon}$ model. Though the $\widetilde{\varepsilon}$-equation, whose boundary condition can be put at 0 at the wall is employed in the model, the turbulent Reynolds number is defined using the net ε. Therefore, the wall-limiting behaviour of the Reynolds shear stress is satisfied exactly like the k–ε model.

Second, to analyze turbulent heat transfer with various thermal boundary conditions, the LRN two-equation heat transfer model is improved. The quasi-dissipation rate of the temperature variance, $\widetilde{\varepsilon_\theta}$, is adopted to the model for calculation stability. The proposed LRN two-equation heat transfer model is used together with the LRN linear k–$\widetilde{\varepsilon}$ or LRN nonlinear k–$\widetilde{\varepsilon}$ model for the calculation, and satisfies exactly the wall-limiting behaviour of turbulent heat-flux in the cases of both existing and non-existing temperature fluctuation at the wall. Agreement with the experimental and the direct numerical simulation (DNS) data is quite satisfactory.

Next, the transport equation for the dissipation rate of the temperature variance, ε_θ, is modeled rigorously (term to term) using the trustworthy DNS database. The DNS database gives some turbulent quantities in detail, in which the budget of ε_θ is contained. In the modelling, the terms of ε_θ-equation are modeled in correspondence with the rigorous terms. The turbulent diffusion terms are especially modeled with the conventional gradient diffusion-type model and new large-scale motion model. Thus, the predicted budgets of ε_θ-equation are in good agreement with the DNS data. Since the ε_θ-equation is modified rigorously, the modeled equation

for temperature variance, k_θ, also predicts exactly the behaviour of its budget and the near-wall profile itself in comparison with DNS. Therefore, the circumstantial transport phenomena of turbulence in the thermal field can be obtained applying the proposed model.

Then, the LRN two-layer turbulence models for both the velocity and thermal fields are proposed using the DNS databases. The advantages of the proposed LRN two-layer models are that a calculation is stabilized, and that the near-wall modelling of the both ε- and ε_θ-equations are simplified. The proposed models are applied to complex turbulent flows such as backward-facing step flow with heat transfer and high Prandtl number flows. The present LRN two-layer models give good agreement with the experiment and the DNS results.

On the other hand, it is well known that the linear k–ε model has a limited application for analysis of flow. Since it is difficult to express the Reynolds normal stress components with the linear k–ε model, a flow in which the Reynolds normal stress components become important can not be exactly predicted such as the rotating channel flow or a square duct turbulent flow with heat transfer. Therefore, the nonlinear k–ε model is effective for an analysis such flows. To improve the LRN nonlinear k–ε model, the existing LRN nonlinear models are evaluated using the DNS databases in both the inertial and noninertial frames. Considering the results of the assessment, the expression of Reynolds stress components is proposed in the nonlinear model which satisfies exactly the wall-limiting behaviour of each component, and reproduces properly the anisotropy of the Reynolds normal stress components. The proposed model adequately provides the wall-limiting behaviour and the anisotropy of the Reynolds normal stress components near the wall in both the inertial and noninertial frames.

Finally, to calculate the rotating shear flows with heat transfer which are often encountered in engineering applications, the LRN nonlinear k–ε model is reconstructed firstly with the above expression of the Reynolds stress component. Though the nonlinear model is effective for calculation of the rotating shear flow, the performance of the nonlinear model applied to such flows remains unclear. Thus, the existing LRN nonlinear models are assessed in the various rotation numbers flows using the DNS database. Introducing the results of the assessment to a reconstruction of the LRN nonlinear k–ε model, the proposed model accurately predicts the various rotation number flows. Especially, in high rotation number flow, the flow tends to indicate laminarization phenomena on the suction side, and the present model can capture this phenomenon adequately.

Contents

List of figures

List of tables

Nomenclature

a_{ij}	anisotropic stress, $= \overline{u_i u_j}/k - 2\delta_{ij}/3$
A_{ij}	additional term in expression of Reynolds stress in nonlinear k–ε model
A	Lumley's stress flatness parameter, $= 1 - (9/8)(A_2 - A_3)$
A_2	second invariant, $= a_{ij}a_{ji}$
A_3	third invariant, $= a_{ij}a_{jk}a_{ki}$
$A_{D1}, A_{D2}, A_\lambda, B_\lambda$	constants in heat-transfer model functions
b_{ij}	anisotropy tensor, $= \overline{u_i u_j}/2k - \delta_{ij}/3$
C_0, C_1, C_2, C_3, C_3, C_4, C_5, C_6, C_7	constants in expression of Reynolds stress in nonlinear k–ε model
C_D, C_η	constants in nonlinear k–ε model
$C_{D1}, C_{D2}, C_{P1}, C_{P2}$	constants in transport equation for ε_t
C_f	mean skin friction coefficient
C_p	mean static pressure coefficient, $= (\bar{P} - \bar{P}_0)/(\rho \bar{U}_0^2/2)$
C_s, C_ε	constants in GGDH type of turbulent diffusions of k and ε, respectively
C_{T1}, C_{T2}, C_{T3}	constants in two-equation heat-transfer model
$C_{\varepsilon 1}, C_{\varepsilon 2}$	constants in transport equation for ε
C_λ, C_m	constants in eddy diffusivity for heat
C_μ	constant in eddy viscosity
c_p	specific heat at constant pressure
D	channel width upstream of step or additional term of k
D_k	molecular diffusion term of k, $= \nu\partial^2 k/\partial x_j \partial x_j$
D_{k_θ}	molecular diffusion term of k_θ, $= \alpha\partial^2 k_\theta/\partial x_j \partial x_j$
D_ε	molecular diffusion term of ε, $= \nu\partial^2 \varepsilon/\partial x_j \partial x_j$
D_{ε_θ}	molecular diffusion term of ε_θ, $= \alpha\partial^2 \varepsilon_\theta/\partial x_j \partial x_j$
D_θ	additional term of k_θ

E	extra production term of ε
E_θ	extra production term of ε_θ
ER	channel expansion ratio, $= (D+H)/D$
f_A	function to account for influence of anisotropy in flow field
f_B	function to guarantee the realizability of anisotropy tensor
$f_{D1}, f_{D2}, f_{P1}, f_{P2}$	functions in transport equation for ε_θ
f_R	function in expression of Reynolds stress component
$f(R)$	function of time scale ratio R
f_{t1}, f_{t2}	functions in GGDH type of turbulent diffusions of k and ε, respectively
f_ε	low-Reynolds-number model function in transport equation for ε
f_λ	low-Reynolds-number model function in eddy diffusivity for heat
f_μ	low-Reynolds-number model function in eddy viscosity
G	temperature gradient parameter, $= \sqrt{\left(\partial\bar{\Theta}/\partial x_j\right)\left(\partial\bar{\Theta}/\partial x_j\right)}$
H	height of backward-facing step
h	duct width at exit of wind tunnel
k	turbulence energy, $= \overline{u_i u_i}/2$
k_θ	temperature variance, $= \overline{\theta^2}/2$
n	local coordinate normal to wall surface
$\bar{P}$	mean static pressure
P_k	production term of k, $= -\overline{u_i u_j}(\partial\bar{U}_i/\partial x_j)$
P_{k_θ}	production term of k_θ, $= -\overline{u_j\theta}(\partial\bar{\Theta}/\partial x_j)$
P_ε^1	mixed production term of ε, $= -2\nu\overline{(\partial u_i/\partial x_j)\,(\partial u_k/\partial x_j)}\left(\partial\bar{U}_i/\partial x_k\right)$
P_ε^2	production by mean velocity gradient term of ε, $= -2\nu\overline{(\partial u_i/\partial x_k)\,(\partial u_i/\partial x_m)}\left(\partial\bar{U}_k/\partial x_m\right)$
P_ε^3	gradient production term of ε, $= -2\nu\overline{u_k\,(\partial u_i/\partial x_m)}\left(\partial^2\bar{U}_i/\partial x_k\partial x_m\right)$
P_ε^4	turbulent production term of ε, $= -2\nu\overline{(\partial u_i/\partial x_k)\,(\partial u_i/\partial x_m)\,(\partial u_k/\partial x_m)}$
$P_{\varepsilon_\theta}^1$	mixed production term of ε_θ, $= -2\alpha\overline{(\partial u_j/\partial x_k)\,(\partial\theta/\partial x_k)}\left(\partial\bar{\Theta}/\partial x_j\right)$
$P_{\varepsilon_\theta}^2$	production by mean velocity gradient term of ε_θ, $= -2\alpha\overline{(\partial\theta/\partial x_j)\,(\partial\theta/\partial x_k)}\left(\partial\bar{U}_j/\partial x_k\right)$
$P_{\varepsilon_\theta}^3$	gradient production term of ε_θ, $= -2\alpha\overline{u_j\,(\partial\theta/\partial x_m)}\left(\partial^2\bar{\Theta}/\partial x_j\partial x_k\right)$
$P_{\varepsilon_\theta}^4$	turbulent production term of ε_θ, $= -2\alpha\overline{(\partial u_j/\partial x_k)\,(\partial\theta/\partial x_k)\,(\partial\theta/\partial x_j)}$
Pr	molecular Prandtl number
Pr_t	turbulent Prandtl number
p	fluctuating static pressure

q_w	wall heat flux
R	time-scale ratio, $= \tau_\theta/\tau_u$
Re_H	Reynolds number based on step height, $= \bar{U}_0 H/\nu$
Re_m	Reynolds number based on channel bulk velocity, $= 2\bar{U}_m\delta/\nu$
Re_τ	Reynolds number based on friction velocity, $= u_\tau\delta/\nu$ or $u_\tau^*\delta/\nu$
Re_0	Reynolds number based on channel centerline velocity, $= 2\bar{U}_0\delta/\nu$
Ro	rotation number based on bulk velocity and angular velocity, $= 2\Omega\delta/\bar{U}_m$
Ro_τ	rotation number based on friction velocity and angular velocity, $= 2\Omega\delta/u_\tau^*$
Rs	shear rate parameter
R_t	turbulent Reynolds number, $= k^2/\nu\varepsilon$
R_θ	Reynolds number based on momentum thickness, $= \bar{U}_0\theta/\nu$
S	strain-rate parameter, $= \sqrt{2S_{ij}S_{ij}}$
S_{ij}	strain-rate tensor, $= \left(\partial\bar{U}_i/\partial x_j + \partial\bar{U}_j/\partial x_i\right)/2$
St	Stanton number, $= q_w/[\rho c_p\bar{U}_0(\bar{\Theta}_w - \bar{\Theta}_0)]$
t	time
T_k	turbulent diffusion term of k, $= -\partial\left[\overline{u_j\left(u_iu_i/2\right)}\right]/\partial x_j$
T_{k_θ}	turbulent diffusion term of k_θ, $= -\partial\left[\overline{u_j\left(\theta^2/2\right)}\right]/\partial x_j$
T_ε	turbulent diffusion term of ε, $= -\nu\partial\left[\overline{u_j\left(\partial u_i/\partial x_k\right)\left(\partial u_i/\partial x_k\right)}\right]/\partial x_j$
T_{ε_θ}	turbulent diffusion term of ε_θ, $= -\alpha\partial\left[\overline{u_j\left(\partial\theta/\partial x_k\right)\left(\partial\theta/\partial x_k\right)}\right]/\partial x_j$
$\bar{U}, \bar{V}, \bar{W}$	mean velocity in x-, y- and z-directions, respectively
$\bar{U}_i$	mean velocity in i-direction
$\bar{U}_m$	bulk velocity of fully-developed channel flow
$\bar{U}^+$	nondimensional mean velocity, $= \bar{U}/u_\tau$
u, v, w	turbulent fluctuation in x-, y- and z-directions, respectively
u_i	turbulent fluctuation in i-direction
u_ε	Kolmogorov velocity scale, $= (\nu\varepsilon)^{1/4}$
u_τ	friction velocity, $= \sqrt{\lvert\tau_w\rvert/\rho}$
u_τ^*	averaged friction velocity on both side walls in channel flow with rotation
W_{ij}	absolute vorticity tensor, $= \Omega_{ij} + \epsilon_{mji}\Omega_m$
X_R	flow reattachment length
x	Cartesian coordinate in streamwise direction
x_i	Cartesian coordinate in i-direction

y	Cartesian coordinate normal to streamwise direction
y_k	nondimensional distance from wall surface, $= \sqrt{k}y/\nu$
y^+	nondimensional distance from wall surface, $= u_\tau y/\nu$
y^*	nondimensional distance from wall surface, $= u_\varepsilon y/\nu$
z	Cartesian coordinate in spanwise direction

Greek symbols

α	molecular diffusivity for heat
α_t	eddy diffusivity for heat
δ	half width of channel or 99% boundary layer thickness
δ_{ij}	Kronecker delta
ε	dissipation rate of turbulence energy, $= \nu\overline{(\partial u_i/\partial x_j)(\partial u_i/\partial x_j)}$
ε_θ	dissipation rate of $\overline{\theta^2}/2$, $= \alpha\overline{(\partial\theta/\partial x_j)(\partial\theta/\partial x_j)}$
η	generalized coordinate in lower to upper wall direction
θ	momentum thickness or temperature fluctuation
θ_τ	friction temperature, $q_w/(\rho c_p u_\tau)$
$\overline{\theta^2}$	temperature variance
κ	Von Kármán's universal constant
ν	kinematic viscosity
ν_t	eddy viscosity
ρ	density
$\sigma_k, \sigma_\varepsilon$	constants in isotropic turbulent diffusions of k and ε, respectively
σ_h, σ_ϕ	coefficients of turbulent diffusion terms in $\overline{\theta^2}$ and ε_t transport equations, respectively
τ_m	characteristic time scale for turbulent heat transfer
τ_R	characteristic time scale for expression of Reynolds stress in nonlinear k–ε model
τ_{Ro}	characteristic time scale for expression of Reynolds stress in nonlinear k–ε model
τ_{Rw}	characteristic time scale for expression of Reynolds stress in nonlinear k–ε model
τ_θ	time scale of temperature field, $= k_\theta/\varepsilon_\theta$
τ_u	time scale of velocity field, $= k/\varepsilon$

τ_w	wall shear stress
Ω	vorticity parameter, $= \sqrt{2\Omega_{ij}\Omega_{ij}}$ or anglar velocity
Ω_m	anglar velocity with x_m axis
Ω_{ij}	vorticity tensor, $\left(\partial\overline{U}_i/\partial x_j - \partial\overline{U}_j/\partial x_i\right)/2$
Π_k	pressure diffusion term of k, $= -\partial\left[\overline{u_j\left(p/\rho\right)}\right]/\partial x_j$
Π_ε	pressure diffusion term of ε, $= -2\nu\partial\left\{\overline{\left[\partial\left(p/\rho\right)/\partial x_m\right]\left(\partial u_k/\partial x_m\right)}\right\}/\partial x_k$
$\bar{\Theta}$	mean temperature
$\bar{\Theta}^+$	nondimensional mean temperature, $= (\bar{\Theta}_w - \bar{\Theta})/t_\tau$
$\bar{\Theta}_r$	reference temperature
$\bar{\Theta}_{ws}$	wall temperateure at step change point
Υ	destruction term of ε, $= 2\nu^2\overline{\left(\partial^2 u_i/\partial x_k\partial x_m\right)\left(\partial^2 u_i/\partial x_k\partial x_m\right)}$
$\Upsilon_{\varepsilon_\theta}$	destruction term of ε_θ, $= 2\alpha^2\overline{\left(\partial^2\theta/\partial x_j\partial x_k\right)\left(\partial^2\theta/\partial x_j\partial x_k\right)}$

Subscripts

e	outer edge of boundary layer
i, j, k, l, m, n	1, 2 and 3 denote x-, y- and z-directions, respectively
R	flow reattachment point
w	wall surface
0	reference value

Special symbols

D/Dt	substantial derivative, $\partial/\partial t + \bar{U}_j\partial/\partial x_j$
$f_{,i}$	partial derivative of variable, f, with respect to coordinate, x_i
$\overline{(\ )}$	ensemble-averaged value
$(\ )^+$	normalization by inner variables

CHAPTER 1

Introduction

1.1 Background

In the analysis of a heat transfer problem, the use of the experimental or numerical techniques is considered, employing methods for experimental fluid dynamics (EFD) or computational fluid dynamics (CFD). Since heat-transfer phenomena in fluid machinery, in the atmosphere, and in fluid motion of river, are almost turbulent flow, numerical techniques solving directly the governing equations are difficult to apply to real flow and conditions of actual machines for which the Reynolds number is large. A flow with hear transfer in a near-wall region, which is important in a turbulent thermal field, is difficult to measure, as is a flow through a very narrow or small duct such as a micro-machine with the EFD method. Thus, the CFD approach can be a valuable tool for the analysis. Also, both the EFD and CFD methods should be used in combination for large-scale motion as in the case of atmosphere phenomena. The conventional CFD method employs a turbulence model to solve an averaged Navier-Stokes equation.

The turbulence model usually is classified into a number of turbulent quantities in the expression of the Reynolds stress, $\overline{u_i u_j}$, or turbulent heat flux, $\overline{u_i \theta}$, in which on the basis of gradient diffusion type modelling, the eddy viscosity or the eddy diffusivity for heat models (EVM or EHM) have been the most widely used for the calculation of turbulent heat transfer phenomena, because the EVM and EHM are easy to handle in a simulation. Especially, k–ε model for the velocity field and k_θ–ε_θ model for the thermal field have been employed for a calculation. In k–ε model, the eddy viscosity, ν_t, is expressed by turbulence energy, k, and its dissipation rate, ε, and in k_θ–ε_θ two-equation heat-transfer model, the eddy diffusivity for heat, α_t, is expressed by the temperature variance, k_θ, its dissipation rate, ε_θ, k and ε. The nonlinear eddy viscosity model (NLEVM), which is composed of the conventional EVM and the quadratic and cubic

gradient tensors, have been improved. Thus, the two-equation model becomes more and more applicable to engineering problems.

On the other hand, in the turbulent heat transfer problems for engineering, since the behaviour of turbulent quantities in the near-wall region is very important, the low-Reynolds-number (LRN) version turbulence model should be employed. The LRN version k–ε model was first proposed by Jones-Launder (1972), and the LRN version k_θ–ε_θ model by Nagano-Kim (1988). Moreover, on a complex shape or terrain, a wall-function is difficult to apply to the wall-boundary conditions. Thus, the LRN version model which can set exactly the physical boundary condition at the wall should be also used in that case. In addition, the wall-limiting behaviour of turbulence should be satisfied in the LRN two-equation model for a prediction of turbulent quantities close to the wall. The Reynolds shear stress is proportional to a distance from the wall cubed, i.e., $\overline{uv} \propto y^3$. The k–ε model satisfying the wall-limiting behaviour was achieved by Nagano & Tagawa (1990a) and Myong & Kasagi (1990a). In the thermal field, the turbulent heat flux, $\overline{v\theta}$ is proportional to y^3 with no temperature fluctuations at the wall, and to y^2 with temperature fluctuations at the wall. The k_θ–ε_θ model satisfying the wall-limiting behaviour of the turbulent heat flux was proposed by Nagano *et al.* (1991). Then, improving Nagano-Tagawa model (1990a), Abe *et al.* (1994, 1995) succeeded in applying the k–ε and k_θ–ε_θ models to the prediction of backward-facing step flows with heat transfer, in which the Kolmogorov velocity scale, $u_\varepsilon = (\nu\varepsilon)^{\frac{1}{4}}$, is adopted for the wall-reflection function instead of y^+ as $y^* = yu_\varepsilon/\nu$.

Usually, the modelling of a two-equation model has been assisted with experimental and direct numerical simulation (DNS) databases. Recently, trustworthy DNS databases containing some turbulent quantities with the budget data of its transport-equation have been supplied through the Internet[1]. Therefore, near-wall turbulence modelling has been improved using DNS databases, and the k–ε model can even predict exactly the budget of transport-equations (Rodi & Mansour 1993; Nagano & Shimada 1995a). In the thermal field, the two-equation model applicable to various Prandtl number fluids is proposed using the DNS database (Nagano & Shimada 1996), so the two-equation models for both the velocity and thermal fields are basically successful. The nonlinear two-equation models have been modified in a way similar to the EVM

[1]e.g., http://ercoftac.mech.surrey.ac.uk/ ;ERCOFTAC, and http://www.thtlab.t.u-tokyo.ac.jp/ ;Turbulence and Heat Transfer Lab., of the University of Tokyo

(e.g., Abe *et al.* 1997; Craft *et al.* 1997), and the performance of the models has been evaluated in various flows with heat transfer.

As mentioned in the foregoing, since two-equation turbulence models which are easy to handle in a scheme of simulation have been expected to predict various more complex flow fields with heat transfer often encountered in engineering problems, such models should be improved and used more and more.

1.2 Concept of EVM and EHM and their classification

In general, the Reynolds stress and turbulent heat flux are modeled using the eddy viscosity model (EVM) and the eddy diffusivity for heat model (EHM).

$$\overline{u_i u_j} = \frac{2}{3}\delta_{ij}k - \nu_t \left(\frac{\partial \bar{U}_i}{\partial x_j} + \frac{\partial \bar{U}_j}{\partial x_i} \right) \tag{1.1}$$

$$\overline{u_j \theta} = -\alpha_t \frac{\partial \bar{\Theta}}{\partial x_j} \tag{1.2}$$

The concept of EVM and EHM is based on the molecular dynamics for the kinematic viscosity as follows:

$$\nu_t \propto V \times L_V \equiv V^2 \times \tau_V, \tag{1.3}$$

$$\alpha_t \propto V \times L_T \equiv V^2 \times \tau_T, \tag{1.4}$$

where V is the characteristic velocity scale for turbulence, L_V is the characteristic length scale for turbulence, τ_V is the characteristic time scale for turbulence, L_T is the characteristic length scale affecting turbulence heat transfer and τ_T is the characteristic time scale affecting turbulence heat transfer. Note that since the characteristic velocity scale in α_t is difficult to define at a thermal field alone, the velocity scale is used commonly similar to the velocity field its. Therefore, the modelling of the characteristic time scale is of importance for each field.

EVM and EHM are classified by numerical values expressing the eddy viscosity and the eddy diffusivity for heat in Eqs. (1.3) and (1.4), respectively, as described in the following sections.

1.2.1 Zero-equation model

The model using this concept is Prandtl's mixing-length theory (1925) which is classified in the zero-equation model for the velocity field as follows:

$$\nu_t \propto V \times L_V \equiv C\ell\frac{d\bar{U}}{dy} \times \ell = C\ell^2\frac{d\bar{U}}{dy}, \tag{1.5}$$

where C is the model constant which is usually put at unity, and ℓ is Prandtl's mixing-length. Since the mixing-length ℓ is defined as $\ell = \kappa y$, the variable to solve the eddy viscosity is not needed, i.e., zero-equation. To apply the zero-equation model to calculation in the near-wall turbulence, the modified mixing-length by van Driest (1956) is employed as follows:

$$\ell = \kappa y\left[1 - \exp\left(-\frac{y^+}{A}\right)\right], \tag{1.6}$$

where $1 - \exp\left(-y^+/A\right)$ is the so-called van Driest's dumping function. Since it is clear from an experiment that the mixing-length scale is not linear versus the distance from the wall near the wall, the above modification is required.

In the thermal field, the EHM is modeled using the concept of turbulent Prandtl number as follows:

$$\alpha_t = \frac{\nu_t}{Pr_t} \tag{1.7}$$

where Pr_t is made a constant in the zero-equation model.

These zero-equation models do not require solving the transport-equations. Therefore, these EVM and EHM formulations cannot follow adequately turbulent heat transfer phenomena in various flows. This makes it difficult to apply the zero-equation models to various flows with heat transfer.

1.2.2 One-equation model

The one-equation model which employed the turbulence energy for the characteristic velocity scale for turbulence (Kolmogorov 1942; Prandtl 1945) may be stated as follows:.

$$\nu_t \propto V \times L_V = C_k\sqrt{k} \times \ell. \tag{1.8}$$

where C_k is the model constant, and k is solved by its transport-equation as follows:

$$\frac{Dk}{Dt} = \frac{\partial}{\partial x_j}\left[\left(\nu + \nu_t\right)\frac{\partial k}{\partial x_j}\right] - \overline{u_i u_j}\frac{\partial \bar{U}_i}{\partial x_j} - \frac{k^{\frac{3}{2}}}{\ell}. \tag{1.9}$$

The one-equation heat transfer model given by Eq. (1.4) can be obtained using the relation between the length scale velocity and thermal fields.

$$\alpha_t \propto V \times L_T = C_k\sqrt{k} \times \ell_t = C_k\sqrt{k}\frac{\ell}{Pr_t}, \tag{1.10}$$

where $\ell/\ell_t = Pr_t$ which is derived from the definition of $Pr_t = \nu_t/\alpha_t = C_k\sqrt{k}\ell/(C_k\sqrt{k}\ell_t)$.

On the other hand, another concept of the one-equation model has been proposed (e.g., Bradshaw *et al.* 1967; Nee & Kovasznay 1969; Spalart & Allmaras 1994; Menter 1997; Nagano *et al.* 2000), in which ν_t is solved directly by its transport equation. Recently, a one-equation model reflecting the two-equation model which can be applied to the prediction of near-wall turbulence has been presented (Pei, Hattori & Nagano 1999a; Nagano, Pei & Hattori 2000). Thus the LRN one-equation model is given by the following equation.

$$\frac{D\nu_t}{Dt} = \frac{\partial}{\partial x_j}\left[\left(\nu + \frac{\nu_t}{\sigma_v}\right)\frac{\partial \nu_t}{\partial x_j}\right] + C_1\nu_t S - E_1 + A_{fv}, \tag{1.11}$$

where C_1 and σ_v are model constants, and $S = \sqrt{S_{ij}S_{ij}}$. The third term on the right-hand side of the equation is the dissipation term, and A_{fv} is the wall-reflection term.

Introducing the similar concept of the LRN one-equation model, the LRN one-equation heat-transfer model has been derived as follows (Pei, Hattori & Nagano 1999b; Pei, Hattori & Nagano 2000):

$$\frac{D\alpha_t}{Dt} = \frac{\partial}{\partial x_j}\left[\left(\alpha + \frac{\alpha_t}{\sigma_t}\right)\frac{\partial \alpha_t}{\partial x_j}\right] + \left(C_{\theta 1} + C_{\theta 2}\frac{\alpha_t}{\nu_t}\right)\nu_t S - E_\theta + D_\theta + A_{fu} + A_{f\theta}, \tag{1.12}$$

where σ_t is the model constant, $C_{\theta 1}$ and $C_{\theta 2}$ are coefficients of the production term, E_θ is the dissipation term, the term D_θ represents the effects of the dissimilarity between velocity and thermal fields, and A_{fu} and $A_{f\theta}$ are the wall-reflection terms.

The traditional one-equation model solves the k-equation for the EVM and EHM. Hence, the one-equation model was expected to have the higher performance than the zero-equation model. However, the characteristic time scale which is the important factor in representing turbulent phenomena, is determined algebraically for the whole region, so the one-equation models may not give proper predictions. On the other hand, as described in the foregoing, the one-equation models reflecting the two-equation model which solve the transport-equation of ν_t and α_t give high performance for analysis of turbulent heat-transfer phenomena (Nagano, Pei & Hattori 2000; Pei, Hattori & Nagano 2000) as well as the result of a two-equation model.

Note that the one-equation model has been employed in the two-layer model, in which the one-equation model is adopted in the near-wall region for the stability of the calculation and the simplicity of model formulation (Rodi *et al.* 1993). In the LRN two-layer model proposed by Rodi *et al.* (1993) referring to Durbin (1991) indicated in Eq. (1.21), the eddy viscosity and the dissipation rate are given near the wall as follows:

$$\nu_t = \sqrt{\overline{v^2}}\ell_{\mu,v}, \tag{1.13}$$

$$\varepsilon = \frac{\sqrt{\overline{v^2}}k}{\ell_{\varepsilon,\nu}}, \tag{1.14}$$

where $\ell_{\mu,v} = C_{\mu,v}y$ and $\ell_{\varepsilon,\nu} = 1.3y/\left[1 + 2.12\nu/\left(\sqrt{\overline{v^2}}y\right)\right]$, respectively, and $\overline{v^2}$ is obtained from algebraic formula as $\overline{v^2}/k = (4.65 \times 10^{-5}R_k^2 + 4.0 \times 10^{-4}R_k)$ with $R_k = y\sqrt{k}/\nu$. The equation is switched from the one-equation model to the two-equation model at $\nu_t/\nu = 16$. The LRN two-layer model has been evaluated in a backward-facing step flow, in which the reattachment point is underpredicted slightly in comparison with the experiment, and the model allows for fast convergence of the solution (Rodi *et al.* 1993).

1.2.3 Two-equation model

Velocity field

The two-equation model adopts k into the characteristic velocity scale identical with the one-equation model. In the two-equation model, the characteristic time scale is solved by the related transport equations. In general, the characteristic time-scale τ_V is the time between producing energy containing eddies and the time when dissipating them in the homogeneous decay turbulence. Therefore, the time τ_V is determined using the dissipation rate of k defined as $dk/dt = -\varepsilon$, which derives the characteristic time-scale $\tau_V = k/\varepsilon$. Consequently, the EVM in the two-equation model is given as follows:

$$\nu_t \propto V \times L_V = V \times V\tau_V = C_\mu\sqrt{k} \times \sqrt{k}\frac{k}{\varepsilon} = C_\mu\frac{k^2}{\varepsilon}, \tag{1.15}$$

where C_μ is the model constant, usually $C_\mu = 0.09$ in the wall turbulence. In general, the modelled transport-equations for k and ε are described as follows:

$$\frac{Dk}{Dt} = \nu\frac{\partial^2 k}{\partial x_j \partial x_j} + \frac{\partial}{\partial x_j}\left(\frac{\nu_t}{\sigma_k}\frac{\partial k}{\partial x_j}\right) - \overline{u_i u_j}\frac{\partial \bar{U}_i}{\partial x_j} - \varepsilon, \tag{1.16}$$

$$\frac{D\varepsilon}{Dt} = \nu\frac{\partial^2 \varepsilon}{\partial x_j \partial x_j} + \frac{\partial}{\partial x_j}\left(\frac{\nu_t}{\sigma_\varepsilon}\frac{\partial \varepsilon}{\partial x_j}\right) - \frac{\varepsilon}{k}\left(C_{\varepsilon 1} f_{\varepsilon 1}\overline{u_i u_j}\frac{\partial \bar{U}_i}{\partial x_j} + C_{\varepsilon 2} f_{\varepsilon 2}\varepsilon\right), \tag{1.17}$$

where the first terms in the right-hand side of Eqs. (1.16) and (1.17) are omitted in the high-Reynolds-number (HRN) version k–ε model, in which the boundary conditions of turbulent quantities are set using the log-law at the wall. Thus, with the HRN k–ε model it is difficult to use a calculation of a flow on a complex terrain or a flow with external forces, etc.

In the wall-bounded flow, since the near-wall characteristic time scale (or the length scale) becomes short, the dumping function should be introduced in the EVM, i.e., the LRN EVM as follows:

$$\nu_t = C_\mu f_\mu \frac{k^2}{\varepsilon}, \tag{1.18}$$

where f_μ is adopted for the van Driest type function as $f_\mu = [1 - \exp(-y^+/A_\mu)]^2$ (Nagano & Hishida 1987). In the LRN EVM, the boundary conditions of turbulent quantities can be set exactly adjusting the physical conditions at the wall, i.e., $\bar{U}_i = k = 0$ and $\varepsilon = \nu(\partial^2 k/\partial y^2)|_w$.

Incidentally, it is well known that the near-wall time scale should be expressed by another time scale for the structure of turbulence affecting a wall (e.g., Nagano & Tagawa 1990a; Myong & Kasagi 1990a). Thus, the characteristic time scale is expressed by the following formula (Nagano & Tagawa 1990a).

$$\tau_V = \frac{k}{\varepsilon} + B_\mu \frac{(\nu^3/\varepsilon)^{\frac{1}{4}}}{\sqrt{k}}, \tag{1.19}$$

where the second term on the right-hand side of Eq. (1.19) is the Taylor microscale for the time which is considered the dominating time scale of the eddy viscosity near the wall. Substituting Eq. (1.19) into Eq. (1.18), the following LRN EVM can satisfy the wall-limiting behaviour of the eddy viscosity as $\nu_t \propto y^3$ which is required from the wall-limiting behaviour of the Reynolds shear stress $\overline{uv}$ (Nagano & Tagawa 1990a):

$$\nu_t = C_\mu f_\mu k\left[\frac{k}{\varepsilon} + B_\mu \frac{(\nu^3/\varepsilon)^{\frac{1}{4}}}{\sqrt{k}}\right] = C_\mu f_\mu \frac{k^2}{\varepsilon}\left(1 + \frac{B_\mu}{R_t^{\frac{3}{4}}}\right). \tag{1.20}$$

This formulation of the EVM is the standard of the latest low-Reynolds-number k–ε model.

On the other hand, a k–ε–$\overline{v^2}$ model has been proposed by Durbin (1991), in which the EVM is defined using the $\overline{v^2}$ for the velocity scale instead of k as follows:

$$\nu_t = C_\mu \overline{v^2} \tau_V = C_\mu \overline{v^2} \max\left[\frac{k}{\varepsilon}, C_T \left(\frac{\nu}{\varepsilon}\right)^{\frac{1}{4}}\right], \tag{1.21}$$

where C_T is the model constant and $(\nu/\varepsilon)^{\frac{1}{4}}$ is the Kolmogorov microscale for the time. Since the Reynolds normal stress in the wall-normal direction, $\overline{v^2}$, implicitly takes the wall effect into account, the damping function is not needed. However, three transport-equations have to be solved for Eq. (1.21).

Again, regarding the wall-reflection function or the dumping function, the function should be adopted properly to reflect the wall effect. To reflect the wall effect appropriately and to avoid the singular points such as the reattachment point where the friction velocity $u_\tau = 0$, Abe *et al.* (1994) has proposed the following wall-reflection function replacing y^+ with $y^* = y u_\varepsilon / \nu$ in the van Driest dumping function.

$$f_\mu = \left[1 - \exp\left(-\frac{y^*}{A_\mu}\right)\right]^2. \tag{1.22}$$

As mentioned in the foregoing, the key point in the modelling with a two-equation model is to consider and adopt a proper time scale and wall-reflection function in the model. Based on this consideration, the transport equations should be modelled appropriately. The modelling of the time scale, in particular, is very important in the two-equation heat transfer model described below.

Thermal field

In general, since the turbulent Prandtl number $Pr_t = \nu_t / \alpha_t$ is not a constant in various flows with heat transfer, the zero- or one-equation models cannot predict a turbulent heat-transfer phenomena. Therefore, Nagano & Kim (1998) have proposed a two-equation heat-transfer model for wall-bounded flows, in which α_t is modelled using the proper turbulent quantities taking into account an experiment in the thermal field. The two-equation heat-transfer model has been successful to analyze various complex flows with heat transfer.

The two-equation heat transfer model usually introduces the mixing time scale for the turbulent heat transfer phenomena affecting both time scales of the velocity and thermal fields

(Nagano & Kim 1988) as follows:

$$\alpha_t \propto V^2 \times \tau_T = C_\lambda f_\lambda k \times \tau_T = C_\lambda f_\lambda k \left(\frac{2k_\theta}{\varepsilon_\theta} \frac{k}{\varepsilon} \right)^{\frac{1}{2}} = C_\lambda f_\lambda \frac{k^2}{\varepsilon} \sqrt{2R}, \tag{1.23}$$

where $R = (\tau_\theta / \tau_u) = (k_\theta / \varepsilon_\theta)/(k/\varepsilon)$ is the time-scale ratio. In Eq. (1.23), k and ε are obtained from Eqs. (1.16) and (1.17), and the modelled k_θ- and ε_θ-equations are described as follows:

$$\frac{Dk_\theta}{Dt} = \alpha \frac{\partial^2 k_\theta}{\partial x_j \partial x_j} + \frac{\partial}{\partial x_j} \left(\frac{\alpha_t}{\sigma_h} \frac{\partial k_\theta}{\partial x_j} \right) - \overline{u_j \theta} \frac{\partial \bar{\Theta}}{\partial x_j} - \varepsilon_\theta, \tag{1.24}$$

$$\begin{aligned} \frac{D\varepsilon_\theta}{Dt} =& \alpha \frac{\partial^2 \varepsilon_\theta}{\partial x_j \partial x_j} + \frac{\partial}{\partial x_j} \left(\frac{\alpha_t}{\sigma_\phi} \frac{\partial \varepsilon_\theta}{\partial x_j} \right) - \frac{\varepsilon_\theta}{k_\theta} \left(C_{P1} f_{P1} \overline{u_j \theta} \frac{\partial \bar{\Theta}}{\partial x_j} + C_{D1} f_{D1} \varepsilon_\theta \right) \\ & - \frac{\varepsilon_\theta}{k} \left(C_{P2} f_{P2} \overline{u_i u_j} \frac{\partial \bar{U}_i}{\partial x_j} + C_{D2} f_{D2} \varepsilon \right), \end{aligned} \tag{1.25}$$

In Eq. (1.23), the wall-reflection function, f_λ, contains the Prandtl number effect and information on the velocity field as follows (Nagano & Kim 1988):

$$f_\lambda = \left[1 - \exp \left(- \frac{\sqrt{Pr}}{A_\lambda} \frac{2}{C_f} Sty^+ \right) \right]^2, \tag{1.26}$$

where C_f is the mean skin friction coefficient and St is the Stanton number.

In the same way as the k–ε model, the characteristic time scale should be reflected in the near-wall effect. The characteristic time scale is expressed including the near-wall dominating scale (Nagano *et al.* 1993).

$$\tau_T = \frac{k}{\varepsilon} \sqrt{2R} + B_{\lambda 1} \frac{(\nu^3/\varepsilon)^{\frac{1}{4}}}{\sqrt{k}} \frac{\sqrt{2R}}{Pr^{\frac{4}{3}}} \exp \left[- \left(\frac{R_t}{B_{\lambda 2}} \right)^2 \right]. \tag{1.27}$$

This time scale takes into account a wide range of Prandtl number effects. Substituting Eq. (1.27) into (1.23) with $f_\lambda = \left[1 - \exp \left(-y^+ / A_\mu \right) \right] \left[1 - \exp \left(-y^+ Pr^{\frac{1}{3}} / A_\mu \right) \right]$ (Nagano *et al.* 1993), we obtain:

$$\begin{aligned} \alpha_t =& C_\lambda f_\lambda k \left\{ \frac{k}{\varepsilon} \sqrt{2R} + \frac{B_{\lambda 1}}{Pr^{\frac{4}{3}}} \frac{(\nu^3/\varepsilon)^{\frac{1}{4}}}{\sqrt{k}} \sqrt{2R} \exp \left[- \left(\frac{R_t}{B_{\lambda 2}} \right)^2 \right] \right\} \\ =& C_\lambda f_\lambda \frac{k^2}{\varepsilon} \sqrt{2R} \left\{ 1 + \frac{1}{Pr^{\frac{4}{3}}} \frac{B_{\lambda 1}}{R_t^{\frac{3}{4}}} \exp \left[- \left(\frac{R_t}{B_{\lambda 2}} \right)^2 \right] \right\}. \end{aligned} \tag{1.28}$$

Equation (1.28) satisfies the wall-limiting behaviour of the eddy diffusivity for heat as $\alpha_t \propto y^3$ with non-existing temperature fluctuation at the wall or $\alpha_t \propto y^2$ with existing temperature fluctuation at the wall, both of which are determined to be requirements of the wall-limiting

behaviour for the turbulent heat flux, $\overline{v\theta}$. Note that in order to satisfy the wall-limiting behaviour of the eddy diffusivity for heat in both the wall conditions $\theta_w = 0$ and $\theta_w \neq 0$, the τ_T should be proportional $\tau_T \propto \tau_V\sqrt{2R}$. In fact, α_t in Eq. (1.28) becomes as follows near the wall:

$$\alpha_t \propto k\frac{(\nu^3/\varepsilon)^{\frac{1}{4}}}{\sqrt{k}}\frac{\sqrt{2R}}{Pr}y^{+2}. \tag{1.29}$$

On the other hand, a harmonic averaged time scale has been proposed (Shikazono & Kasagi 1996, Abe *et al.* 1995). To express the near-wall time scale, the following formulation for τ_T is presented (Abe *et al.* 1995):

$$\tau_T = \frac{k}{\varepsilon}\left(\frac{2R}{0.5+R}\right) + B_{\lambda 1}\frac{(\nu^3/\varepsilon)^{\frac{1}{4}}}{\sqrt{k}}\frac{\sqrt{2R}}{Pr}\exp\left[-\left(\frac{R_t}{B_{\lambda 2}}\right)^2\right], \tag{1.30}$$

where the first term of the right-hand side of Eq. (1.30) is the harmonic averaged time scale. This time scale characteristically takes a too short scale in the large-scale motion of the thermal field. This is because the shortest time scale serves as the large scale for dominating eddy diffusivity for heat, α_t. Considering the ratio between the velocity and temperature time scales for dissipative motions, near the wall is represented by $\sqrt{R/Pr}$ (Shikazono & Kasagi 1996). Therefore, the eddy diffusivity for heat using Eq. (1.30) with the wall-reflection function $f_\lambda = [1-\exp(-y^*/A_\mu)]\left[1-\exp(-y^*\sqrt{Pr}/A_\mu)\right]$ takes the following relation near the wall (Abe *et al.* 1995):

$$\alpha_t \propto k\frac{(\nu^3/\varepsilon)^{\frac{1}{4}}}{\sqrt{k}}\frac{\sqrt{2R}}{\sqrt{Pr}}y^{*2}. \tag{1.31}$$

Moreover, from further consideration of the Prandtl number effects, the following characteristic time scale for α_t has been suggested (Nagano & Shimada 1996):

$$\tau_T = \frac{k}{\varepsilon}\left[\frac{2R}{1/(5Pr^{\frac{1}{4}})+R}\right] + \frac{B_{\lambda 1}}{(1+2\sqrt{Pr})^{\frac{1}{4}}}\left(\frac{\nu}{k}\right)\frac{\sqrt{2R}}{\sqrt{Pr}}\exp\left[-\left(\frac{R_{\varepsilon t}}{B_{\lambda 2}}\right)^{\frac{3}{4}}\right], \tag{1.32}$$

where $R_{\varepsilon t} = (1+2\sqrt{Pr})R_\varepsilon$ and $R_\varepsilon = y/(\nu^3/\widetilde{\varepsilon})^{\frac{1}{4}}$. In this model, with the wall-reflection function $f_\lambda = 1-\exp\left[-\left(1+2\sqrt{Pr}\right)^{\frac{1}{4}}R_\varepsilon^2\right]$, α_t is expressed near the wall as follows:

$$\alpha_t \propto k\left(\frac{\nu}{k}\right)\frac{\sqrt{2R}}{\sqrt{Pr}}R_\varepsilon. \tag{1.33}$$

The time scale ν/k means a low turbulent Reynolds number effect, because $\nu/k \gg k/\varepsilon$ yields $R_t = (k/\varepsilon)/(\nu/k) \to 0$ near the wall.

The k–$\widetilde{\varepsilon}$ and k_θ–$\widetilde{\varepsilon}_\theta$ models

To stabilize the calculation, the k–$\widetilde{\varepsilon}$ equation model has been proposed (Jones & Launder 1972; Nagano & Hishida 1987). The quasi-dissipation rate of k, $\widetilde{\varepsilon}$, is defined as:

$$\widetilde{\varepsilon} = \begin{cases} \varepsilon - 2\nu \dfrac{\partial\sqrt{k}}{\partial y}\dfrac{\partial\sqrt{k}}{\partial y} & : \dfrac{\partial\sqrt{k}}{\partial y} \geq 0 \\ \varepsilon & : \dfrac{\partial\sqrt{k}}{\partial y} < 0. \end{cases} \tag{1.34}$$

This relation proposed by Jones & Launder (1972) is derived from the theory of the wall-limiting behaviour of turbulence (see section 2.3). The k–$\widetilde{\varepsilon}$ equation model has been employing the following transport equations.

$$\frac{Dk}{Dt} = \frac{\partial}{\partial x_j}\left[\left(\nu + \frac{\nu_t}{\sigma_k}\right)\frac{\partial k}{\partial x_j}\right] - \overline{u_i u_j}\frac{\partial \bar{U}_i}{\partial x_j} - \left(\widetilde{\varepsilon} + 2\nu\frac{\partial\sqrt{k}}{\partial y}\frac{\partial\sqrt{k}}{\partial y}\right), \tag{1.35}$$

$$\frac{D\widetilde{\varepsilon}}{Dt} = \frac{\partial}{\partial x_j}\left[\left(\nu + \frac{\nu_t}{\sigma_\varepsilon}\right)\frac{\partial\widetilde{\varepsilon}}{\partial x_j}\right] - \frac{\widetilde{\varepsilon}}{k}\left(C_{\varepsilon 1} f_{\varepsilon 1}\overline{u_i u_j}\frac{\partial \bar{U}_i}{\partial x_j} + C_{\varepsilon 2} f_{\varepsilon 2}\widetilde{\varepsilon}\right) + \nu\nu_t\left(1 - f_\mu\right)\frac{\partial^2 \bar{U}_i}{\partial x_j \partial x_k}\frac{\partial^2 \bar{U}_i}{\partial x_j \partial x_k}, \tag{1.36}$$

where the last term on the right-hand side of Eq. (1.36) is the extra production term introduced to correct a near-wall profile of $\widetilde{\varepsilon}$. Since the boundary condition of $\widetilde{\varepsilon}$-equation in Eq. (1.36) can be put to zero at the wall, the calculation used for the $\widetilde{\varepsilon}$-equation is performed more stably than the ε-equation used for the calculation.

In the thermal field, the quasi-dissipation rate of k_θ is also proposed (Nagano & Kim 1988) as follows:

$$\widetilde{\varepsilon_\theta} = \begin{cases} \varepsilon_\theta - 2\alpha \dfrac{\partial\sqrt{k_\theta}}{\partial y}\dfrac{\partial\sqrt{k_\theta}}{\partial y} & : \dfrac{\partial\sqrt{k_\theta}}{\partial y} \geq 0 \\ \varepsilon_\theta & : \dfrac{\partial\sqrt{k_\theta}}{\partial y} < 0. \end{cases} \tag{1.37}$$

However, this relation can not be employed for the case of existing temperature fluctuation at the wall, because Eq. (1.37) does not satisfy the wall-limiting behaviour in that case. Thus, the modified definition for the $\widetilde{\varepsilon_\theta}$ which can apply to both cases of non-existing k_θ and existing k_θ at the wall is proposed (Youssef *et al.* 1992) as follows:

$$\widetilde{\varepsilon_\theta} = \begin{cases} \varepsilon_\theta - 2\alpha \dfrac{\partial\sqrt{\Delta k_\theta}}{\partial y}\dfrac{\partial\sqrt{\Delta k_\theta}}{\partial y} & : \dfrac{\partial\sqrt{\Delta k_\theta}}{\partial y} \geq 0 \\ \varepsilon_\theta & : \dfrac{\partial\sqrt{\Delta k_\theta}}{\partial y} < 0, \end{cases} \tag{1.38}$$

where $\Delta k_\theta = k_\theta(x,y,z) - k_\theta(x,0,z) = k_\theta - k_\theta|_w$. The k_θ–$\widetilde{\varepsilon}_\theta$ model has been using the following modeled transport equations.

$$\frac{Dk_\theta}{Dt} = \frac{\partial}{\partial x_j}\left[\left(\alpha + \frac{\alpha_t}{\sigma_h}\right)\frac{\partial k_\theta}{\partial x_j}\right] - \overline{u_j\theta}\frac{\partial \bar{\Theta}}{\partial x_j} - \left(\widetilde{\varepsilon}_\theta + 2\alpha\frac{\partial\sqrt{\Delta k_\theta}}{\partial y}\frac{\partial\sqrt{\Delta k_\theta}}{\partial y}\right), \tag{1.39}$$

$$\begin{aligned}\frac{D\widetilde{\varepsilon}_\theta}{Dt} = \frac{\partial}{\partial x_j}\left[\left(\alpha + \frac{\alpha_t}{\sigma_\phi}\right)\frac{\partial\widetilde{\varepsilon}_\theta}{\partial x_j}\right] &- \frac{\widetilde{\varepsilon}_\theta}{k_\theta}\left(C_{P1}f_{P1}\overline{u_j\theta}\frac{\partial\bar{\Theta}}{\partial x_j} + C_{D1}f_{D1}\widetilde{\varepsilon}_\theta\right)\\ &- \frac{\widetilde{\varepsilon}_\theta}{k}\left(C_{P2}f_{P2}\overline{u_iu_j}\frac{\partial\bar{U}_i}{\partial x_j} + C_{D2}f_{D2}\widetilde{\varepsilon}\right)\\ &+ \alpha\alpha_t\left(1-f_\lambda\right)\frac{\partial^2\bar{\Theta}}{\partial x_j\partial x_k}\frac{\partial^2\bar{\Theta}}{\partial x_j\partial x_k},\end{aligned} \tag{1.40}$$

where the last term on the right-hand side of Eq. (1.40) is the extra production term introduced to correct a near-wall profile of $\widetilde{\varepsilon}_\theta$. Since the boundary condition of $\widetilde{\varepsilon}_\theta$-equation in Eq. (1.40) can be put to zero at the wall similar to the $\widetilde{\varepsilon}$-equation, the stability of calculation is achieved.

Nonlinear two-equation model and algebraic stress model

The model reflecting the Reynolds stress model (RSM) or the turbulent heat-flux model (THM) in the EVM or EHM is the so-called nonlinear two-equation model (e.g., Pope 1975, Gatski & Speziale 1993; Abe *et al.* 1997). The nonlinear two-equation model is a kind of algebraic stress model (ASM), also called the explicit ASM. The traditional ASMs for $\overline{u_iu_j}$ and $\overline{u_i\theta}$ are obtained from the assumption of the structure parameters $\overline{u_iu_j}/k$=constant and $\overline{u_i\theta}/\sqrt{kk_\theta}$=constant in various flows with heat transfer (Rodi 1976; Hossain & Rodi 1982; Launder 1988). In general, the Reynolds stress and turbulent heat flux in the ASM can be written as follows:

$$\overline{u_iu_j} = \frac{k\left(P_{ij} + \Phi_{ij} - \varepsilon_{ij}\right)}{P_k - \varepsilon}, \tag{1.41}$$

$$\overline{u_i\theta} = \frac{2kk_\theta\left(P_{i\theta} + \Phi_{i\theta} - \varepsilon_{i\theta}\right)}{k_\theta\left(P_k - \varepsilon\right) + k\left(P_{k_\theta} - \varepsilon_\theta\right)}, \tag{1.42}$$

where

$$
\begin{aligned}
P_k =& -\overline{u_i u_j}\frac{\partial \bar{U}_i}{\partial x_j} \\
P_{ij} =& -\overline{u_i u_k}\frac{\partial \bar{U}_j}{\partial x_k} - \overline{u_j u_k}\frac{\partial \bar{U}_i}{\partial x_k}, \\
\Phi_{ij} =& \overline{\frac{p}{\rho}\left(\frac{\partial u_i}{\partial x_j} + \frac{\partial u_j}{\partial x_i}\right)}, \\
\varepsilon_{ij} =& 2\nu\overline{\frac{\partial u_i}{\partial x_k}\frac{\partial u_j}{\partial x_k}},
\end{aligned}
$$

$$
\begin{aligned}
P_{k\theta} =& -\overline{u_j\theta}\frac{\partial \bar{\Theta}}{\partial x_j} \\
P_{i\theta} =& -\overline{u_i u_j}\frac{\partial \bar{\Theta}}{\partial x_j} - \overline{u_j\theta}\frac{\partial \bar{U}_i}{\partial x_j}, \\
\Phi_{i\theta} =& \overline{\frac{p}{\rho}\left(\frac{\partial \theta}{\partial x_i}\right)}, \\
\varepsilon_{i\theta} =& (\alpha+\nu)\overline{\frac{\partial u_i}{\partial x_j}\frac{\partial \theta}{\partial x_j}}.
\end{aligned}
$$

Here the terms Φ_{ij}, ε_{ij}, $\Phi_{i\theta}$ and $\varepsilon_{i\theta}$ should be modelled.

With the two-equation models, the Reynolds stress components $\overline{u_i u_j}$ and the turbulent heat fluxes $\overline{u_i\theta}$ are obtained algebraically from Eqs. (1.41) and (1.42), respectively. Since there is no need to solve the transport equations of $\overline{u_i u_j}$ and $\overline{u_i\theta}$, the ASM is employed for the calculation of the complex flow and thermal field with two-equation models. However, Eqs. (1.41) and (1.42) include $\overline{u_i u_j}$ and $\overline{u_i\theta}$ on both sides of the equation, so to obtain $\overline{u_i u_j}$ and $\overline{u_i\theta}$, an implicit calculation is required. Therefore, the ASM often causes an unstable calculation.

On the other hand, in the EASM, i.e., nonlinear two-equation models, the Reynolds stress components $\overline{u_i u_j}$ and the turbulent heat fluxes $\overline{u_i\theta}$ are solved explicitly. The EASM for the velocity field can be written formally as follows (for a detailed formulation of EASM, see section 2.1):

$$
\begin{aligned}
\overline{u_i u_j} = \frac{2}{3}\delta_{ij}k - \nu_t\left(\frac{\partial \bar{U}_i}{\partial x_j} + \frac{\partial \bar{U}_j}{\partial x_i}\right) \\
+C_q k\tau^2 \times (\text{quadratic terms for combination of } S_{ij} \text{ and } \Omega_{ij}) \\
+C_c k\tau^3 \times (\text{cubic terms for combination of } S_{ij} \text{ and } \Omega_{ij}),
\end{aligned}
\tag{1.43}
$$

where C_q and C_c are the model constants.

Equation (1.43) is based on Eq. (1.41). However, the right-hand side of the equation does not include $\overline{u_i u_j}$ like Eq. (1.41). Thus, the Reynolds stress components $\overline{u_i u_j}$ are solved explicitly by Eq. (1.43). Consequently, the calculation using the EASM becomes more stable than the calculation using the ASM.

Several nonlinear two-equation heat-transfer models have been proposed (Yoshizawa 1988; Sommer & So 1996). The latest version of the nonlinear two-equation heat-transfer model has been presented by Abe *et al.* (1996) as follows:

$$\begin{aligned}\overline{u_j\theta} = &- \alpha^t_{jk}\frac{\partial\bar{\Theta}}{\partial x_k} \\ &+ \frac{1}{f_{RT}}\overline{u_\ell u_k}\tau_m^2\left[\left(C_{T2}-C_{T3}\right)S_{j\ell}\frac{\partial\bar{\Theta}}{\partial x_k}+\left(C_{T2}+C_{T3}\right)\Omega_{j\ell}\frac{\partial\bar{\Theta}}{\partial x_k}\right],\end{aligned} \tag{1.44}$$

where C_{T2} and C_{T3} are the model constants, and the model function f_{RT} is given as:

$$f_{RT} = \frac{C_{T1}}{1+\frac{1}{2}\tau_m^2\left[\left(C_{T2}+C_{T3}\right)^2\Omega^2-\left(C_{T2}-C_{T3}\right)^2S^2\right],} \tag{1.45}$$

where C_{T1} is the model constant.

α^t_{jk} is an anisotropic eddy diffusivity for heat tensor as follows:

$$\alpha^t_{jk} = C_\lambda f_\lambda \delta_{j\ell}\overline{u_\ell u_k}\tau_T. \tag{1.46}$$

where $C_\lambda = 1/f_{RT}$. In Eq. (1.46), the characteristic velocity scale is taken as an anisotropy scale, and the characteristic time scale τ_T is given by:

$$\tau_T = \frac{k}{\varepsilon}\left(\frac{2R}{0.5+R}\right)f_A + B_{\lambda1}\frac{(\nu^3/\varepsilon)^{\frac{1}{4}}}{\sqrt{k}}\frac{\sqrt{2R}}{\sqrt{Pr}}\exp\left[-\left(\frac{R_t}{B_{\lambda2}}\right)^{\frac{3}{4}}\right], \tag{1.47}$$

where

$$f_A = \left(\frac{2}{1+3.5\sqrt{b^2}}\right)\left[1+\left(1+\frac{1+3.5\sqrt{b^2}}{2}-1\right)\right]\exp\left[-\left(\frac{y^*}{26}\right)^2\right], \tag{1.48}$$

$$f_\lambda = 1-\exp\left[-\left(\frac{y^*}{26}\right)^2\right] \tag{1.49}$$

here $b^2 = b_{ij}b_{ij}$. The behaviour of α_t near the wall is similar to that in Eq. (1.31).

Although the nonlinear two-equation heat transfer model has not yet been applied to calculation of the various flows with heat transfer, the model may become a powerful tool for an analysis of turbulent heat-transfer problems in the engineering.

1.3 Objectives

The objectives of the present study are the development of two-equation turbulence models which are applicable to turbulent heat-transfer problems in engineering as described below:

1. To construct a low-Reynolds-number k–ε model satisfying both the wall-limiting behaviour of turbulence and stability of calculation, and applicable to predictions of the boundary layer flows with pressure gradient;

2. To develop a low-Reynolds-number k_θ–ε_θ model satisfying both the wall-limiting behaviour of turbulence and a stability of calculation, and applicable to predictions of thermal boundary layer flows with arbitrary wall boundary conditions;

3. To evaluate the prediction accuracy of the existing modeled equation for the dissipation rate of temperature variance using DNS databases, and to model rigorously the ε_θ-equation employing the assessment results;

4. To show the performance of reconstructed two-equation heat-transfer models taking prediction accuracy of the budget in transport equations into account in a thermal boundary layer flow with a pulse heat-input wall boundary condition;

5. To construct new low-Reynolds-number two-layer heat-transfer models allowing fast convergence of a calculation, and applicable to heat transfer problems in complex turbulent flows and various Prandtl number flows;

6. To assess the prediction accuracy of the Reynolds stress components' expression of low-Reynolds-number nonlinear k–ε models in inertial and noninertial frames using DNS databases.

7. To improve the Reynolds stress components' expression of a low-Reynolds-number nonlinear k–ε model introducing a new wall-reflected time scale for nonlinear terms and satisfying the wall-limiting behaviour of each Reynolds stress components exactly in both inertial and noninertial frames;

8. To reconstruct a low-Reynolds-number nonlinear k–ε model applicable to various rotation number flows.

1.4 Organization of Dissertation

The subject of this thesis consists of four main areas of inquiry. The first is concerned with the construction of low-Reynolds-number two-equation heat transfer models for predicting boundary layer flows with pressure gradient and thermal boundary layer flows with arbitrary wall boundary conditions. The second deals with the assessment of the existing modeled equation for the dissipation rate of temperature variance, ε_θ, using DNS databases. The ε_θ-equation is modeled rigorously in comparison with the budget of its transport equation obtained from DNS, and the set of two-equation heat-transfer models is reconstructed using the new modeled ε_θ-equation. The third is concerned with the new proposal of two-equation heat-transfer models for predicting a complex flow with heat transfer and various Prandtl number flows. The fourth deals with the evaluation of the existing low-Reynolds-number nonlinear models in inertial and noninertial frames using DNS databases, and the reconstruction of a nonlinear k–ε model for predicting various rotation number flows. Chapter 3 and 4 deal with the first area, Chapter 5 with the second, Chapter 6 with the third, and Chapter 7 and 8 with the fourth.

Chapter 2 presents ensemble-averaged governing equations for the turbulent velocity and temperature fields used in this study, and the theory of the wall-limiting behaviour of turbulence.

In Chapter 3, an improvement of the k–$\widetilde{\varepsilon}$ model for predicting boundary layer flows with pressure gradients is proposed (Hattori & Nagano 1993; Hattori & Nagano 1995a), which satisfies the wall-limiting behaviour of Reynolds shear stress exactly and allows the calculation stability. The proposed model is based on the Nagano & Hishida model which employs the $\widetilde{\varepsilon}$-equation but not satisfy the wall-limiting behaviour and the Nagano & Tagawa model (1990a) which satisfies the wall-limiting behaviour but does not allow calculation stability. The principal improvement is introducing the nondimensional pressure gradient parameter, $P^+ = \nu(d\bar{P}/dx)/(\rho u_\tau^3)$, in the wall-reflection function, and the modified turbulent Reynolds number $R_t = k^2/[(\widetilde{\varepsilon} + D)\nu]$ where $D = 2\nu(\partial\sqrt{k}/\partial y)^2$ is proposed for satisfying the wall-limiting behaviour similar to the Nagano & Tagawa model (1990a).

Chapter 4 presents a two-equation heat transfer model for predicting thermal boundary layer flows in arbitrary wall boundary conditions (Hattori *et al.* 1993; Nagano, Hattori & Abe 1995; Nagano & Hattori 1997), which satisfies the wall-limiting behaviour of turbulent heat flux in both wall-boundary conditions, $\theta_w = 0$ and $\theta_w \neq 0$. The present heat-transfer model based on both the Nagano & Kim model (k_θ–$\widetilde{\varepsilon}_\theta$ model) and the Youssef *et al.* model (k_θ–ε_θ model), in

which the $\widetilde{\varepsilon}_\theta$-equation is adopted, so the model allows calculation stability. The principal improvement is modification of the correction term, D_t, for $\widetilde{\varepsilon}_\theta$ applicable to the $\theta_w \neq 0$ condition at the wall.

In Chapter 5, a rigorous model for ε_θ-equation for the modification of the behaviour for k_θ and ε_θ close to the wall is proposed (Hattori & Nagano 1995b; Hattori & Nagano 1995c; Hattori & Nagano 1998), in which, first, the assessment of the existing modelled ε_θ -equations is carried out using the DNS database. Considering the results of the assessment, the modelled ε_θ-equation is then improved to predict the near-wall behaviour of ε_θ with its budget indicated in DNS. The set of two-equation models for both the velocity and thermal fields is also proposed with the modified ε_θ-equation.

Chapter 6 presents the low-Reynolds number two-layer models for both the velocity and thermal fields for predicting complex flows with heat transfer and various Prandtl number flows (Hattori & Nagano 1999), which is modelled by dividing the near-wall region from the over the log-law region. Since the ε and ε_θ are solved by the algebraic formulas for the near-wall region, the models allow stable calculation. In the modelling, the new algebraic formulas ε and ε_θ are suggested for giving the characteristic time scale of ν_t and α_t. The indicator functions for switching properly from algebraic formulas to the equations are also proposed.

In Chapter 7, the Reynolds stress expression in a nonlinear k–ε model for satisfying the wall-limiting behaviour of the Reynolds stress components individually is improved (Hattori, Hiramatsu & Nagano 2002). For improvement of the model, the Reynolds stress expressions in existing nonlinear models are evaluated using the DNS databases in both inertial and noninertial frames. The principal improvement is the introduction of the wall-reflection term in the expression of the Reynolds stress component, in which a new characteristic time scale is proposed to satisfy exactly the wall-limiting behaviour and to reproduce anisotropy of the Reynolds stress components in both the inertial and noninertial frames.

Chapter 8 presents an improvement of the nonlinear k–ε model for predicting various rotation number flows (Nagano & Hattori 2001a: Nagano & Hattori 2001b; Hattori & Nagano 2002), which adopts the additional rotational term in ε-equation for reproducing the rotational effects in the channel flow. The results of the assessment for the expression of Reynolds stress component are reflected in the proposed model as described in Chapter 7.

The important overall conclusions of this study are described in Chapter 9.

CHAPTER 2

Governing equations

2.1 Equations for velocity field

In this study, the following conditions are imposed in calculating a tubrulent velocity field:

- All fluid properties are constant within the flow
- Fluid is imcompressible and Newtonian

Under the above-mentioned conditions, the ensemble-averaged governing equations for a velocity fields are described as follows:

$$\frac{\partial \bar{U}_i}{\partial x_i} = 0, \tag{2.1}$$

$$\frac{D\bar{U}_i}{Dt} = -\frac{1}{\rho}\frac{\partial \bar{P}}{\partial x_i} + \frac{\partial}{\partial x_j}\left[\nu\left(\frac{\partial \bar{U}_i}{\partial x_j} + \frac{\partial \bar{U}_j}{\partial x_i}\right) - \overline{u_i u_j}\right], \tag{2.2}$$

where $D/Dt = \partial/\partial t + \bar{U}_j + \partial/\partial x_j$ implies the substantial derivative, and the Einstein summation convention applies to repeated indices. On the other hand, the momentum transport equation of the rotating flow described in the noninertial frame can be written as:

$$\frac{D\bar{U}_i}{Dt} = -\frac{1}{\rho}\frac{\partial}{\partial x_i}\left(\bar{P} - \frac{\rho}{2}\Omega^2 r^2\right) + \frac{\partial}{\partial x_j}\left[\nu\left(\frac{\partial \bar{U}_i}{\partial x_j} + \frac{\partial \bar{U}_j}{\partial x_i}\right) - \overline{u_i u_j}\right] - 2\Omega_m \epsilon_{ijm}\bar{U}_j, \tag{2.3}$$

where $-\rho\Omega^2 r^2/2$ is the centrifugal force which can be included in the pressure under the above-mentioned conditions, r denotes the distance from the axis of rotation.

In two-equation turbulence modelling, the unknown Reynolds stress $\overline{u_i u_j}$ in Eq. (2.2) and (2.3) can be expressed the usage of the concept of the gradient diffusion approximation through the eddy viscosity ν_t as follows:

$$\overline{u_i u_j} = \frac{2}{3}\delta_{ij}k - \nu_t\left(\frac{\partial \bar{U}_i}{\partial x_j} + \frac{\partial \bar{U}_j}{\partial x_i}\right), \tag{2.4}$$

$$\nu_t = C_\mu f_\mu k \tau_V, \tag{2.5}$$

where τ_V denotes the characteristic time scale for turbulnce in velocity field, and is generally a function of the turbuelence energy k and its dissipation rate ε. On the other hand, the above relation in Eq. (2.4) is employed in a linear eddy viscosity equation model (EVM), a nonlinear eddy viscosity equation model (NLEVM) adopts the following expression for the Reynolds stress (Craft *et al.* 1997):

$$\begin{aligned}
\overline{u_i u_j} =& \frac{2}{3}k\delta_{ij} - C_0\nu_t\left(\frac{\partial \bar{U}_i}{\partial x_j} + \frac{\partial \bar{U}_j}{\partial x_i}\right) \\
&+ C_1 k\tau_R^2\left(\Omega_{jk}S_{ki} + \Omega_{ik}S_{kj}\right) \\
&+ C_2 k\tau_R^2\left(S_{ik}S_{kj} - \frac{1}{3}S_{mn}S_{mn}\delta_{ij}\right) \\
&+ C_3 k\tau_R^2\left(\Omega_{ik}\Omega_{jk} - \frac{1}{3}\Omega_{mn}\Omega_{mn}\delta_{ij}\right) \\
&\quad \text{— quadratic model —} \\
&+ C_4 k\tau_R^3\left(S_{ki}\Omega_{\ell j} + S_{kj}\Omega_{\ell i}\right)S_{k\ell} \\
&+ C_5 k\tau_R^3\left(\Omega_{i\ell}\Omega_{\ell m}S_{mj} + S_{i\ell}\Omega_{\ell m}\Omega_{mj} - \frac{2}{3}S_{\ell m}\Omega_{mn}\Omega_{n\ell}\delta_{ij}\right) \\
&+ C_6 k\tau_R^3 S_{ij}S_{k\ell}S_{k\ell} \\
&+ C_7 k\tau_R^3 S_{ij}\Omega_{k\ell}\Omega_{k\ell} \\
&\quad \text{— cubic model —} \\
&+ A_{ij}, \qquad (2.6)
\end{aligned}$$

where $C_0 \sim C_7$ are the model constants, τ_R is the characteristic time-scale, A_{ij} is the additional term. Note that, in the noninertial frame, the vorticity tensor should be replaced with the absolute vorticity tensor, i.e., $W_{ij} = \Omega_{ij} + \epsilon_{mji}\Omega_m$ for satisfying the material frame indifference (MFI) (Speziale *et al.* 1997).

The futher unknown quntities k and ε in Eq. 2.5 are given by the following equations:

$$\frac{Dk}{Dt} = D_k + T_k + \Pi_k + P_k - \varepsilon, \qquad (2.7)$$

where

$$
\begin{aligned}
D_k =& \nu \frac{\partial^2 k}{\partial x_j \partial x_j} && \text{: Molecular diffusion,} \\
T_k =& -\frac{\partial}{\partial x_j}\left[\overline{u_j\left(\frac{u_i u_i}{2}\right)}\right] && \text{: Turbulent diffusion,} \\
\Pi_k =& -\frac{\partial}{\partial x_j}\overline{\left(u_j \frac{p}{\rho}\right)} && \text{: Pressure diffusion,} \\
P_k =& -\overline{u_i u_j}\frac{\partial \bar{U}_i}{\partial x_j} && \text{: Production,} \\
\varepsilon =& \nu \overline{\frac{\partial u_i}{\partial x_j}\frac{\partial u_i}{\partial x_j}} && \text{: Dissipation,}
\end{aligned}
$$

and

$$
\frac{D\varepsilon}{Dt} = D_\varepsilon + T_\varepsilon + \Pi_\varepsilon + P_\varepsilon^1 + P_\varepsilon^2 + P_\varepsilon^3 + P_\varepsilon^4 - \Upsilon, \tag{2.8}
$$

where

$$
\begin{aligned}
D_\varepsilon =& \nu \frac{\partial^2 \varepsilon}{\partial x_j \partial x_j} && \text{: Molecular diffusion,} \\
T_\varepsilon =& -\nu \frac{\partial}{\partial x_j}\left(\overline{u_j \frac{\partial u_i}{\partial x_m}\frac{\partial u_i}{\partial x_m}}\right) && \text{: Turbulent diffusion,} \\
\Pi_\varepsilon =& -2\nu \frac{\partial}{\partial x_j}\left[\overline{\frac{\partial (p/\rho)}{\partial x_m}\frac{\partial u_j}{\partial x_m}}\right] && \text{: Pressure diffusion,} \\
P_\varepsilon^1 =& -2\nu \overline{\frac{\partial u_i}{\partial x_j}\frac{\partial u_k}{\partial x_j}}\frac{\partial \bar{U}_i}{\partial x_k} && \text{: Mixed production,} \\
P_\varepsilon^2 =& -2\nu \overline{\frac{\partial u_i}{\partial x_k}\frac{\partial u_i}{\partial x_m}}\frac{\partial \bar{U}_k}{\partial x_m} && \text{: Production by mean velocity gradient,} \\
P_\varepsilon^3 =& -2\nu \overline{u_k \frac{\partial u_i}{\partial x_m}}\frac{\partial^2 \bar{U}_i}{\partial x_k \partial x_m} && \text{: Gradient production,} \\
P_\varepsilon^4 =& -2\nu \overline{\frac{\partial u_i}{\partial x_k}\frac{\partial u_i}{\partial x_m}\frac{\partial u_k}{\partial x_m}} && \text{: Turbulent production,} \\
\Upsilon =& 2\nu^2 \overline{\frac{\partial^2 u_i}{\partial x_k \partial x_m}\frac{\partial^2 u_i}{\partial x_k \partial x_m}} && \text{: Destruction,}
\end{aligned}
$$

where the terms T_k and Π_k in Eq. (2.7), and T_ε, Π_ε, P_ε^1, P_ε^2, P_ε^3, P_ε^4 and Υ in Eq. (2.8) are should be modelled. In general, the terms P_ε^1, P_ε^2 and P_ε^4 together with Υ is modelled as follows:

$$
P_\varepsilon^1 + P_\varepsilon^2 + P_\varepsilon^4 - \Upsilon = \frac{\varepsilon}{k}\left(C_{\varepsilon 1} P_k - C_{\varepsilon 2} f_\varepsilon \varepsilon\right). \tag{2.9}
$$

Therefore, the modelled transport-eqautions for k and ε can be written as follows:

$$\frac{Dk}{Dt} = \nu\frac{\partial^2 k}{\partial x_j \partial x_j} + T_k - \overline{u_i u_j}\frac{\partial \bar{U}_i}{\partial x_j} - \varepsilon + D, \tag{2.10}$$

$$\frac{D\varepsilon}{Dt} = \nu\frac{\partial^2 \varepsilon}{\partial x_j \partial x_j} + T_\varepsilon - \frac{\varepsilon}{k}\left(C_{\varepsilon 1}\overline{u_i u_j}\frac{\partial \bar{U}_i}{\partial x_j} + C_{\varepsilon 2} f_\varepsilon \varepsilon\right) + E, \tag{2.11}$$

where D is the additional term and E is the extra production term.

2.2 Equations for thermal field

In calculating turbulent heat transfer, we consider the following conditions in addtion to those imposed on a velocity field as described in Section 2.1:

- Within the flow, there is no heat generation due to chemical or biological reactions.
- Internal heat generation originating from the viscous dissipation is negligibly small compared with the heat input from wall surfaces.
- Temperature dependence of various flow properties is negligibly small.

Under these condition, we can deal with a thermal filed as a forced convection field. Thus, the ensemble-averaged governing equation for a thermal field can be described as follows:

$$\frac{D\bar{\Theta}}{Dt} = \frac{\partial}{\partial x_j}\left(\alpha\frac{\partial \bar{\Theta}}{\partial x_j} - \overline{u_j\theta}\right), \tag{2.12}$$

The unknown turbulent heat flux $\overline{u_j\theta}$ in Eq. (2.12) can be expressed the usage of the concept of the gradient diffusion approximation through the eddy diffusivity for heat α_t as follows:

$$\overline{u_j\theta} = -\alpha_t\frac{\partial \bar{\Theta}}{\partial x_j}, \tag{2.13}$$

$$\alpha_t = C_\lambda f_\lambda k \tau_T, \tag{2.14}$$

where τ_T denotes the characteristic time scale affected turbulence heat transfer, and is constructed generally k/ε with a function of the time-scale ratio $R = (k_\theta/\varepsilon_\theta)/(k/\varepsilon)$. The transport equations for temperature variance k_θ and its dissipation rate ε_θ can be wrtten as follows:

$$\frac{Dk_\theta}{Dt} = D_{k_\theta} + T_{k_\theta} + P_{k_\theta} - \varepsilon_\theta, \tag{2.15}$$

where

$$
\begin{aligned}
D_{k_\theta} =& \alpha \frac{\partial^2 k_\theta}{\partial x_j \partial x_j} && \text{: Molecular diffusion,} \\
T_{k_\theta} =& -\frac{\partial}{\partial x_j}\left(\overline{u_j \frac{\theta^2}{2}}\right) && \text{: Turbulent diffusion,} \\
P_{k_\theta} =& -\overline{u_j\theta}\frac{\partial \bar{\Theta}}{\partial x_j} && \text{: Production,} \\
\varepsilon_\theta =& \alpha \overline{\frac{\partial \theta}{\partial x_j}\frac{\partial \theta}{\partial x_j}} && \text{: Dissipation,}
\end{aligned}
$$

and

$$
\frac{D\varepsilon_\theta}{Dt} = D_{\varepsilon_\theta} + T_{\varepsilon_\theta} + P^1_{\varepsilon_\theta} + P^2_{\varepsilon_\theta} + P^3_{\varepsilon_\theta} + P^4_{\varepsilon_\theta} - \Upsilon_{\varepsilon_\theta}, \tag{2.16}
$$

where

$$
\begin{aligned}
D_{\varepsilon_\theta} =& \alpha \frac{\partial^2 \varepsilon_\theta}{\partial x_j \partial x_j} && \text{: Molecular diffusion,} \\
T_{\varepsilon_\theta} =& -\alpha \frac{\partial}{\partial x_j}\left(\overline{u_j \frac{\partial \theta}{\partial x_m}\frac{\partial \theta}{\partial x_m}}\right) && \text{: Turbulent diffusion,} \\
P^1_{\varepsilon_\theta} =& -2\alpha \overline{\frac{\partial u_j}{\partial x_k}\frac{\partial \theta}{\partial x_k}}\frac{\partial \bar{\Theta}}{\partial x_j} && \text{: Mixed production,} \\
P^2_{\varepsilon_\theta} =& -2\alpha \overline{\frac{\partial \theta}{\partial x_k}\frac{\partial \theta}{\partial x_j}}\frac{\partial \bar{U}_j}{\partial x_k} && \text{: Production by mean velocity gradient,} \\
P^3_{\varepsilon_\theta} =& -2\alpha \overline{u_j \frac{\partial \theta}{\partial x_k}}\frac{\partial^2 \bar{\Theta}}{\partial x_j \partial x_k} && \text{: Gradient production,} \\
P^4_{\varepsilon_\theta} =& -2\alpha \overline{\frac{\partial u_j}{\partial x_k}\frac{\partial \theta}{\partial x_k}\frac{\partial \theta}{\partial x_j}} && \text{: Turbulent production,} \\
\Upsilon_{\varepsilon_\theta} =& 2\alpha^2 \overline{\frac{\partial^2 \theta}{\partial x_k \partial x_j}\frac{\partial^2 \theta}{\partial x_k \partial x_j}} && \text{: Destruction,}
\end{aligned}
$$

where the terms T_{k_θ} in Eq. (2.15), and T_{ε_θ}, $P^1_{\varepsilon_\theta}$, $P^2_{\varepsilon_\theta}$, $P^3_{\varepsilon_\theta}$, $P^4_{\varepsilon_\theta}$ and $\Upsilon_{\varepsilon_\theta}$ in Eq. (2.16) are should be modelled. In general, the terms $P^1_{\varepsilon_\theta}$, $P^2_{\varepsilon_\theta}$ and $P^4_{\varepsilon_\theta}$ together with $\Upsilon_{\varepsilon_\theta}$ is modelled as follows:

$$
P^1_{\varepsilon_\theta} + P^2_{\varepsilon_\theta} + P^4_{\varepsilon_\theta} - \Upsilon_{\varepsilon_\theta} = \frac{\varepsilon_\theta}{k_\theta}\left(C_{P1} f_{P1} P_\theta - C_{D1} f_{D1} \varepsilon_\theta\right) + \frac{\varepsilon_\theta}{k}\left(C_{P2} f_{P2} P_k - C_{D2} f_{D2} \varepsilon\right). \tag{2.17}
$$

Therefore, the modelled transport-eqautions for k_θ and ε_θ can be written as follows:

$$
\frac{Dk_\theta}{Dt} = \alpha \frac{\partial^2 k_\theta}{\partial x_j \partial x_j} + T_{k_\theta} - \overline{u_j\theta}\frac{\partial \bar{\Theta}}{\partial x_j} - \varepsilon_\theta + D_\theta, \tag{2.18}
$$

$$
\begin{aligned}
\frac{D\varepsilon_\theta}{Dt} =& \alpha \frac{\partial^2 \varepsilon_\theta}{\partial x_j \partial x_j} + T_{\varepsilon_\theta} - \frac{\varepsilon_\theta}{k_\theta}\left(C_{P1} f_{P1} \overline{u_j\theta}\frac{\partial \bar{\Theta}}{\partial x_j} + C_{D1} f_{D1} \varepsilon_\theta\right) \\
& - \frac{\varepsilon_\theta}{k}\left(C_{P2} f_{P2} \overline{u_i u_j}\frac{\partial \bar{U}_i}{\partial x_j} + C_{D2} f_{D2} \varepsilon\right) + E_\theta,
\end{aligned} \tag{2.19}
$$

where D_θ is the additional term and E_θ is the extra production term.

2.3 Wall-limiting behaviour of turbulence

The wall-limiting behaviour of turbulence is obtained from the Taylor series expansions for fluctuating velocities and temperature in terms of x_2.

$$u_1 = a_1 + b_1 x_2 + c_1 x_2^2 + d_1 x_2^3 + \cdots , \tag{2.20}$$

$$u_2 = a_2 + b_2 x_2 + c_2 x_2^2 + d_2 x_2^3 + \cdots , \tag{2.21}$$

$$u_3 = a_3 + b_3 x_2 + c_3 x_2^2 + d_3 x_2^3 + \cdots , \tag{2.22}$$

$$\theta = \theta_w + h_1 x_2 + h_2 x_2^2 + h_3 x_2^3 + \cdots , \tag{2.23}$$

where $a_1 \sim h_3$ are the expansion coefficients of Taylor series expansions. Since the velocity components must vanish due to the non-slip condition at the wall, a_1, a_2 and a_3 are equal to zero, and considering the continuity on the wall, b_2 goes to zero in the velocity field. Therefore, the wall-limiting behaviour of turbulent quantities can be written as follows (Nagano & Tagawa 1990; Youssef *et al.* 1992):

$$\bar{U}_1 = B_1 x_2 + C_1 x_2^2 + D_1 x_2^3 + \cdots \propto x_2^1, \tag{2.24}$$

$$\bar{U}_2 = C_2 x_2^2 + D_2 x_2^3 + \cdots \propto x_2^2, \tag{2.25}$$

$$\bar{U}_3 = B_3 x_2 + C_3 x_2^2 + D_3 x_2^3 + \cdots \propto x_2^1, \tag{2.26}$$

$$\bar{\Theta} = \bar{\Theta}_w + H_1 x_2 + H_2 x_2^2 + H_3 x_2^3 + \cdots \propto x_2^0, \tag{2.27}$$

$$\overline{u_1^2} = \overline{b_1^2} x_2^2 + 2\overline{b_1 c_1} x_2^3 \cdots \propto x_2^2, \tag{2.28}$$

$$\overline{u_2^2} = \overline{c_2^2} x_2^4 + \cdots \propto x_2^4, \tag{2.29}$$

$$\overline{u_3^2} = \overline{b_3^2} x_2^2 + 2\overline{b_3 c_3} x_2^3 + \cdots \propto x_2^2, \tag{2.30}$$

$$\overline{u_1 u_2} = \overline{b_1 c_2} x_2^3 + \cdots \propto x_2^3, \tag{2.31}$$

$$\overline{u_1 u_3} = \overline{b_1 b_3} x_2^2 + \cdots \propto x_2^2, \tag{2.32}$$

$$\overline{u_2 u_3} = \overline{c_2 b_3} x_2^3 + \cdots \propto x_2^3, \tag{2.33}$$

$$k = \frac{\overline{u_1^2} + \overline{u_2^2} + \overline{u_3^2}}{2} = \frac{\overline{b_1^2} + \overline{b_3^2}}{2} x_2^2 + \left(\overline{b_1 c_1} + \overline{b_3 c_3}\right) x_2^3 + \cdots \propto x_2^2, \tag{2.34}$$

$$\varepsilon = \nu \overline{\frac{\partial u_i}{\partial x_j} \frac{\partial u_i}{\partial x_j}} = \nu \left(\overline{b_1^2} + \overline{b_3^2}\right) + 4\nu \left(\overline{b_1 c_1} + \overline{b_3 c_3}\right) x_2 + \cdots \propto x_2^0, \tag{2.35}$$

$$k_\theta = \frac{\overline{\theta^2}}{2} = \frac{\overline{\theta_w^2}}{2} + \overline{h_1 \theta_w} x_1 + \frac{\overline{h_1^2} + 2\overline{h_2 \theta_w}}{2} x^2 + \cdots \begin{cases} \propto x_2^0 & : \theta_w \neq 0 \\ \propto x_2^2 & : \theta_w = 0 \end{cases} \tag{2.36}$$

$$\varepsilon_\theta = \alpha \overline{\frac{\partial \theta}{\partial x_j} \frac{\partial \theta}{\partial x_j}} = \alpha \overline{h_1^2} + 4\alpha \overline{h_1 h_2} x_2 + \alpha \left(4\overline{h_2^2} + 6\overline{h_1 h_3}\right) x_2^2 + \cdots \propto x_2^0, \tag{2.37}$$

$$\overline{u_1 \theta} = \overline{b_1 \theta_w} x_2 + \left(\overline{b_1 h_1} + \overline{c_1 \theta_w}\right) x_2^2 + \cdots \begin{cases} \propto x_2^1 & : \theta_w \neq 0 \\ \propto x_2^2 & : \theta_w = 0 \end{cases} \tag{2.38}$$

$$\overline{u_2 \theta} = \overline{c_2 \theta_w} x_2^2 + \left(\overline{c_2 h_1} + \overline{d_2 \theta_w}\right) x_2^3 + \cdots \begin{cases} \propto x_2^2 & : \theta_w \neq 0 \\ \propto x_2^3 & : \theta_w = 0 \end{cases} \tag{2.39}$$

$$\overline{u_3 \theta} = \overline{b_3 \theta_w} x_2 + \left(\overline{b_3 h_1} + \overline{c_3 \theta_w}\right) x_2^2 + \cdots \begin{cases} \propto x_2^1 & : \theta_w \neq 0 \\ \propto x_2^2 & : \theta_w = 0 \end{cases} \tag{2.40}$$

where the coefficient $\overline{h_1 \theta_w}$ of k_θ in Eq. (2.36) vanishes for the heat-input conditions, i.e., $h_1 = 0$ $(q'_w = 0)$ with $\theta_w \neq 0$ and $\theta_w = 0$ with the constant wall-temperature condition, and the coefficient of x_2 in Eq. (2.36) becomes 0 for the equation balance. Therefore, the wall-limiting bahaviour of k_θ and ε_θ is given finally as follows:

$$k_\theta = \frac{\overline{\theta_w^2}}{2} + \frac{\overline{h_1^2} + 2\overline{h_2 \theta_w}}{2} x^2 + \cdots \begin{cases} \propto x_2^0 & : \theta_w \neq 0 \\ \propto x_2^2 & : \theta_w = 0 \end{cases} \tag{2.41}$$

$$\varepsilon_\theta = \alpha \overline{h_1^2} + \alpha \left(4\overline{h_2^2} + 6\overline{h_1 h_3}\right) x_2^2 + \cdots \propto x_2^0, \tag{2.42}$$

The wall-limiting behaviour of ν_t and α_t should be satisfied by relations between Eq. (2.4) and Eq. (2.31), and Eq. (2.13) and Eq. (2.39) as follows:

$$\nu_t \propto x_2^3 \tag{2.43}$$

$$\alpha_t \propto \begin{cases} \propto x_2^2 & : \theta_w \neq 0 \\ \propto x_2^3 & : \theta_w = 0 \end{cases} \tag{2.44}$$

The wall-limiting behaviour of the major strain-rate and vorticity tensors is described in a

fully developed two-dimensional wall shear flow as follows:

$$S_{12} = C_{S0} + C_{S1}x_2 + C_{S2}x_2^2 + \cdots \propto x_2^0, \tag{2.45}$$

$$S_{21} = S_{12} \quad , \tag{2.46}$$

$$\Omega_{12} = C_{\Omega 0} + C_{\Omega 1}x_2 + C_{\Omega 2}x_2^2 + \cdots \propto x_2^0, \tag{2.47}$$

$$\Omega_{21} = -\Omega_{12} \quad , \tag{2.48}$$

where $C_{S0} \sim C_{\Omega 2}$ are the expansion coefficients of Taylor series expansions. Since $\partial \bar{U}_2/\partial x_1\big|_w = 0$ at the wall, the relation $C_{S0} = \partial \bar{U}_1/\partial x_2\big|_w /2 = C_{\Omega 0}$ holds.

On the other hand, in the noninertial frame, if the frame is rotating with the x_3-axis, the absolute vorticity tensors W_{12} or W_{21} behave as follows:

$$W_{12} = C_{\Omega 0} + C_{\Omega 1}x_2 + C_{\Omega 2}x_2^2 + \cdots + \epsilon_{321}\Omega_3 \propto x_2^0, \tag{2.49}$$

$$W_{21} = -W_{12} \quad , \tag{2.50}$$

where Ω_3 is proportional to x_2^0, thus, the leading term of W_{12} is $C_{\Omega 0} - \Omega_3$ near the wall. Therefore, the coefficient of the wall-limiting behaviour in the terms containing the vorticity tensor in Eq. (2.6) is affected. The wall-limiting behaviour of the other turbulent quantities are identical with Eq. (2.24)–(2.46) of the inertial frame.

CHAPTER 3

Improvement of k–$\widetilde{\varepsilon}$ model for turbulent flows with pressure gradients

The low-Reynolds-number type k–ε models include: [i] the basic models of problems encountered, as represented by the models of Jones & Launder (hereinafter referred to as JL) (1973) and Nagano & Hishida (NH) (1987); [ii] improvements in the above models by Nagano & Tagawa (NT) (1990a) and Myong & Kasagi (MK) (1990) taking into account the wall limiting behaviour of velocity fluctuations; and [iii] the models in which the dissipation rate of turbulence energy profile near the wall is corrected by the recent direct numerical simulation (DNS) data, e.g., the models of Rodi & Mansour (1993), Nagano & Shimada (1995a) and Kawamura & Hada (1992).

Models mentioned in [i] were for computational expediency, in which the dissipation rate of turbulence energy is set equal to zero at a wall, and consequently the turbulence energy equation has an additional term. However, these models give no consideration to the wall limiting behaviour; thus, the models are less accurate in predicting the heat transfer in the high-Prandtl-number fluids. On the other hand, the NT and MK models in category [ii] exactly take into account the wall limiting behaviour of velocity fluctuations. The differences in each model lie in their way of expressing the contribution of small-scale eddies. The models in category [iii] reproduce the wall limiting behaviour of the dissipation rate of turbulence energy near the wall as shown by the DNS data. Compared with [i] and [ii] models, however, these model formulae are more complex. Therefore, we propose a modified k–ε turbulence model in which the dissipation rate of turbulence energy is set as zero at the wall though the wall limiting behaviour of velocity fluctuations is reproduced exactly.

In this Chapter, we propose a modified k–$\widetilde{\varepsilon}$ turbulence model in which the dissipation rate

of turbulence energy is set as zero at the wall though the wall limiting behaviour of velocity fluctuations is reproduced exactly. The model also reflects the effect of pressure gradients near the wall. The validity of the present k–$\widetilde{\varepsilon}$ model was tested by application to a channel flow and boundary layers with pressure gradients flows, and we compare the present predictions with the available experimental and DNS data.

3.1 Turblence modelling

In the JL and NH models, in order to make the dissipation rate zero at a wall, $\widetilde{\varepsilon}$ defined as $\widetilde{\varepsilon} = \varepsilon - 2\nu(\partial\sqrt{k}/\partial y)^2$ is substituted for ε in Eqs. (2.5), (2.10) and (2.11). Therefore, these models have the additional term $D = -2\nu\left(\partial\sqrt{k}/\partial y\right)^2$ in Eq. (2.10), and the near-wall limiting behaviour of $\widetilde{\varepsilon}$ can be inferred from Taylor series expansion in terms of y as follows (Nagano & Hishida 1987):

$$\widetilde{\varepsilon} = 2\nu by + O(y^2) \tag{3.1}$$

with $k = ay^2 + by^3 + O(y^4)$ and coefficients a and b independent of the y coordinate.

On the other hand, the MK and NT models do not have the additional term in Eq. (2.10), since the dissipation rate is set equal to $\nu(\partial^2 k/\partial y\partial y)$ at a wall. Hence, the wall limiting behaviour of ε near the wall becomes (Nagano an Tagawa1990a):

$$\varepsilon = 2\nu a + 6\nu by + O(y^2). \tag{3.2}$$

Near the wall, the Reynolds shear stress, $-\overline{uv}$, and the eddy viscosity, ν_t, are both proportional to y^3. Then, from Eq. (2.5), the model function f_μ has to satisfy $f_\mu \propto y^0$ with Eq. (3.1), and $f_\mu \propto y^{-1}$ with Eq. (3.2). Nagano and Tagawa (1990a) have proposed the following model function f_μ to satisfy the limiting behaviour of $-\overline{uv}$ and ν_t with Eq. (3.2).

$$f_\mu = \left[1 - \exp\left(-\frac{y^+}{A_\mu}\right)\right]^2 \left(1 + \frac{B_{\mu 1}}{{R_t}^{3/4}}\right), \tag{3.3}$$

where the model constants $A_\mu = 26$ and $B_{\mu 1} = 4.1$ and the turbulence Reynolds number R_t is defined by $k^2/\nu\varepsilon$.

Jones and Launder (1973) have suggested the model function f_μ with Eq. (3.1) as follows:

$$f_\mu = \exp\left(-\frac{2.5}{1 + R_t/50}\right), \tag{3.4}$$

where R_t is defined by $k^2/\nu\widetilde{\varepsilon}$, as a result of which the calculated Reynolds shear stress $-\overline{uv}$ satisfies the limiting behaviour $-\overline{uv} \propto y^3$. However, it is known that the JL model is less accurate in predicting wall shear flows (Nagano & Hishida 1987).

In this study, we set the dissipation rate of turbulence energy at a wall equal to zero similarly to the NH model. However, in order to satisfy the wall limiting behaviour of velocity fluctuations, we employed the following representations of ε in the eddy viscosity ν_t and the turbulent Reynolds number R_t.

$$\varepsilon = \widetilde{\varepsilon} + D = \widetilde{\varepsilon} + 2\nu \left(\frac{\partial \sqrt{k}}{\partial y} \right)^2, \quad \frac{\partial \sqrt{k}}{\partial y} \geq 0 \tag{3.5}$$

$$\nu_t = C_\mu f_\mu \frac{k^2}{(\widetilde{\varepsilon} + D)} = C_\mu f_\mu \frac{k^2}{\varepsilon}, \tag{3.6}$$

$$R_t = \frac{k^2}{\nu(\widetilde{\varepsilon} + D)} = \frac{k^2}{\nu\varepsilon}. \tag{3.7}$$

In Eq. (3.5), since the limiting behaviour of ε is consistent with Eq. (3.2), the model function f_μ has to satisfy $f_\mu \propto y^{-1}$. Therefore, we adopt the representation similar to Eq. (3.3).

It was found by Nagano *et al.* (1992) that in a flow under APG conditions, a Van Driest constant A_μ decreases with increasing P^+. Cebeci *et al.* (1970) and Launder (1981) have proposed replacing the wall shear stress with the total shear $\tau_a = \mu \left(\partial \bar{U}/\partial y \right) - \rho\overline{uv}$ in the Van Driest damping function, because the original function depends only on the wall shear stress and, thus, does not explicitly represent a change in mixing length with a pressure gradient.

In view of the above factors, we propose the following formula for f_μ:

$$f_\mu = \left[1 - \exp\left(-\frac{y^+}{A^+} \right) \right]^2 \left\{ 1 + \left(\frac{B_{\mu 1}}{R_t{}^{\frac{3}{4}}} \right) \exp\left[-\left(\frac{R_t}{B_{\mu 2}} \right)^2 \right] \right\}, \tag{3.8}$$

where $A^+ = A_\mu/\tau^+$. Near the wall, the dimensionless shear stress τ^+ is given by

$$\tau^+ = \frac{\tau_a}{\tau_w} \simeq 1 + y^+ P^+. \tag{3.9}$$

In the present model, we model τ^+ by replacing y^+ with a constant;

$$\tau^+ = 1 + 11.8 P^+. \tag{3.10}$$

The constant of 11.8 in Eq. (3.10) is consistent with that of Cebeci *et al.* (1970).

The model constants A_μ and $B_{\mu 1}$ may be determined by the following relation and DNS database (Moser *et al.* 1999). With the asymptotic expansion for $-\overline{uv}$ near the wall and f_μ

given by Eq. (3.8), we obtain

$$-\overline{uv}^{+} = \frac{-\overline{uv}}{u_\tau} \simeq C_\mu \left(\frac{B_{\mu 1}}{A^{+2}} \right) y^{+2} {R_t}^{1/4}. \tag{3.11}$$

The turbulent Reynolds number R_t is about 5×10^{-2}, and the Reynolds shear stress $-\overline{uv}^{+}$ is about 1×10^{-3} at $y^{+} \simeq 1$ from the DNS database (Moser *et al.* 1999). Thus, we let $A_\mu = 30$ and $B_{\mu 1} = 20$. The model constant $B_{\mu 2}$ is determined by numerical optimization. The other model constants and functions are the same as for the NH model (Nagano & Hishida 1987).

DNS databases (Moser *et al.* 1999; Spalart 1988) showed that the profile of ε becomes maximum at the wall, which is different from previous model predictions. In the present model, the profile of ε is not in agreement with DNS data. According to recent studies (Rodi & Monsour 1993; Nagano & Shimada 1995a; Kawamura & Hada 1992), for the near wall ε profile to conform to DNS data, some additional terms (e.g., pressure diffusion term) should be incorporated in k- and ε-equations, with the consequence that the modelling becomes more complex. However, the present study aims at constructing a turbulence model that is easily applicable to engineering calculations. Thus we retain the model formulation within the framework of categories [i] and [ii]. Note that, although the present model predictions for turbulence energy and its dissipation rate in the immediate neighborhood of the wall disagree with DNS data, this disagreement does not affect the overall performance of model predictions. Also, it should be mentioned again that $\widetilde{\varepsilon}$ is substituted for ε in Eqs. (2.5) and (2.10), and ε in Eq. (2.11) [or (3.6)] is given by Eq. (3.5). The model constants and functions are listed in Table 3.1.

Finally, the turbulent diffusion terms in Eqs (2.10) and (2.11) are given as follows:

$$T_k = \frac{\partial}{\partial x_j} \left(\frac{\nu_t}{\sigma_k} \frac{\partial k}{\partial x_j} \right), \tag{3.12}$$

$$T_\varepsilon = \frac{\partial}{\partial x_j} \left(\frac{\nu_t}{\sigma_\varepsilon} \frac{\partial \varepsilon}{\partial x_j} \right). \tag{3.13}$$

3.2 Discussion of predictions with the proposed model

3.2.1 Numerical scheme

The numerics sometimes affect the results of the turbulence models both in the algorithm chosen and in the number and distribution of grid points (Kline 1981). Therefore, special attention was paid to the numerics to enable a more meaningful model appraisal. The numerical

Table 3.1: Model constants and functions in the present model

C_μ	$C_{\varepsilon 1}$	$C_{\varepsilon 2}$	σ_k	σ_ε	f_μ	$B_{\mu 1}$	$B_{\mu 2}$
0.09	1.45	1.9	1.4	1.3	$\left[1-\exp\left(-\frac{y^+}{A^+}\right)\right]^2\left\{1+\left(\frac{B_{\mu 1}}{R_t{}^{\frac{3}{4}}}\right)\exp\left[-\left(\frac{R_t}{B_{\mu 2}}\right)^2\right]\right\}$	20	120

A^+	f_ε	D	E	f_w
$\frac{30}{1+11.8P^+}$	$1-0.3\exp\left(-{R_t}^2\right)$	$-2\nu\left(\frac{\partial\sqrt{k}}{\partial y}\right)^2$	$\nu\nu_t(1-f_w)\left(\frac{\partial^2\bar{U}}{\partial y^2}\right)^2$	$\left[1-\exp\left(-\frac{y^+}{30}\right)\right]^2$

technique used is a finite-volume method developed by Patankar (1980) and Leschziner (1982). The coordinate for regions of very large gradients should be expanded near the wall. Thus, for internal flows, a transformation is introduced so that $\eta = (y/h)^{\frac{1}{2}}$. For external flows, the following nonuniform grid (Nagano & Tagawa 1990a) across the layer is employed:

$$y_j = \Delta y_1 \frac{K^j - 1}{K - 1}, \tag{3.14}$$

where Δy_1, the length of the first step, and K, the ratio of two successive steps, are chosen as 10^{-5} and 1.03, respectively. For both internal and external flows, 201 cross-stream grid points were used to obtain grid-independent solutions. To confirm numerical accuracy, the cross-stream grid interval was cut in half for internal flow cases. No significant differences were seen in the results.

The boundary conditions are: $\bar{U} = k = \widetilde{\varepsilon} = 0$ at $y = 0$ (wall), $\partial\bar{U}/\partial y = \partial k/\partial y = \partial\widetilde{\varepsilon}/\partial y = 0$ at the axis for internal flows (symmetry); $\bar{U} = \bar{U}_e$, $k = \widetilde{\varepsilon} = 0$ at the outside boundary layer where $\bar{U}_e$ or $d\bar{P}/dx$ is prescribed from experiments.

The criterion for convergence is:

$$\frac{\max|X^{(i+1)} - X^{(i)}|}{\max|X^{(i)}|} < 10^{-5}, \tag{3.15}$$

where $X = \bar{U}$, k and $\widetilde{\varepsilon}$, and i denotes the number of iterations. The computations were performed on a PC386 personal computer and a TITAN 3000 computer.

3.2.2 Channel flow

First, we have calculated a fully developed channel flow. This test case involves the most fundamental actual flows, and often occurs in engineering-related problems.

The prediction of mean velocity profile in a channel is shown in Fig. 3.1. The result is compared with the DNS data (Moser *et al.* 1999) ($Re = \bar{U}_m h/\nu = 1.375 \times 10^4$). The proposed model predicts exactly the universal velocity profile given by the DNS data as follows:

$$\bar{U}^+ = 2.5 \ln y^+ + 5.0. \tag{3.16}$$

The prediction of Reynolds shear stress near the wall, which is the most important turbulent quantity to be calculated, is shown in Fig. 3.2. The prediction reproduces well the wall limiting behaviour $-\overline{uv}^+ \propto y^{+3}$, and agreement with the DNS data is very good.

The calculated profiles of turbulence energy k and its dissipation rate ε near the wall are shown in Figs. 3.3 and 3.4. The wall limiting behaviour of k predicted by the present model is compared with the DNS data. Although the near-wall limiting behaviour, $k^+ \propto y^{+2}$, is satisfied, there is a slight underprediction of the DNS data which may be attributed to the difference in the calculated dissipation rate very near the wall. As mentioned in section 3.1, however, this difference does not affect the overall performance of model predictions.

3.2.3 Boundary layer flows

Turbulent boundary layers with pressure gradients are particularly important in practical applications; for example, atmosphere flow, flow around an aerofoil and flow in a gas turbine.

We have calculated the boundary layer with and without pressure gradients, namely, with a zero pressure gradient (ZPG; $P^+ = 0$), with an adverse pressure gradient (APG; $P^+ > 0$), and with a favorable pressure gradient (FPG; $P^+ < 0$).

Zero pressure gradient flows

In Fig. 3.5, the prediction of mean velocity profile in the ZPG flow is presented in comparison with the experimental data of Nagano *et al.* (1992) ($R_\theta = 1620$) and the DNS data of Spalart (1988) ($R_\theta = 1410$). The present prediction is in almost perfect agreement with the

standard log-law profile:

$$\bar{U}^+ = 2.44 \ln y^+ + 5.0. \tag{3.17}$$

The prediction of Reynolds shear stress in the ZPG flow is shown in Fig. 3.6. The calculated profile of Reynolds shear stress is again in close agreement with the experimental and DNS results.

Figure 3.7 shows the profiles of turbulence energy at various Reynolds numbers based on a momentum thickness, R_θ. From comparison of the model predictions with the experimental (Nagano *et al.* 1992; Verriopoulos 1983; Klebanoff 1955) and DNS (Spalart 1988) data, it can be seen that the present model correctly reproduces the significant Reynolds-number dependence of the turbulence energy distribution.

Adverse pressure gradient flows

Predictions of flows under APG conditions are shown in Figs. 3.8–3.10, in comparison with the experimental data of Nagano *et al.* (1992). Following the proposals made by Nagano and Tagawa (1990a), calculations are performed with the aid of the algebraic stress model (ASM). The ASM used in the NT model, however, is modified for the present model by replacing ε with ε of Eq. (3.5).

We can see the change of mean velocity profiles in the APG flows with increasing R_θ in Fig. 3.8, where the experimental results and the calculated results with $A^+ \equiv 30$ in f_μ are included for comparison. Obviously, the model predictions with $A^+ = A_0^+/(1 + 11.8P^+)$ are much better than those with A^+ as a constant.

Figure 3.9 compares the predicted results with experimental data of the Reynolds shear stress in the APG flows. The proposed model reproduces well the phenomenon of increasing $-\overline{uv}^+$ in the outer region along the flow. These cannot be observed in the ZPG flow.

The predictions of turbulence energy are shown in Fig. 3.10. It can be seen that good agreement is obtained between the present predictions and the experimental data (Nagano *et al.* 1992).

Favorable pressure gradient flows

The last test case for which calculations have been performed is that for the FPG flows. This test case simulates the DNS of Spalart (1986) at the acceleration parameters $K = (\nu/\bar{U}_e^2)(d\bar{U}_e/dx) = 1.5 \times 10^{-6}$ and 2.5×10^{-6}. The results of calculations with the present model are shown in Figs. 3.11 and 3.12, where the DNS data of Spalart and the calculated results for a ZPG flow are included for comparison. Figure 3.11 shows the mean velocity profiles in FPG flows and Fig. 3.12 the Reynolds shear stress. Both predicted quantities show the character of the FPG flow, where a decrease in the Reynolds shear stress along flow laminarization is exactly predicted by the present model.

3.2.4 Calculation stability

We assess the calculation stability of the present model and the NT model which lets ε be equal to $\nu(\partial^2 k/\partial y^2)$ at a wall, with the calculation of the pipe flow at various Reynolds numbers using the initial profiles at $Re = 10000$. The results of assessment are shown in Table 3.2. The proposed model can perform stable calculation as shown in the table which includes the CPU times and the number of iterations with the present model and with the NT model. When the Reynolds number becomes higher, the expenditure of the CPU times of the present model is much smaller than of the NT model, since the wall boundary condition for the dissipation-rate equation (2.11) of the proposed model is always equal to zero, whereas that of the NT model is determined by the diffusion of turbulence energy which is dependent on the Reynolds number.

Table 3.2: Assessment of calculation stability

Initial data $Re = 10,000$(pipe flow)

	NT model		Present(HN)		time ratio
	CPU	(No.	CPU	(No.	(HN/NT)
Re	time(sec)	itera.)	time(sec)	itera.)	
2×10^4	27	(54)	24	(41)	0.889
3×10^4	26	(53)	25	(42)	0.962
4×10^4	31	(63)	25	(42)	0.806
5×10^4	34	(68)	25	(43)	0.735
1×10^5	38	(78)	25	(43)	0.658
5×10^5	40	(81)	25	(39)	0.625

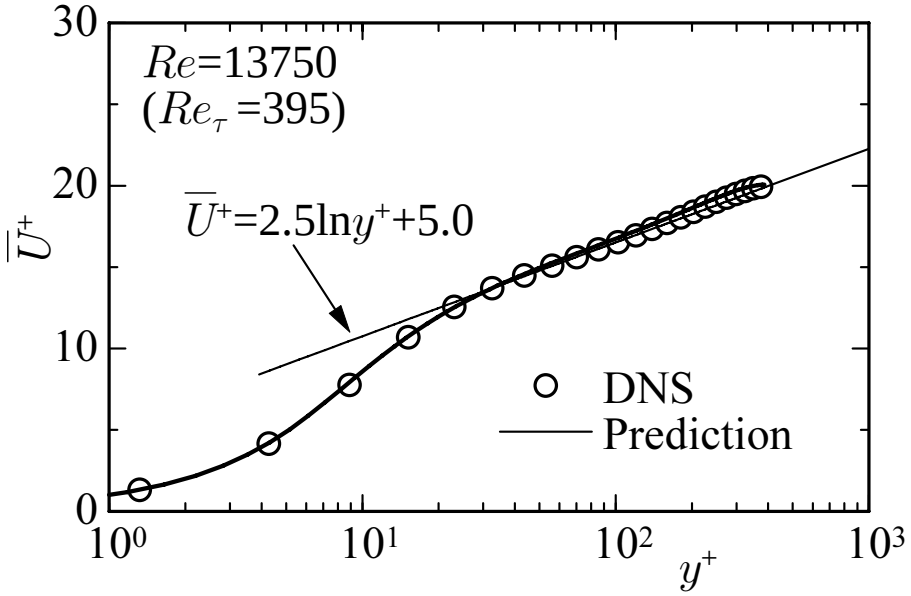

Figure 3.1: Mean velocity profile in a channel.

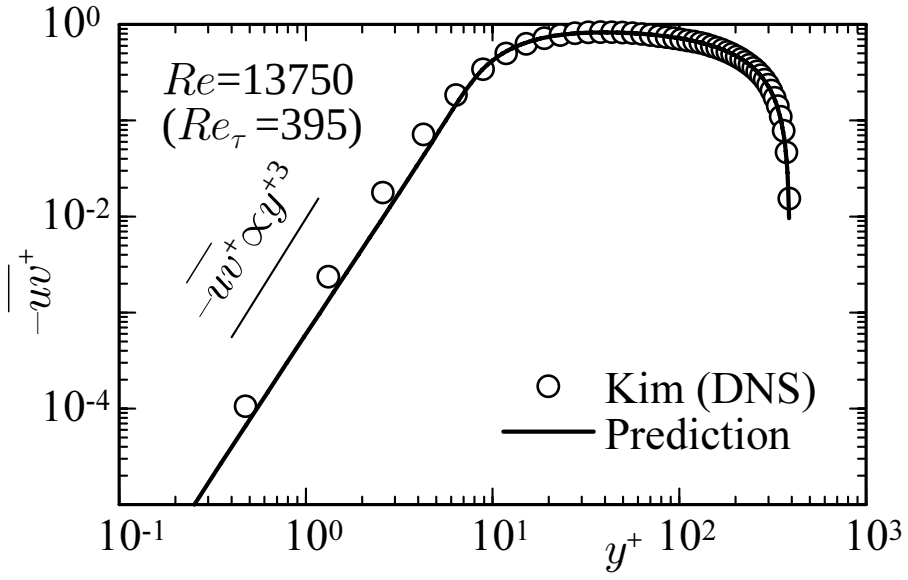

Figure 3.2: Near-wall behaviour of Reynolds shear stress.

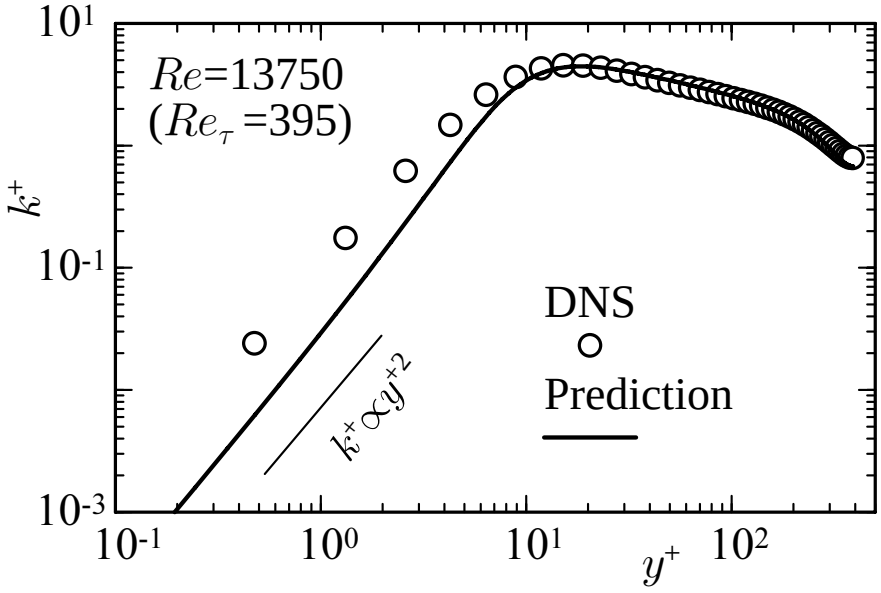

Figure 3.3: Near-wall behaviour of turbulence energy.

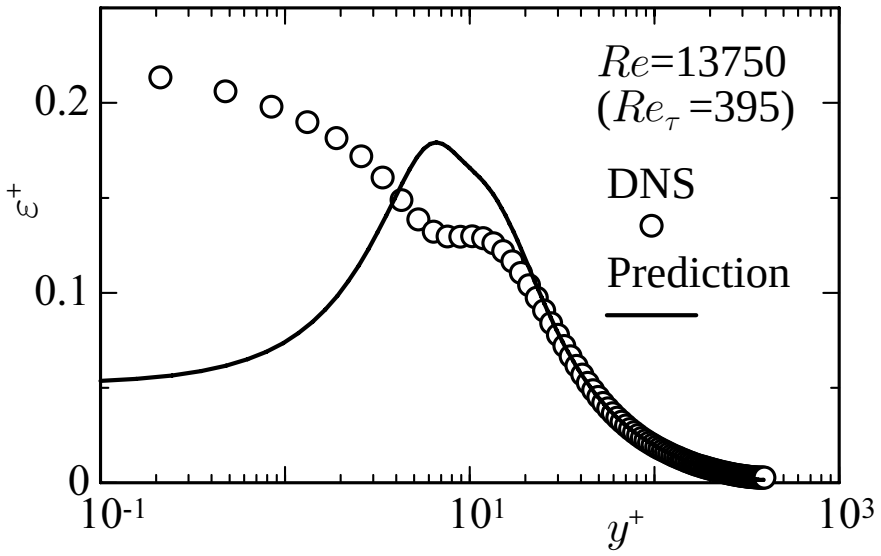

Figure 3.4: Near-wall behaviour of dissipation rate of turbulence energy.

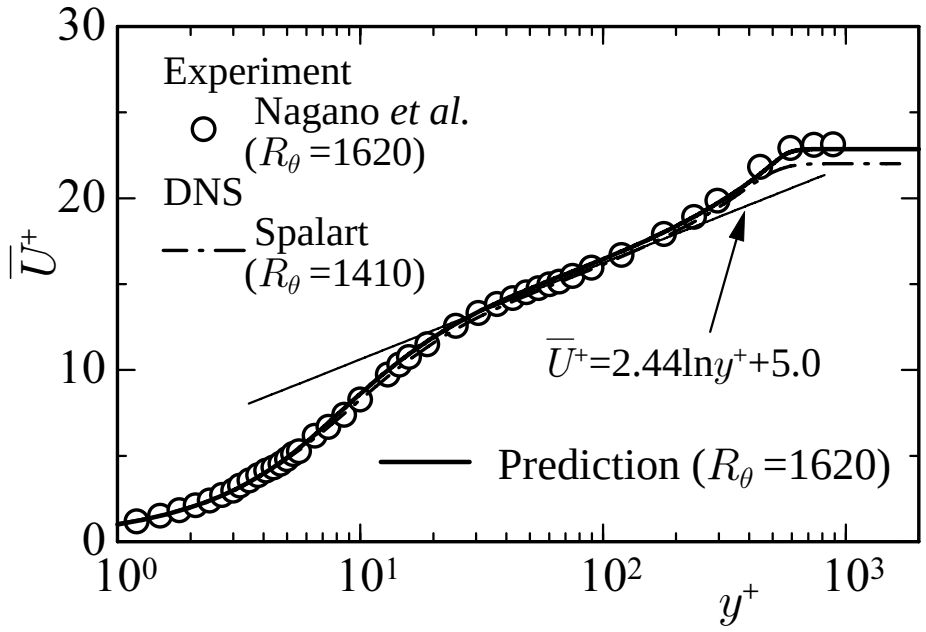

Figure 3.5: Mean velocity profile in a boundary layer.

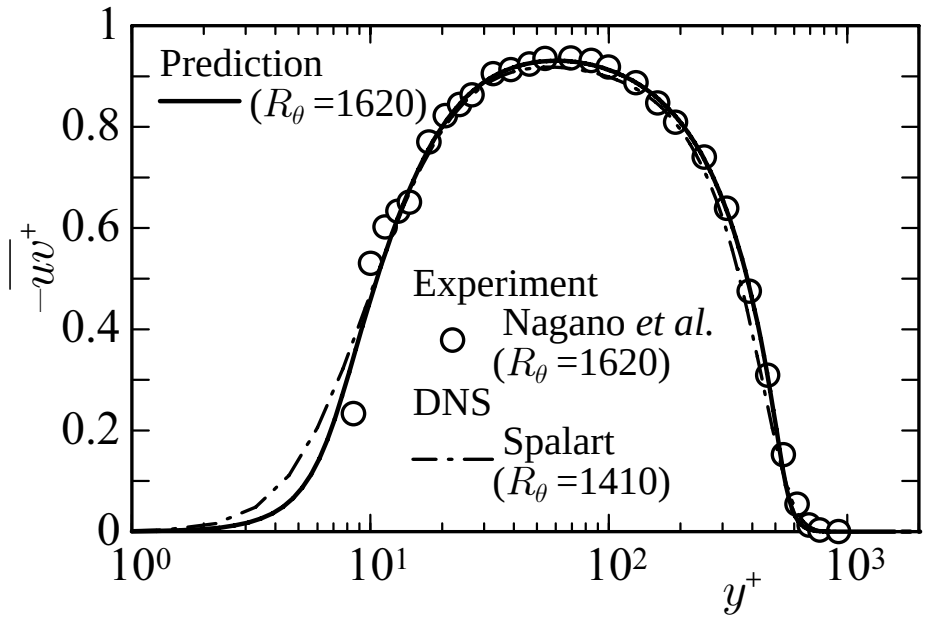

Figure 3.6: Reynolds shear stress profile in a ZPG flow.

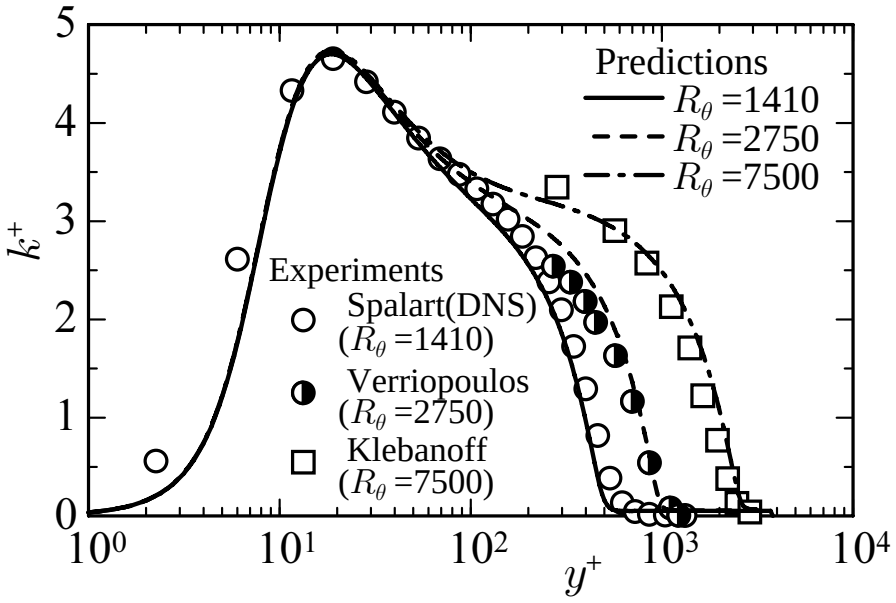

Figure 3.7: Turbulence energy profiles in boundary layers.

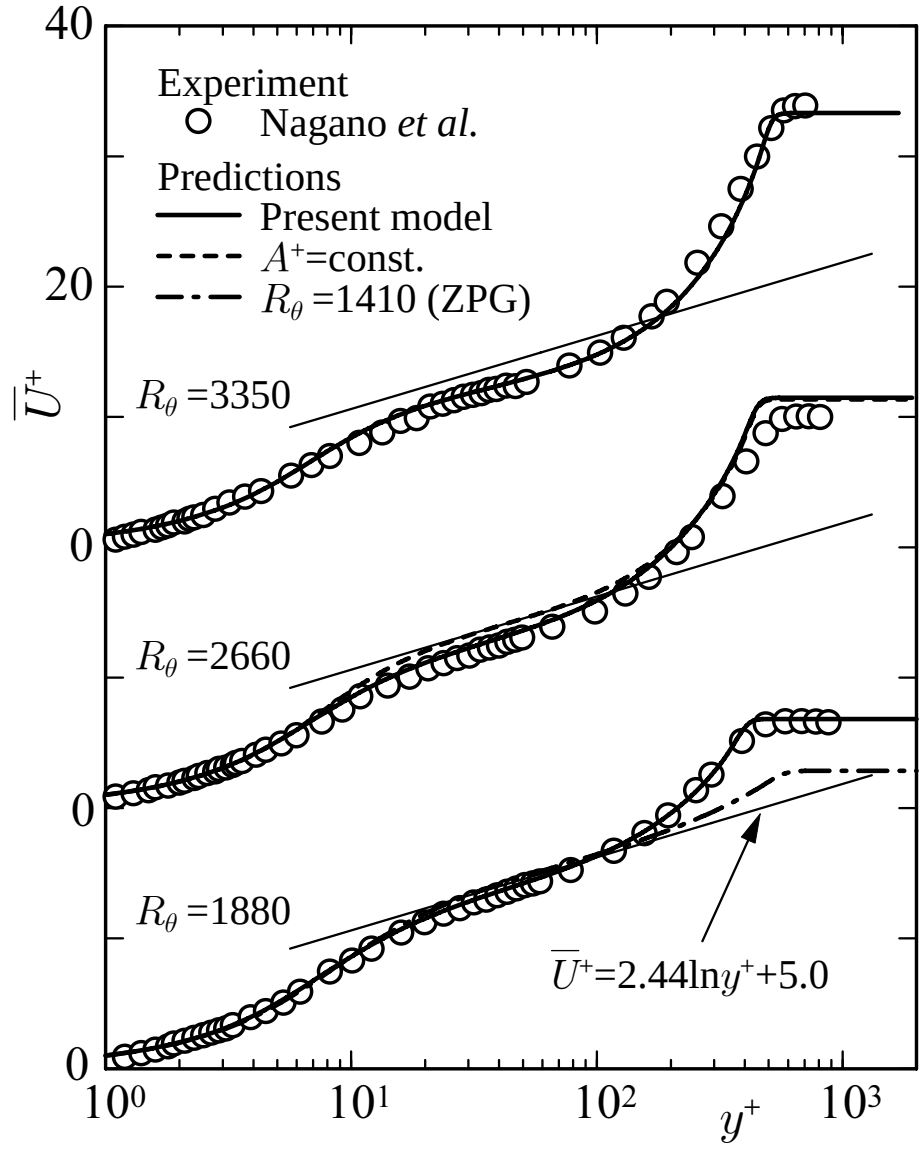

Figure 3.8: Mean velocity profiles in APG flows.

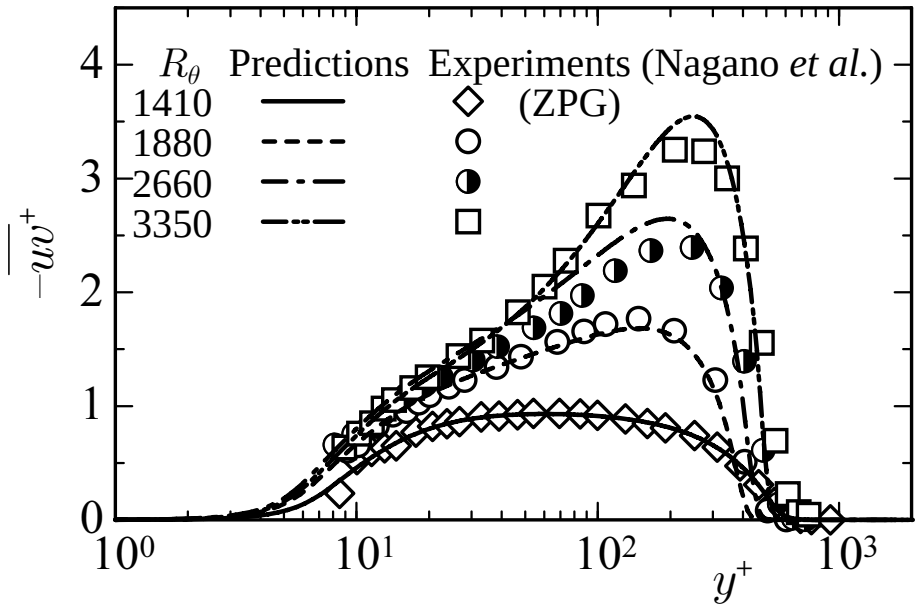

Figure 3.9: Reynolds shear stress profiles in APG flows.

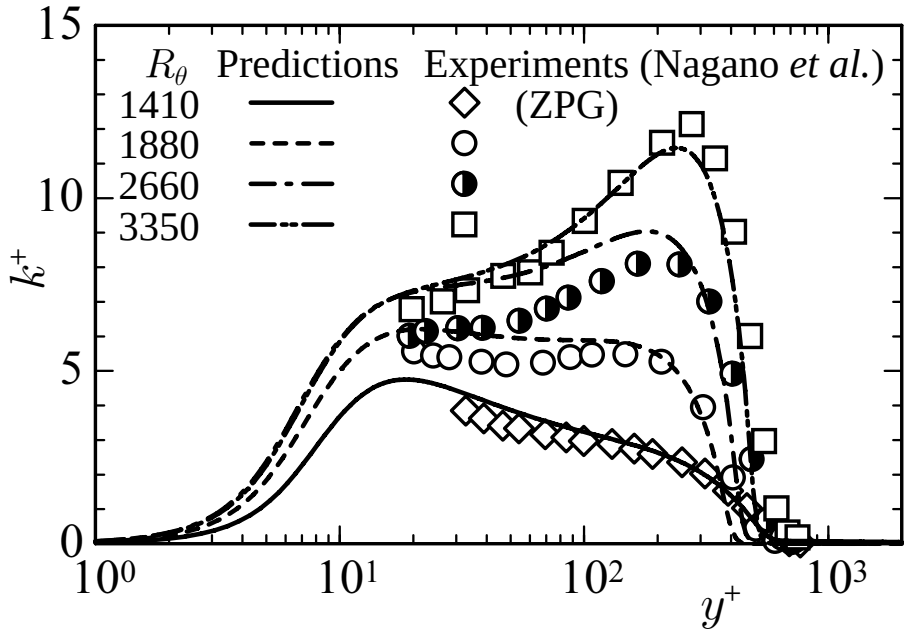

Figure 3.10: Turbulence energy profiles in APG flows.

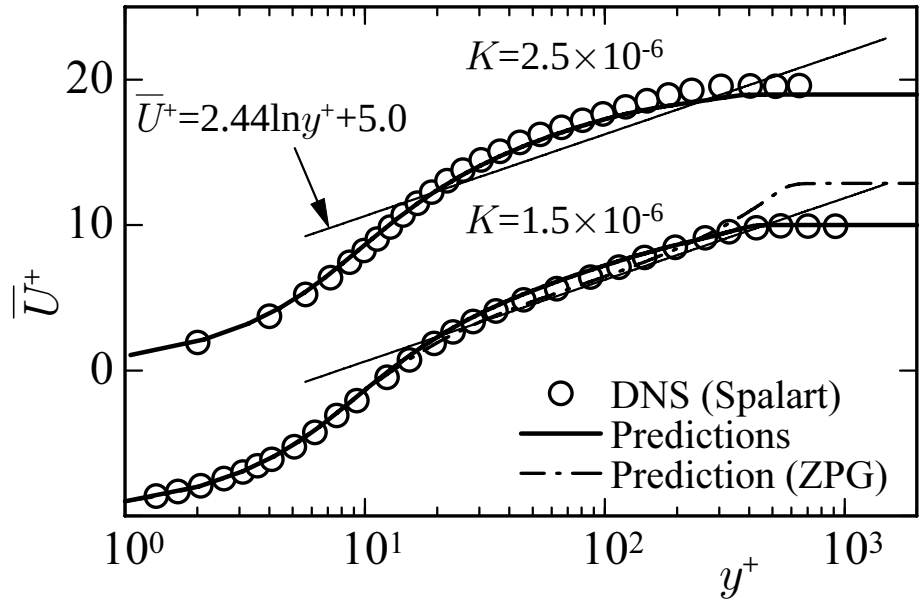

Figure 3.11: Mean velocity profiles in FPG flows.

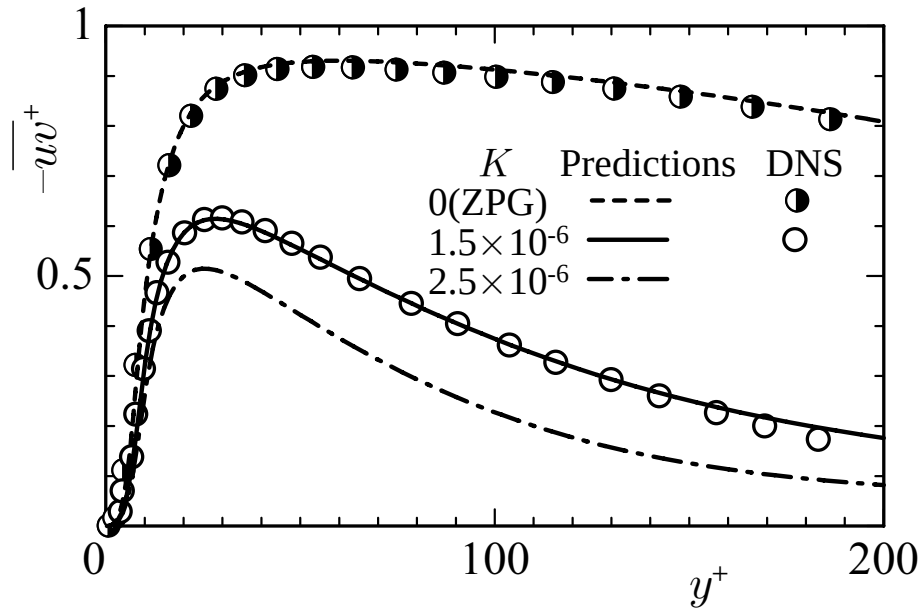

Figure 3.12: Reynolds shear stress profiles in FPG flows.

CHAPTER 4

Modeling the turbulent heat and momentum transfer in flows under different thermal conditions

In this Chapter, we propose modified two-equation models in which the apparent dissipation rates of both turbulence energy and temperature variance are set to zero at the wall though the wall limiting behaviour is reproduced exactly. The present k-ε model is a nonlinear k-ε model of Abe *et al*. (1995) type which incorporates some essential characteristics of Reynolds stress and algebraic stress models. The proposed k-ε turbulence model was tested by application to a channel flow and boundary layers with/without pressure gradients. The proposed heat-transfer model was tested in a channel flow and in turbulent boundary layers with four different wall thermal conditions; i.e., a uniform wall temperature, a uniform wall heat flux, a constant wall temperature followed by an adiabatic wall, and intermittent stepwise heat-flux input at the wall.

4.1 Modeling

4.1.1 Nonlinear k-ε model

In this Chapter, we adopt a nonlinear formulation for the k-ε model constructed by Abe *et al.*(1995b) (hereinafter referred to as the AKN model), and modify it so that we can make ε zero at the wall. This formulation includes a new type of expression for the Reynolds stress $\overline{u_i u_j}$ by introducing the explicit algebraic stress model concept (Pope 1975; Taulbee 1992; Gatski and Speziale 1993) to the nonlinear k-ε representation. The present nonlinear k-ε model is thus

described with the following equation (Abe *et al.* 1995b):

$$\begin{aligned}\overline{u_i u_j} =& \frac{2}{3}k\delta_{ij} - \frac{1}{f_R}2\nu_t S_{ij} \\ &+ \frac{4C_D}{f_R}k\tau_R^2\left[(S_{ik}\Omega_{kj} - \Omega_{ik}S_{kj}) - \left(S_{ik}S_{kj} - \frac{\delta_{ij}}{3}S_{mn}S_{mn}\right)\right],\end{aligned} \tag{4.1}$$

where $f_R = 1+(C_D\tau_R)^2\left[(22/3)\Omega^2 + (2/3)\left(\Omega^2 - S^2\right)f_B\right]$. According to Abe *et al.* (1995b), in Eq. (4.1), the parameter $(C_D\tau_R)^2(\Omega^2 - S^2)$ is one of the most important measures in turbulence since it indicates how the flow field deviates from the condition of pure shear flow. In complex flows, sometimes the normal strain rate becomes much larger than the shear strain rate, i.e., $S^2 \gg \Omega^2$. Therefore, to guarantee non-negative turbulent intensities, the model function f_B is introduced as follows:

$$f_B = 1 + C_\eta\left(\Omega^2 - S^2\right). \tag{4.2}$$

The eddy viscosity ν_t in Eq. (4.1) is expressed as

$$\nu_t = C_\mu f_\mu \frac{k^2}{\varepsilon}. \tag{4.3}$$

Note that the following time scale is employed as the characteristic time scale of turbulence:

$$\tau_R = \frac{\nu_t}{k} = C_\mu f_\mu \frac{k}{\varepsilon}, \tag{4.4}$$

where f_μ is the model function to account for the near-wall and LRN effects originating from the rigorous physical requirements.

We employ the following representation of ε in the eddy viscosity ν_t and the turbulent Reynolds number $R_t = k^2/(\nu\varepsilon)$:

$$\varepsilon = \widetilde{\varepsilon} + 2\nu\left(\frac{\partial\sqrt{k}}{\partial y}\right)^2, \quad \frac{\partial\sqrt{k}}{\partial y} \geq 0 \tag{4.5}$$

with $\widetilde{\varepsilon} \equiv 0$ at the wall ($y = 0$). Since the above representation is used, we should solve the transport equation for the pseudo-dissipation $\widetilde{\varepsilon}$. Thus, we replace ε with $\widetilde{\varepsilon}$ in Eq. (2.11). In Eq. (4.3), because the limiting behaviour of ε is $\varepsilon \propto y^0$, the model function f_μ has to satisfy $f_\mu \propto y^{-1}$, where y is the distance from wall. Therefore, we adopt the representation similar to Abe *et al.*(1995b) as follows:

$$f_\mu = \left\{1 + \frac{23}{R_t^{3/4}}\exp\left[-\left(\frac{R_t}{150}\right)^2\right]\right\}\left[1 - f_w(28)\right], \tag{4.6}$$

where $f_w(\xi)$ is the wall reflection function (Nagano and Shimada 1995a) given in the present model by

$$f_w(\xi) = \exp\left[-\left(\frac{y^*}{\xi}\right)^2\right], \tag{4.7}$$

where $y^* = u_\varepsilon y/\nu$ is the dimensionless distance from the wall based on the Kolmogorov velocity scale $u_\varepsilon = (\nu\varepsilon)^{1/4}$. It must be appropriate to discuss the argument regarding the use of the wall distance in the model functions. In this study, the wall distance at a point, y, is definitely determined by the definition as "the distance between that point and the nearest point on all the wall surfaces in a flow field" (Abe *et al.* 1995b; Abe *et al.* 1996). By following this definition, we can uniquely determine the wall distance y used in the model functions in any geometrical configuration and in any coordinate system. Even near the corner, it can be determined by considering the limit of a wall with a very small curvature. The distance between two points is not essentially harmful to the tensorial invariance, as is readily recognized by some expressions of the two-point-correlation equations and general solution of the pressure-strain correlation. Furthermore, Abe *et al.* (1995b; 1996) have confirmed that the calculations with the AKN model, in which the wall distance is uniquely determined by the above-mentioned definition, give the identical solution when the coordinate system is rotated some degrees, e.g., 45 deg, in backward-facing step flows. Thus, the use of the wall distance may not violate the tensorial invariance, so long as the wall distance is determined uniquely in the problem, e.g., the nearest distance from all the wall surface as employed in the present study[1].

An important feature of the present model functions is the introduction of the Kolmogorov velocity scale, $u_\varepsilon = (\nu\varepsilon)^{1/4}$, instead of the friction velocity u_τ. In adverse pressure gradient(APG) flows, as will be discussed in the later section, the friction velocity changes more rapidly in the streamwise direction than turbulent quantities such as Reynolds stresses. Therefore, in our previous study (Hattori *et al.* 1995) the dimensionless pressure-gradient parameter $P^+[= \nu(d\bar{P}/dx)/\rho u_\tau^3]$ was adopted in order to restrain the variation of the friction velocity, leading to reasonable predictions of the APG flows. In addition, it is elucidated in this study that model functions with y^*, i.e. u_ε, work more appropriately than those with y^+ for APG flow predictions even though we have excluded P^+ (see section 4.2.3). Abe *et al.*(1994) have also

[1]From a practical viewpoint, a further effort to develop a new model without the wall distance is now being made (Shimada and Nagano 1996).

confirmed that in backward-facing step flows, the model functions with y^* improve the prediction accuracy in the region downstream of the reattachment point, where the flow is subjected to a strong adverse pressure gradient. The above discussions, however, do not directly indicate that the Kolmogorov velocity scale is more suitable for scaling the near-wall turbulence than the friction velocity. The law of scaling the near-wall turbulence in APG flows is now investigated on the basis of the experiment of Nagano *et al.* (1992), the detail of which will be reported in an another paper.

Turbulent diffusion terms T_k and T_ε in Eqs. (2.10) and (2.11) are modeled using the generalized gradient diffusion hypothesis by Daly and Harlow(1970) as follow:

$$T_k + \Pi_k = \frac{\partial}{\partial x_j}\left(C_s f_{t1}\, \frac{\nu_t}{k}\, \overline{u_j u_\ell} \frac{\partial k}{\partial x_\ell} \right), \tag{4.8}$$

$$T_\varepsilon + \Pi_\varepsilon = \frac{\partial}{\partial x_j}\left(C_\varepsilon f_{t2}\, \frac{\nu_t}{k}\, \overline{u_j u_\ell} \frac{\partial \widetilde{\varepsilon}}{\partial x_\ell}, \right), \tag{4.9}$$

where $C_s = 1.4$ and $C_\varepsilon = 1.4$ are the model constants, and $f_{t1} = 1 + 6.0 f_w(5)$ and $f_{t2} = 1 + 5.0 f_w(5)$ are the model functions activating in the vicinity of the wall. Other model constants are assigned the same value as those in the AKN model, i.e., $C_\mu = 0.12$, $C_D = 0.8$, $C_\eta = 5.0$, $C_{\varepsilon 1} = 1.45$ and $C_{\varepsilon 2} = 1.9$, respectively. For f_ε, we adopt the conventional model function: $f_\varepsilon = 1 - 0.3\exp[-(R_t/6.5)^2]$; and the extra production term E in Eq. (2.11) is $E = 0.01 f_w(28)\nu(k/\widetilde{\varepsilon})\overline{u_\ell u_k}\left(\partial^2 \bar{U}_i/\partial x_\ell \partial x_k\right)\left(\partial^2 \bar{U}_i/\partial x_j \partial x_k\right)$.

4.1.2 Two-equation heat transfer model

Main issue in improving a two-equation heat transfer model is to obtain a simplified form satisfying the wall limiting behaviour. Under the nonuniform wall temperature conditions, k_θ is generally not null at the wall, and the pseudo-dissipation rate $\widetilde{\varepsilon}_\theta = \varepsilon_\theta - 2\alpha(\partial\sqrt{k_\theta}/\partial y)^2$ in the NK model cannot be applied as it is. Thus, we propose a new expression for ε_θ, with reference to Youssef *et al.*(1992):

$$\varepsilon_\theta = \widetilde{\varepsilon}_\theta + 2\alpha\left(\frac{\partial\sqrt{\Delta k_\theta}}{\partial y}\right)^2, \quad \frac{\partial\sqrt{\Delta k_\theta}}{\partial y} \geq 0, \tag{4.10}$$

where $\Delta k_\theta = k_\theta(x,y,z) - k_\theta(x,0,z) = k_\theta - k_{\theta w}$. With a Taylor series expansion of θ near the wall, i.e., $\theta = \theta_w + b_1 y + b_2 y^2 + O(y^3)$, we obtain that the wall limiting behaviour of ε_θ is

$\alpha\overline{b_1^2} + O(y)$ for $t_w = 0$ and $2\alpha\overline{b_2 t_w} + O(y)$ for $\theta_w \neq 0$ (see Youssef *et al.*1992). It can be readily seen that Eq. (4.10) satisfies this requirement since $\widetilde{\varepsilon}_\theta = 0$ at the wall.

The turbulent diffusivity for heat can be written as

$$\alpha_t = C_\lambda f_\lambda k \tau_m, \tag{4.11}$$

where $C_\lambda = 0.1$ is the model constant, τ_m is the hybrid (mixed) time scale proposed by Nagano and Kim(1988) and f_λ is the wall reflection function.

In the present model, using ε in Eq. (4.5) and ε_θ in Eq. (4.10), we write τ_m with reference to some recent studies(Abe *et al.* 1995a; Shikazono & Kasagi 1996) as follows:

$$\tau_m = \frac{k}{\varepsilon}\left\{\frac{2R}{0.5+R} + \left(\frac{23\sqrt{2R}/Pr^{\frac{4}{3}}}{R_t^{\frac{3}{4}}}\right)\exp\left[-\left(\frac{R_t}{150}\right)^2\right]\right\}, \tag{4.12}$$

where $R = (k_\theta/\varepsilon_\theta)/(k/\varepsilon)$ is the time-scale ratio with ε and ε_θ defined by Eqs. (4.5) and (4.10). The following wall reflection function f_λ is adopted on the basis of the discussion by Cebeci(1973):

$$f_\lambda = \left[1 - f_w(A)\right]^{\frac{1}{2}}\left[1 - f_w(B)\right]^{\frac{1}{2}}, \tag{4.13}$$

where the constants A and B are set to $A = 26$ and $B = A/Pr^{\frac{1}{3}}$. Turbulent diffusion terms T_{k_θ} and T_{ε_θ} should be modeled. We adopt gradient-type diffusion modeling, and write T_{k_θ} and T_{ε_θ} as

$$T_{k_\theta} = \frac{\partial}{\partial x_j}\left[f_{t3}\left(\frac{\alpha_t}{\sigma_h}\right)\frac{\partial k_\theta}{\partial x_j}\right], \tag{4.14}$$

$$T_{\varepsilon_\theta} = \frac{\partial}{\partial x_j}\left[f_{t4}\left(\frac{\alpha_t}{\sigma_\phi}\right)\frac{\partial \widetilde{\varepsilon}_\theta}{\partial x_j}\right], \tag{4.15}$$

where $\sigma_h = 1.4$ and $\sigma_\phi = 1.0$ are the model constants for diffusion, $f_{t3} = 1 + 9.0 f_w(5)$ and $f_{t4} = 1 + 1.0 f_w(5)$ are the model functions activating in the neighborhood of the wall. Other model constants and functions in the present k_θ–ε_θ model are assigned the standard values: $C_{P1} = 0.85$, $C_{P2} = 0.64$, $C_{D1} = 1.0$, $C_{D2} = 0.9$, $f_{D1} = f_{P1} = f_{P2} = 1.0$ and $f_{D2} = (1/C_{D2})(C_{\varepsilon 2} f_\varepsilon - 1)$. The extra production term E_θ has a form similar to the NK model: $E_\theta = \alpha\alpha_t f_w(26)\left(\partial\bar{\Theta}/\partial x_j \partial x_k\right)^2$.

4.2 Discussion on predictions with the proposed models

To assess the performance of the present $k-\varepsilon$ and k_θ–ε_θ models, several representative test cases are calculated. The numerical technique used are a finite-volume method in the wall-bounded flows and a Runge-Kutta method in the homogeneous shear flow. Full details of the present numerical method of solution are given in Hattori and Nagano(1995) and Abe *et al.*(1995b; 1996). The computations were performed on an SGI Indigo 2 computer.

4.2.1 Rotating homogeneous shear flow

In this study, we propose a new model formulation including the invariants of not only the strain rate but also the vorticity tensor. It is highly expected that this new formulation gives more reasonable predictions for a flow field where there exist considerable differences between the strain rate and the vorticity tensor. Thus, we first applied the proposed model to the rotating homogeneous shear flow, which is a typical test case to evaluate the model performance in the above-mentioned flow field.

In the rotating homogeneous shear flow, the most important phenomenon which a turbulence model should reproduce is the "bifurcation" as follows:

- Unsteady (developing with time) solutions are obtained under the condition of $0 \leq \Omega/S \leq 0.5$.
- Steady (decaying with time) solutions are obtained under the condition of $\Omega/S \ll 0$ and $\Omega/S \gg 0.5$.

Note that S is the shear rate and Ω is the frame-rotating speed. The present model is applicable to the rotating homogeneous shear flow just by defining the non-dimensional vorticity tensor Ω^*_{ij} as follows:

$$\Omega^*_{ij} = 2C_D\tau\left(W_{ij} - 1.2\epsilon_{ijk}\Omega_k\right), \qquad W_{ij} = \Omega_{ij} - \epsilon_{ijk}\Omega_k, \tag{4.16}$$

where Ω_k is the angular-velocity vector of the frame rotation, i.e., $\Omega = |\Omega_k|$. If $\Omega_k = 0$, the above expression completely coincides with that in the inertial frame. This model extension follows the discussion by Gatski and Speziale (1993).

The "bifurcation diagram" for the rotating homogeneous shear flow, which is the variation of the equilibrium values of ε/kS versus Ω/S, is shown in Fig. 4.1. The computational results

obtained by the standard k–ε model and the GS model (Gatski and Speziale, 1993) are also included for comparison. From Fig. 4.1, we can readily see that the present and the GS model sufficiently predict the above-mentioned bifurcation phenomenon, whereas the standard k–ε model evidently fails to predict it. This is a definite advantage.

4.2.2 Channel flow

We have calculated a fully developed channel flow. This test case is the most fundamental in actual flows, and often occurs in engineering relevant problems.

Figures 4.2–4.5 show the present results of the channel flow calculated under both the DNS conditions of Moser *et al.* (1999) ($\mathrm{Re}_\tau = u_\tau \delta/\nu = 395$) and of Kasagi *et al.*(1992) ($\mathrm{Re}_\tau = 150$). From Figs. 4.2, 4.3 and 4.4, it can be seen that the mean velocity, Reynolds shear stress and turbulence energy are quite successfully predicted for both cases. Figure 4.5 shows all the terms of the turbulence energy budget. The predicted dissipation and molecular diffusion terms give the profiles slightly different from the DNS very near the wall ($y^+ < 3$). It seems, however, that this difference does not affect the overall performance of model predictions.

Next, we perform the model assessment in a fully developed channel flow with heat transfer, for which trustworthy DNS database(Kasagi *et al.* 1992) ($\mathrm{Re}_\tau = 150$ and Pr=0.71) is available. Comparisons of the predicted mean temperature and temperature variance with DNS is shown in Fig. 4.6. The model predictions are in almost perfect agreement with the DNS data. Figure 4.7 shows the predicted budget of temperature variance, compared with the DNS data. Obviously, agreement of each term with DNS is also very good.

4.2.3 Boundary layer flows with and without pressure gradients

We have calculated boundary layers with/without pressure gradients, i.e., with a zero pressure gradient (ZPG; $d\bar{P}/dx = 0$), with an adverse pressure gradient (APG; $d\bar{P}/dx > 0$) and with a favorable pressure gradient (FPG; $d\bar{P}/dx < 0$). In Fig. 4.8, the prediction of mean velocity profile in the ZPG flow is presented in comparison with the experimental data of Nagano *et al.*(1992) ($R_\theta = 1620$) and the DNS data of Spalart(1988) ($R_\theta = 1410$). Again, the present predictions are in almost perfect agreement with the experiment, the DNS and the standard log-law profile: $\bar{U}^+ = 2.44 \ln y^+ + 5.0$.

Predictions of flows under different pressure-gradient conditions are shown in Figs. 4.9–4.11, in comparison with the experimental data of Nagano *et al.*(1992) (APG, ZPG) and with the DNS data of Spalart(1986) (FPG). Note that including the additional production of ε due to irrotational strains is significant in calculating APG flows (Hanjalić and Launder 1980; Hanjalić 1994; Nagano and Tagawa 1990a; Hattori and Nagano 1995) as:

$$\frac{\mathrm{D}\widetilde{\varepsilon}}{\mathrm{D}\tau} = D_\varepsilon + T_\varepsilon + \Pi_\varepsilon - C_{\varepsilon 1}\frac{\widetilde{\varepsilon}}{k}\overline{uv}\frac{\partial \bar{U}}{\partial y} - C'_{\varepsilon 1}\frac{\widetilde{\varepsilon}}{k}\left(\overline{u^2} - \overline{v^2}\right)\frac{\partial \bar{U}}{\partial x} - C_{\varepsilon 2}f_\varepsilon\frac{\widetilde{\varepsilon}^2}{k} + E. \tag{4.17}$$

Here, the velocity fluctuation components $\overline{u^2}$ and $\overline{v^2}$ are calculated by the present nonlinear k-ε model, and the model constant of $C'_{\varepsilon 1} = 2.5C_{\varepsilon 1}$ is given as in the NT model. Figure 4.9 shows the mean velocity profiles. Obviously, the present model works very satisfactorily in flows with a variety of pressure gradients.

Figure 4.10 compares the predicted results with the experimental and DNS data of Reynolds shear stresses in APG, FPG and ZPG flows . The proposed model reproduces well the phenomena of increasing $-\overline{uv}^+$ in the outer region along the flow on APG and decreasing one on FPG. These cannot be observed in the ZPG flow.

The predictions of turbulence energy are shown in Fig. 4.11. Again, it can be seen that good accordance with the experimental data(Nagano *et al.* 1992) is achieved.

4.2.4 Heat transfer from uniform temperature or uniform heat-flux wall

In the following, we assess the present two-equation heat transfer model in boundary layer flows. The most basic situations encountered in engineering applications are the heat transfer from a uniform temperature or uniform heat-flux wall. The results of thermal-field calculations under the constant wall temperature or the constant wall heat-flux condition along a flat plate, are shown in Fig. 4.12. The present predictions indicate good agreement with the experimental data(Gibson *et al.* 1982; Antonia *et al.* 1977).

4.2.5 Stepwise change in wall temperature

To further verify the effectiveness of the present model for calculating various kinds of turbulent thermal fields, the predictions of mean temperature profiles for a constant wall temperature ($\bar{\Theta}_w = \bar{\Theta}_e + 16°\mathrm{C}$) followed by another constant wall temperature ($\bar{\Theta}_w = \bar{\Theta}_e$) are

shown in Fig. 4.13. Also, included for comparison are the experimental data of Charnay *et al.* (1979) and the calculations of Browne and Antonia (1981) at the same streamwise location. Note that the model for the velocity field proposed in Chapter 3 is used here.

The present model gives a little overpredictions, though the overall predictions are much better than those of Browne and Antonia. This is mainly due to difficulties of reproducing the initial conditions, as experienced by Browne and Antonia (1981).

The predictions of the rms temperature fluctuations $\sqrt{\overline{k_\theta}}/(\bar{\Theta}_{ws}-\bar{\Theta}_e)$ are shown in Fig. 4.14. Again, owing to the same reason mentioned above, the predictions give a little overpredictions.

4.2.6 Constant wall temperature followed by adiabatic wall

The next test case for which calculations have been performed is concerned with a more complex thermal field in a boundary layer along a uniformly heated wall followed by an adiabatic wall. This case is of interest in the de-icing of aircraft wings. The same situations also occur frequently in compact heat exchangers. Figure 4.15 shows a comparison of the predicted results with the experimental data(Reynolds *et al.* 1958) of temperature differences between the wall and the free-stream $\Delta\bar{\Theta}$. The proposed model gives generally good predictions for the rapidly changing thermal field.

4.2.7 Double-pulse heat input

To further verify the effectiveness of the present model for calculating various kinds of turbulent thermal fields, comparison of the predicted variation of wall temperature ($\Delta\bar{\Theta}_w = \bar{\Theta}_w - \bar{\Theta}_e$; $\bar{\Theta}_w$ and $\bar{\Theta}_e$ being the wall and free-stream temperatures) with the measurement (Reynolds *et al.* 1958) for double-pulse heat input case is shown in Fig. 4.16. Figure 4.17 shows how a wall turbulent thermal layer changes when heat input is intermittent, in which $\Delta\Theta = \bar{\Theta} - \bar{\Theta}_e$ is normalized by the temperature difference between the wall and free-stream $\Delta\bar{\Theta}_0 = \bar{\Theta}_{w0} - \bar{\Theta}_e$ just before the first heat-input/cut-off point. It can be seen that very abrupt decrease and increase in mean fluid-temperature occur in the wall region, which is the consequence of no heat-input condition followed by heat input, i.e., $\partial\bar{\Theta}/\partial y|_w = 0 \rightarrow \partial\bar{\Theta}/\partial y|_w =$ constant. Within a short distance from the discontinuity point, the mean temperature profile becomes uniform over most of the thermal layer. Also, variations of the temperature variance are shown in Fig. 4.18. It

can been seen that the temperature fluctuations are growing along the thermal boundary layer, then sudden heat cut-off at the wall makes the temperature variance decrease close to the wall. This phenomenon agrees with the experimental evidence obtained by Subramanian and Antonia (1981a).

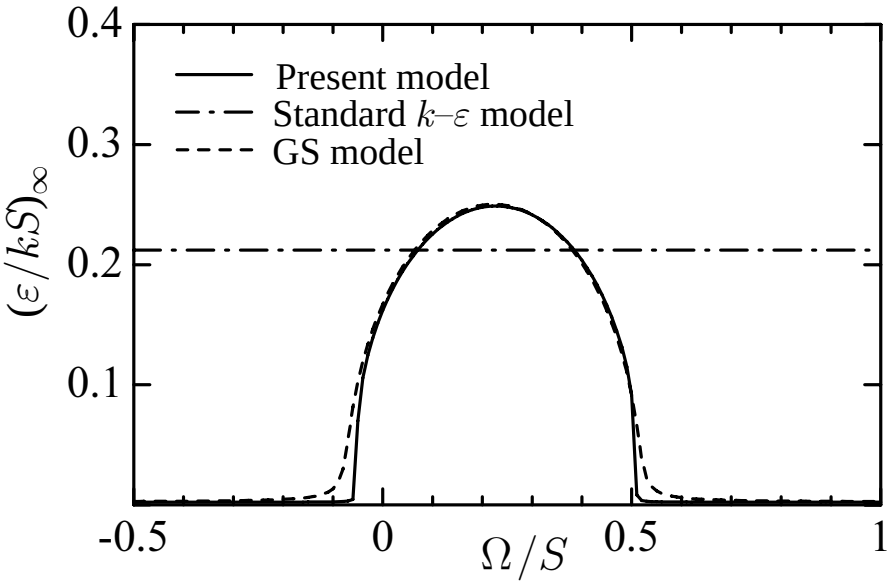

Figure 4.1: Bifurcation diagram for rotating homogeneous shear flow

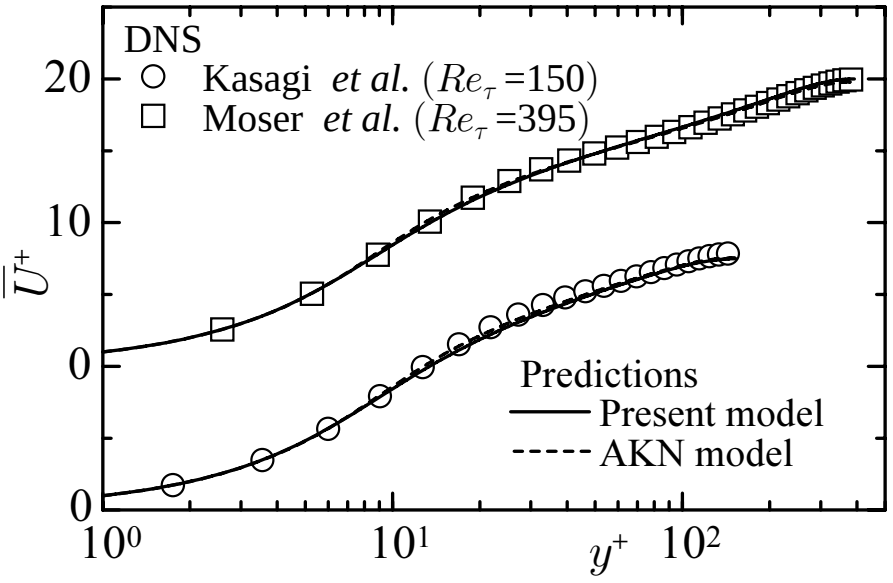

Figure 4.2: Profiles of mean velocity in a channel

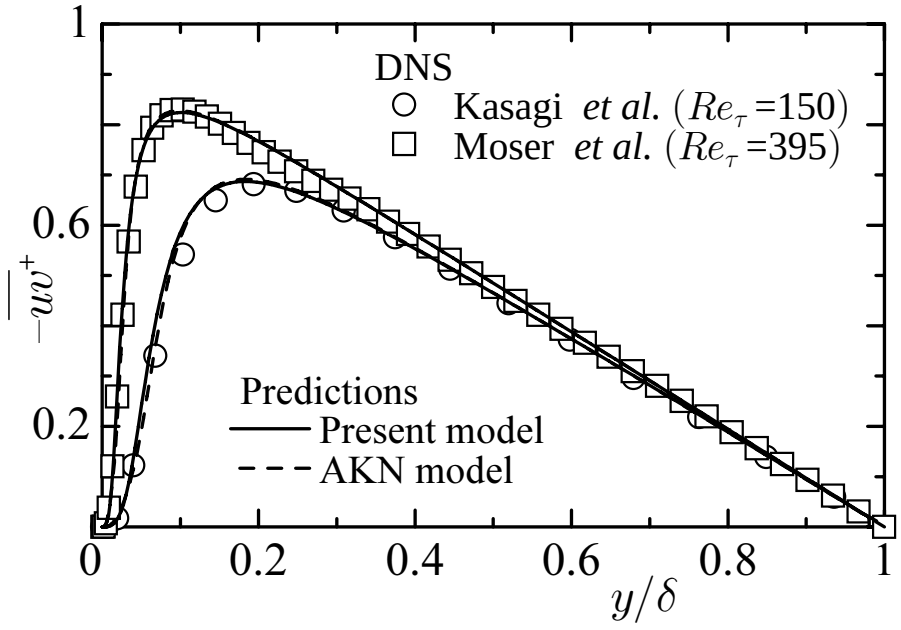

(a)

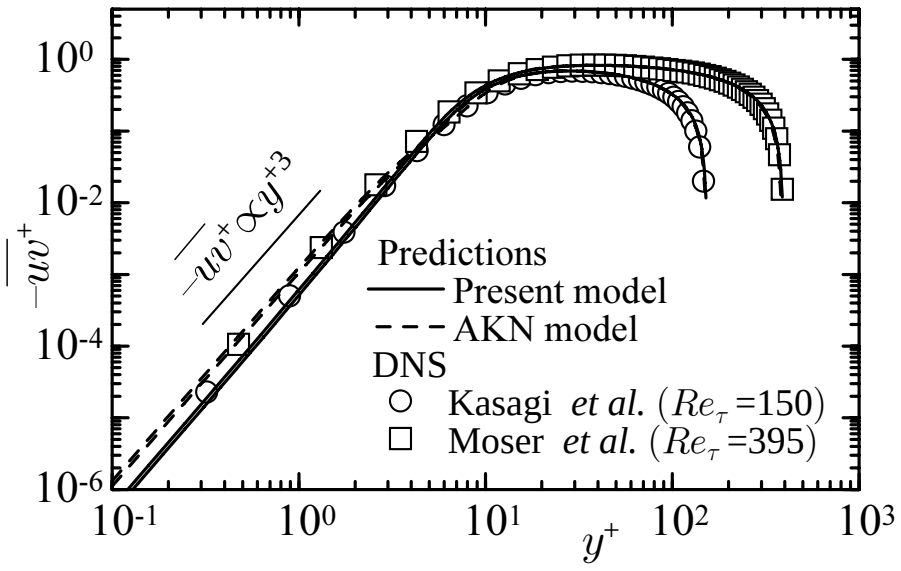

(b)

Figure 4.3: Profiles of Reynolds shear stress in a channel: (a) overall (b) wall-limiting behaviour

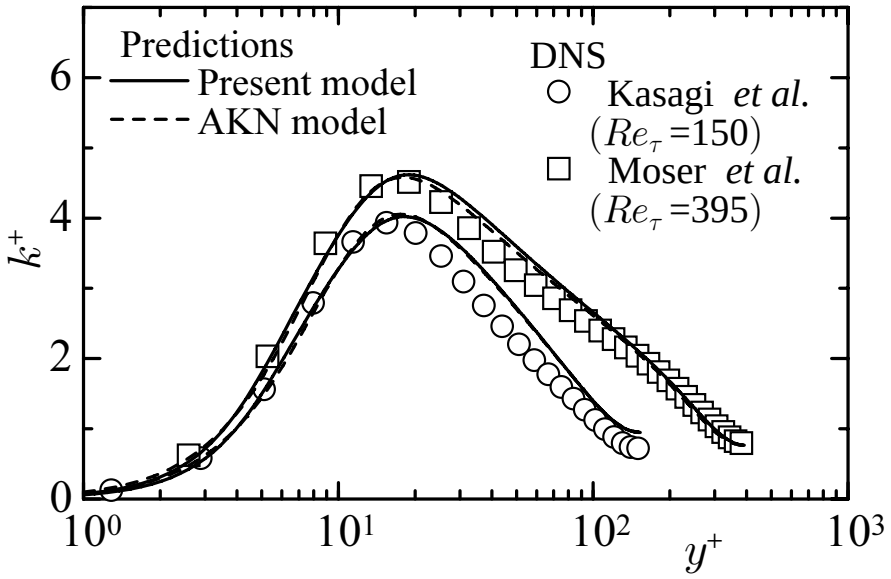

Figure 4.4: Profiles of turbulence energy in a channel

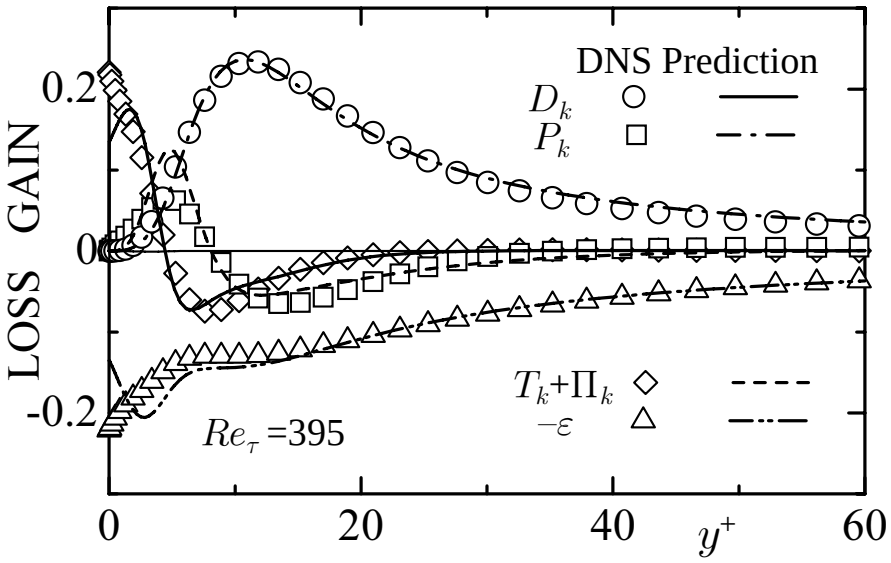

Figure 4.5: Budget of turbulence energy in channel flow

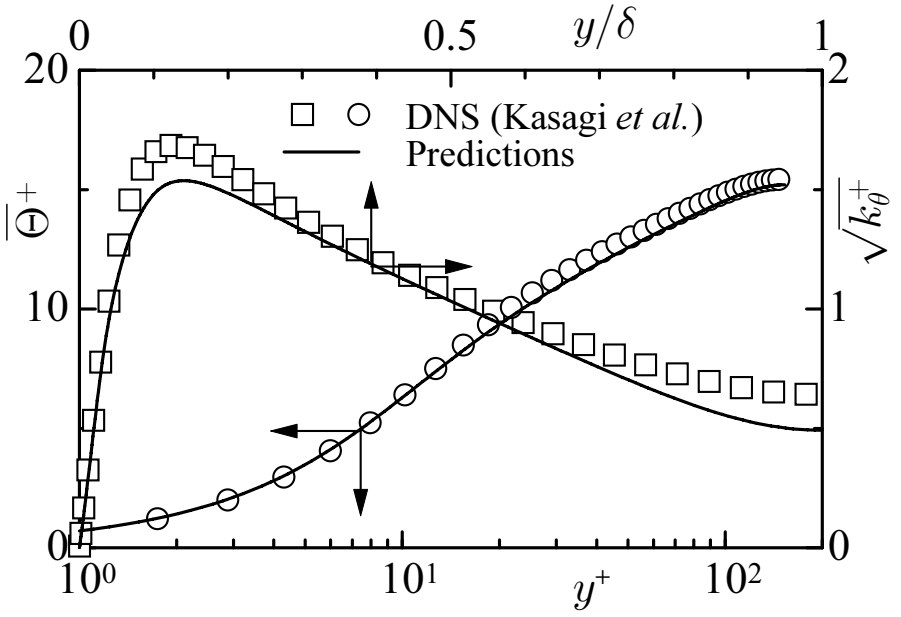

Figure 4.6: Profiles of mean temperature and temperature variance in a channel

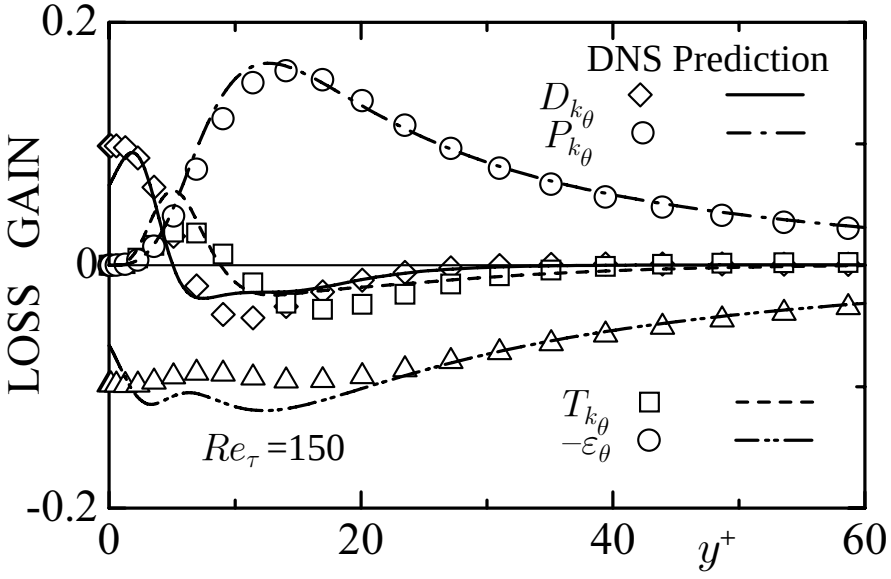

Figure 4.7: Budget of temperature variance in channel flow

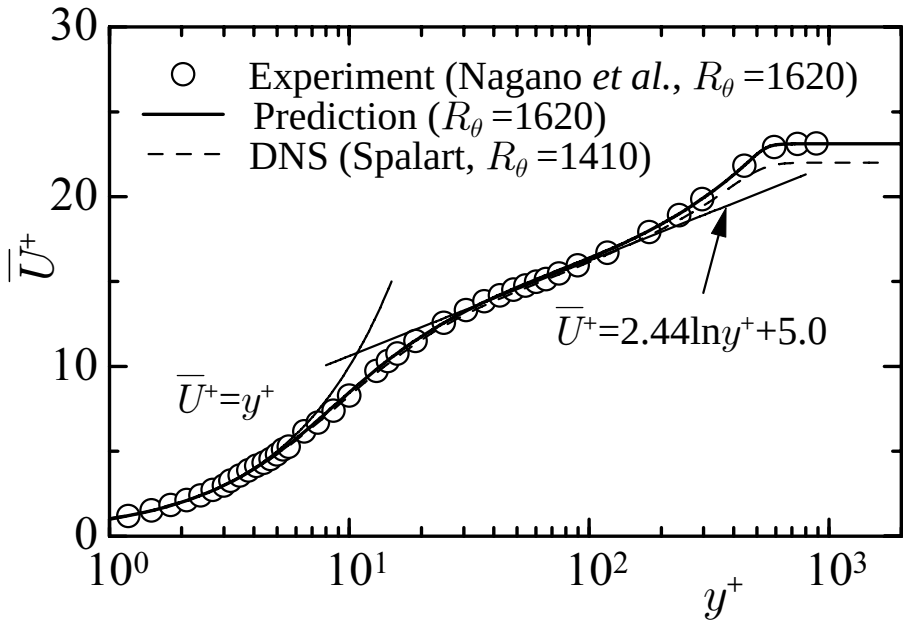

Figure 4.8: Mean Velocity profiles in boundary-layer flow $(d\bar{P}/dx = 0)$

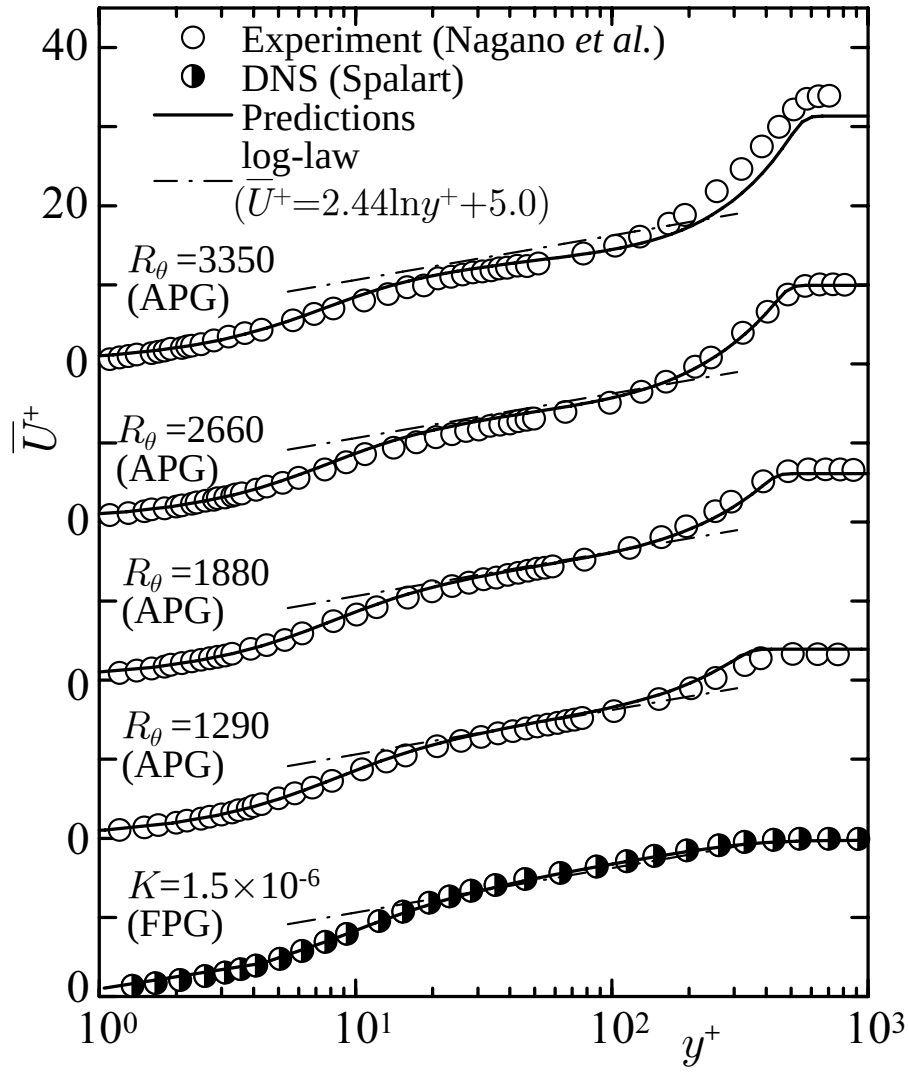

Figure 4.9: Mean velocity profiles in flows with various pressure gradients

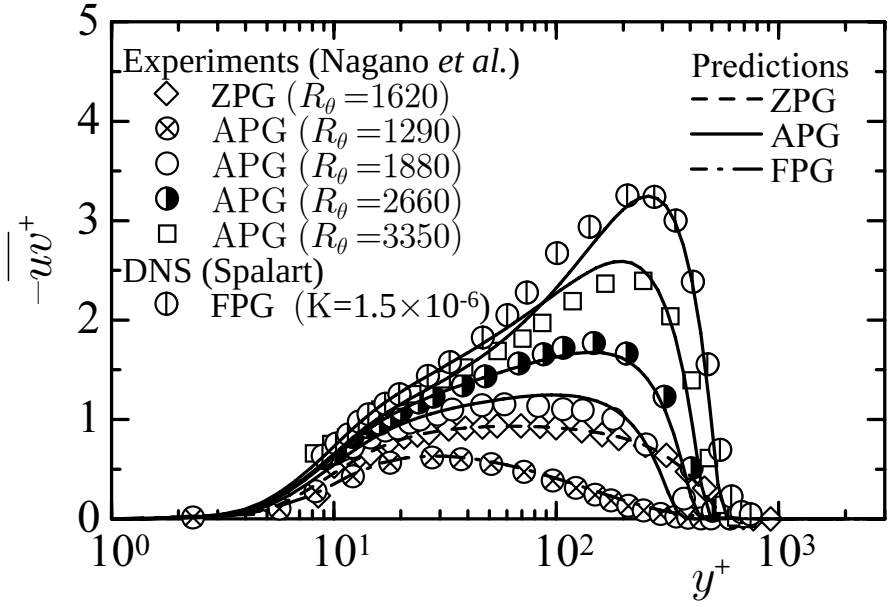

Figure 4.10: Profiles of Reynolds shear stresses in flows with various pressure gradients

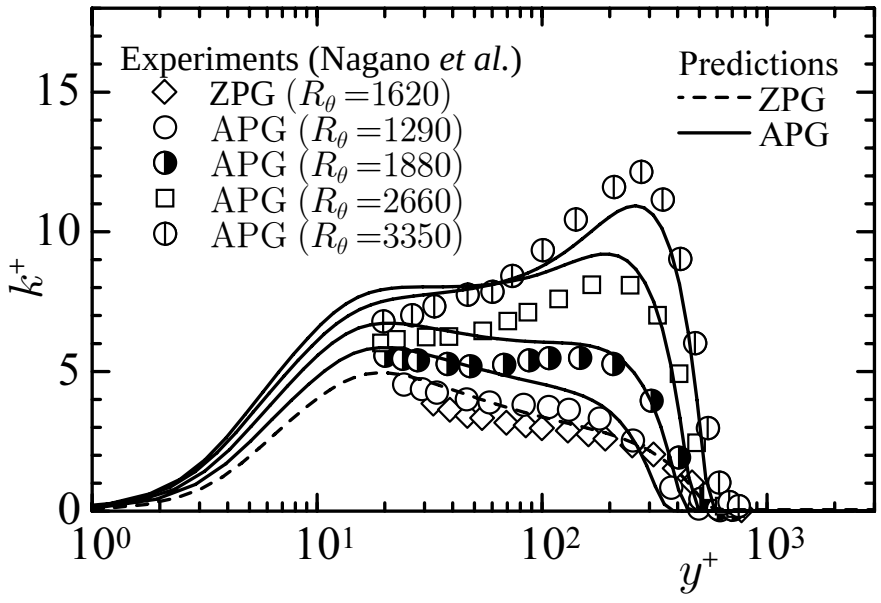

Figure 4.11: Profiles of turbulence energy in flows with various pressure gradients

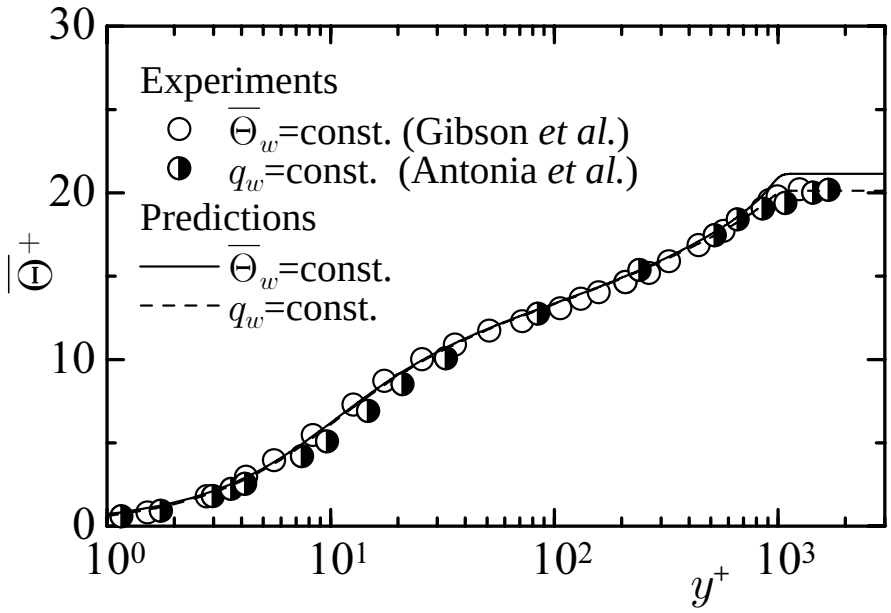

Figure 4.12: Mean temperature profiles in boundary layer flows

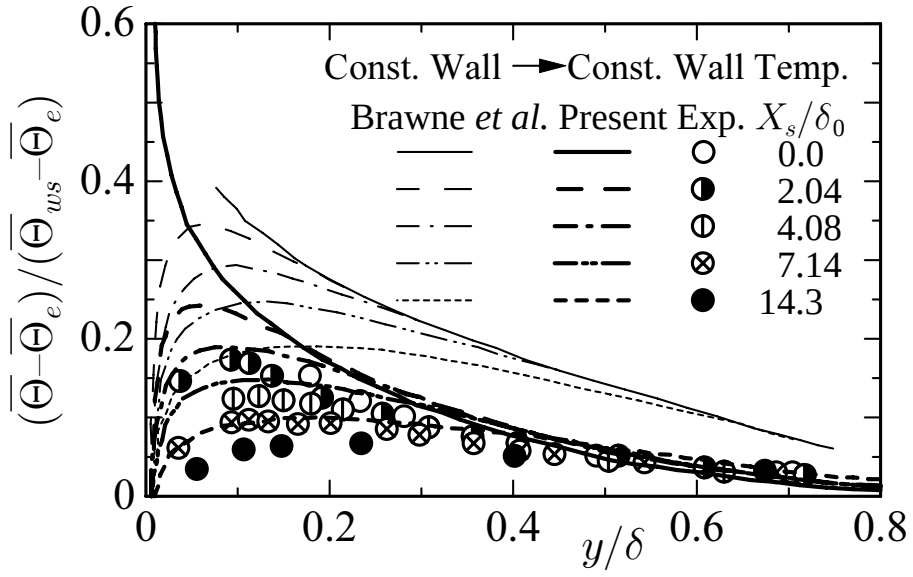

Figure 4.13: Comparison of the predicted mean temperature profile with the measurements

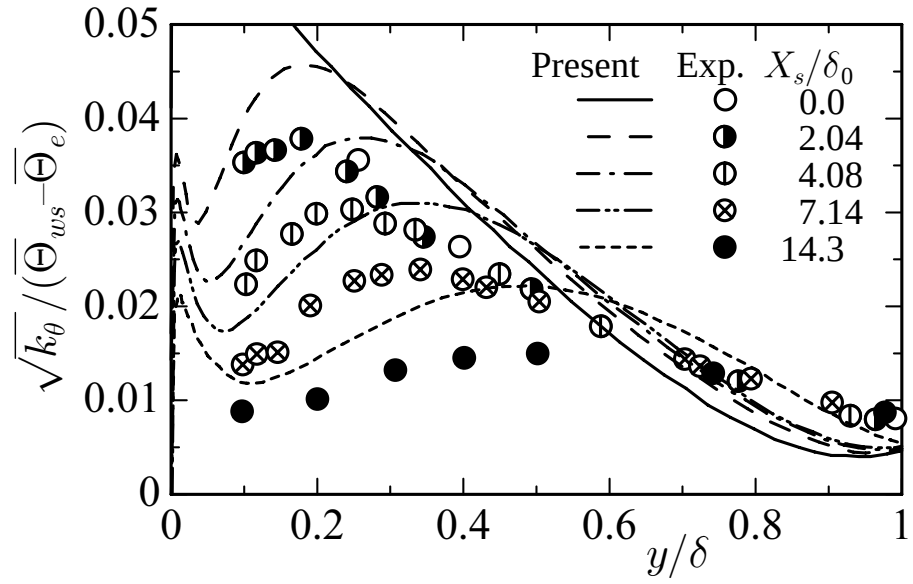

Figure 4.14: Comparison of the predicted rms temperature fluctuations with the measurements

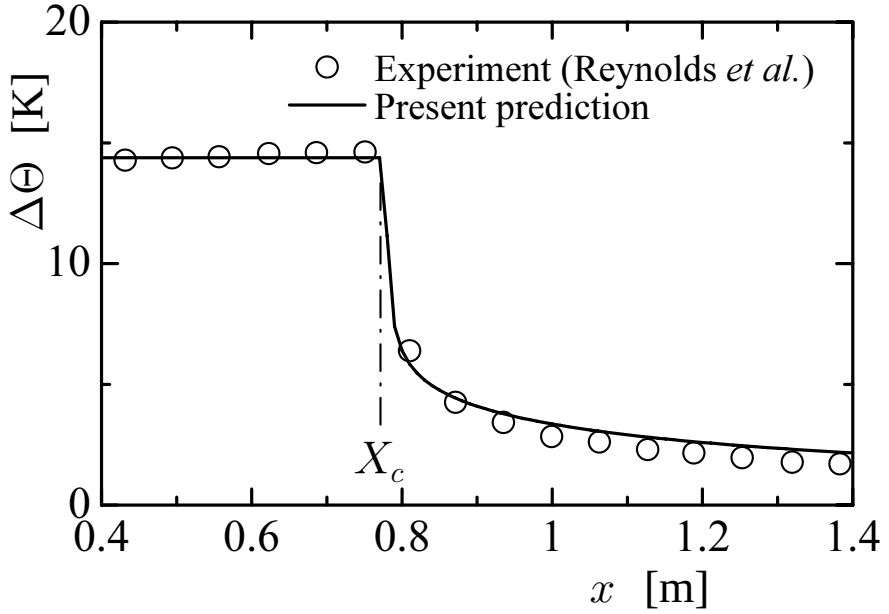

Figure 4.15: Comparison of the predicted variation of wall temperature with the measurement

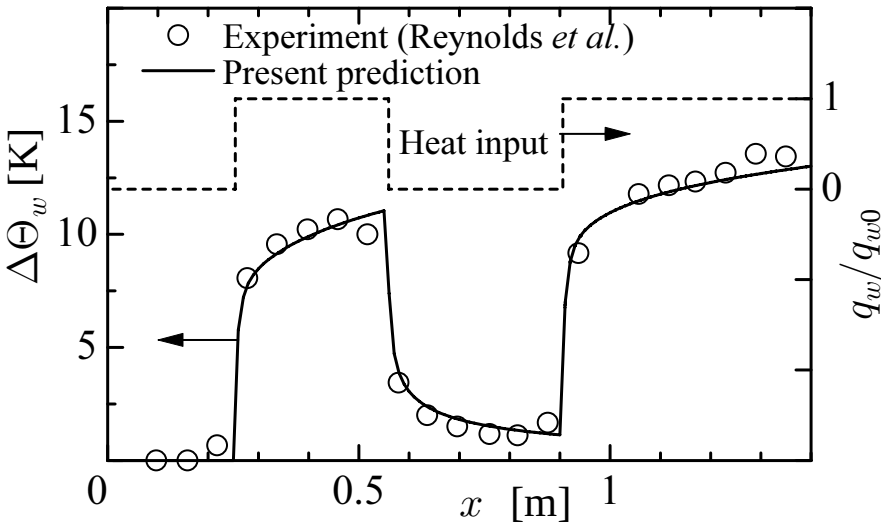

Figure 4.16: Comparison of the predicted variation of wall temperature with the measurement (double-pulse heat input)

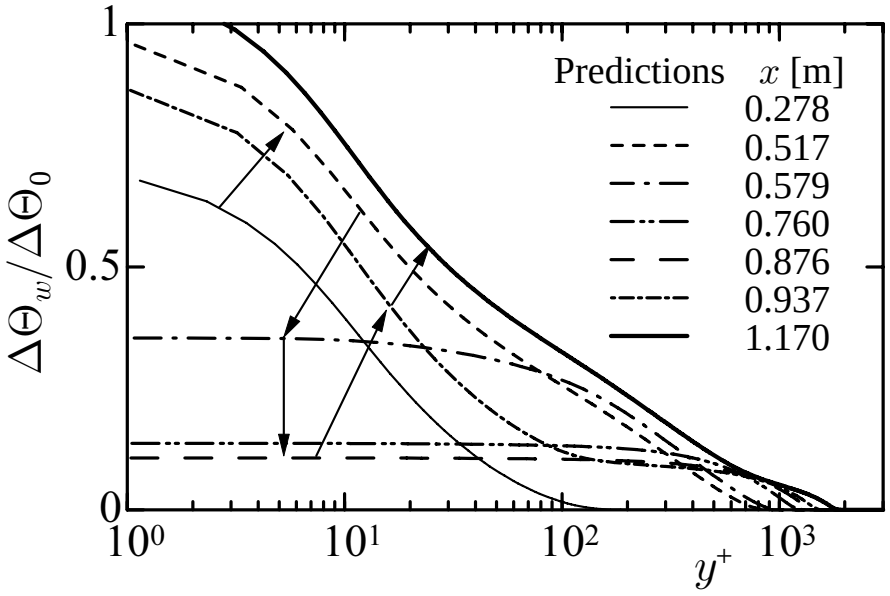

Figure 4.17: Mean temperature profiles for double-pulse heat input

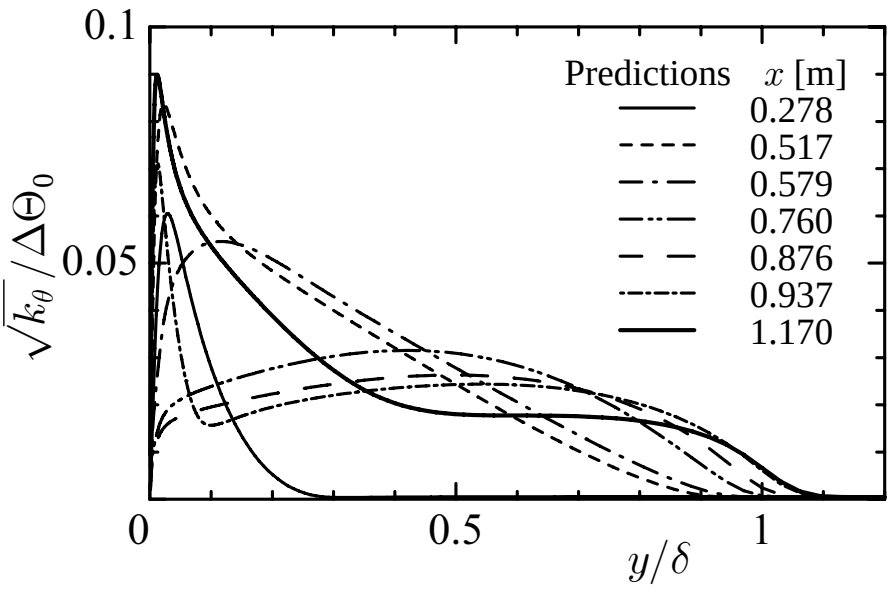

Figure 4.18: Variation of temperature variance for double-pulse heat input

CHAPTER 5

Rigorous formulation of two-equation heat-transfer model of turbulence using direct simulations

The direct numerical simulations (DNS) for wall shear flows provided the details of turbulent quantities near the wall (e.g., Moser *et al.* 1999; Kasagi *et al.* 1992). It was shown from these DNS data that the near-wall profiles of the dissipation-rates of turbulent kinetic energy and temperature variance were completely different from the existing model predictions. Recently, Rodi & Mansour (1993), and Nagano & Shimada (1995a) improved the $k-\varepsilon$ model using DNS databases, in which all the budget terms in the exact ε–equation were incorporated in the modeled ε–equation. The performance of the existing ε–equation models was assessed by Nagano & Shimada (1995b), and a rational ε–equation was reconstructed by Nagano *et al.* (1994).

Similarly, two-equation heat-transfer models (k_θ–ε_θ) have been improved, since Nagano & Kim (1988) proposed the first model for wall turbulent shear flows. The two-equation heat-transfer model is a powerful tool for predicting the heat transfer in flows with almost complete dissimilarity between velocity and thermal fields. Also, the characteristic time scale for a thermal field needed in a second-order closure model is now calculated with the two-equation heat-transfer model (Shikazono & Kasagi 1996).

In this Chapter, we develop a rigorous k_θ–ε_θ model. In particular, modeling of the ε_θ–equation is performed by taking into account all the budget terms in the exact ε_θ–equation. First, we make a critical assessment of existing ε_θ– and $\widetilde{\varepsilon}_\theta$–equations for both two-equation and second-order closure models. Secondly, we rebuild a more sophisticated ε_θ–equation reflecting the assessment results. Then, we propose a set of k_θ–ε_θ models to match with the present rigorous ε_θ–equation. Finally, we verify a set of model equations using DNS data and experi-

mental data. In order to show the proposed two-equation heat-transfer model performance, we analyze the system of a sudden change wall thermal condition, which is hard to measure using conventional tools, then we investigate physical phenomenon of the system using the results of analysis.

5.1 Assessment of modeled ε_θ–equations

5.1.1 Modeled ε_θ–equations

The modeled dissipation-rate equations for temperature variance used in the current k_θ–ε_θ models for wall shear flows are written in either of two ways:

$$\begin{aligned}\frac{D\varepsilon_\theta}{D\tau} =&\alpha\frac{\partial^2\varepsilon_\theta}{\partial x_j\partial x_j} + T_{\varepsilon_\theta} + C_{P1}f_{P1}\frac{\varepsilon_\theta}{k_\theta}P_{k_\theta} + C_{P2}f_{P2}\frac{\varepsilon_\theta}{k}P_k\\ &- C_{D1}f_{D1}\frac{{\varepsilon_\theta}^2}{k_\theta} - C_{D2}f_{D2}\frac{\varepsilon_\theta\varepsilon}{k} + \text{Additional term}, \qquad (5.1)\\ \frac{D\widetilde{\varepsilon}_\theta}{D\tau} =&\alpha\frac{\partial^2\widetilde{\varepsilon}_\theta}{\partial x_j\partial x_j} + T_{\widetilde{\varepsilon}_\theta} + C_{P1}f_{P1}\frac{\widetilde{\varepsilon}_\theta}{k_\theta}P_{k_\theta} + C_{P2}f_{P2}\frac{\widetilde{\varepsilon}_\theta}{k}P_k\\ &- C_{D1}f_{D1}\frac{\widetilde{\varepsilon}_\theta^2}{k_\theta} - C_{D2}f_{D2}\frac{\widetilde{\varepsilon}_\theta\widetilde{\varepsilon}}{k} + \text{Additional term}. \qquad (5.2)\end{aligned}$$

The turbulent diffusion term T_{ε_θ} in Eq. (2.19) is generally modeled as follows:

$$T_{\varepsilon_\theta} = \begin{cases}\dfrac{\partial}{\partial x_j}\left(\dfrac{\alpha_t}{\sigma_\phi}\dfrac{\partial\varepsilon_\theta}{\partial x_j}\right) & : \text{at a two-equation level,}\\ \dfrac{\partial}{\partial x_j}\left(C_s\dfrac{k}{\varepsilon}f(R)\overline{u_iu_j}\dfrac{\partial\varepsilon_\theta}{\partial x_i}\right) & : \text{at a second-order closure level.}\end{cases} \qquad (5.3)$$

The $T_{\widetilde{\varepsilon}_\theta}$ term is also modeled in the same manner as in Eq. (5.3).

In Eq. (5.2), quantities $\widetilde{\varepsilon}$ and $\widetilde{\varepsilon}_\theta$, called the isotropic dissipation rates of k and k_θ, are defined by the following equations, respectively:

$$\widetilde{\varepsilon} = \varepsilon - \widehat{\varepsilon}, \qquad (5.4)$$

$$\widetilde{\varepsilon}_\theta = \varepsilon_\theta - \widehat{\varepsilon}_\theta, \qquad (5.5)$$

where $\widehat{\varepsilon} = 2\nu(\partial\sqrt{k}/\partial y)^2$, $\widehat{\varepsilon}_\theta = 2\alpha(\partial\sqrt{\Delta k_\theta}/\partial y)^2$ and $\Delta k_\theta = k_\theta - k_{\theta w}$.

5.1.2 Assessment Procedure

In Eqs. (5.1) and (5.2), ε_θ and $\widetilde{\varepsilon}_\theta$ are the only unknown variables, and all turbulence quantities except ε_θ and $\widetilde{\varepsilon}_\theta$ are given directly from the DNS data; i.e., $\bar{U}_i$, $\overline{u_iu_j}$, k, ε, $\widetilde{\varepsilon}$, $\bar{\Theta}$, and k_θ are

not calculated from any modeled equation, but given as the "true" values from the DNS data.

We perform the model assessment in a fully developed channel flow with heat transfer for which the trustworthy DNS database is available (Kasagi *et al.* 1992) . The Reynolds number based on the friction velocity and a channel half-width, Re_τ, is 150 and the Prandtl number is 0.71.

5.1.3 Models for Assessment

We assess the six temperature dissipation-rate equations proposed by Nagano and Kim (NK) (1988), Hattori, Nagano and Tagawa (HNT) (1993) and Shikazono and Kasagi (SK) (1996), which are the $\widetilde{\varepsilon}_\theta$–equations, and those by Nagano *et al.* (NTT) (1991), Abe *et al.* (AKN) (1995) and Sommer *et al.* (SSL) (1992), which are the ε_θ–equations. The abbreviations in parentheses are introduced for ease of reference. The details of the above six modeled equations are listed in Table 5.1. It should be mentioned that the SSL model has partly introduced $\widetilde{\varepsilon}$ and $\widetilde{\varepsilon}_\theta$ to prevent divergence in calculation caused by finite values of ε and ε_θ at the wall, while the NTT and AKN models avoid it by introducing the proper f_{D1} and f_{D2} functions. In the SSL model, the turbulent heat-flux $\overline{u_i\theta}$ in the P_{k_θ} term is modeled using α_t, but the Reynolds shear-stress $\overline{u_iu_j}$ and turbulent diffusion term T_{ε_θ} are modeled at a second-order closure level [see Eq. (5.3)]. The AKN model has put $f_{P1} = f_{D1}$ to avoid divergence in calculation of flows with complete dissimilarity between velocity and thermal fields. In the SK model, where the k_θ–ε_θ model is employed to calculate the time scale of thermal field, the turbulent diffusion and production terms are modeled at a second-order closure level.

A characteristic time scale τ_m, whose importance was demonstrated by Nagano and Kim (1988), has been used in all the two-equation heat-transfer models for wall shear flows. It can be shown that the eddy diffusivity for heat α_t is governed near the wall by the Kolmogorov microscale in the NTT, HNT and AKN models, and by the Taylor microscale in the SSL model.

5.1.4 Assessment Results

The results of assessment for $\widetilde{\varepsilon}_\theta$– and ε_θ–equation models at a two-equation level and those at a second-order closure level are shown in Fig. 5.1, where in $\widetilde{\varepsilon}_\theta$–equation modeling ε_θ is obtained from $\varepsilon_\theta = \widetilde{\varepsilon}_\theta + \widehat{\varepsilon}_\theta$. The resultant characteristic time scale τ_θ is assessed in Fig. 5.2.

To assess the NK model, the time scale τ_u in α_t is given by $k/\widetilde{\varepsilon}$ from the DNS, because the NK model is usually combined with Nagano and Hishida model (1987) ($\widetilde{\varepsilon}$–equation model).

As can be seen from Figs. 5.1 and 5.2, the results of assessment for $\widetilde{\varepsilon}_\theta$– and ε_θ–equation models indicate that none of the four models can reproduce accurately the DNS behaviour. Especially, predicted ε_θ tends to increase in the buffer layer $(5 < y^+ < 40)$. In Figs. 5.1(c) and 5.2(c), only the SK model qualitatively and quantitatively reproduces a trend similar to DNS. However, the constants C_{P1} and C_{P2} in the SK model do not satisfy the relation for "constant-stress and constant-heat-flux layer" as follows:

$$\frac{\kappa^2/Pr_t}{\sqrt{C_\mu}} + \frac{C_{P1} - C_{D1}}{2R} + C_{P2} - C_{D2} = 0, \tag{5.6}$$

where $\kappa = 0.39 \sim 0.41$, Pr_t=0.9, $C_\mu = 0.09$ and $R = 0.5$ are typical values in the wall bounded flows.

Next, we discuss the gradient of ε_θ at the wall. The near-wall behaviour of ε_θ without θ_w fluctuations can be inferred from a Taylor series expansion in terms of y as follows (Yossef *et al.* 1992):

$$\varepsilon_\theta = h_1 + 4h_2 y + O(y^2), \tag{5.7}$$

where coefficients h_1 and h_2 are independent of the y coordinate. On the other hand, from Eq. (2.18), the molecular diffusion term balances with the dissipation term at $y = 0$:

$$\varepsilon_\theta = \alpha \frac{\partial^2 k_\theta}{\partial y^2} \text{ with } \alpha \frac{\partial^2 k_\theta}{\partial y^2} = h_1 + 6h_2 y + O(y^2). \tag{5.8}$$

From Eq. (5.7) and Eq. (5.8), the coefficient $h_2[= (1/4)(\partial\varepsilon_\theta/\partial y)|_w]$ should be zero. This can be, of course, seen in the DNS data.

In theory, the wall limiting behaviour of $\widetilde{\varepsilon}_\theta$ must be $\widetilde{\varepsilon}_\theta \propto y^2$. But in the $\widetilde{\varepsilon}_\theta$–equation of the NK and HNT models, the molecular diffusion term balances with $C_{D1}\widetilde{\varepsilon}_\theta{}^2/k_\theta$ term at $y = 0$. As a result, the wall limiting behaviour of $\widetilde{\varepsilon}_\theta$ becomes $\widetilde{\varepsilon}_\theta \propto y^1$. Therefore, in the $\widetilde{\varepsilon}_\theta$–equation, adding the extra term to reproduce the correct wall limiting behaviour of $\widetilde{\varepsilon}_\theta$ is of the first importance to obtain the correct profile of ε_θ near the wall. The SK model has an additional term to balance, at the wall, with the molecular diffusion term in the $\widetilde{\varepsilon}_\theta$–equation, as suggested by Kawamura and Kawashima (1994).

The sum total of budget data for $\widetilde{\varepsilon}_\theta$– and ε_θ–equations are shown in Fig. 5.3. The budget in the $\widetilde{\varepsilon}_\theta$–equation is represented by $\alpha(\partial^2\varepsilon_\theta/\partial y^2) = \alpha(\partial^2\widetilde{\varepsilon}_\theta/\partial y^2) - 2\alpha^2(\partial^2[(\sqrt{\Delta k_\theta})^2]/\partial y^2)$.

Table 5.1: Existing ε_θ and $\widetilde{\varepsilon}_\theta$ equation models.

	Nagano-Kim(1988)	Nagano *et al.*(1991)
C_λ	0.11	0.1
C_s	—	—
C_{P1}	0.9	0.85
C_{P2}	0.72	0.64
C_{D1}	1.1	1.0
C_{D2}	0.8	0.9
σ_ϕ	1.0	1.0
τ_m	$\left(\frac{k}{\widetilde{\varepsilon}}\right)(2\widetilde{R})^{\frac{1}{2}}$	$\left(\frac{k}{\varepsilon}\right)\left[(2R)^2+\frac{3.4(2R)^{\frac{1}{2}}}{R_t{}^{\frac{3}{4}}}\right]$
f_λ	$\left[1-\exp\left(-\frac{y^+}{A_\lambda}\right)\right]^2$	$\left[1-\exp\left(-\frac{y^+}{A_\lambda}\right)\right]^2$
A_μ	—	—
A_λ	$\left(\frac{30.5}{\sqrt{Pr}}\right)\left(\frac{C_f}{2St}\right)$	$\frac{26}{\sqrt{Pr}}$
$f(R)$	—	—
f_{P1}	1.0	1.0
f_{P2}	1.0	1.0
f_{D1}	1.0	$\left[1-\exp\left(-\frac{y^+}{5.8}\right)\right]^2$
f_{D2}	1.0	$\frac{1}{C_{D2}}(C_{\varepsilon 2}f_\varepsilon-1)\left[1-\exp\left(-\frac{y^+}{6}\right)\right]^2$
Additional term	$\alpha\alpha_t(1-f_\lambda)\left(\frac{\partial^2\bar{\Theta}}{\partial x_j\partial x_k}\right)^2$	—
	$\widetilde{R}=\frac{k_\theta/\widetilde{\varepsilon}_\theta}{k/\widetilde{\varepsilon}}$	$C_{\varepsilon 2}=1.9$ $f_\varepsilon=1-\exp\left[-\left(\frac{R_t}{6.5}\right)^2\right]$

Table 5.1: (continued)

	Shikazono-Kasagi(1996)	Abe-Kondoh-Nagano(1995)
C_λ	—	0.1
C_s	0.3	—
C_{P1}	0.8	1.9
C_{P2}	0.3	0.6
C_{D1}	1.0	2.0
C_{D2}	0.3	0.9
σ_ϕ	—	1.6
τ_m	—	$\frac{k}{\varepsilon}\left[f(R)+\frac{3(2R)^{\frac{1}{2}}}{R_t{}^{\frac{3}{4}}Pr}f_d\right]$
f_λ	—	$\left[1-\exp\left(-\frac{y^*}{A_\mu}\right)\right]\left[1-\exp\left(-\frac{y^*}{A_\lambda}\right)\right]$
A_μ	—	14
A_λ	—	$\frac{A_\mu}{\sqrt{Pr}}$
$f(R)$	$\frac{2R}{0.7+R}$	$\frac{2R}{0.5+R}$
f_{P1}	1.0	$[1-\exp(-y^*)]^2$
f_{P2}	1.0	1.0
f_{D1}	1.0	$[1-\exp(-y^*)]^2$
f_{D2}	1.0	$\frac{1}{C_{D2}}(C_{\varepsilon 2}f_\varepsilon-1)\left[1-\exp\left(-\frac{y^*}{5.7}\right)\right]^2$
Additional term	$2\alpha C_{w2}\left(\frac{k_\theta}{\varepsilon_\theta}\right)\overline{v^2}\left(\frac{\partial^2\bar{\Theta}}{\partial y^2}\right)^2-\frac{\widetilde{\varepsilon}_\theta\widehat{\varepsilon}_\theta}{k_\theta}$	—
		$f_d=\exp\left[-\left(\frac{R_t}{200}\right)^2\right]$
	$C_{w2}=\max[0.1, 0.35-0.21Pr]$	$C_{\varepsilon 2}=1.9$
		$f_\varepsilon=1-\exp\left[-\left(\frac{R_t}{6.5}\right)^2\right]$

Table 5.1: (continued)

	Sommer-So-Lai(1992)	Hattori-Nagano-Tagawa(1993)
C_λ	0.11	0.1
C_s	0.11	—
C_{P1}	0.9	0.85
C_{P2}	0.72	0.64
C_{D1}	1.1	1.0
C_{D2}	0.8	0.9
σ_ϕ	—	1.0
τ_m	$\frac{k}{\varepsilon}\left[(2R)^{\frac{1}{2}}+\frac{0.1(2R)^{\frac{1}{2}}}{R_t^{\frac{1}{4}}}\left(\frac{f_{\varepsilon t}}{f_\lambda}\right)\right]$	$\frac{k}{\varepsilon}\left[(2R)^{\frac{1}{2}}+\frac{7.9(2R)^{\frac{1}{2}}}{R_t^{\frac{3}{4}}}f_d\right]$
f_λ	$\left[1-\exp\left(-\frac{y^+}{A_\lambda}\right)\right]^2$	$\left[1-\exp\left(-\frac{y^+}{A_\mu}\right)\right]\left[1-\exp\left(-\frac{y^+}{A_\lambda}\right)\right]$
A_μ	—	$\frac{30}{1+11.8P^+}$
A_λ	30	$\frac{A_\mu}{Pr^{\frac{1}{3}}}$
$f(R)$	1.0	—
f_{P1}	1.0	1.0
f_{P2}	1.0	1.0
f_{D1}	$\frac{\widetilde{\varepsilon}_\theta}{\varepsilon_\theta}$	1.0
f_{D2}	$\frac{\widetilde{\varepsilon}}{\varepsilon}$	$\frac{1}{C_{D2}}(C_{\varepsilon 2}f_\varepsilon-1)$
Additional term	$f_{\varepsilon t}\left[(C_{D1}-2)\frac{\widetilde{\varepsilon}_\theta}{k_\theta}\varepsilon_\theta+C_{D2}\frac{\widetilde{\varepsilon}}{k}\varepsilon_\theta\right.$ $\left.-\frac{\varepsilon_\theta^{*2}}{2k_\theta}+(1-C_{P1})\frac{\varepsilon_\theta}{k_\theta}P_\theta^*\right]$	$\alpha\alpha_t(1-f_w)\left(\frac{\partial^2\bar{\Theta}}{\partial x_j\partial x_k}\right)^2$
	$f_{\varepsilon t}=\exp\left[-\left(\frac{R_t}{80}\right)^2\right]$	$f_d=\exp\left[-\left(\frac{R_t}{120}\right)^2\right]$
	$\varepsilon_\theta^*=\varepsilon_\theta-2\alpha\frac{k_\theta}{y^2}$	$f_w=\left\{1-\exp\left[-\frac{y^+}{(30/Pr^{\frac{1}{3}})}\right]\right\}^2$
	$P_\theta^*=\overline{u\theta}\left(\frac{\partial\bar{\Theta}}{\partial x}\right)$	$P^+=\frac{\nu}{\rho u_\tau^3}\left(\frac{d\bar{P}}{dx}\right)$
		$C_{\varepsilon 2}=1.9$
		$f_\varepsilon=1-0.3\exp\left(-R_t^2\right)$

Obviously, the two-equation model predictions are not in agreement with the DNS data. As seen from Fig. 5.3(c), the sum total of the budget in the SK model is the closest to the DNS. This is the consequence of smaller model constants C_{P2} and C_{D2} used, which render the production and destruction terms smaller in magnitude. In the ε_θ–equation models, the NTT model is rather close to the DNS. This is because the NTT model has no additional production term.

From these assessments it becomes clear that solutions for ε_θ are significantly influenced by an additional production term, model constants and a formulation of characteristic time scale.

5.2 Modeling of ε_θ–equation

As shown in the previous section, none of the existing $\widetilde{\varepsilon}_\theta$ and ε_θ models at a two-equation level give qualitative and quantitative agreement with the DNS. Hence, we will construct an ε_θ–equation model based on the NTT model by taking into account all the budget terms in the exact ε_θ–equation.

5.2.1 Modeling of $P^1_{\varepsilon_\theta}$, $P^2_{\varepsilon_\theta}$, $P^4_{\varepsilon_\theta}$ and $\Upsilon_{\varepsilon_\theta}$

The $P^1_{\varepsilon_\theta}$, $P^2_{\varepsilon_\theta}$, $P^4_{\varepsilon_\theta}$ and $\Upsilon_{\varepsilon_\theta}$ terms can be modeled in a way similar to the NK model (1987) and NTT model (1991):

$$\begin{aligned} & P^1_{\varepsilon_\theta} + P^2_{\varepsilon_\theta} + P^4_{\varepsilon_\theta} - \Upsilon_{\varepsilon_\theta} \\ = & - C_{P1} f_{P1} \frac{\varepsilon_\theta}{k_\theta} \overline{u_j \theta} \frac{\partial \bar{\Theta}}{\partial x_j} - C_{D1} f_{D1} \frac{{\varepsilon_\theta}^2}{k_\theta} - C_{P2} f_{P2} \frac{\varepsilon_\theta}{k} \overline{u_i u_j} \frac{\partial \bar{U}_i}{\partial x_j} - C_{D2} f_{D2} \frac{\varepsilon_\theta \varepsilon}{k}. \end{aligned} \tag{5.9}$$

The DNS data indicates that the $P^1_{\varepsilon_\theta}$ and $P^2_{\varepsilon_\theta}$ terms exert a great influence on the production of ε_θ near the wall. The modeling given by Eq. (5.9) is based on $P^4_{\varepsilon_\theta}$ and $\Upsilon_{\varepsilon_\theta}$, so that other terms' effects are not sufficiently reflected. Therefore, we model the contributions from the $P^1_{\varepsilon_\theta}$ and $P^2_{\varepsilon_\theta}$ terms using an order-of-magnitude analysis, as done in modeling ε by Rodi and Mansour (1993) and Nagano and Shimada (1995a). With k_θ and $\ell_\theta = \sqrt{k}\tau_\theta$ (thermal turbulence length

scale), we can estimate an order of magnitude of the $P^1_{\varepsilon_\theta}$, $P^2_{\varepsilon_\theta}$ and $P^4_{\varepsilon_\theta}$ terms as

$$\left.\begin{aligned} P^1_{\varepsilon_\theta} &= O\left[\left(\frac{k\sqrt{k_\theta}}{\ell_\theta}\right)\left(\frac{\lambda_\theta}{\lambda}\right)G\right] \\ P^2_{\varepsilon_\theta} &= O\left[\left(\frac{\sqrt{k}k_\theta}{\ell_\theta}\right)S\right] \\ P^4_{\varepsilon_\theta} &= O\left[\left(\frac{kk_\theta}{{\ell_\theta}^2}\right)\left(\frac{\ell_\theta}{\lambda}\right)\right] \end{aligned}\right\}, \tag{5.10}$$

where $G = [(\partial\bar{\Theta}/\partial x_j)(\partial\bar{\Theta}/\partial x_j)]^{\frac{1}{2}}$ represents the mean temperature gradient, $S = [(\partial\bar{U}_i/\partial x_j)(\partial\bar{U}_i/\partial x_j)]^{\frac{1}{2}}$ is the mean strain rate, and $\lambda = \sqrt{k\nu/\varepsilon}$ and $\lambda_\theta = \sqrt{k_\theta\alpha/\varepsilon_\theta}$ are the Taylor microscales for the velocity and temperature fields, respectively. The above relations give $P^1_{\varepsilon_\theta}/P^4_{\varepsilon_\theta} \sim (\lambda_\theta/\sqrt{k_\theta})G = G/(\varepsilon_\theta/\alpha)^{\frac{1}{2}}$, $P^2_{\varepsilon_\theta}/P^4_{\varepsilon_\theta} \sim (\lambda/\sqrt{k})S = S/(\varepsilon/\nu)^{\frac{1}{2}}$. Consequently, we define the parameters R_T and R_U as

$$R_T = \frac{\left[\left(\partial\bar{\Theta}/\partial x_j\right)^2\right]^{\frac{1}{2}}}{\left[\,\overline{\left(\partial\theta/\partial x_j\right)^2}\,\right]^{\frac{1}{2}}} = \frac{G}{(\varepsilon_\theta/\alpha)^{\frac{1}{2}}}, \tag{5.11}$$

$$R_U = \frac{\left[\left(\partial\bar{U}_i/\partial x_j\right)^2\right]^{\frac{1}{2}}}{\left[\,\overline{\left(\partial u_i/\partial x_j\right)^2}\,\right]^{\frac{1}{2}}} = \frac{S}{(\varepsilon/\nu)^{\frac{1}{2}}}. \tag{5.12}$$

These parameters represent the ratio of the gradient of mean flow to that of fluctuating components. Apparently, the relations $P^1_{\varepsilon_\theta}/P^4_{\varepsilon_\theta} \sim R_T$ and $P^2_{\varepsilon_\theta}/P^4_{\varepsilon_\theta} \sim R_U$ hold. Since the structure of turbulent shear flows near the wall is mainly governed by the gradient of mean flow (see, e.g., Hinze 1975), contributions of $P^1_{\varepsilon_\theta}$ and $P^2_{\varepsilon_\theta}$ terms must appear when $R_T > 1$ and $R_U > 1$. We replace the mean temperature gradient G and the strain rate parameter S with the well-known relations for the constant heat-flux layer $[G = (q_w/\rho c_p)/(\alpha+\alpha_t) = u_\tau\theta_\tau/(\alpha+\alpha_t)]$ and the constant stress layer $[S = (\tau_w/\rho)/(\nu+\nu_t) = {u_\tau}^2/(\nu+\nu_t)]$. Then, Eqs. (5.11) and (5.12) lead to

$$R_T = \frac{u_\tau\theta_\tau}{(1/\operatorname{Pr}+\alpha_t/\nu)(\operatorname{Pr}\varepsilon_\theta/\nu)^{\frac{1}{2}}} f_w(6), \tag{5.13}$$

$$R_U = \frac{{u_\tau}^2}{(1+\nu_t/\nu)(\varepsilon/\nu)^{\frac{1}{2}}} f_w(6). \tag{5.14}$$

The contributions of $P^1_{\varepsilon_\theta}$ and $P^2_{\varepsilon_\theta}$ are now able to be included in the model functions f_{P1} and f_{P2} as follows:

$$\left.\begin{aligned} f_{P1} &= (1 - f'_{P1}) f_p \\ f'_{P1} &= \exp(-7 \times 10^{-5} {R_T}^{10})[1 - \exp(-2.2 {R_T}^{\frac{1}{2}})] \end{aligned}\right\}, \tag{5.15}$$

$$\left.\begin{aligned} f_{P2} &= (1 - f'_{P2}) f_p \\ f'_{P2} &= \exp(-7 \times 10^{-5} {R_U}^{10})[1 - \exp(-2.2 {R_U}^{\frac{1}{2}})] \end{aligned}\right\}, \tag{5.16}$$

where $f_p \left(= 1 + 0.75 \exp\left[-(R_h/40)^{\frac{1}{2}} \right] \right)$ is introduced for correcting overproduction near the wall and $R_h = k\tau_m/\nu = R_t[2R/(0.5 + R)]$ is the turbulence Reynolds number based on the harmonic-averaged time scale $\tau_m = (k/\varepsilon)[2R/(0.5 + R)]$. Note that τ_m becomes identical to $\tau_u = k/\varepsilon$ in local-equilibrium flows with $R = 0.5$.

The wall-reflection function employed in the present model is

$$f_w(\xi) = \exp\left[-\left(\frac{y^*}{\xi} \right)^2 \right], \tag{5.17}$$

where $y^* = u_\varepsilon y/\nu$ is the dimensionless distance from the wall based on the Kolmogorov velocity scale $u_\varepsilon = (\nu\varepsilon)^{\frac{1}{4}}$. This model function is more useful for analysis of various complex flows, as confirmed by Abe *et al.* (1995) and Nagano *et al.* (1997).

5.2.2 Modeling of $P^3_{\varepsilon_\theta}$

The $P^3_{\varepsilon_\theta}$ term is negligibly small in comparison with $P^1_{\varepsilon_\theta}$, $P^2_{\varepsilon_\theta}$, $P^4_{\varepsilon_\theta}$ and $\Upsilon_{\varepsilon_\theta}$. However, when compared with the sum of these terms, i.e., $P^1_{\varepsilon_\theta} + P^2_{\varepsilon_\theta} + P^4_{\varepsilon_\theta} - \Upsilon_{\varepsilon_\theta}$, the $P^3_{\varepsilon_\theta}$ term becomes of the same order, so that modeling of $P^3_{\varepsilon_\theta}$ is also important.

In the present model, we adopt the following form similar to that proposed in the k–ε model by Nagano and Shimada (1995a):

$$P^3_{\varepsilon_\theta} = \alpha\alpha_t f_w(12) \left(\frac{\partial^2 \bar{\Theta}}{\partial x_j \partial x_k} \right)^2 + C_{P3} \alpha \frac{k}{\varepsilon} f(R) \frac{\partial k}{\partial x_k} \frac{\partial \bar{\Theta}}{\partial x_j} \frac{\partial^2 \bar{\Theta}}{\partial x_j \partial x_k}, \tag{5.18}$$

where $f(R) = 2R/(0.5 + R)$.

5.2.3 Modeling of T_{ε_θ}

A gradient-type diffusion plus convection by large-scale motions may effectively represent turbulent diffusion for scalar (see, e.g., Hinze 1975). Thus, considering the relation $\varepsilon_\theta \simeq 2(\varepsilon/k)k_\theta$ at $R \simeq 0.5$ and the near-wall limiting behaviour of T_{ε_θ}, we write T_{ε_θ} as

$$T_{\varepsilon_\theta} = \frac{\partial}{\partial x_j}\left(\frac{\alpha_t}{\sigma_\phi}\frac{\partial \varepsilon_\theta}{\partial x_j}\right) + C_{\varepsilon_\theta}\alpha\frac{\partial}{\partial x_j}\left\{[1-f_w(3)]^{\frac{3}{2}}\frac{\varepsilon}{k}\frac{\partial k_\theta}{\partial x_j}f_w(3)\right\}. \tag{5.19}$$

For the eddy diffusivity for heat α_t, we adopt the following representation similar to the AKN model (1995):

$$\alpha_t = C_\lambda \frac{k^2}{\varepsilon}\left[f(R) + \frac{B_{\lambda 1}}{{R_t}^{\frac{3}{4}}}\exp\left(-\frac{R_h}{B_{\lambda 2}}\right)\right][1-f_w(A_\mu)]^{\frac{1}{2}}[1-f_w(A_\lambda)]^{\frac{1}{2}}. \tag{5.20}$$

The model constants and functions in the modeled ε_θ–equation at a two-equation level are listed in Table 5.2.

5.2.4 Case of second-order closure modeling

In the second-order closure modeling, the turbulent diffusion term T_{ε_θ} and the production term $P^3_{\varepsilon_\theta}$ should be slightly modified, since the second-order closure model needs neither ν_t nor α_t. Hence, the gradient parameters R_T and R_U are changed as follows:

$$R_T = \frac{u_\tau\theta_\tau + \overline{v\theta}}{(\varepsilon_\theta\nu/\,\mathrm{Pr})^{\frac{1}{2}}}f_w(6), \tag{5.21}$$

$$R_U = \frac{{u_\tau}^2 + \overline{uv}}{(\varepsilon\nu)^{\frac{1}{2}}}f_w(6). \tag{5.22}$$

The model functions f'_{P1} and f'_{P2} in Eqs. (5.15) and (5.16) are defined by

$$\left.\begin{aligned} f'_{P1} &= \exp\left(-7\times 10^{-5}{R_T}^{10}\right)\left[1-\exp(-1.1{R_T}^{\frac{1}{2}})\right] \\ f'_{P2} &= \exp\left(-7\times 10^{-5}{R_U}^{10}\right)\left[1-\exp(-1.1{R_U}^{\frac{1}{2}})\right] \end{aligned}\right\}. \tag{5.23}$$

The turbulent diffusion term T_{ε_θ} can be written as

$$T_{\varepsilon_\theta} = \frac{\partial}{\partial x_k}\left(C_s\frac{k}{\varepsilon}f(R)\overline{u_ju_k}\frac{\partial \varepsilon_\theta}{\partial x_j}\right) + C_{\varepsilon_\theta}\alpha\frac{\partial}{\partial x_j}\left\{[1-f_w(3)]^{\frac{3}{2}}\frac{\varepsilon}{k}\frac{\partial k_\theta}{\partial x_j}f_w(3)\right\}, \tag{5.24}$$

where $C_s = 0.11$, and $f(R)$ and C_{ε_θ} are exactly the same as those used in the two-equation heat-transfer model.

The $P^3_{\varepsilon_\theta}$ term may be written [see Eq. (5.18)] as

$$P^3_{\varepsilon_\theta} = C_{P4}\alpha\overline{u_ju_k}\frac{k}{\varepsilon}f(R)\frac{\partial^2\bar{\Theta}}{\partial x_k\partial x_\ell}\frac{\partial^2\bar{\Theta}}{\partial x_j\partial x_k} + C_{P3}\alpha\frac{k}{\varepsilon}f(R)\frac{\partial\overline{u_ju_\ell}}{\partial x_k}\frac{\partial\bar{\Theta}}{\partial x_\ell}\frac{\partial^2\bar{\Theta}}{\partial x_j\partial x_k} \tag{5.25}$$

with $C_{P3} = 0.1$ and $C_{P4} = 0.25$.

Table 5.2: Model constants and functions in the present ε_θ model

C_λ	0.1	f_R	$\dfrac{2R}{0.5+R}$
C_s	—	f_{P1}	$(1-f'_{P1})\,f_p\,[1-f_w(12)]$
C_{P1}	0.9	f_{P2}	$(1-f'_{P2})\,f_p$
C_{P2}	0.77	f_{D1}	$1-f_w(12)$
C_{P3}	0.05	f_{D2}	$\dfrac{1}{C_{D2}}\,(C_{\varepsilon 2}f_\varepsilon - 1)\,[1-f_w(12)]$
C_{D1}	1.0	Additional term	$\left(=P^3_{\varepsilon_\theta}\right)$
C_{D2}	0.9	f_d	$\exp\left(-\dfrac{R_h}{220}\right)$
C_{ε_θ}	1.6	$C_{\varepsilon 2}$	1.9
σ_ϕ	1.8	f_ε	$1-0.3\exp\left[-\left(\dfrac{R_t}{6.5}\right)^2\right]$
τ_m	$\dfrac{k}{\varepsilon}\left[f(R)+\dfrac{26(2R)^{\frac{1}{2}}}{Pr^{\frac{4}{3}}R_t^{\frac{3}{4}}}f_d\right]$	f'_{P1}	$\exp\left(-7\times10^{-5}R_T^{10}\right)\left[1-\exp(-2.2R_T^{\frac{1}{2}})\right]$
f_λ	$[1-f_w(A_\mu)]^{\frac{1}{2}}\,[1-f_w(A_\lambda)]^{\frac{1}{2}}$	f'_{P2}	$\exp\left(-7\times10^{-5}R_U^{10}\right)\left[1-\exp(-2.2R_U^{\frac{1}{2}})\right]$
$f_w(\xi)$	$\exp\left[-\left(\dfrac{y^*}{\xi}\right)^2\right]$	f_p	$1+0.75\exp\left[-\left(\dfrac{R_h}{40}\right)^{\frac{1}{2}}\right]$
A_μ	28	R_T	$f_w(6)\dfrac{u_\tau\theta_\tau}{(\alpha+\alpha_t)(\varepsilon_\theta/\alpha)^{\frac{1}{2}}}$
A_λ	$\dfrac{A_\mu}{Pr^{\frac{1}{3}}}$	R_U	$f_w(6)\dfrac{{u_\tau}^2}{(\nu+\nu_t)(\varepsilon/\nu)^{\frac{1}{2}}}$

5.2.5 Assessment of proposed ε_θ-equation models

Figure 5.4 shows the solutions obtained from new ε_θ–equations. As shown previously, the existing two-equation level models have never reproduced the correct near-wall behaviour of ε_θ, whereas the present predictions give excellent agreement with the DNS data. Owing to the inclusion of the model for α_t, the proposed model at a two-equation level gives predictions slightly different from those at a second-order closure level. The overall predictions, however, are much better than with the existing models. It should also be noted that, for the budget balance in the ε_θ–equation [Fig. 5.4(c)], excellent agreement is now achieved.

5.3 Construction of set of model equations

5.3.1 Two-equation model for velocity field

In this study, for the basic formulation in k–ε model, we adopt the Nagano–Shimada model (1995a) (hereinafter referred to as the NS model) which reproduces turbulence energy and its dissipation rate including these budgets exactly. An incompressible turbulent velocity field is described with the following governing equations (the equation of continuity, the ensemble-averaged Navier-Stokes equation, and the transport equations of the turbulence energy and its dissipation rate):

$$\frac{\partial \bar{U}_i}{\partial x_i} = 0, \tag{5.26}$$

$$\frac{D\bar{U}_i}{D\tau} = -\frac{1}{\rho}\frac{\partial \bar{P}}{\partial x_i} + \frac{\partial}{\partial x_j}\left(\nu\frac{\partial \bar{U}_i}{\partial x_j} - \overline{u_i u_j}\right), \tag{5.27}$$

$$-\overline{u_i u_j} = \nu_t\left(\frac{\partial \bar{U}_i}{\partial x_j} + \frac{\partial \bar{U}_j}{\partial x_i}\right) - \frac{2}{3}\delta_{ij}k, \tag{5.28}$$

$$\nu_t = C_\mu f_\mu \frac{k^2}{\varepsilon}, \tag{5.29}$$

$$\frac{Dk}{D\tau} = \frac{\partial}{\partial y}\left[\left(\nu + \frac{\nu_t}{\sigma_k^*}\right)\frac{\partial k}{\partial y}\right] - \overline{uv}\frac{\partial \bar{U}}{\partial y} - \varepsilon + \max\left[-0.5\nu\frac{\partial}{\partial y}\left(\frac{k}{\varepsilon}\frac{\partial \varepsilon}{\partial y}f_{w1}\right), 0\right], \tag{5.30}$$

$$\begin{aligned}\frac{D\varepsilon}{D\tau} =& \frac{\partial}{\partial y}\left[\left(\nu + \frac{\nu_t}{\sigma_\varepsilon^*}\right)\frac{\partial \varepsilon}{\partial y}\right] - C_{\varepsilon 1}\frac{\varepsilon}{k}\overline{uv}\frac{\partial \bar{U}}{\partial y} - C_{\varepsilon 2}f_2\frac{\varepsilon^2}{k} + f_{w2}\nu\nu_t\left(\frac{\partial^2 \bar{U}}{\partial y^2}\right)^2 \\ &+ C_{\varepsilon 3}\nu\frac{k}{\varepsilon}\frac{\partial k}{\partial y}\frac{\partial \bar{U}}{\partial y}\frac{\partial^2 \bar{U}}{\partial y^2} + C_{\varepsilon 4}\nu\frac{\partial}{\partial y}\left[\left(1 - f_{w1}\right)\frac{\varepsilon}{k}\frac{\partial k}{\partial y}f_{w1}\right].\end{aligned} \tag{5.31}$$

The NS model employed the wall friction velocity u_τ in the wall reflection function f_w. However, we introduce the Kolmogorov velocity u_ε in this function described in the previous section [see Eq. (5.17)], and the model constants and functions were optimized for the proposed function. These are listed in Table 5.3.

5.3.2 Modeling of k_θ–equation

Figure 5.5 shows the budget of temperature variance predicted by the NTT model (Nagano *et al.* 1991) which is the basis for the proposed model and the AKN model (Abe *et al.* 1995). Obviously, the model predictions are different from DNS data near the wall because of the solution given by ε_θ–equation and the modeling of turbulent diffusion term in the k_θ–equation.

Table 5.3: Constants and fuctions for the k–ε model.

σ_k^*	$1.4/f_t$
σ_ε^*	$1.3/f_t$
f_t	$1+6f_{w1}$
f_{w1}	$f_w(4)$
f_{w2}	$f_w(26)$
$C_{\varepsilon 1}$	1.45
$C_{\varepsilon 2}$	1.9
$C_{\varepsilon 3}$	0.005
$C_{\varepsilon 4}$	0.5
f_2	$(1+f_2')(1-f_{w1})\left\{1-0.6\exp\left[-\left(\frac{R_t}{45}\right)^{\frac{1}{2}}\right]\right\}$
f_2'	$\exp\left(-2\times10^{-4}R_v^{13}\right)\left[1-\exp\left(-2.2R_v^{0.5}\right)\right]$
R_v	$\left(\frac{k}{\varepsilon}\right)\frac{1}{1+\nu_t/\nu}\left(\frac{1}{R_t{}^{\frac{1}{2}}}\right)f_{w1}$
f_μ	$(1-f_{w2})\left\{1+\left(\frac{60}{R_t{}^{\frac{3}{4}}}\right)\exp\left[-\left(\frac{R_t}{55}\right)^{\frac{1}{2}}\right]\right\}$

Therefore, in the k_θ–equation given by Eq. (2.18), it is the turbulent diffusion term T_{k_θ} that should be modeled. We adopt the foregoing turbulent diffusion modeling, and write T_{k_θ} as

$$T_{k_\theta}=\frac{\partial}{\partial x_j}\left(\frac{\alpha_t}{\sigma_h^*}\frac{\partial k_\theta}{\partial x_j}\right)+C_\theta\frac{\partial}{\partial x_j}\left\{\sigma_{\overline{u_k u_\ell}}d_k n_\ell e_j[1-f_w(28)]^{\frac{1}{2}}\sqrt{k}\;k_\theta[f_w(28)]^{\frac{1}{2}}\right\}, \tag{5.32}$$

where $C_\theta=0.1$ and $\sigma_h^*=1.8/\left[1+0.5f_w(28)\right]$, and d_k, n_ℓ and e_j are unit vectors in the stream-wise, wall-normal and x_j directions, respectively and $\sigma_{\overline{u_k u_\ell}}$ is a sign function, first introduced by Nagano and Tagawa (1990b). The sign function $\sigma_{\overline{u_k u_\ell}}$ is necessary to make a model independent of a coordinate system, which is defined as

$$\sigma_x=\begin{cases}1 & (x\geq 0),\\ -1 & (x<0).\end{cases} \tag{5.33}$$

5.4 Discussion of predictions with proposed models

In general, a turbulence model must give a prediction of great precision for both fundamental internal and external flows. For instance, if the model predicting does not indicate good agreement with both cases, the model obtains a no-confidence prediction and can hardly predict complex flows of technological interest. In this study, the modeling takes into account full turbulence quantities and these budgets obtained by DNS results, so that we confirm the precision of model prediction in basically both fields. Then, we assess the proposed model performance in flow fields under different thermal conditions at the wall for turbulent quantities and these budgets.

The numerical technique used are a finite-volume method in the wall-bounded flows. Full details of the present numerical method of solution are given in Hattori and Nagano(1995).

In this Chapter, the boundary conditions are: $\bar{U}_w = k_w = k_{\theta w} = 0$, $\varepsilon_w = 2\nu(\partial\sqrt{k}/\partial y)^2$, $\varepsilon_{\theta w} = 2\alpha(\partial\sqrt{\Delta k_\theta}/\partial y)^2$ and $\bar{\Theta}_w$ or q_w are determined by experimental or DNS data at a wall, $\partial\bar{U}/\partial y = \partial k/\partial y = \partial\varepsilon/\partial y = \partial\bar{\Theta}/\partial y = \partial k_\theta/\partial y = \partial\varepsilon_\theta/\partial y = 0$ at the axis for internal flows (symmetry); $\bar{U} = \bar{U}_e$, $k = \varepsilon = k_\theta = \varepsilon_\theta = 0$ and $\bar{\Theta} = \bar{\Theta}_e$ at the outside boundary layer where $\bar{U}_e$ and $\bar{\Theta}_e$ are prescribed from experiments. The computations were performed on a PC personal computer and a DEC Alpha Work Station.

5.4.1 Channel flow with heat transfer (constant heat-flux wall and constant temperature wall)

It is important to predict the velocity field precisely for relevant temperature field prediction. The framework of the proposed k–ε model is based on the NS model, which has been confirmed to show highly accurate prediction of the wall-bounded turbulent flows (Nagano & Shimada 1995a). In this study, however, the wall-reflection function is corrected on the model, so that the model is tested in the channel flow calculated under both DNS conditions of Moser *et al.* (1999) ($Re_\tau = 395$) and of Kasagi *et al.* (1992) ($Re_\tau = 150$) shown in Fig. 5.6. From Fig. 5.6, it can be seen that the mean velocity and turbulence energy are quite successfully predicted for both cases.

Next, we assess the constructed two-equation heat-transfer model with the k–ε model in a fully developed channel flow under both constant temperature (Kim & Moin 1989) ($Re_\tau = 180$

and Pr=0.71) and constant heat-flux wall conditions (Kasagi *et al.* 1992) ($Re_\tau = 150$ and Pr=0.71). Comparisons of the predicted mean temperature, turbulent heat-flux and temperature variance with DNS are shown in Fig. 5.7(a), 5.7(b) and 5.7(c), respectively. The model predictions are in almost perfect agreement with the DNS data. As shown Figs. 5.8(a) and 5.8(b), the model predictions reproduce exactly the wall limiting behaviour of temperature variance and turbulent heat-flux near the wall for both thermal wall conditions, i.e., $\theta_w = 0$ and $\theta_w \neq 0$. Figures 5.9 and 5.10 show the predicted budget of temperature variance and of its dissipation-rate, compared with the DNS data. Obviously, agreement of each term in both budgets with DNS is also very good. An important point of the present study is the modeling for turbulent diffusion term T_{k_θ} in the k_θ–equation. From a comparison of Fig. 5.5 with 5.9, the calculated budget of the proposed model is seen to improve over previous models near the wall ($y^+ < 15$). These facts indicate that the modeling of a gradient-type diffusion plus convection by large-scale motions is effective for the turbulent diffusion term, and that the proposed modeling is appropriate for construction of a set of heat-transfer models.

5.4.2 Boundary layer flows with uniform temperature or uniform heat-flux wall

In the following, we assess the present two-equation heat transfer model in boundary layer flows under different thermal conditions. The most basic situations encountered are the heat transfer from a uniform temperature or uniform heat-flux wall. The results of thermal-field calculations under the constant wall temperature or the constant wall heat-flux condition along a flat plate compared with experimental data of Gibson *et al.* (1982) (uniform temperature wall) and of Antonia *et al.* (1977) (uniform heat-flux wall), are shown in Fig. 5.11. It is known that the NTT model for reference gives good prediction of turbulent thermal fields under these wall thermal conditions (Youssef *et al.* 1992), and the present predictions also indicate good agreement with the experimental data.

5.4.3 Constant wall temperature followed by adiabatic wall

The next test case for which calculations have been performed is concerned with a more complex thermal field in a boundary layer along a uniformly heated wall followed by an adi-

abatic wall. Figure 5.12 shows a comparison of the predicted results with the experimental data (Reynolds *et al.* 1958) of temperature differences between the wall and the free-stream $\Delta\bar{\Theta}(=\bar{\Theta}_e-\bar{\Theta}_w)$. It can be seen that the proposed model gives generally good predictions for the rapidly changing thermal field. And the present model gives no prediction inferior to the AKN model (Abe *et al.* 1995) for comparison.

5.4.4 Constant heat flux followed by adiabatic wall

To further verify the effectiveness of the present model for calculating various kinds of turbulent thermal fields, we have carried out the calculation of a boundary layer flow along a uniform heat-flux wall followed by an adiabatic wall, which has been reported by Subramanian-Antonia (1981a) in detail. The calculated distributions of rms temperature fluctuations normalized by temperature difference between free-stream and wall, $\Delta\bar{\Theta}_c$, at a step change in surface thermal condition, are shown in Fig. 5.13, compared with the experimental data (Subramanian & Antonia 1981a) and the prediction of AKN model. Both models indicate a slight underprediction for the peak value of rms temperature. The proposed model, however, shows the variation of physical phenomena of rms temperature in the thermal layer along a uniform heat-flux followed by adiabatic wall. Especially, a rapid decrease in fluctuation of temperature from the inner region has been captured by the proposed model.

As shown in the foregoing, the proposed model accurately reproduces a distribution of temperature and of rms temperature in arbitrary wall thermal conditions.

5.4.5 Double-pulse heat input

As a final test case, we have calculated more complex heat transfer, where heat input is intermittent in a double-pulse manner. Then we have investigated the mechanism of turbulent heat transfer in such a rapidly changing thermal layer.

The temperature difference between free-stream and wall, $\Delta\bar{\Theta}=\bar{\Theta}_w-\bar{\Theta}_e$, and the Stanton number reported by Reynolds *et al.* (1958), are shown in Fig. 5.14 compared with the prediction of the present model. It is indicated that both the velocity and the thermal fields are well predicted, and the turbulent heat transfer characteristics in the thermal entrance region are reproduced very well. Figure 5.15(a) shows how a wall turbulent thermal layer changes when

heat input is intermittent, in which $\Delta T = \bar{\Theta} - \bar{\Theta}_e$ is normalized by the temperature difference between the wall and free-stream $\Delta\bar{\Theta}_c = \bar{\Theta}_{wc} - \bar{\Theta}_e$ just before the first heat-input/cut-off point. It can be seen that a very abrupt decrease and increase in mean fluid-temperature occur in the wall region, which is the consequence of no heat-input condition followed by heat input, i.e., $\partial\bar{\Theta}/\partial y|_w = 0 \rightarrow \partial\bar{\Theta}/\partial y|_w = \text{constant}$. Within a short distance from the discontinuity point, the mean temperature profile becomes uniform over most of the thermal layer. The following discussion deals with how these phenomena affect other turbulent quantities. Figure 5.15(b) shows distribution of turbulent heat-flux normalized by u_τ and $\Delta\bar{\Theta}_c$. At just after the first heat-input/cut-off point, with vanishing the mean temperature gradient near the wall, the turbulent heat-flux $\overline{v\theta}$ decreases rapidly. Then just before the second heat-input point, $\overline{v\theta}$ remains a little in the outer layer only. At the reheated wall, $\overline{v\theta}$ shows again a quick increase near the wall. This is qualitatively consistent with the experiment result (Antonia *et al.* 1977) for thermal entrance region of boundary layer on a flat plate.

Next, variations of the rms temperature are shown in Fig. 5.15(c). Just after the heat cut-off point, distributions of the rms temperature tend to be similar to the experimental evidence obtained by Subramanian & Antonia (1981a) discussed in the previous section. It can be seen that just before the second heat-input point the rms temperature remains in the outer region only, and it increases very rapidly near the wall after that point. Figures 5.16(a)–(d) show budgets of temperature variance at locations just before the first heat cut-off ($x = 0.517$ m), just after the heat cut-off ($x = 0.579$ m), just before the second heat-input ($x = 0.876$ m) and just after the second heat-input ($x = 0.936$ m), respectively. In these figures, each term is normalized by the peak value of the production P_{k_θ} at the respective locations. Since the mean temperature gradient vanishes near the wall as shown in Fig. 5.15(a) at x=0.579 m, the peak value of the production term tends to increase in the outer region and the rapidly decreasing temperature fluctuation is restrained by an increase of the convective term there. Accordingly, the fluctuating temperature is transported actively by the turbulent diffusion from the outer to wall region, though the dissipation also increases away from the wall. Since the molecular diffusion and the dissipation preserve the near-wall structure and no temperature fluctuation is yielded by the mean temperature gradient, the temperature fluctuation is virtually non-existent just before the second heat-input point as shown in Fig. 5.15(c). From the above-mentioned, after the first cut-off point, it is understandable that the near-wall structure of thermal turbulence is preserved

mainly by diffusion from the outer to inner region, and the temperature fluctuation decreases remarkably. Then, just after the second heat-input point, the near-wall profile of temperature fluctuation returns to the unperturbed initial profile rapidly. The remaining fluctuation in the outer region does not participate in the re-production. Since the proposed model is rigorously constructed by considering the budget profiles of turbulence quantities obtained by DNS, we may expect that the model could be used to investigate the detailed mechanism of heat transfer in complex applications, as illustrated in this section.

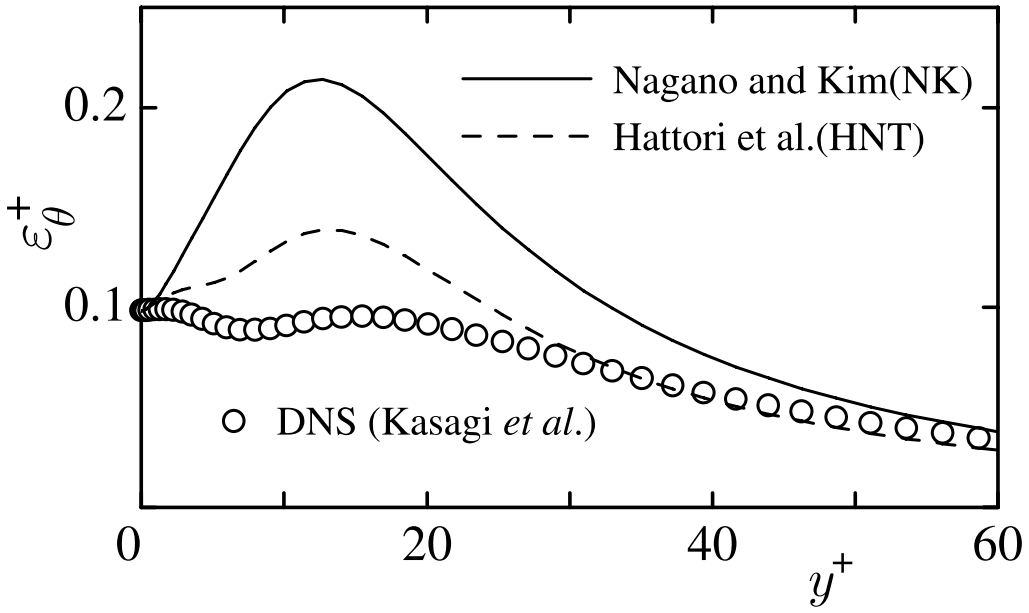

(a)

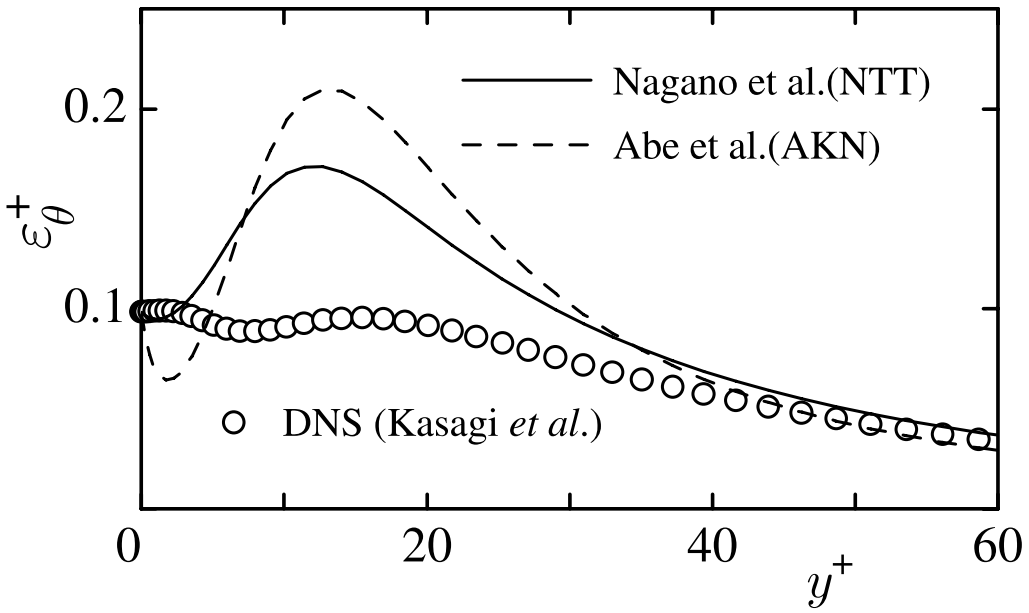

(b)

Figure 5.1: Assessment of $\widetilde{\varepsilon}_\theta$– and ε_θ–equations: (a) $\widetilde{\varepsilon}_\theta$–equations ($\varepsilon_\theta = \widetilde{\varepsilon}_\theta + \widehat{\varepsilon}_\theta$) at a two-equation level; (b) ε_θ–equations at a two-equation level; (c) $\widetilde{\varepsilon}_\theta$– and ε_θ–equations at a second-order closure level

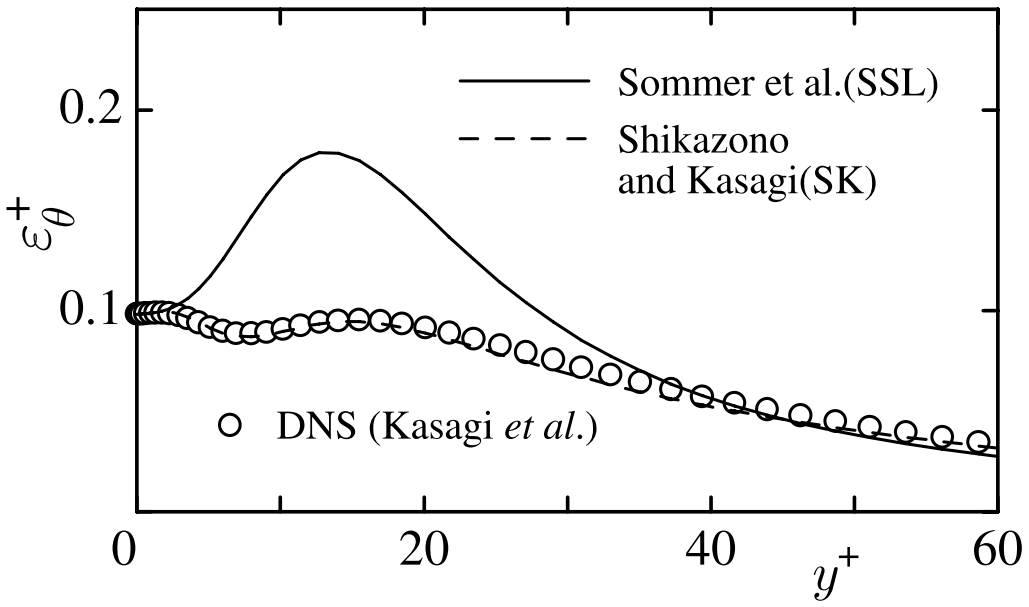

(c)

Figure 5.1: (continued)

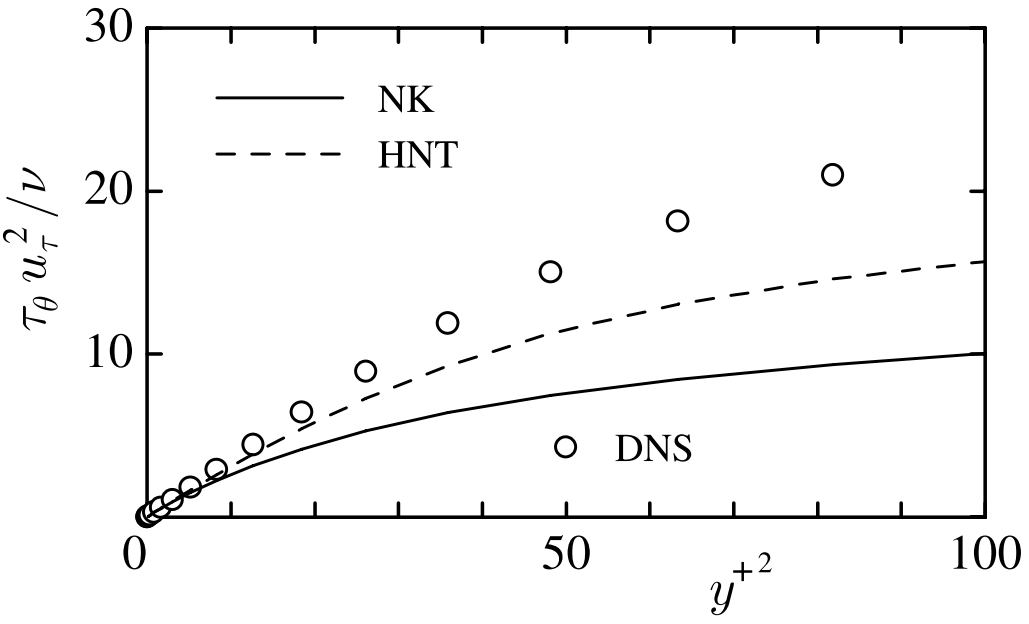

(a)

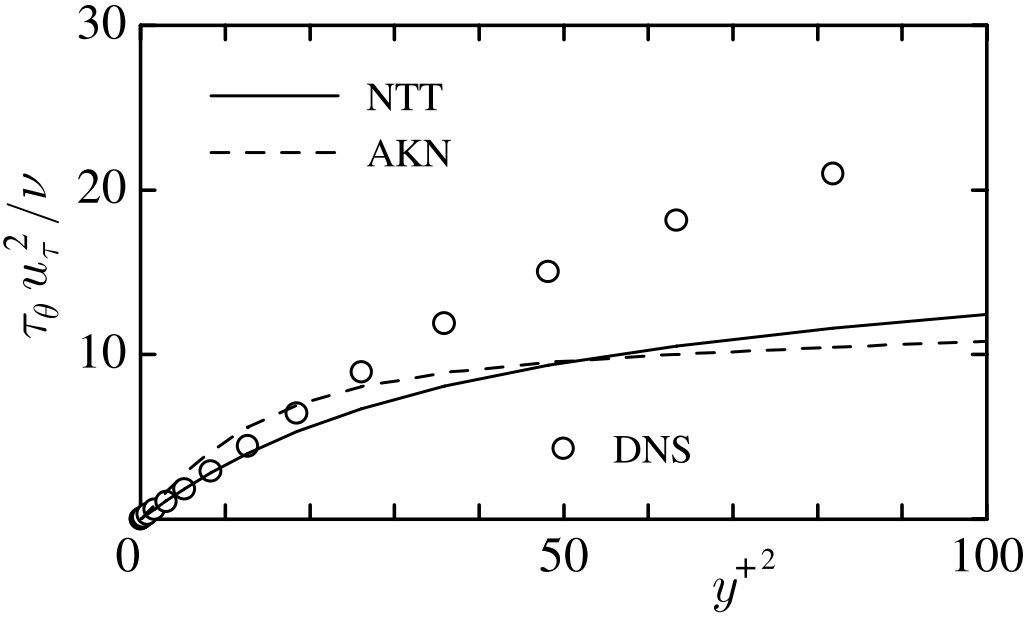

(b)

Figure 5.2: Profiles of time scale τ_θ: (a) In $\widetilde{\varepsilon}_\theta$–equations at a two-equation level; (b) In ε_θ–equations at a two-equation level; (c) In $\widetilde{\varepsilon}_\theta$– and ε_θ–equations at a second-order closure level

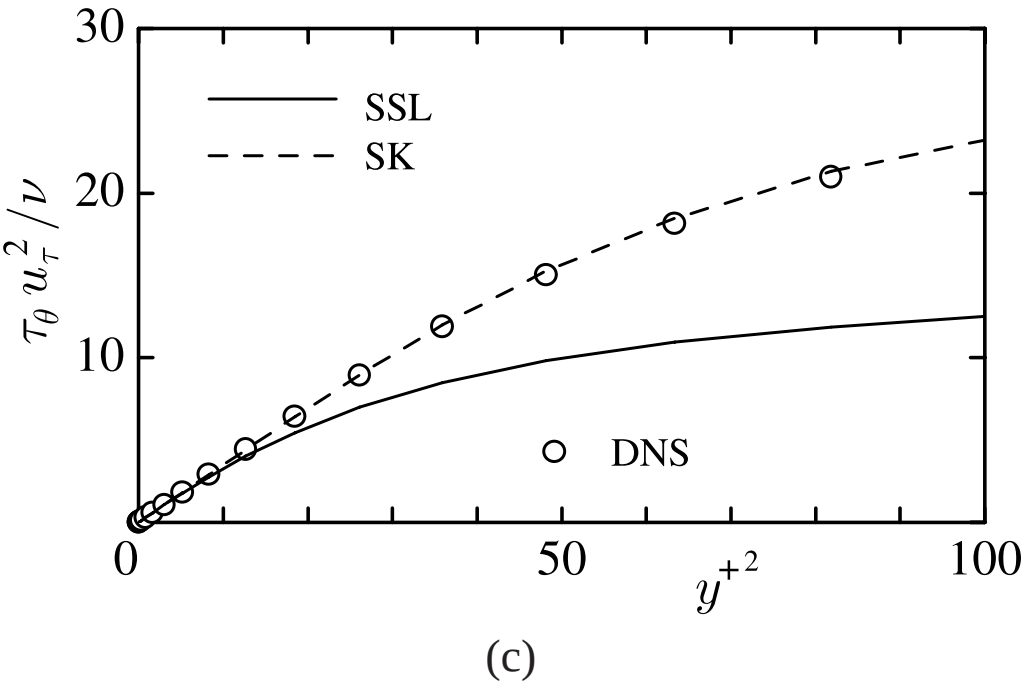

(c)

Figure 5.2: (continued)

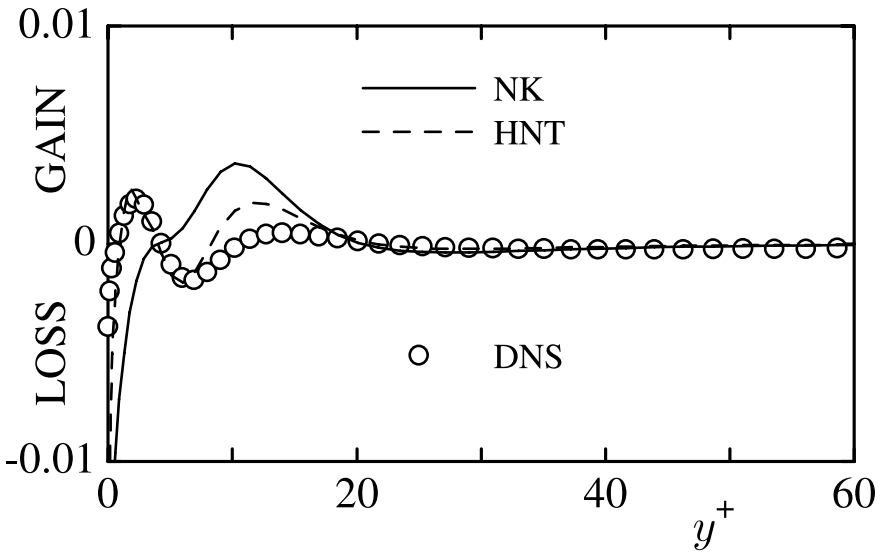

(a)

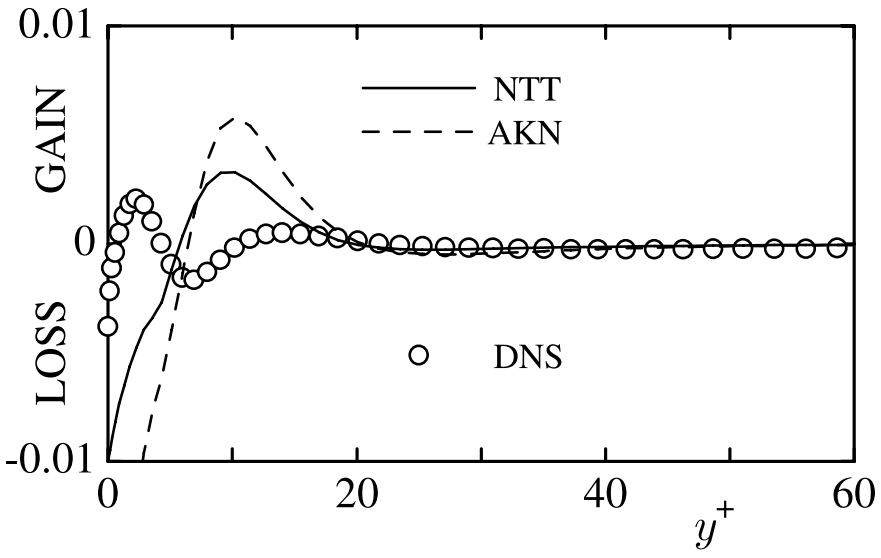

(b)

Figure 5.3: Budgets of modeled $\widetilde{\varepsilon_\theta}$–equations ($P^1_{\widetilde{\varepsilon_\theta}}+P^2_{\widetilde{\varepsilon_\theta}}+P^3_{\widetilde{\varepsilon_\theta}}+P^4_{\widetilde{\varepsilon_\theta}}+T_{\widetilde{\varepsilon_\theta}}-\Upsilon_{\widetilde{\varepsilon_\theta}}$) and ε_θ–equations ($P^1_{\varepsilon_\theta}+P^2_{\varepsilon_\theta}+P^3_{\varepsilon_\theta}+P^4_{\varepsilon_\theta}+T_{\varepsilon_\theta}-\Upsilon_{\varepsilon_\theta}$): (a) Two-equation level $\widetilde{\varepsilon_\theta}$–equations; (b) Two-equation level ε_θ–equations; (c) Second-order closure level $\widetilde{\varepsilon_\theta}$– and ε_θ–equations

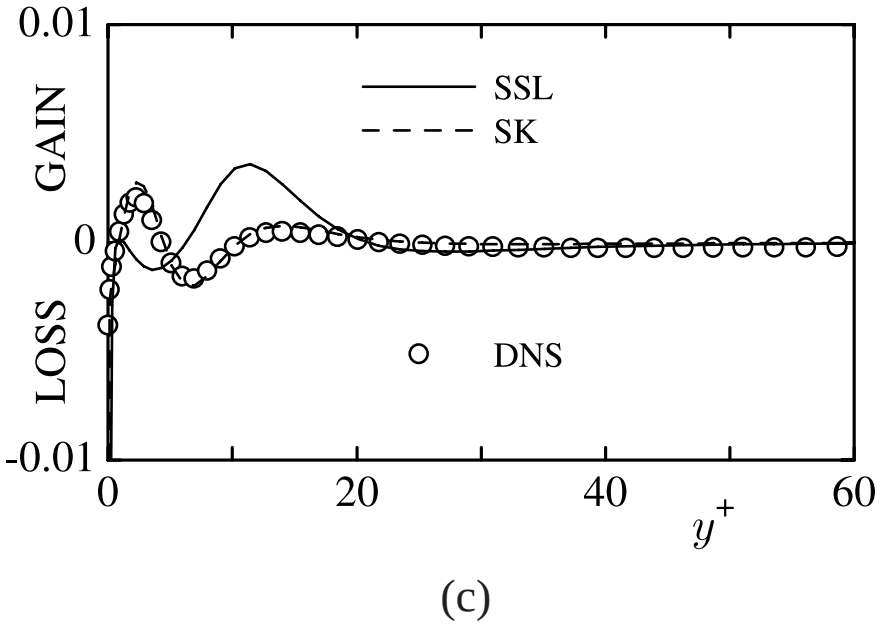

(c)

Figure 5.3: (continued)

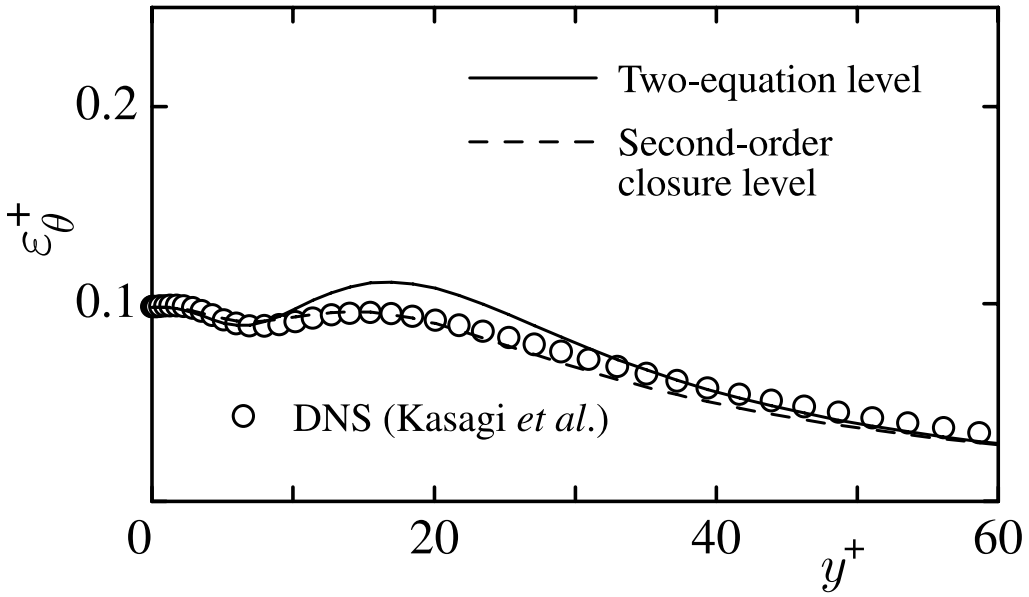

(a)

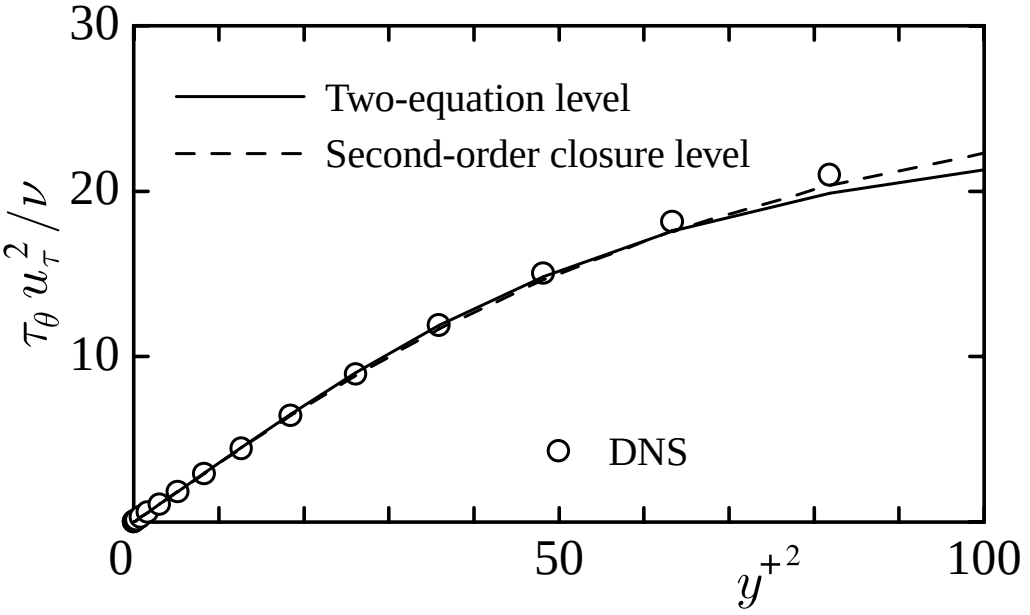

(b)

Figure 5.4: Assessment of the proposed ε_θ–equation models: (a) Profiles of ε_t near the wall; (b) Profiles of time scale τ_θ near the wall; (c) Budget of the proposed ε_θ–equation models ($P^1_{\varepsilon_\theta} + P^2_{\varepsilon_\theta} + P^3_{\varepsilon_\theta} + P^4_{\varepsilon_\theta} + T_{\varepsilon_\theta} - \Upsilon_{\varepsilon_\theta}$)

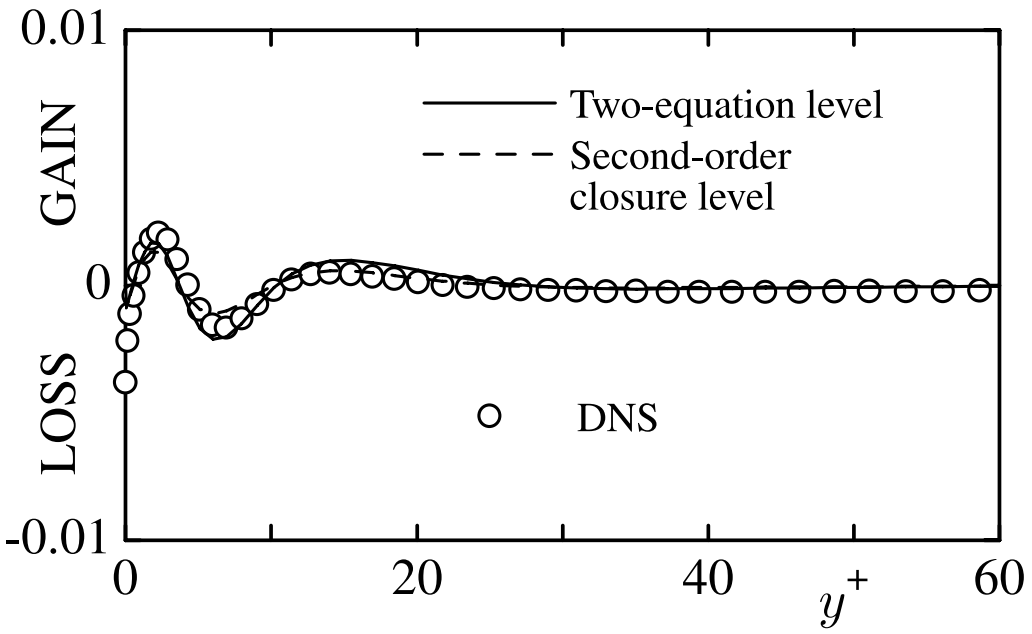

(c)

Figure 5.4: (continued)

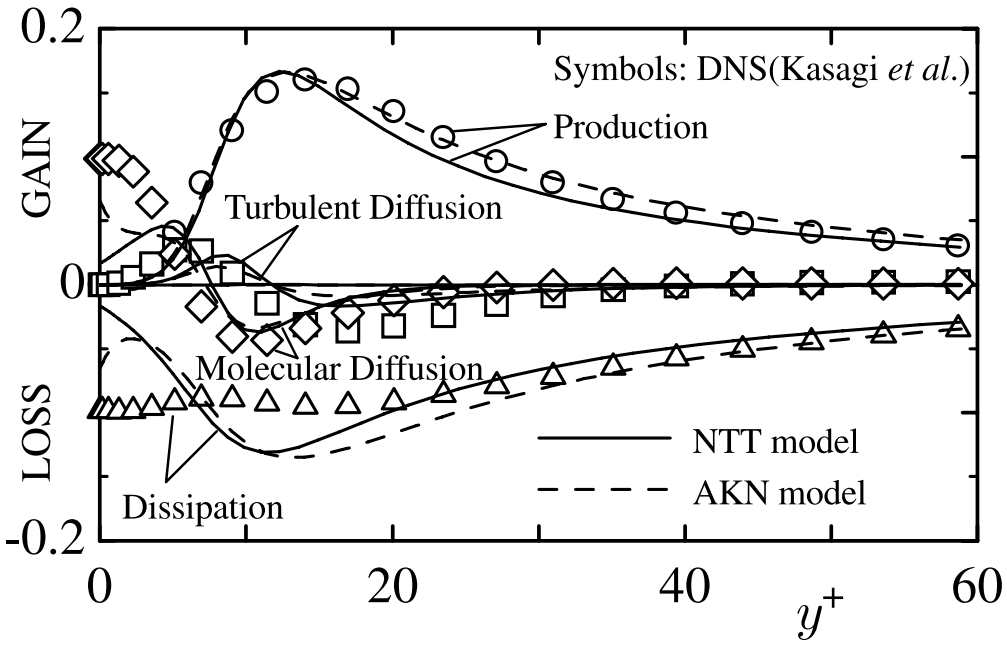

Figure 5.5: Budget of temperature variance k_θ

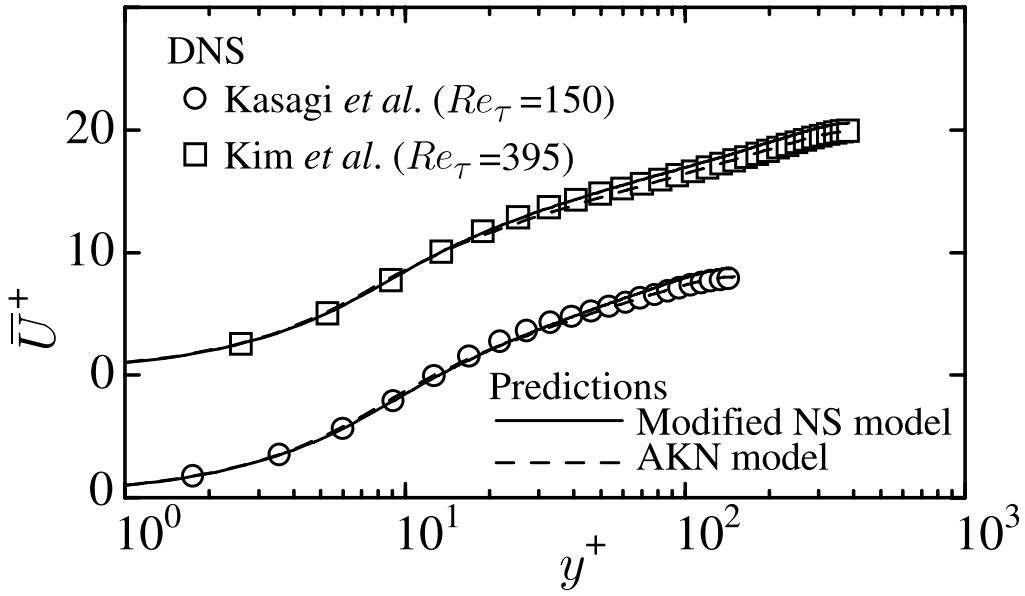

(a)

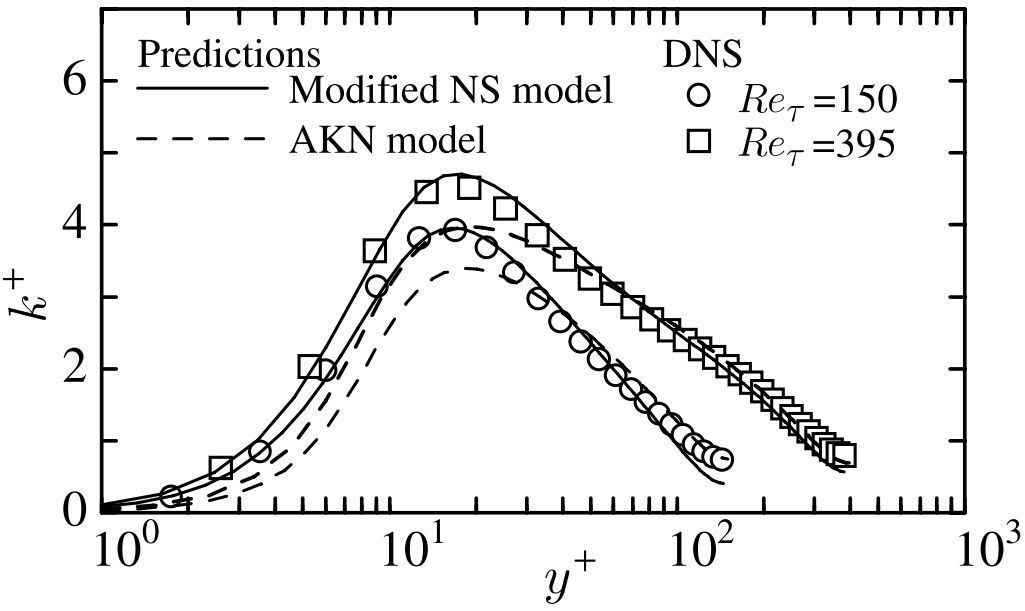

(b)

Figure 5.6: Channel flow predictions: (a) Mean velocity; (b) turbulence energy

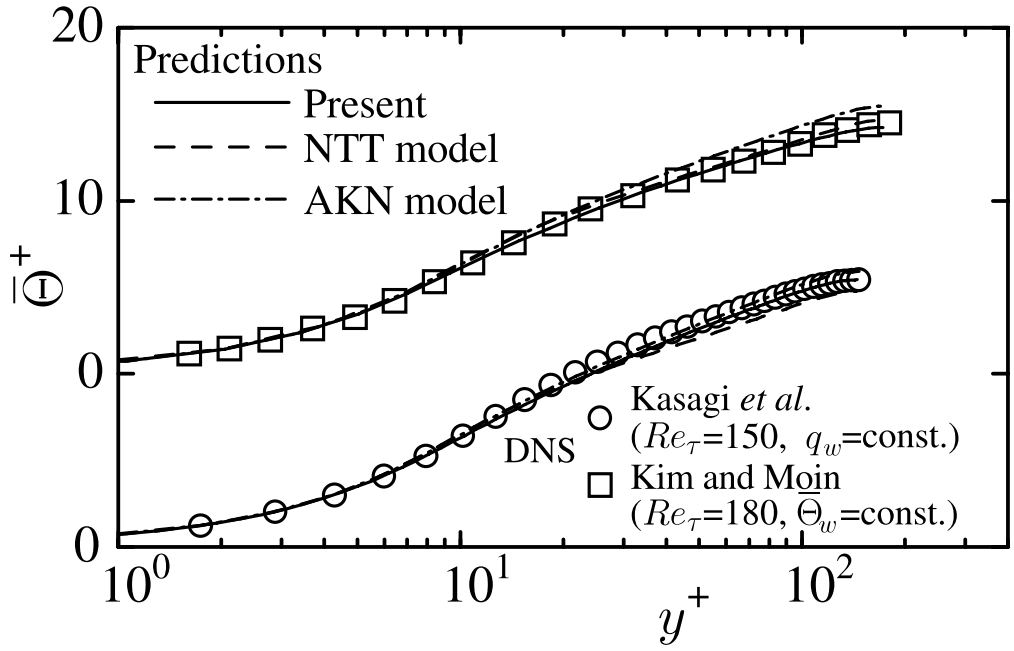

(a)

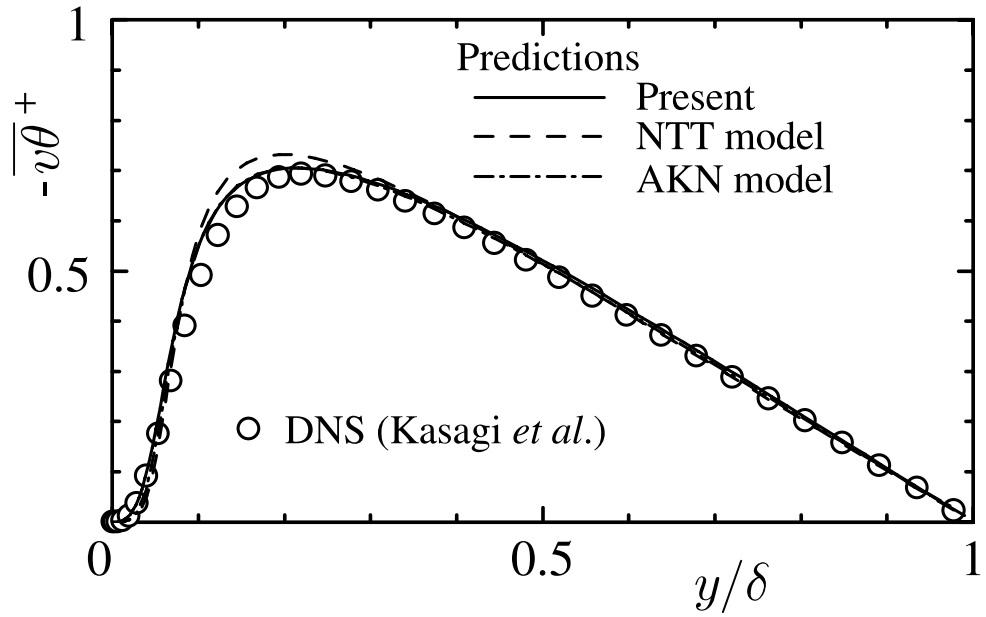

(b)

Figure 5.7: Thermal field predictions in channel flow: (a) Mean temperature; (b) Turbulent heat-flux; (c) Temperature variance

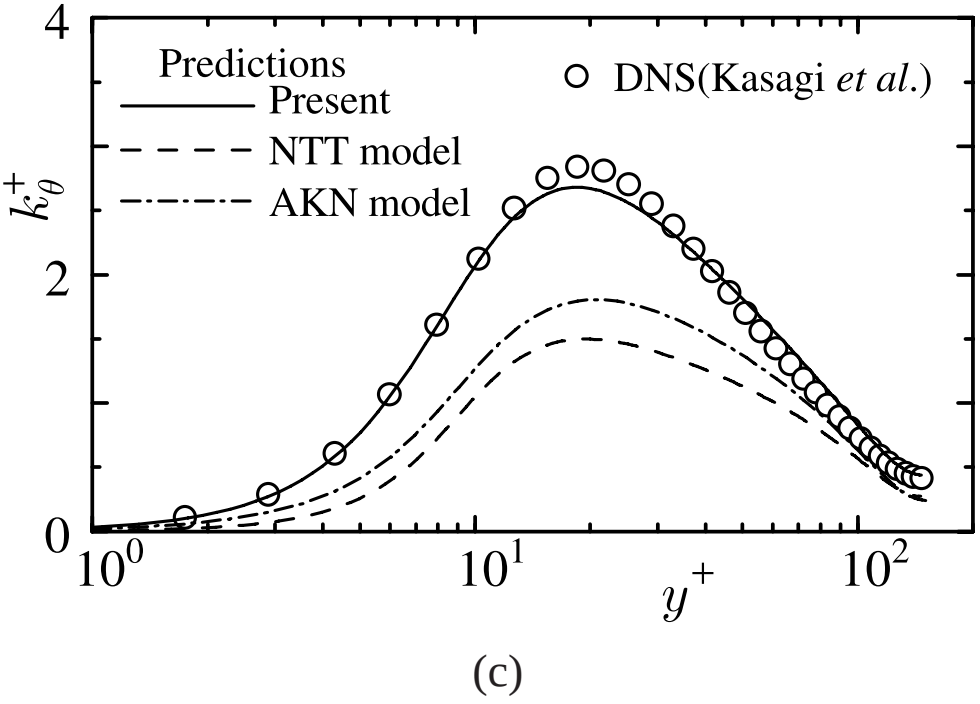

Figure 5.7: (continued)

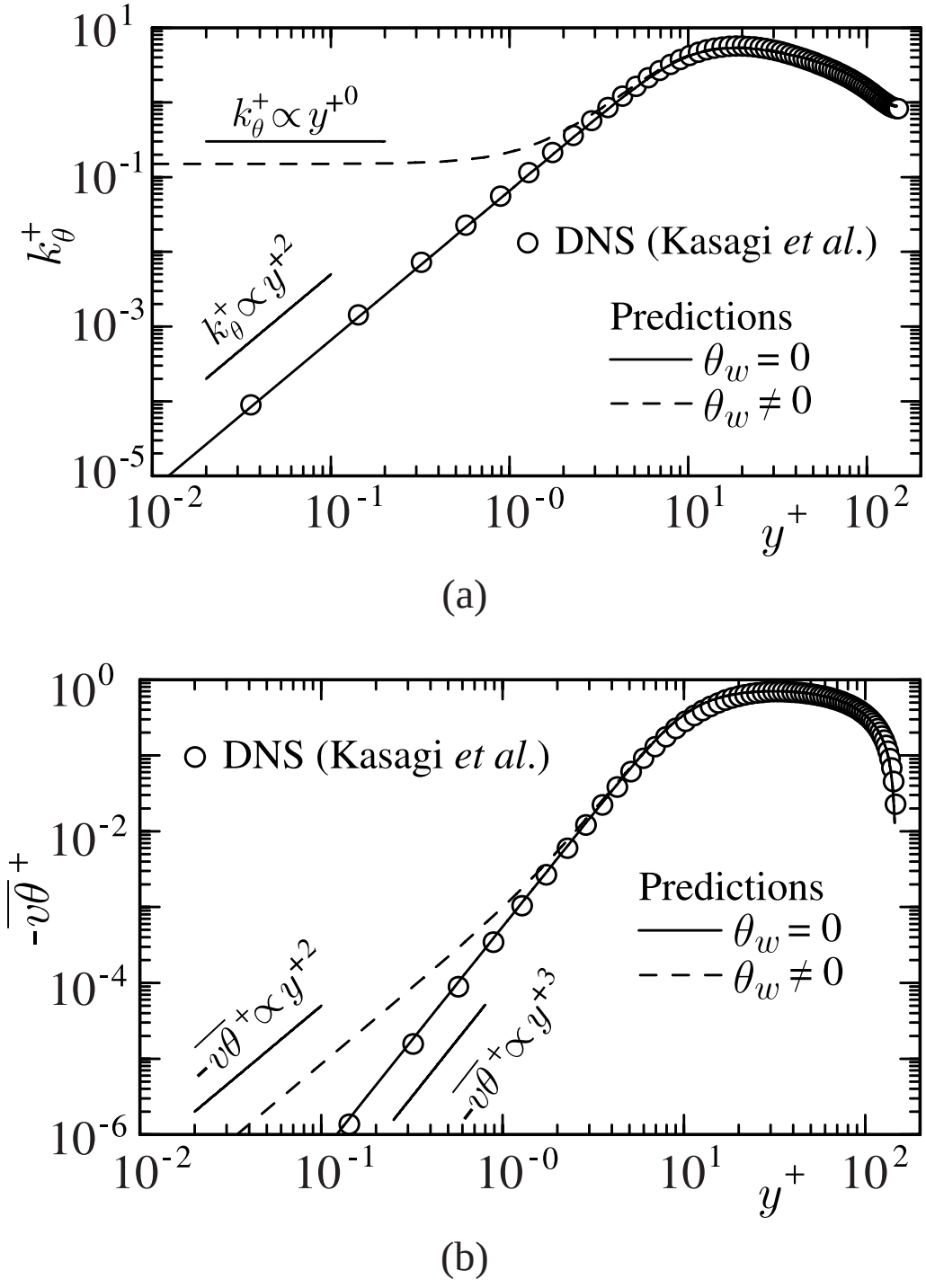

Figure 5.8: Near-wall behaviour of turbulence quantities: (a) Temperature variance; (b) Turbulent heat-flux

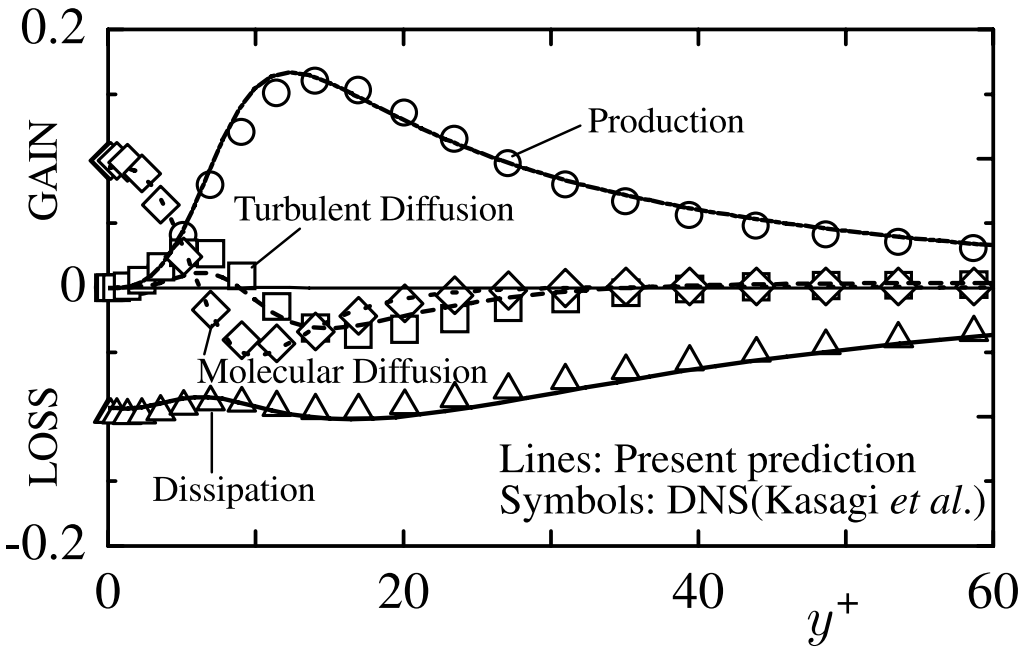

Figure 5.9: Budget of temperature variance in channel flow

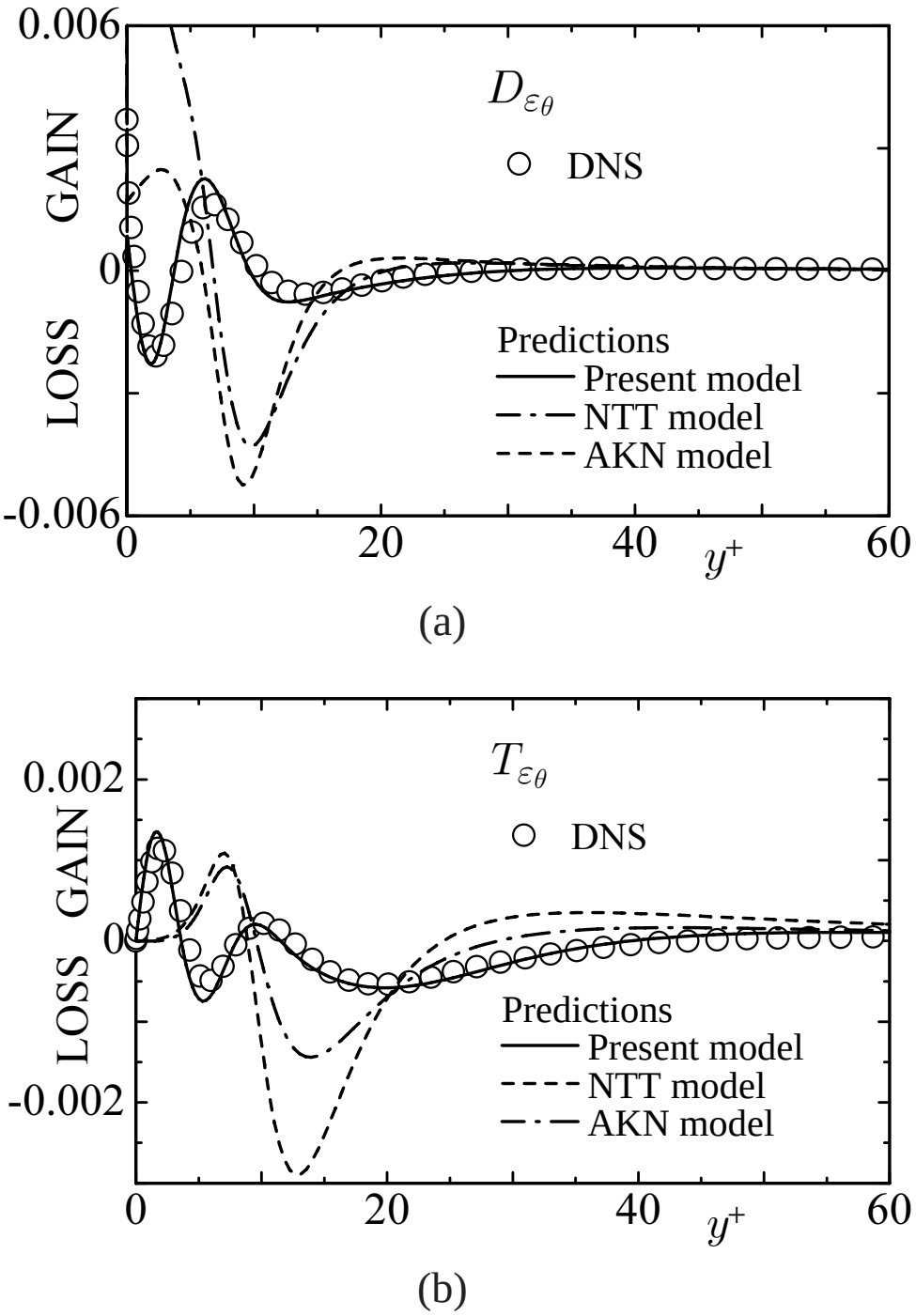

Figure 5.10: Calculated budget of ε_θ in channel flow: (a) Molecular diffusion; (b) Turbulent diffusion; (c) Gradient production; (d) Production + destruction

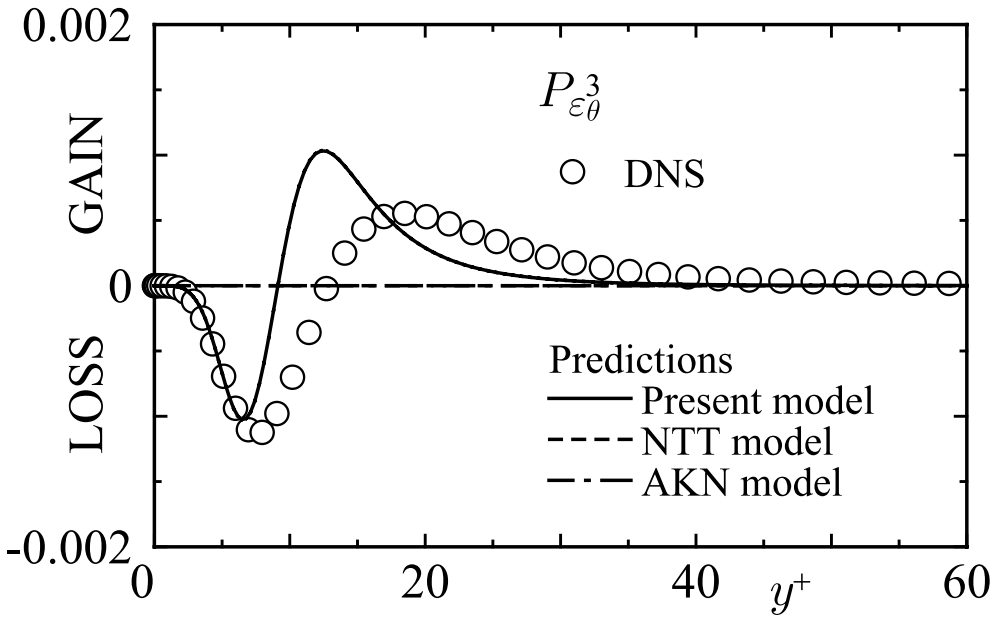

(c)

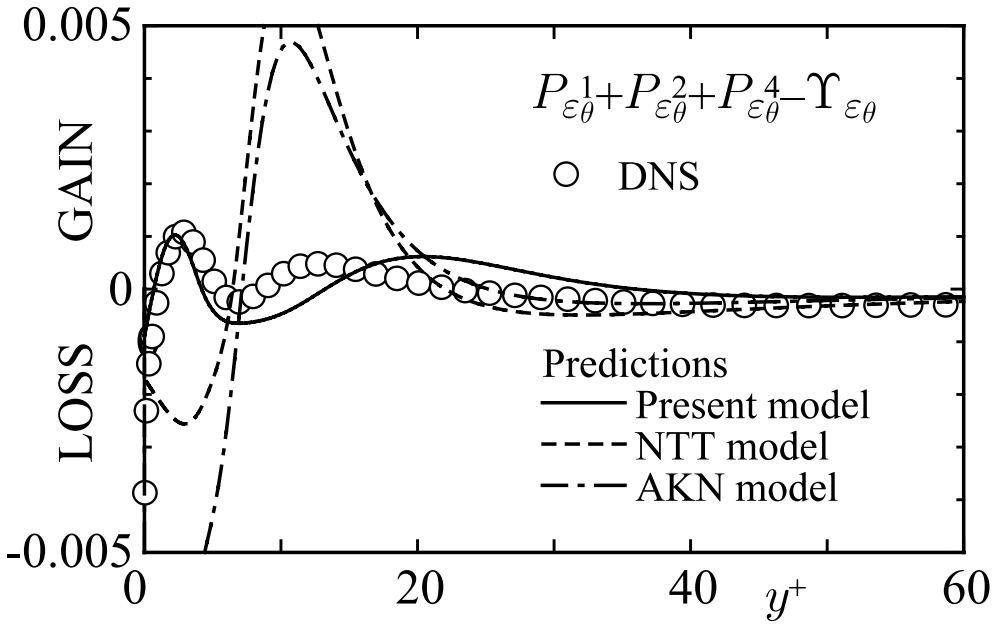

(d)

Figure 5.10: continued

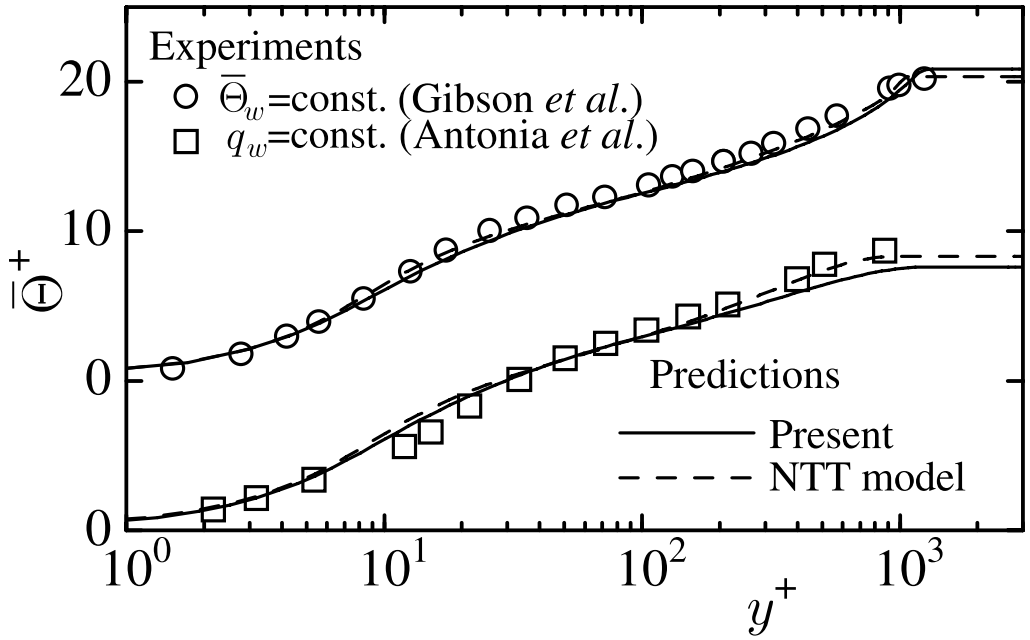

(a)

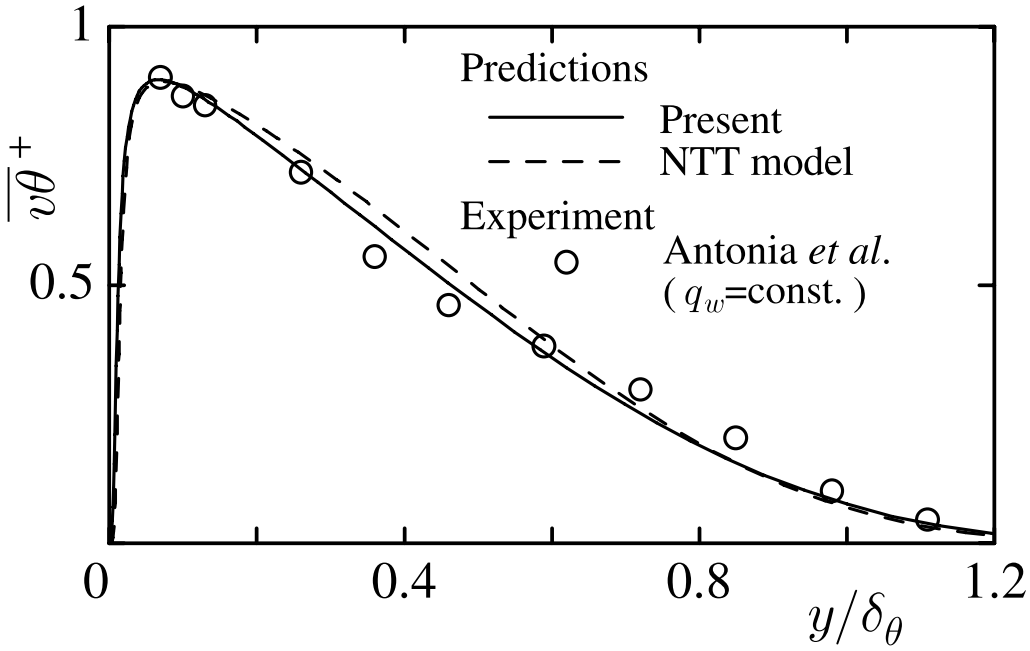

(b)

Figure 5.11: Profiles of turbulent quantities in a boundary layer: (a) Mean temperature; (b) Turbulent heat-flux; (c) Rms temperature

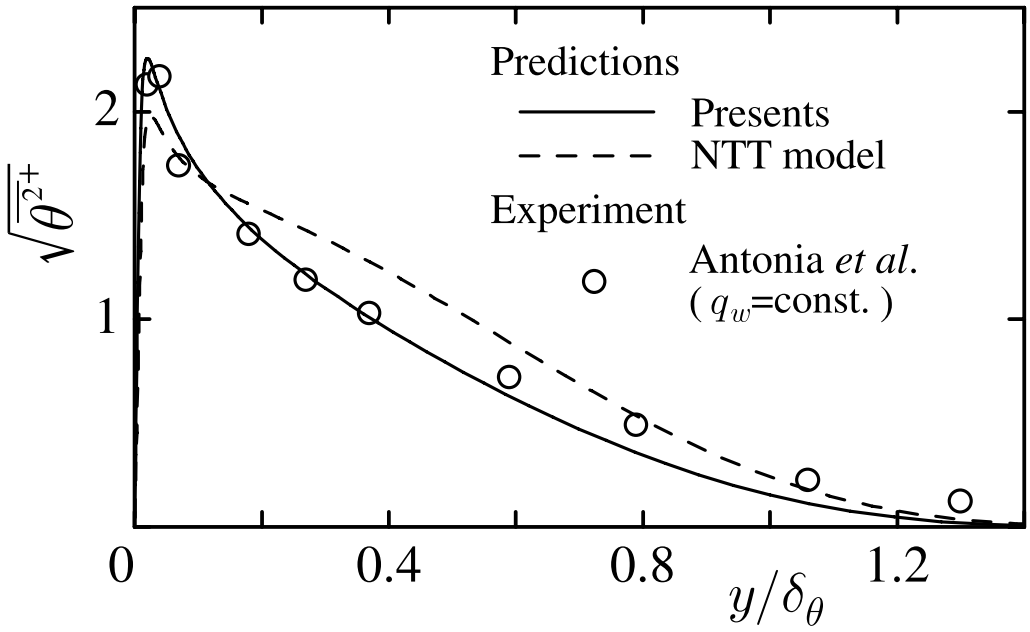

(c)

Figure 5.11: (continued)

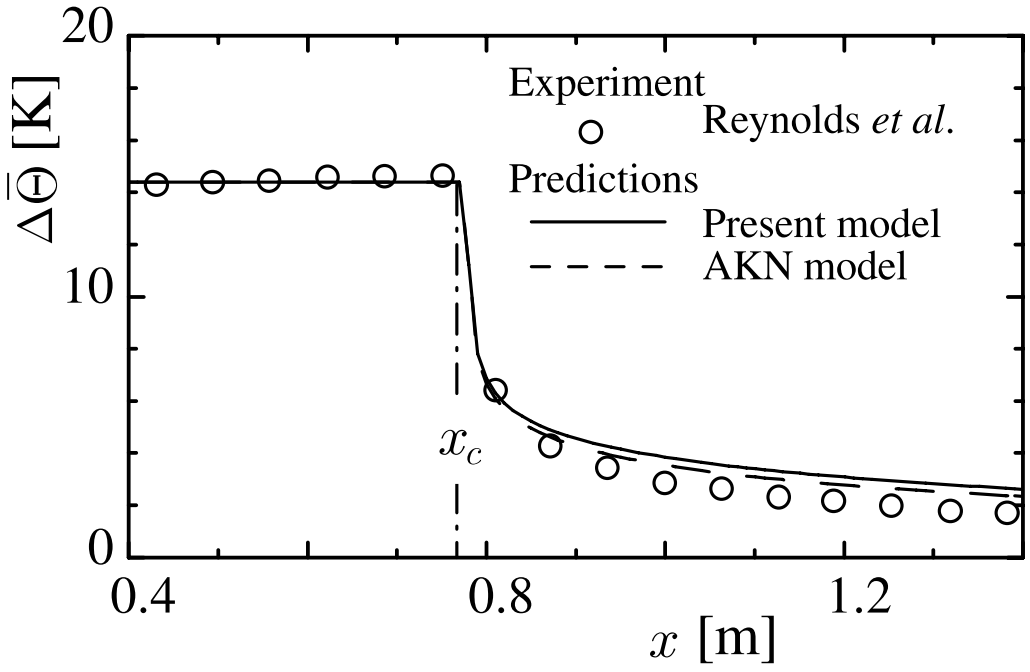

Figure 5.12: Comparison of the predicted variations of wall temperature with the measurement

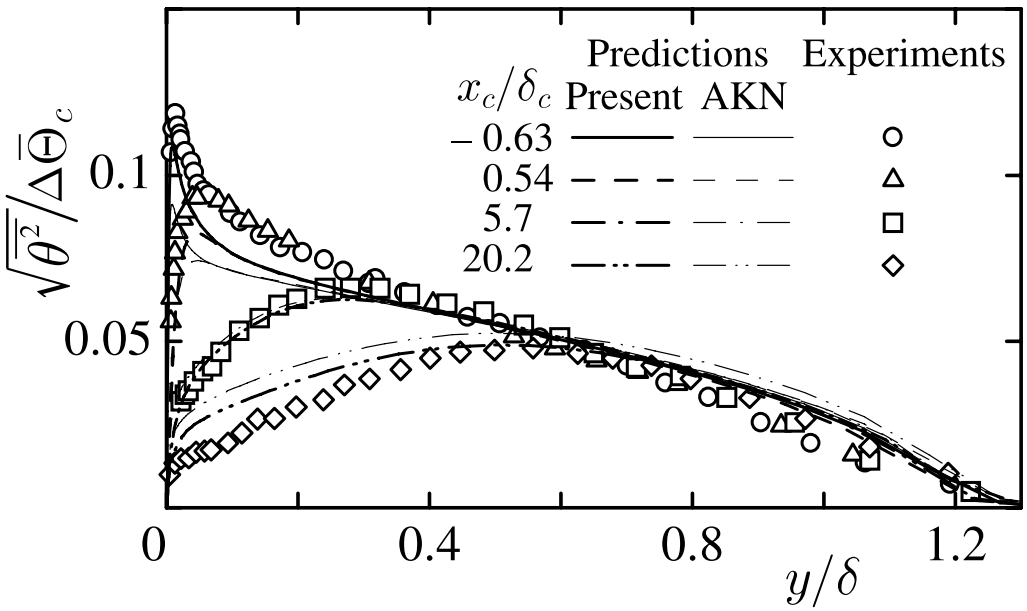

Figure 5.13: Comparison of the predicted rms temperature profiles and measurements (sudden decrease in wall heat flux)

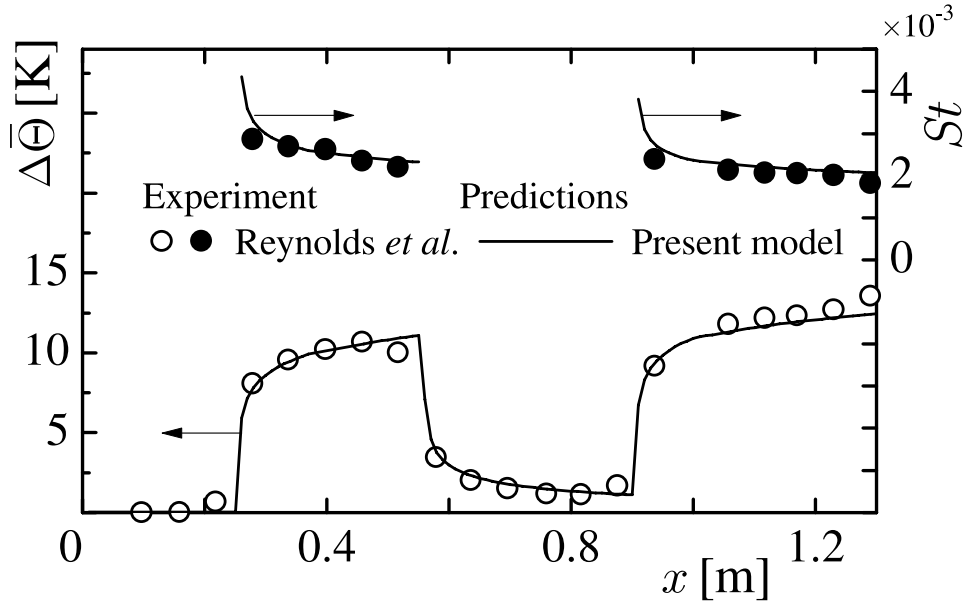

Figure 5.14: Comparison of the predicted variations of wall temperature and Stanton number with the measurements (double-pulse heat input)

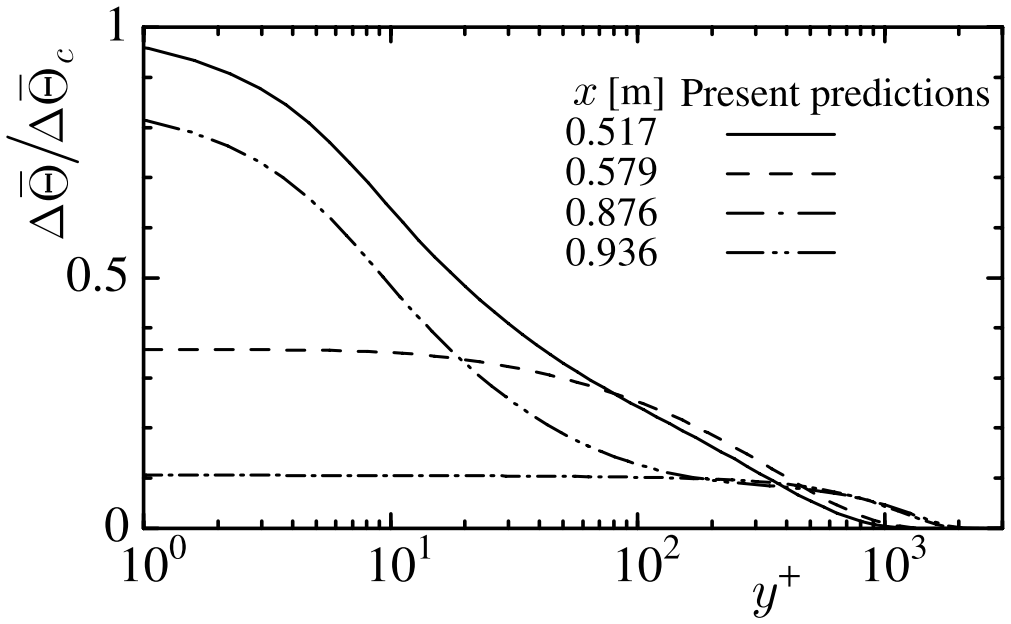

(a)

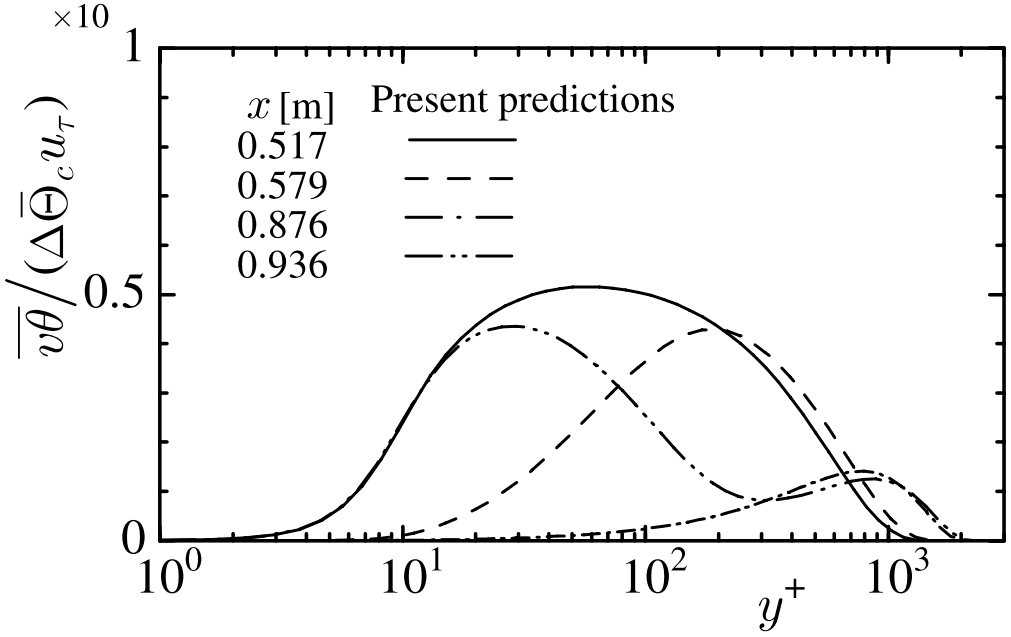

(b)

Figure 5.15: Variations of turbulent quantities for double-pulse heat input: (a) Mean temperature; (b) Turbulent heat-flux; (c) Rms temperature

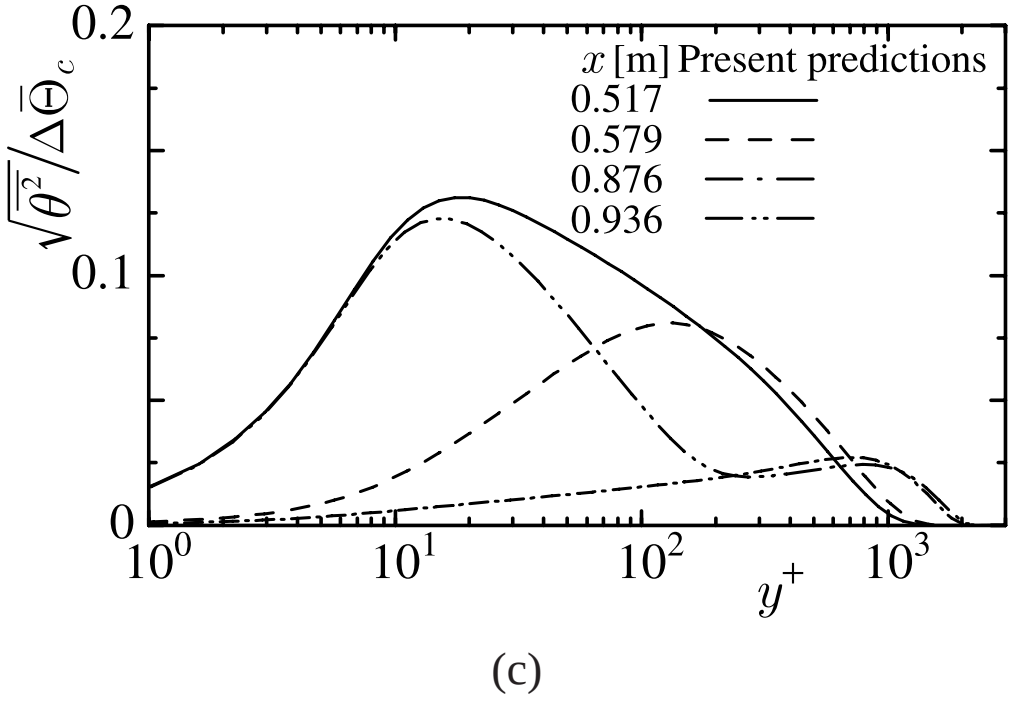

(c)

Figure 5.15: (continued)

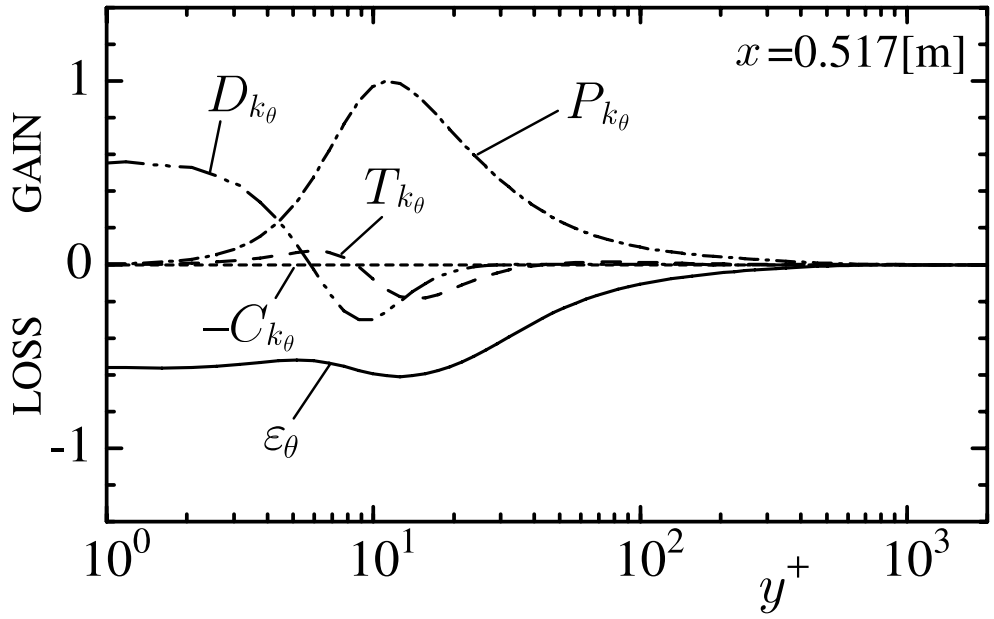

(a)

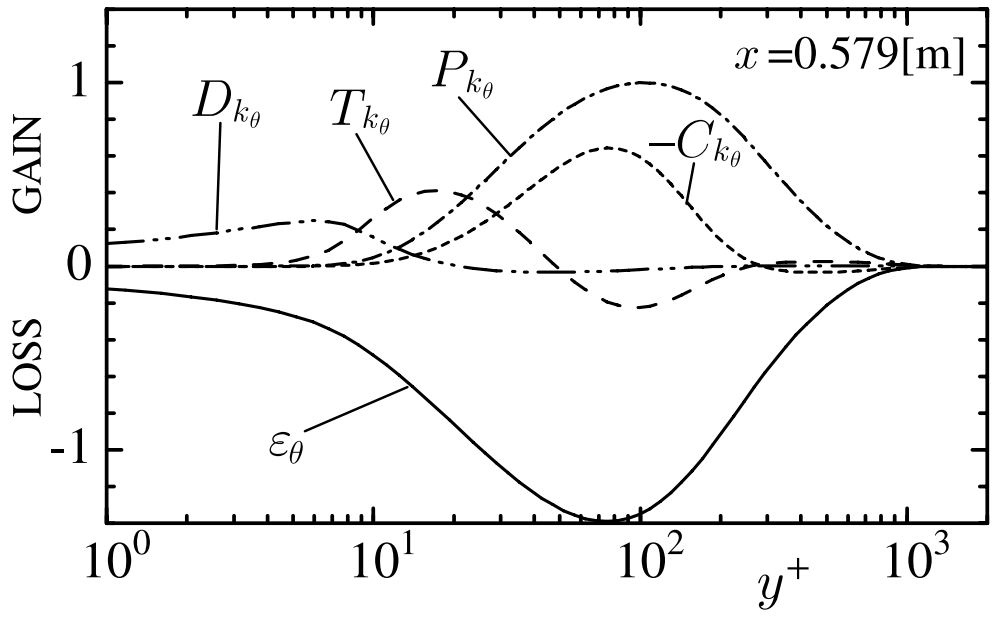

(b)

Figure 5.16: Budget of temperature variance for double-pulse heat input: (a)$x = 0.517$ [m]; (b)$x = 0.579$ [m]; (c)$x = 0.876$ [m]; (d)$x = 0.936$ [m]

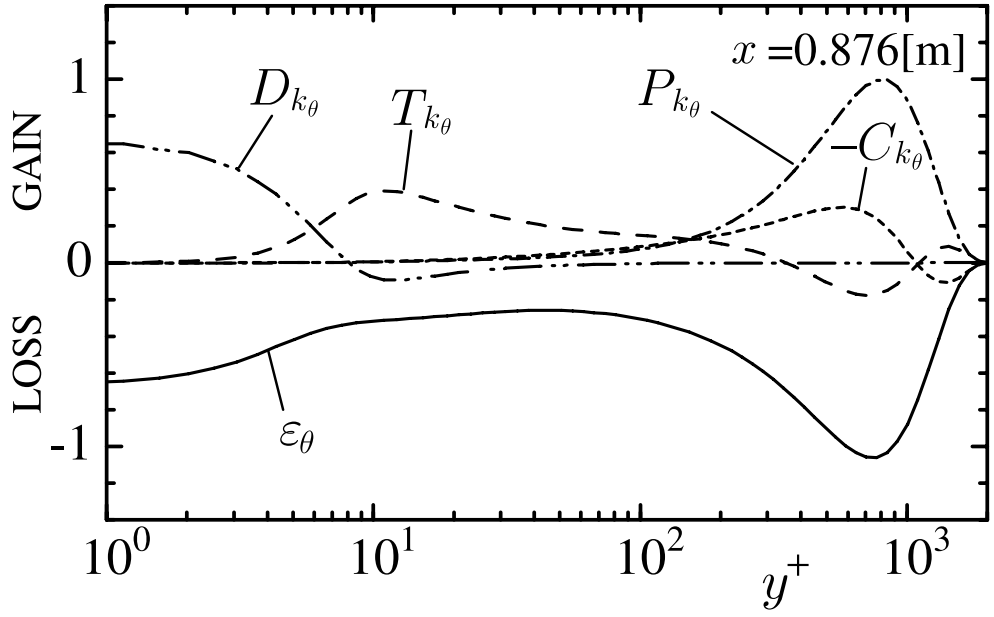

(c)

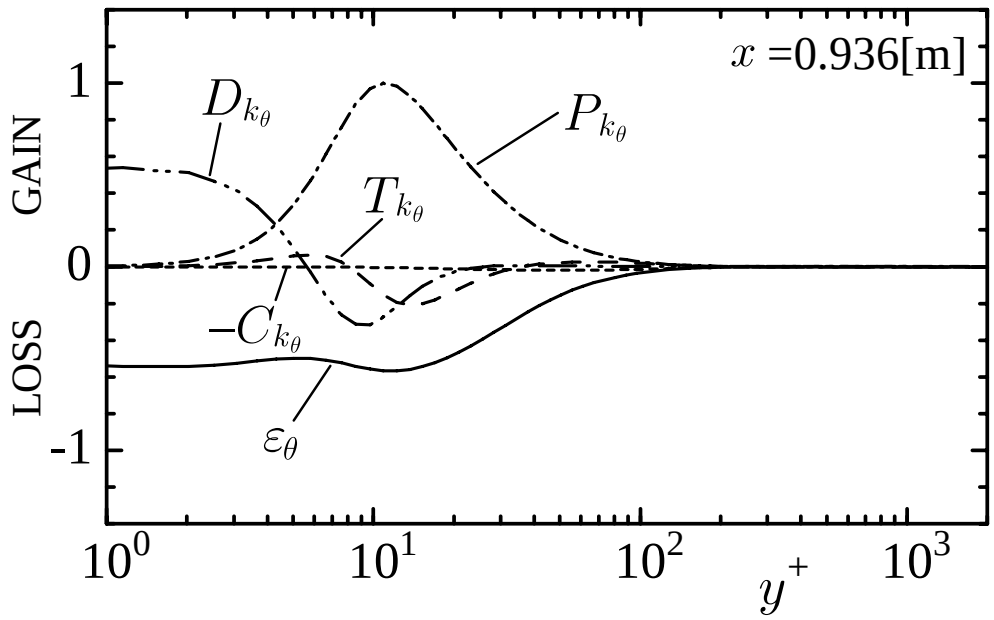

(d)

Figure 5.16: (continued)

CHAPTER 6

Two-layer turbulence model for heat transfer in wall turbulent shear flows

In this Chapter, we propose a new two-layer model, in which both the dissipation rate for turbulent kinetic energy and temperature variance are given in terms of algebraic expressions near the wall based on recent two-equation modeling. The models also take the Prandtl number effects into account according to Nagano & Shimada model (1996). The proposed models are tested in turbulent boundary layer flows with/without pressure gradients, in detaching and reattaching flows and in various Prandtl number flows, and then the model performance is discussed.

6.1 Construction of two-layer model

6.1.1 Two-layer modeling for ε and ε_θ

The two-layer model proposed by Rodi *et al.* (1993) (hereafter referred to as the RMM model) was based on the one-equation model very near the wall, in which two length scales appearing in the relations for the eddy viscosity and dissipation-rate must be prescribed as indicated in Eqs. (1.13) and (1.14). In this study, however, we propose a new two-layer model based on the two-equation model taking modeling for thermal field into account. Thus, modeling of the time scale for eddy viscosity is needed; i.e., the dissipation-rate must be modeled.

We represent ε and ε_θ near the wall with the following conjugate forms:

$$\varepsilon = \widetilde{\varepsilon}_a + D, \tag{6.1}$$

$$\varepsilon_\theta = \widetilde{\varepsilon}_{\theta a} + D_\theta, \tag{6.2}$$

where $D = 2\nu \left[\left(\partial\sqrt{k}/\partial x_j \right) \left(\partial\sqrt{k}/\partial x_j \right) \right]$ and $D_\theta = 2\alpha \left[\left(\partial\sqrt{\Delta k_\theta}/\partial x_j \right) \left(\partial\sqrt{\Delta k_\theta}/\partial x_j \right) \right]$ are the additional terms to correct the near-wall behavior of both dissipation rates, and a subscript a indicates quantities given by algebraic formulas. The above formulation has been employed in the previous $\widetilde{\varepsilon}$– and $\widetilde{\varepsilon}_t$–equation models (e.g., Nagano & Shimada 1996), in which the first terms of the right hand side in Eqs. (6.1) and (6.2) are solved with the relevant transport equations. In the present study, however, we model $\widetilde{\varepsilon}_a$ and $\widetilde{\varepsilon}_{\theta a}$ by the following algebraic expressions:

$$\widetilde{\varepsilon}_a \simeq \left(\frac{k}{\tau_b} \right) f_b = \left[\frac{k}{\nu / \left(\nu S + k \right)} \right] f_b, \tag{6.3}$$

$$\widetilde{\varepsilon}_{\theta_a} \simeq \left(\frac{k_\theta}{\tau_{b\theta}} \right) f_{b\theta} = \left[\frac{k_\theta}{\nu / \left(k + \nu S + \nu G \sqrt{k/k_\theta} \right)} \right] f_{b\theta}, \tag{6.4}$$

where, $G \left[= \sqrt{\left(\partial\bar{\Theta}/\partial x_j \right) \left(\partial\bar{\Theta}/\partial x_j \right)} \right]$ is the temperature gradient parameter, $S \left(= \sqrt{2 S_{ij} S_{ij}} \right)$ is the mean shear-rate, and τ_b and $\tau_{b\theta}$ are the hybrid time-scales determining ε and ε_θ in the near-wall region, respectively. It should be noted that in order to express a complex thermal field, the hybrid time-scale $\tau_{b\theta}$ is represented by using the three characteristic time-scales, i.e., $\sqrt{k_\theta/k}(1/G)$ derived from the order-of-magnitude modeling for the production term in the ε_θ–equation (Hattori-Nagano, 1998), ν/k determining the fluctuating velocity time-scale and $1/S$ reflecting the mean velocity gradient. Moreover, the model functions, f_b and $f_{b\theta}$, which include the effect of Prandtl numbers are defined as follows:

$$f_b = \left(\frac{1}{90} \right) \exp \left[- \left(1.0 \times 10^{-4} R_s \right)^{\frac{1}{2}} \right], \tag{6.5}$$

$$f_{b\theta} = \frac{1}{130\sqrt{Pr}} \exp \left[- \left(\frac{R_{c\theta}}{13} \right)^{\frac{1}{2}} \right], \tag{6.6}$$

where $R_s = k/(\nu S)$ and $R_{c\theta} (= \tau_{b\theta} k/\nu)$ are the turbulent Reynolds numbers.

We assess the proposed algebraic formulas to substitute DNS data for Eqs. (6.3) and (6.4). From Fig. 6.1, it can be seen that the proposed algebraic formulas are in good agreement with the DNS results for various Reynolds number and Prandtl number flows.

6.2 Construction of two-equation models

The models for ν_t and α_t are similar to the AKN model (Abe *et al.* 1994) and the NS model (Nagano & Shimada 1996):

$$\nu_t = C_\mu f_\mu \frac{k^2}{\varepsilon}\left\{1+\left(\frac{40}{R_t^{3/4}}\right)\exp\left[-\left(\frac{R_t}{25}\right)^{1/2}\right]\right\}, \tag{6.7}$$

$$\alpha_t = C_\lambda f_\lambda \frac{k^2}{\varepsilon}\left\{f(R)+\sqrt{\frac{2R}{Pr}}\frac{55}{\left(1+2\sqrt{Pr}\right)^{\frac{1}{4}}}\frac{1}{R_t^{\frac{3}{4}}}\exp\left[-\left(\frac{R_t f(R)}{12}\right)^{\frac{1}{2}}\right]\right\}, \tag{6.8}$$

where the wall reflection functions used in Eqs. (6.7) and (6.8) are given as follows:

$$f_\mu = 1-\exp\left[-\left(\frac{n^*}{24}\right)^2\right], \tag{6.9}$$

$$f_\lambda = 1-\exp\left(-7.5\times10^{-4}{n^*}^{\frac{7}{4}}{n_\theta^*}^{\frac{1}{4}}\right). \tag{6.10}$$

The nondimensional wall distance $n^*\ (=u_\varepsilon n/\nu)$ is introduced to calculate a flow with separation and reattachment (Abe *et al.* 1994) and $n_\theta^*\left[=\left(1+2\sqrt{Pr}\right)n^*\right]$ is defined by the mixed length of the Kolmogorov and the Batchelor microscales (Nagano & Shimada 1996), where u_ε is the Kolmogorov velocity scale and n is the distance between a point n and the nearest point on all the wall surfaces in a flow field (Abe *et al.* 1994). Note that the use of the wall distance does not violate the tensorial invariance, as long as the wall distance is determined uniquely in the problem.

In addition, the modeling for the turbulent diffusion term of k_θ is made by considering the gradient-type diffusion plus convection by large-scale motion as proposed by Hattori & Nagano (1998) and that for k accounts for the gradient-type diffusion and pressure diffusion. It should be noted, however, that the corresponding near-wall model functions are not needed in the dissipation-rate equations, since the proposed models adopt the algebraic formulas for the dissipation-rates near the wall. Thus, the equations for T_ε and T_{ε_θ} are identical with the

high-Reynolds-number turbulence models:

$$T_k + \Pi_k = \frac{\partial}{\partial x_j}\left[\left(\frac{\nu_t}{\sigma_k^*}\right)\frac{\partial k}{\partial x_j}\right], \tag{6.11}$$

$$T_\varepsilon = \frac{\partial}{\partial x_j}\left[\left(\frac{\nu_t}{\sigma_\varepsilon}\right)\frac{\partial \varepsilon}{\partial x_j}\right], \tag{6.12}$$

$$T_{k_\theta} = \frac{\partial}{\partial x_j}\left[\left(\frac{\alpha_t}{\sigma_h^*}\right)\frac{\partial k_\theta}{\partial x_j}\right] + C_\theta \frac{\partial}{\partial x_j}\left[\sigma_{\overline{u_k u_\ell}} d_k n_\ell e_j \sqrt{k}\, k_\theta \sqrt{f_\lambda(1-f_\lambda)}\right], \tag{6.13}$$

$$T_{\varepsilon_\theta} = \frac{\partial}{\partial x_j}\left[\left(\frac{\alpha_t}{\sigma_\phi}\right)\frac{\partial \varepsilon_\theta}{\partial x_j}\right], \tag{6.14}$$

where d_k, n_ℓ and e_j are unit vectors in the streamwise, wall-normal and x_j directions, respectively, and $\sigma_{\overline{u_k u_\ell}}$ is a sign function which is necessary to make a model independent of a coordinate system (Nagano & Tagawa 1990b), i.e., $\sigma_{\overline{u_k u_\ell}} = -1$ when $\overline{u_k u_\ell} \le 0$: $\sigma_{\overline{u_k u_\ell}} = 1$ when $\overline{u_k u_\ell} > 0$. Especially, in Eqs. (6.11) and (6.13), the model constants σ_k and σ_h are not constants as observed from the DNS results near the wall. Thus we adopt the following modifications near the wall (Nagano-Shimada 1995a; Hattori-Nagano 1998):

$$\sigma_k^* = \frac{\sigma_k}{f_k} = \frac{\sigma_k}{1+5f_w}, \tag{6.15}$$

$$\sigma_h^* = \frac{\sigma_h}{f_\theta} = \frac{\sigma_h}{1+9f_w}, \tag{6.16}$$

where the wall reflection function f_w is defined as follows:

$$f_w = \exp\left[-\left(\frac{n^*}{10}\right)^2\right]. \tag{6.17}$$

The other model constants and functions used in the present new two-layer heat-transfer model are summarized in Table 6.1.

6.2.1 Connecting the algebraic formulas

The conjunct turbulence Reynolds numbers based on τ_b and ν/k, $R_c(=\tau_b k/\nu)$, and $\tau_{b\theta}$ and ν/k, $R_{c\theta}(=\tau_{b\theta}k/\nu)$ are employed as the switching indicators to connect the algebraic formulas close to the wall and the two-equation modeling away from the wall. The criterion functions are:

$$f_c = \left(\frac{0.5}{R_c}\right)\left\{1-\exp\left[-1\times 10^4\left(\frac{S\nu}{\bar{U}_i^2}\right)\right]\right\}, \tag{6.18}$$

$$f_{c\theta} = \left(\frac{1.0}{R_{c\theta}}\right)\left\{1-\exp\left[-1\times 10^4\left(\frac{S\nu}{\bar{U}_i^2}\right)\right]\right\}\exp\left(-\sqrt{\frac{R_{c\theta}}{10}}\right). \tag{6.19}$$

Table 6.1: Constants and functions in proposed models

C_μ	$C_{\varepsilon 1}$	$C_{\varepsilon 2}$	f_ε
0.09	1.5	1.9	$1-0.3\exp\left[-\left(R_t/6.5\right)^2\right]$

σ_k	σ_ε	C_λ	C_θ	C_{P1}	C_{P2}	C_{D1}
1.4	1.4	0.1	0.05	0.9	0.77	1.0

C_{D2}	σ_h	σ_ϕ	f_{P1}	f_{P2}	f_{D1}
0.9	1.8	1.8	1.0	1.0	1.0

f_{D2}	$f(R)$
$(1/C_{D2})\,(1.9f_\varepsilon - 1.0)$	$2R/(R+0.2/Pr^{\frac{1}{4}})$

When values of the above functions become larger than unity, the corresponding algebraic formulas are used. In a typical channel flow, a point of connection is located at about $y^+ \simeq 10$ for both velocity and temperature fields.

6.3 Dscussion of predictions with proposed models

To assess the performance of the present two-layer models, several representative test cases are calculated. The numerical technique used is the finite-volume method applied for parabolic equations in channel and boundary layer flows (Hattori & Nagano 1995) and for elliptic equations in backward-facing step flows (Nakayama 1995). Especially, in the calculation of backward-facing step flows, the third-order upwind difference for the convection term is used and the grid system is staggered.

6.3.1 Channel flows with heat transfer at various Reynolds and Prandtl numbers

Comparisons of mean velocity profiles of channel flows at various Reynolds numbers are made between the model predictions and the DNS (Moser *et al.* 1999; Kim & Moin 1989;

Kasagi *et al.* 1992) in Fig. 6.2. The agreement between the DNS data and the predicted results is very good. Figure 6.5 shows the prediction for the budget of turbulent kinetic energy near the wall, compared with the DNS data (Moser *et al.* 1999). It can be seen that the modeled algebraic dissipation-rate reproduces quite well the near-wall profile given by DNS.

Figures 6.6–6.10 show the predicted profiles of mean temperature $\bar{\Theta}$, turbulent heat flux $\overline{v\theta}$, temperature variance k_θ, budget of k_θ at $Pr = 0.71$, and that at $Pr = 0.025$, respectively. Also, the predicted the mean temperature, turbulent heat flux and temperature variance in the constant wall-temperature condition of various Prandtl number fluilds ($Pr = 0.1$, 0.71 and 2.0) are indicated in Figs. 6.11–6.13. In a variety of Prandtl number fluids, the present predictions for the detailed turbulent heat transport show good agreement with the corresponding DNS data (Kasagi *et al.* 1992; Kasagi & Ohtsubo 1992; Kim & Moin 1989).

6.3.2 High Prandtl number fluids

The evaluations for the proposed model in the high Prandtl number fluids are shown in Figs. 6.14 and 6.15. In comparison with experimental data (Kader 1981), it can been seen that the proposed model reproduces adequately the mean temperature in a fully developed channel flow of technical oil ($Pr = 95$ and $Re = 10000$). To assess the proposed model at various high Prandtl number fluids, we have compared predictions and the following empirical equation by Kader (1981):

$$\bar{\Theta}^+ = Pry^+ \exp(-\Gamma) + \left\{ 2.12 \ln \left[(1+y^+) \frac{2.5(2-y/\delta)}{1+4(1-y/\delta)^2} \right] + \beta(Pr) \right\} \exp\left(-\frac{1}{\Gamma} \right), \tag{6.20}$$

where

$$\beta(Pr) = (3.85 Pr^{\frac{1}{3}} - 1.3)^2 + 2.12 \ln Pr,$$
$$\Gamma = \frac{10^{-2}(Pry^+)^4}{1 + 5Pr^3 y^+}.$$

It can been seen that the proposed model gives proper predictions of mean temperature at various high Prandtl number fluids as shown in Fig. 6.15.

6.3.3 Boundary layer flows with or without pressure gradients

We have calculated boundary layers with/without pressure gradients, i.e., with a zero-pressure gradient (ZPG) and with an adverse pressure gradient (APG). Especially, since the standard log-law, $\bar{U}^+ = 2.44 \ln y^+ + 5.0$ is not valid in an APG flow (Nagano *et al.* 1992), these are good test cases for the wall function reflecting the effect of the pressure gradients. In Figs. 6.16–6.19, the predictions of mean velocity, Reynolds shear stress, turbulence energy and dissipation rate of turbulence energy profiles in ZPG flows are compared with the DNS (Spalart 1988) and experimental data (Nagano *et al.* 1992). The present predictions are in almost perfect agreement with the experiment and the DNS data.

Predictions of flow under APG condition are shown in Figs. 6.20, 6.21 and 6.22, in comparison with the experimental data (Nagano *et al.* 1992), and the prediction with the AKN and RMM models. Note that including the additional production term for ε due to irrotational strains is significant in calculating APG flows (Nagano *et al.* 1997) as:

$$\frac{D\varepsilon}{D\tau} = \frac{\partial}{\partial y}\left[\left(\nu + \frac{\nu_t}{\sigma_\varepsilon}\right)\frac{\partial \varepsilon}{\partial y}\right] - \frac{\varepsilon}{k}\left[C_{\varepsilon 1}\overline{uv}\frac{\partial \bar{U}}{\partial y} + C'_{\varepsilon 1}\left(\overline{u^2} - \overline{v^2}\right)\frac{\partial \bar{U}}{\partial x} + C_{\varepsilon 2} f_\varepsilon \varepsilon\right], \qquad (6.21)$$

where, $\overline{u^2}$ and $\overline{v^2}$ are calculated by the nonlinear k–ε model as shown in Chapter 5, and the model constant is $C'_{\varepsilon 1} = 2.5 C_{\varepsilon 1}$. In the RMM model, although an empirical relation between $\overline{v^2}/k$ and the wall distance is used instead of the wall reflection function, it can not, however, reflect the varying APG effects on mean velocity profiles as indicated in Fig. 6.20. Obviously, the present model works very satisfactorily in flow with an APG similar to the AKN model.

6.3.4 Boundary layer flows with heat transfer

We assess the performance of the proposed two-layer models by comparing with experiments and DNS in boundary layer flows with heat transfer. Mean temperature profiles in boundary-layer flows along uniform-temperature and uniform-heat-flux walls are shown in Fig. 6.23. The present predictions indicate good agreement with the experimental data (Gibson *et al.* 1982; Antonia *et al.* 1977). Comparisons of the predicted mean temperature an temperature variance profiles with DNS (Bell & Ferziger 1993) in various Prandtl number fluids are shown in Figs. 6.24 and 6.25. Again, excellent agreement between the predictions and DNS results is achieved for each profile.

As shown in the foregoing, the proposed two-layer models accurately reproduce a fundamental flow system. From Fig. 6.26 and the foregoing figures, it can be seen that objectionable disconnections between the algebraic formulas and the solutions from the transport equations do not exist in both ε and ε_θ.

6.3.5 Backward-facing step flows with or without heat transfer

We have calculated a backward-facing step flow to assess the model performance in a complex flow. In Fig. 6.27, the predicted mean velocities are presented, compared with the experimental data (Kasagi & Matsunaga 1995) and with the AKN and RMM model, where the reattachment length obtained is 6.52 for the AKN model (Abe *et al.* 1994) and 6.26 for the RMM model, respectively. The predicted streamline is also indicated in Fig. 6.28. The reattachment length obtained is $x_R/H = 6.23$ for the present two-layer model, which is almost in agreement with the experimental data of $x_R/H = 6.51$. Other turbulent quantities are also in good agreement with the experimental data. Figure 6.29 shows the comparison of the predicted dissipation rates with the experimental data. The predicted dissipation rate gives profiles slightly different from those of the AKN model very near the wall. This difference seems to affect the predicted turbulent energy levels which are larger than for the AKN model in the central recirculation region. Thus, the reattachment length is slightly underpredicted.

Finally, we have carried out a simulation of backward-facing step flow with heat transfer reported by Vogel & Eaton (1985). The streamline, mean velocity and skin friction coefficient in the velocity field are shown in Fig. 6.30, and mean temperature and Stanton number are shown in Fig. 6.31, in comparison with experimental data. Note that x^* denotes the streamwise distance normalized by the reattachment length x_R, that is $x^* = (x - x_R)/x_R$ in the figure. The present model predicts the reattachment length $x_R = 6.0$, which is slightly shorter than the experimental result (=6.7). However, the NS model, which serves as the basis for the proposed two-layer model, predicts a similar reattachment length in this case, for the same reasons (Nagano & Shimada, 1996) mentioned above. Both the mean velocity and mean temperature profiles are significant factors for the Stanton number. It can be seen that the present model predicts well both profiles, and good accordance with the experimental data is achieved for the Stanton number.

Table 6.2: Assessment of calculation stability

Model	AKN	HN	Present
Re	No. itera.	No. itera.	No. itera.
10,000	199	55	47
20,000	98	51	46
30,000	75	49	50
40,000	68	47	50
50,000	65	46	49
100,000	58	42	49

6.3.6 Calculation stability and grid dependence

We assess the calculation stability of the present model, the AKN model which lets ε be equal to $\nu\,(\partial^2 k/\partial y^2)$ at a wall and the HN model (Hattori & Nagano 1995) which employs the pseudo-dissipation $\widetilde{\varepsilon}$ set to zero at the wall, with the calculation of channel flows at various Reynolds numbers using the initial profiles calculated from the log-law. The results of assessment are shown in Table 6.2. The proposed model can perform stable calculation as shown in the table which includes the number of iterations with each model. When the Reynolds number becomes smaller, the number of iterations with the present model is much smaller than with other models, since the dissipation-rate equation (2.11) is not solved near the wall for the proposed two-layer model, whereas that for other models must be calculated in this near-wall region.

Moreover, we assess the grid dependence of the present model predictions. For instance, in the channel flow, the DNS at the present Reynolds number needs the number of 97 grid points for half channel width in the normal direction (Moser *et al.* 1999). The Reynolds-averaged turbulence model must give mean profiles identical to the DNS data with less grid points. Figure 6.32 shows the dependency of grid numbers, varying from 21 to 11 for the proposed model with JL model (Jones & Launder 1972) for comparison. From the figure, it is evident that the present model can predict mean velocity profiles exactly with considerably fewer grid points.

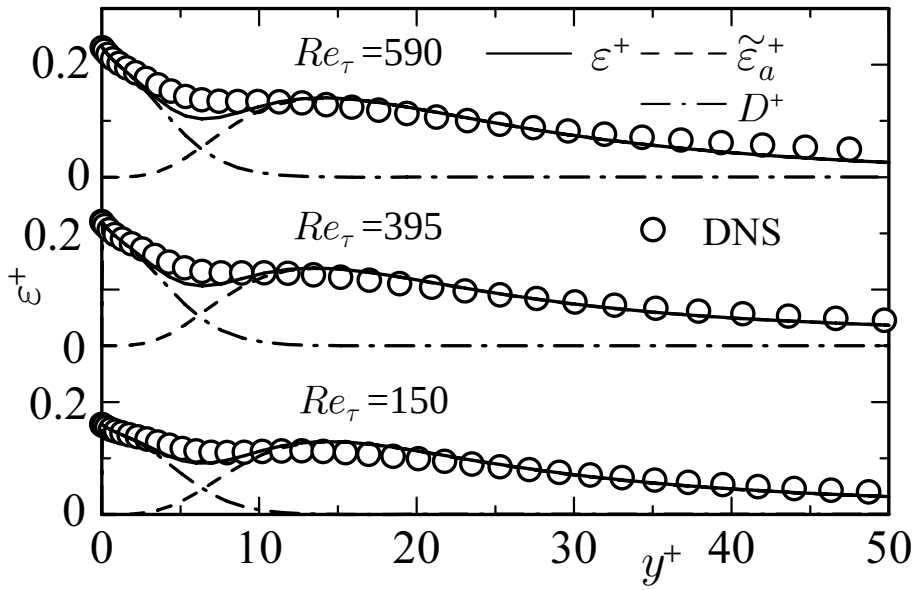

(a)

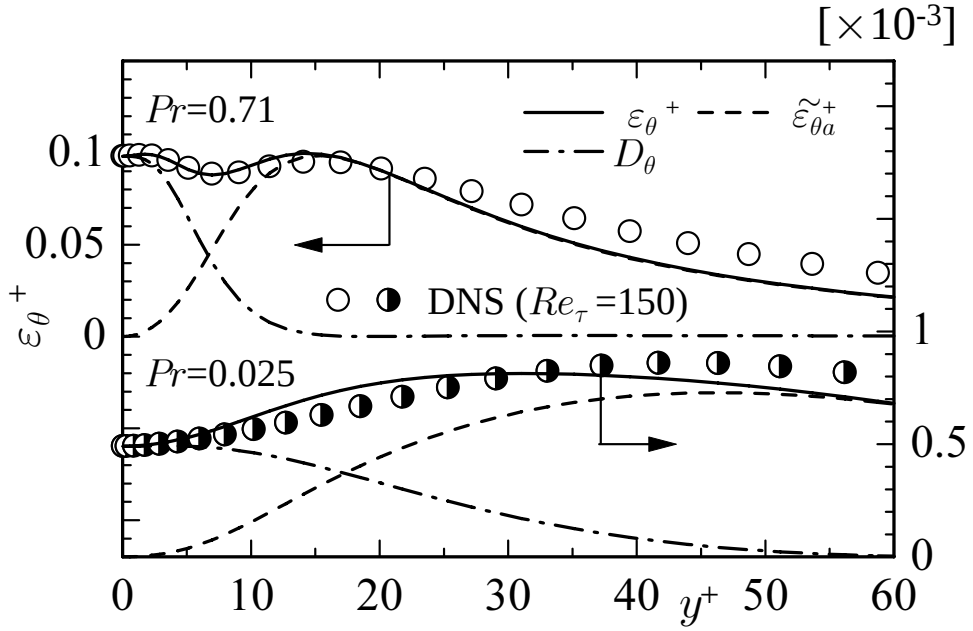

(b)

Figure 6.1: Assessment of proposed algebraic formulas for ε and ε_θ: (a) Velocity field; (b) Thermal field

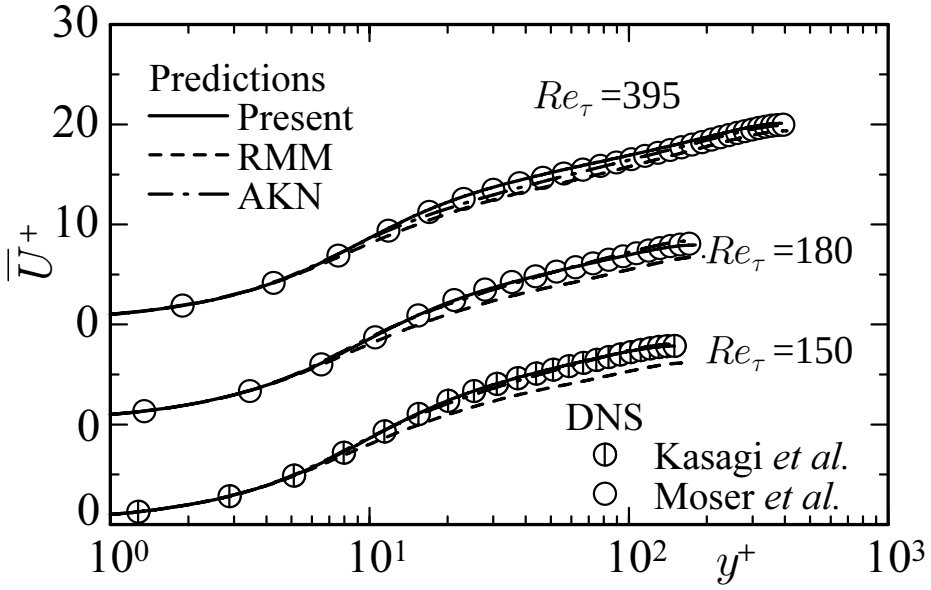

Figure 6.2: Mean velocity profiles in a channel

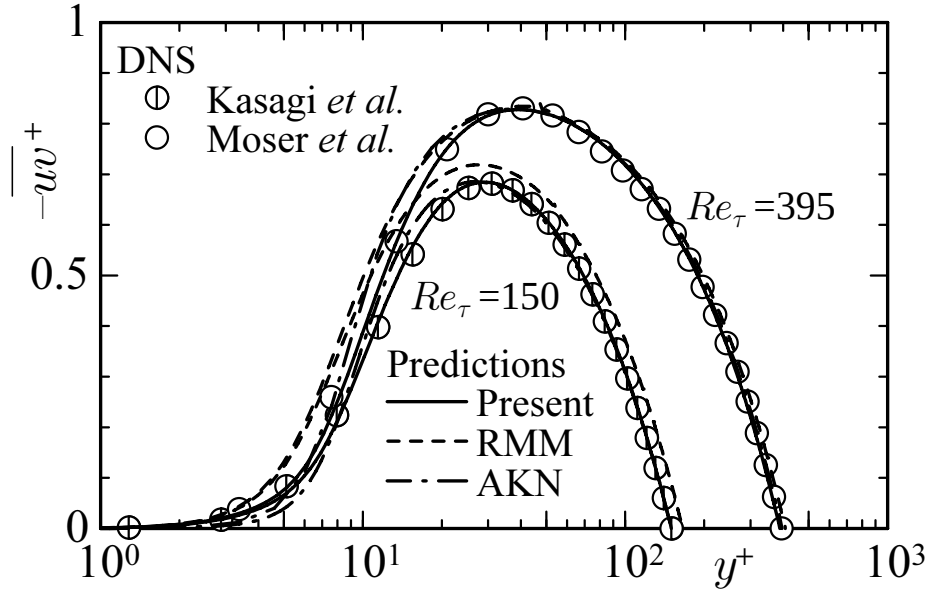

Figure 6.3: Distributions of Reynolds shear stress in a channel

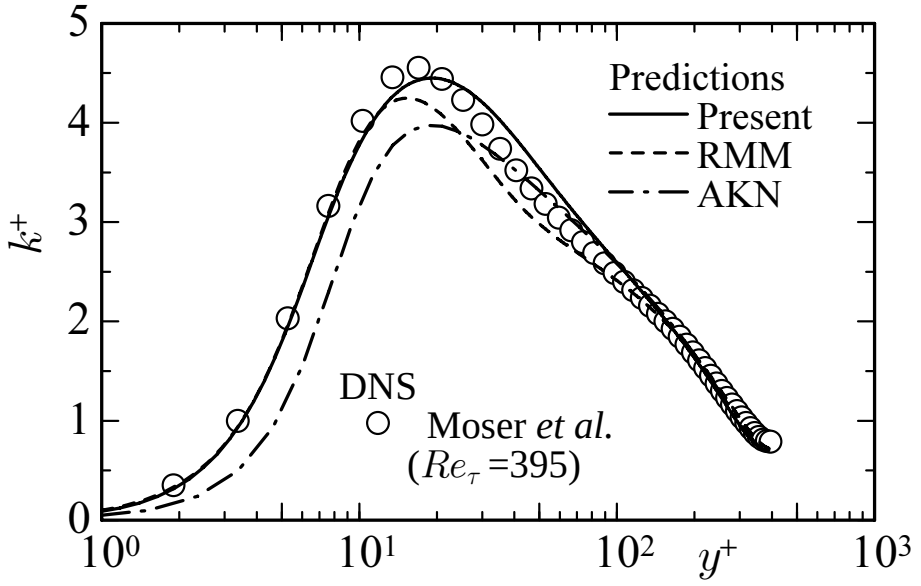

Figure 6.4: Distributions of turbulence energy in a channel $(Re_\tau = 395)$

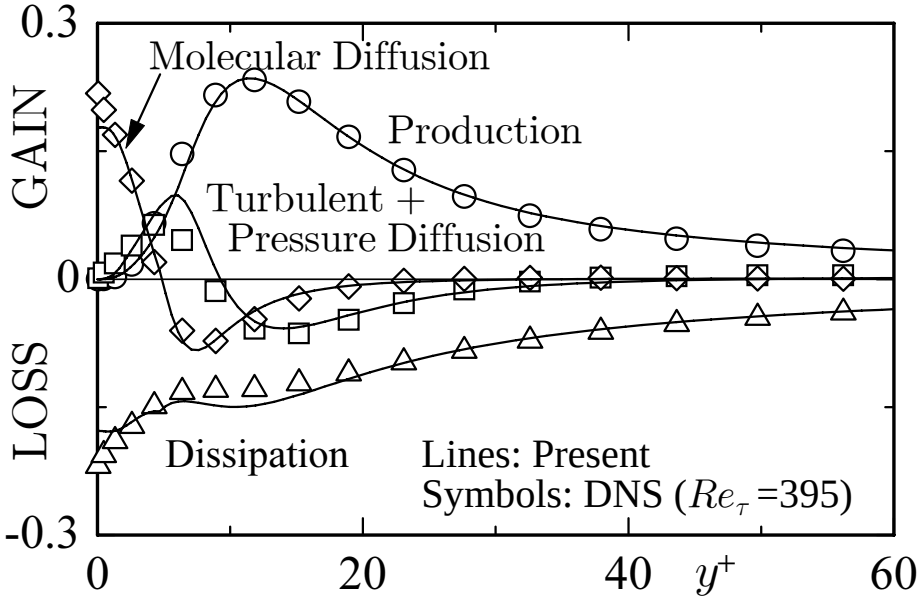

Figure 6.5: Budget of turbulent kinetic energy

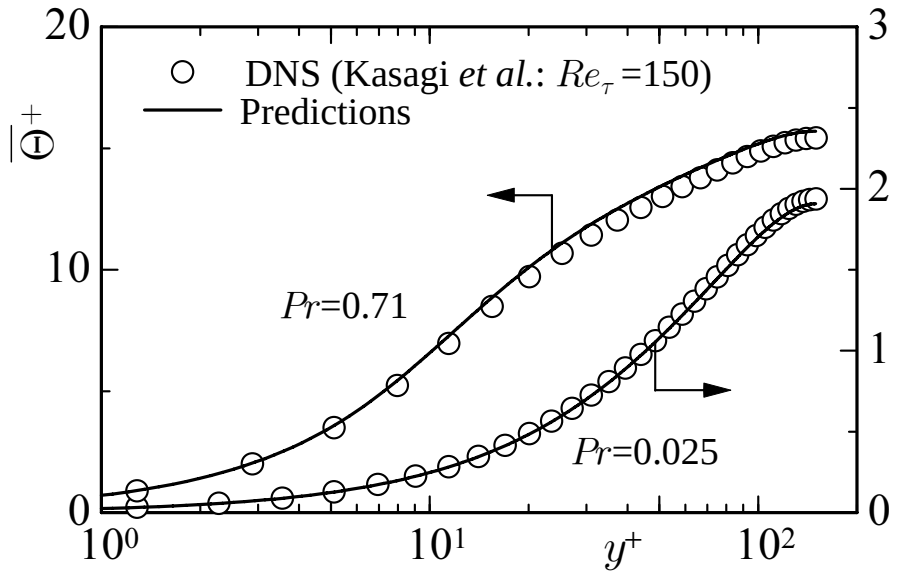

Figure 6.6: Mean temperature profiles in air and mercury channel flows (q_w=const.)

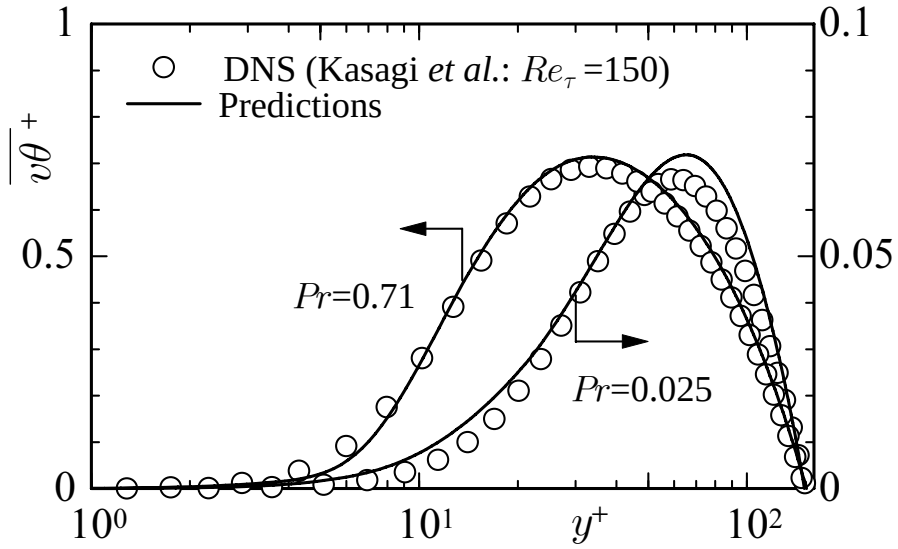

Figure 6.7: Distributions of turbulent heat flux in air and mercury channel flows (q_w=const.)

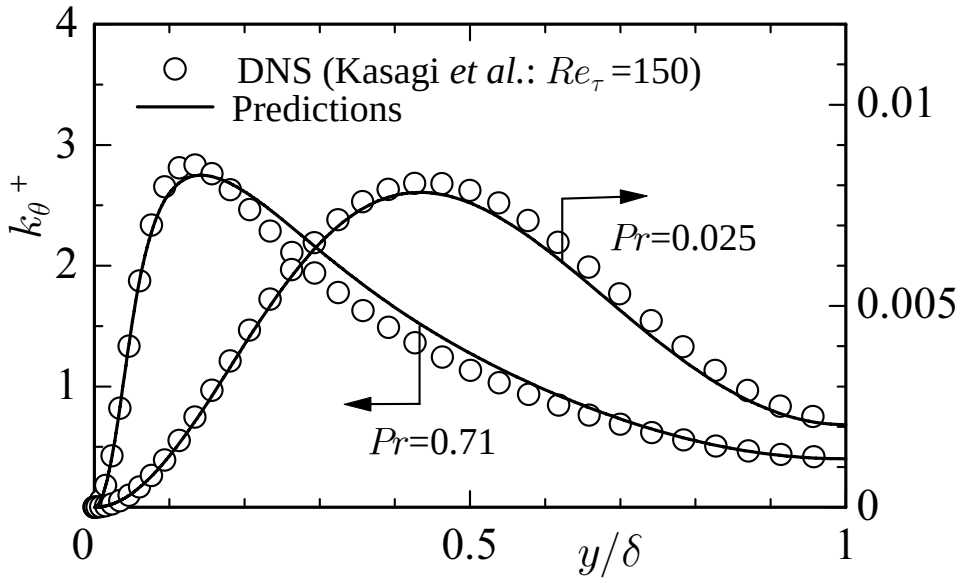

Figure 6.8: Temperature variance in air and mercury channel flows (q_w=const.)

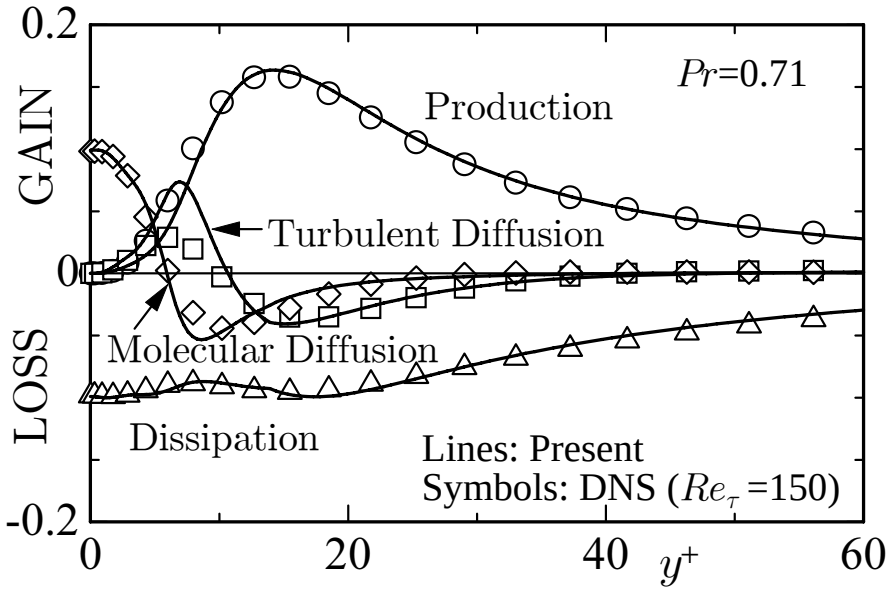

Figure 6.9: Budget of temperature variance $(Pr = 0.71)$

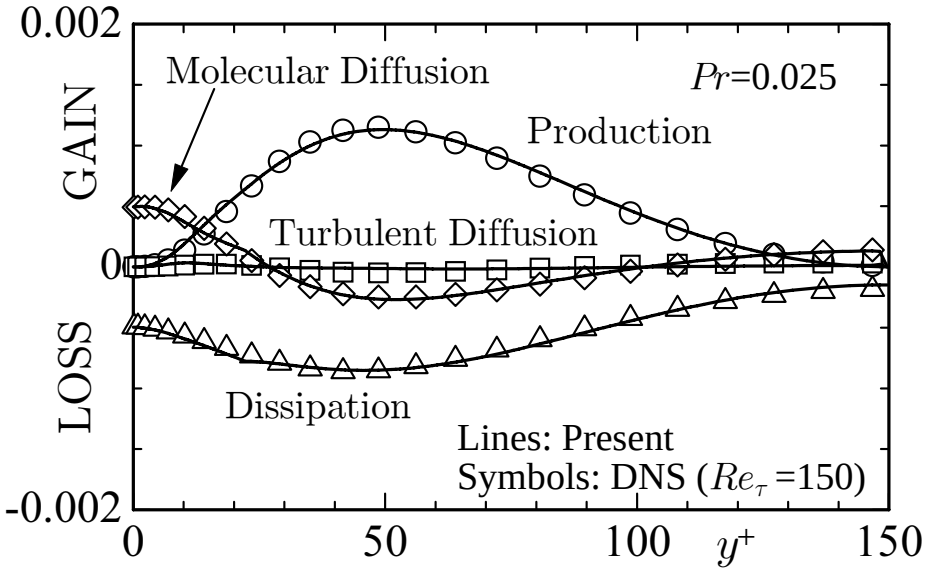

Figure 6.10: Budget of temperature variance $(Pr = 0.025)$

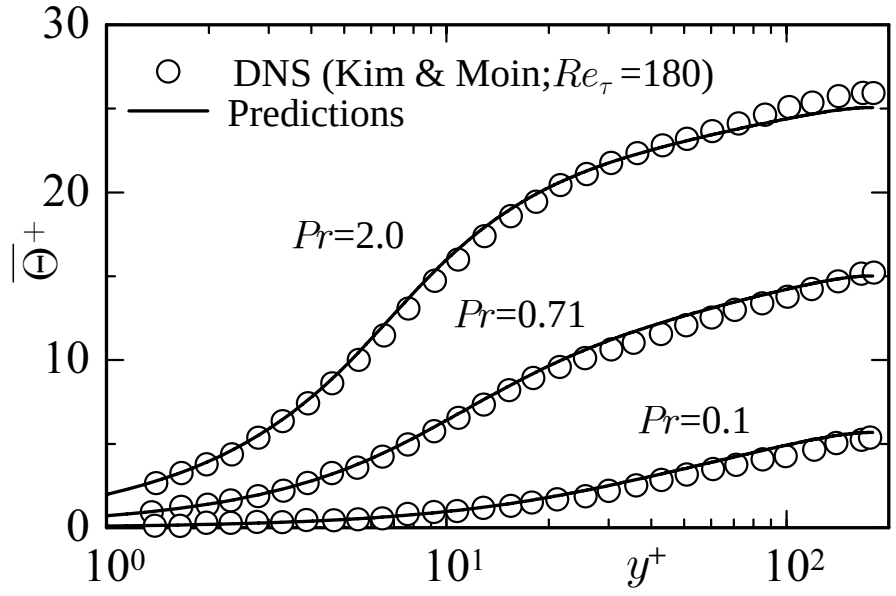

Figure 6.11: Temperature profiles in various Prandtl number flows ($\bar{\Theta}_w$=const.)

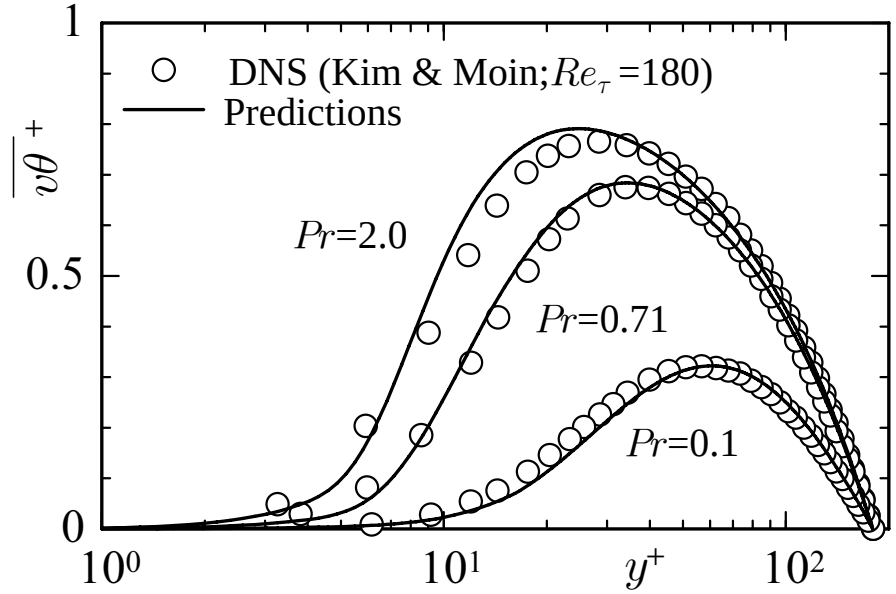

Figure 6.12: Profiles of turbulent heat flux in various Prandtl number flows ($\bar{\Theta}_w$=const.)

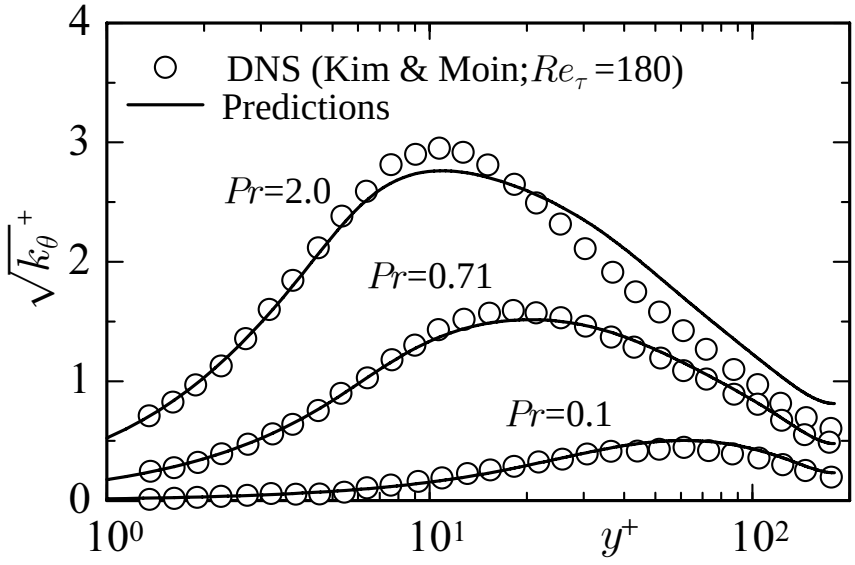

Figure 6.13: Temperature variance in various Prandtl number flows ($\bar{\Theta}_w$=const.)

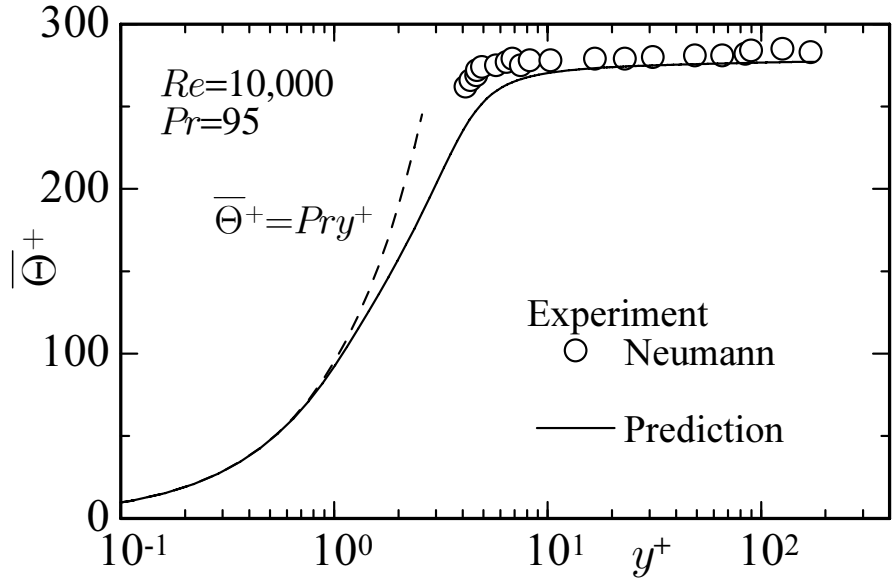

Figure 6.14: Mean temperature profile at high Prandtl number flow ($Pr = 95, Re = 10000$)

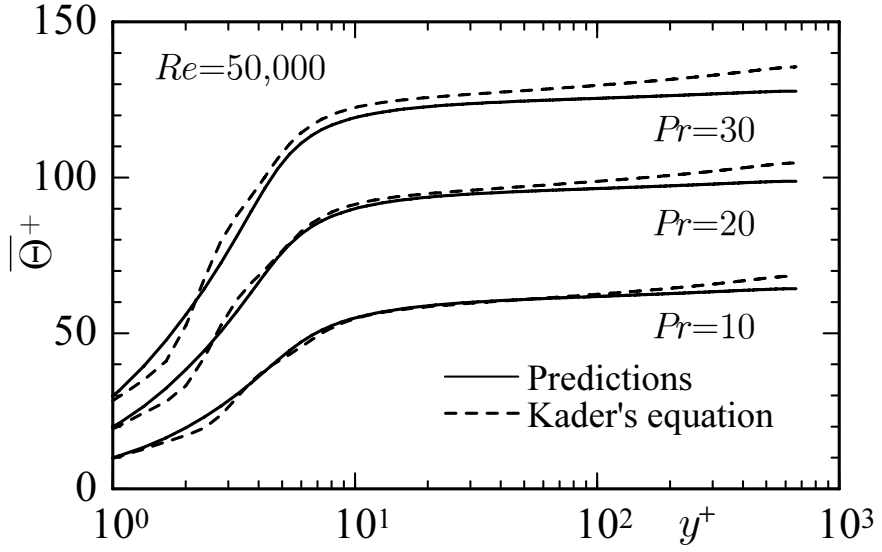

Figure 6.15: Mean temperature profile in various high Prandtl number flows

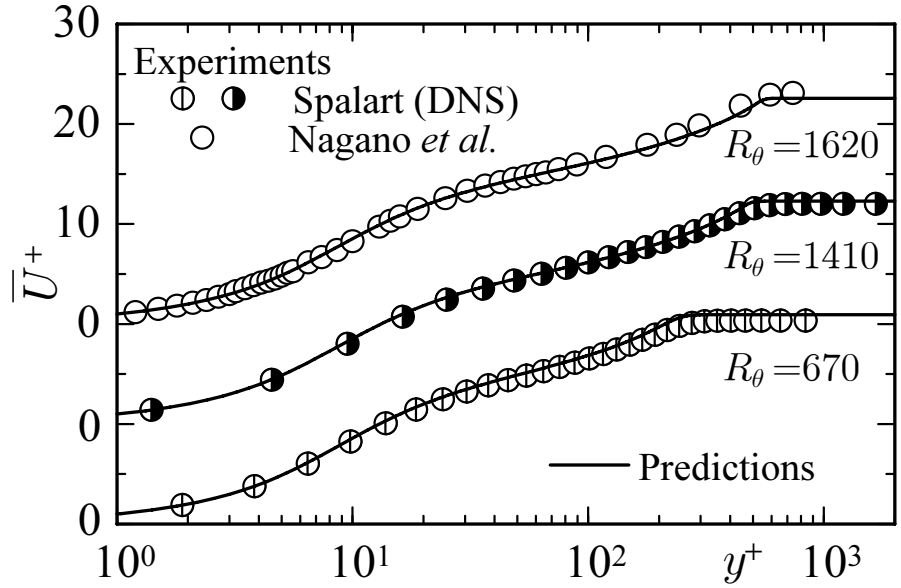

Figure 6.16: Profiles of mean velocity in boundary layer flows

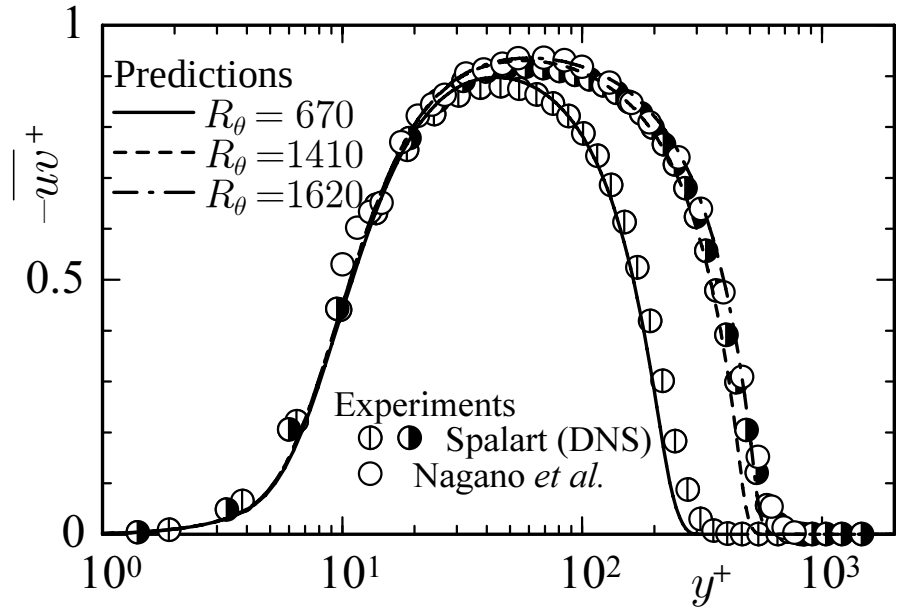

Figure 6.17: Profiles of Reynolds shear stress in boundary layer flows

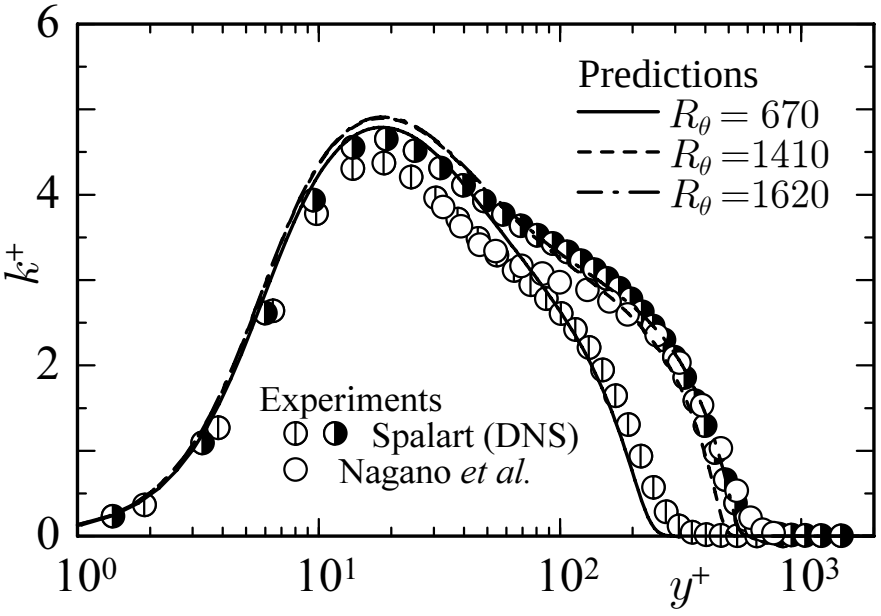

Figure 6.18: Profiles of turbulence energy in boundary layer flows

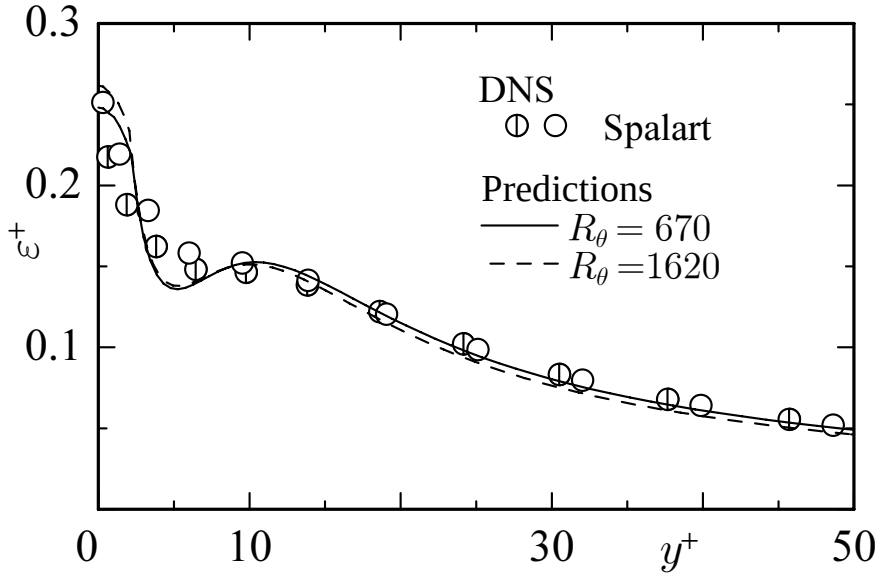

Figure 6.19: Distributions of dissipation rate of turbulence energy in boundary layer flows

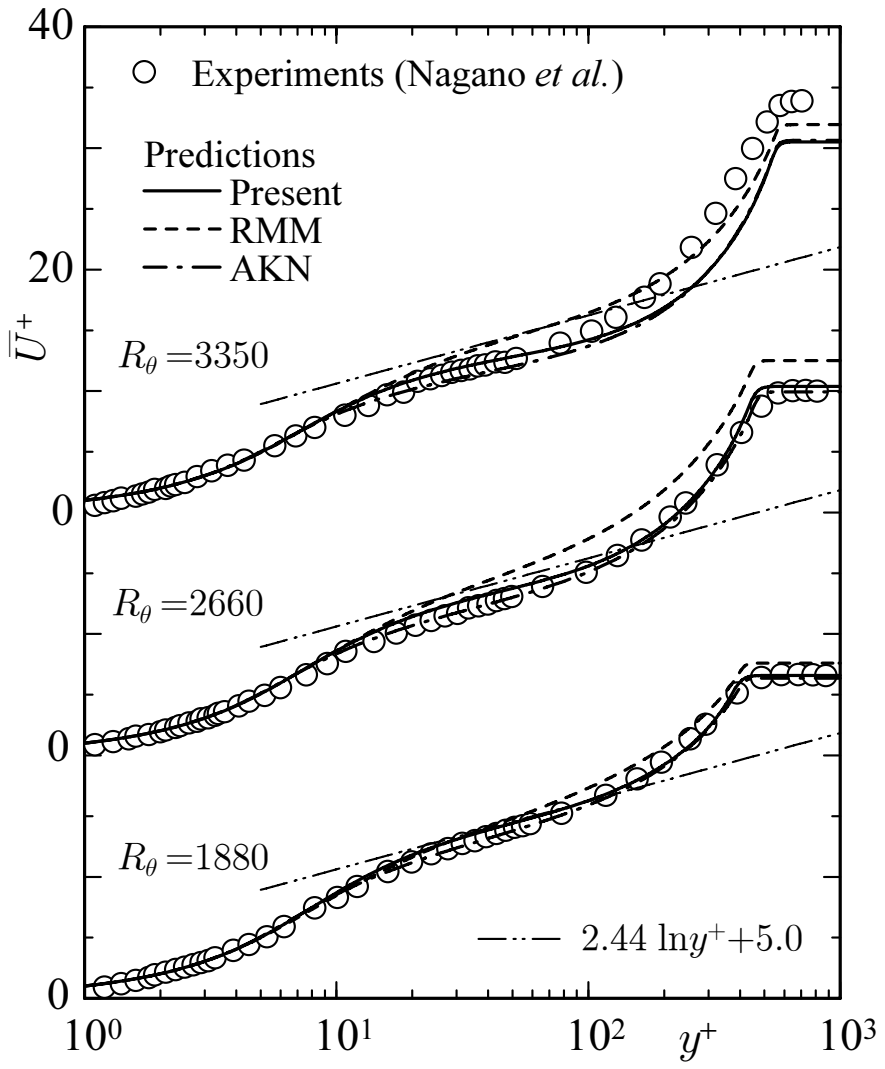

Figure 6.20: Distributions of mean velocity in APG flows

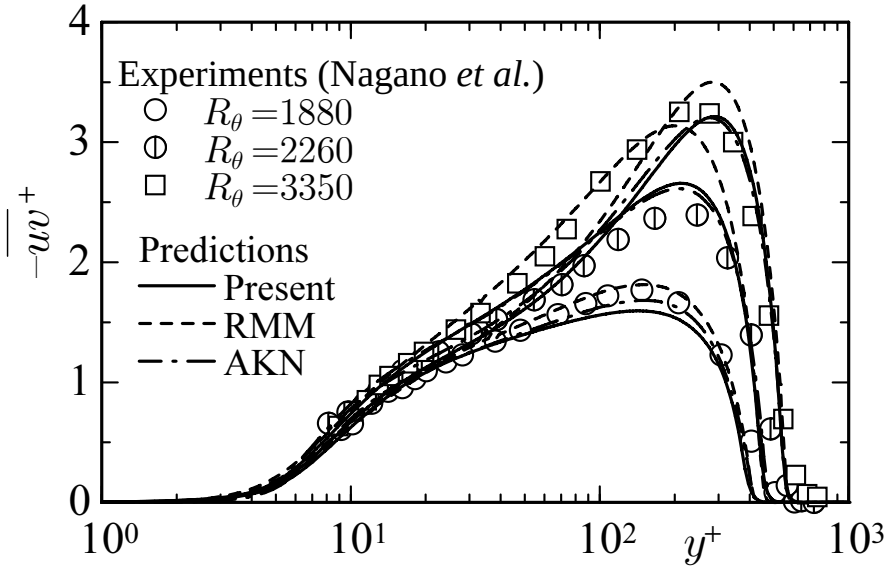

Figure 6.21: Distributions of Reynolds shear stress in APG flows

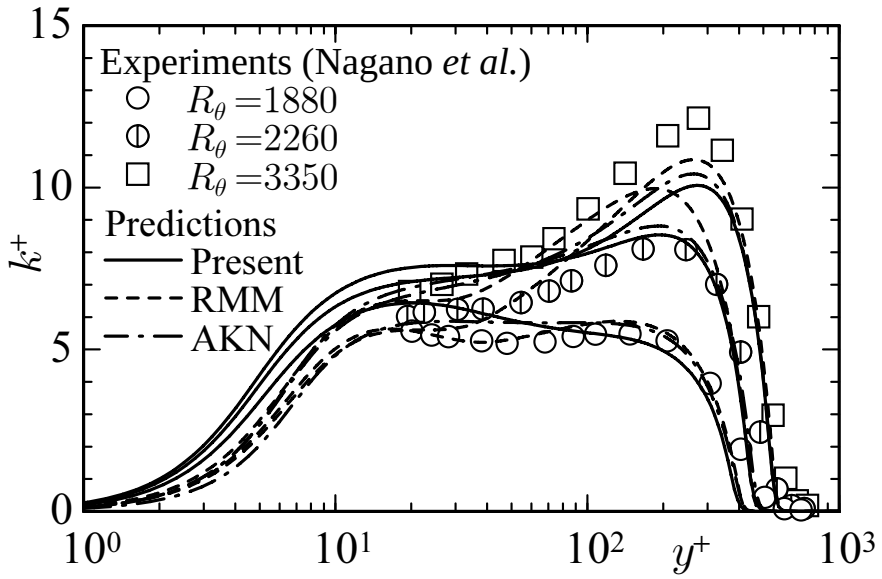

Figure 6.22: Distributions of turbulent kinetic energy in APG flows

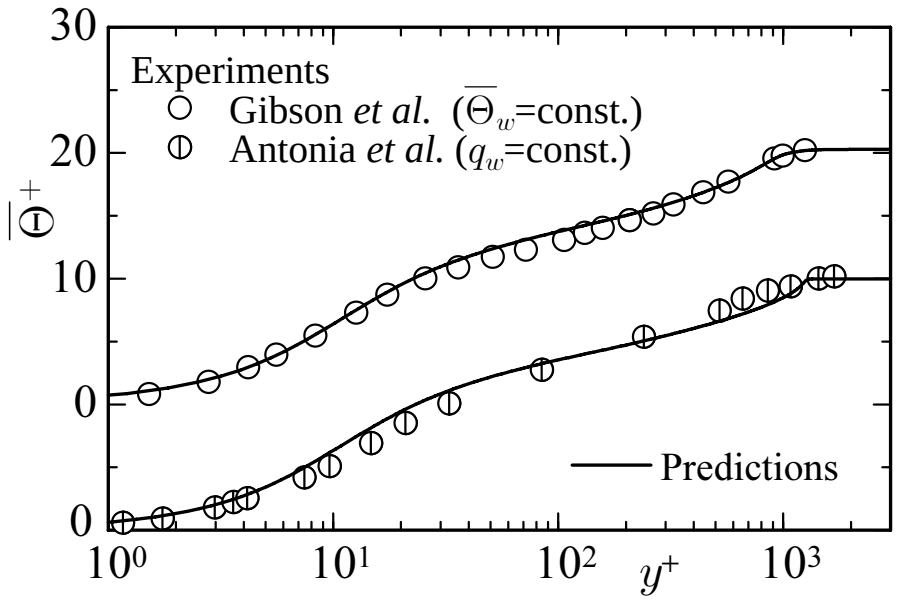

Figure 6.23: Profiles of mean temperature in boundary layer flows

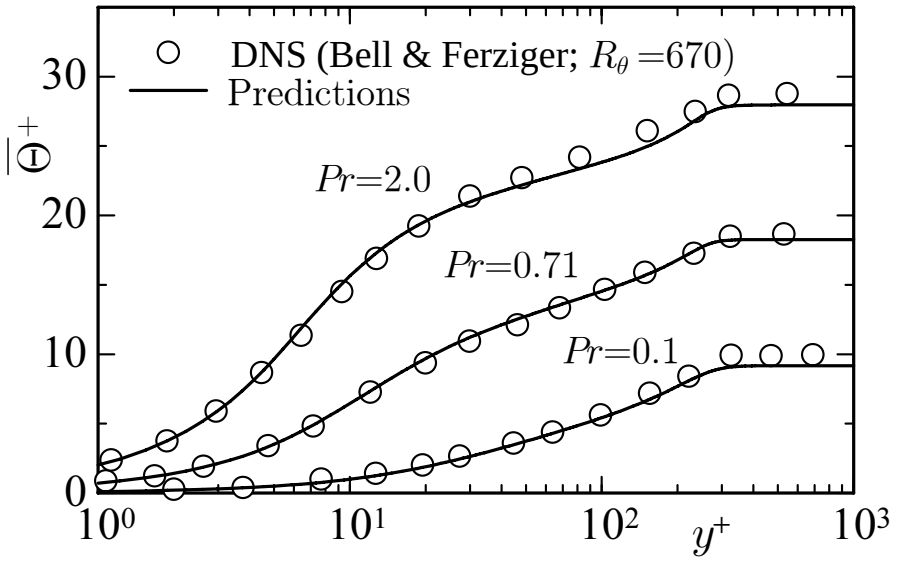

Figure 6.24: Mean temperature profiles in boundary layer flows at various Prandtl numbers

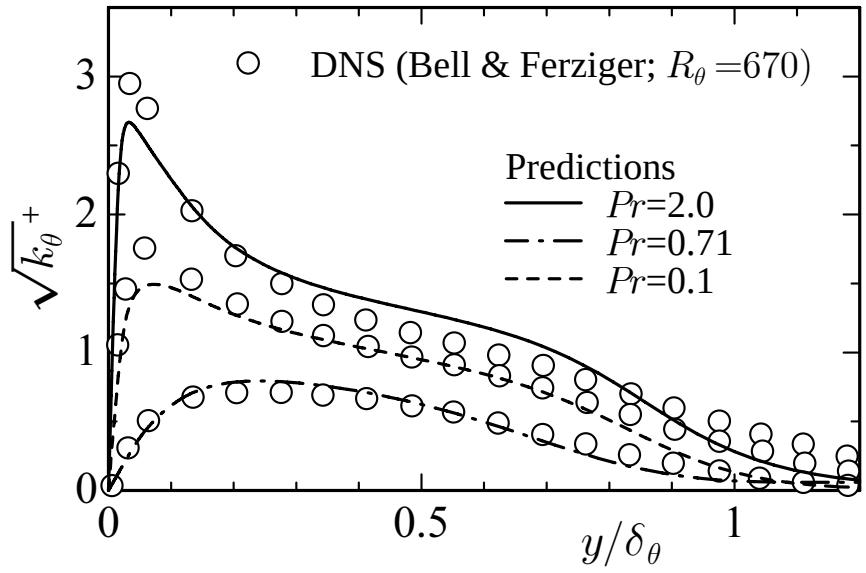

Figure 6.25: Temperature variances in boundary layer flows at various Prandtl numbers

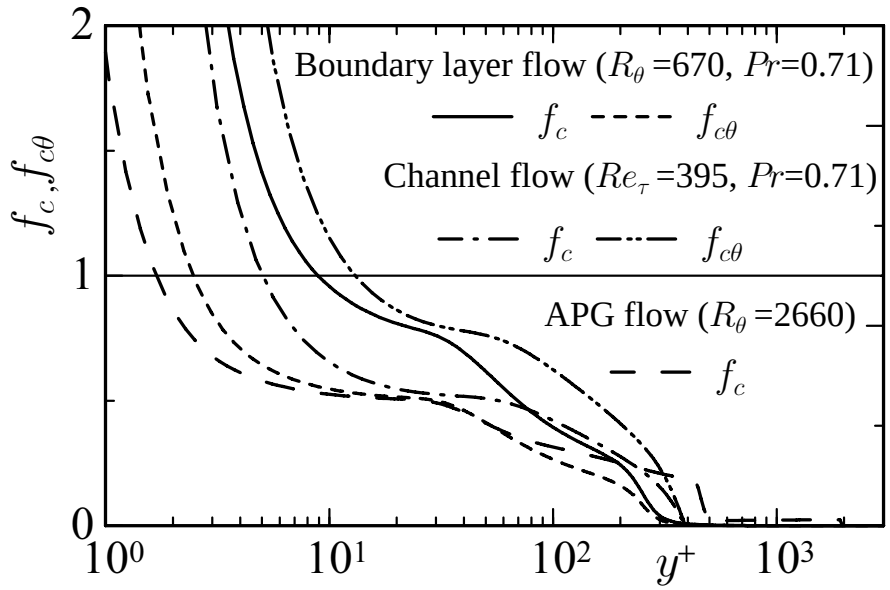

Figure 6.26: Values of criterion functions in various flows

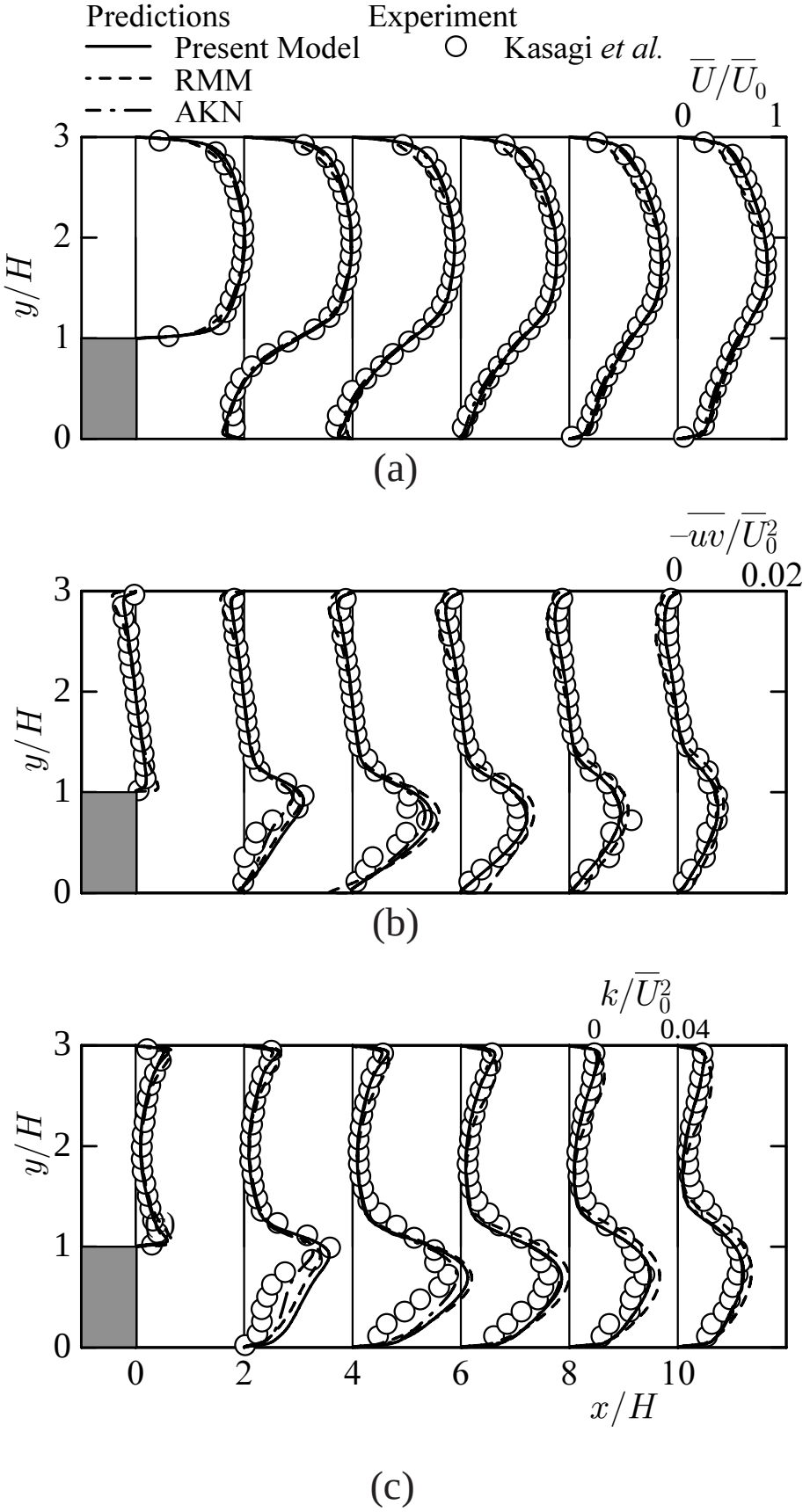

Figure 6.27: Comparison with experiment in backward-facing step flow: (a) mean velocity; (b) Reynolds shear stress; (c) turbulence energy

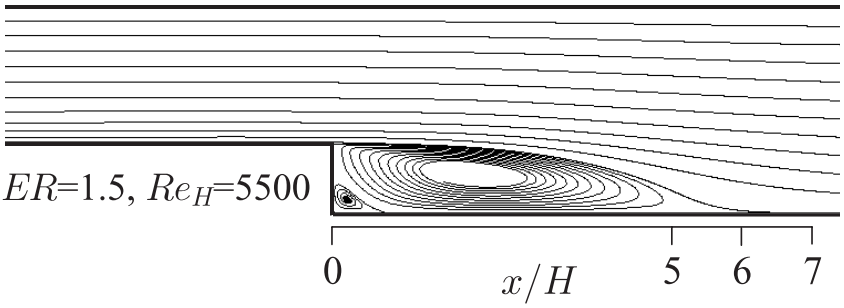

Figure 6.28: Predicted streamline of backward-facing step flow at $Re_H = 5500$

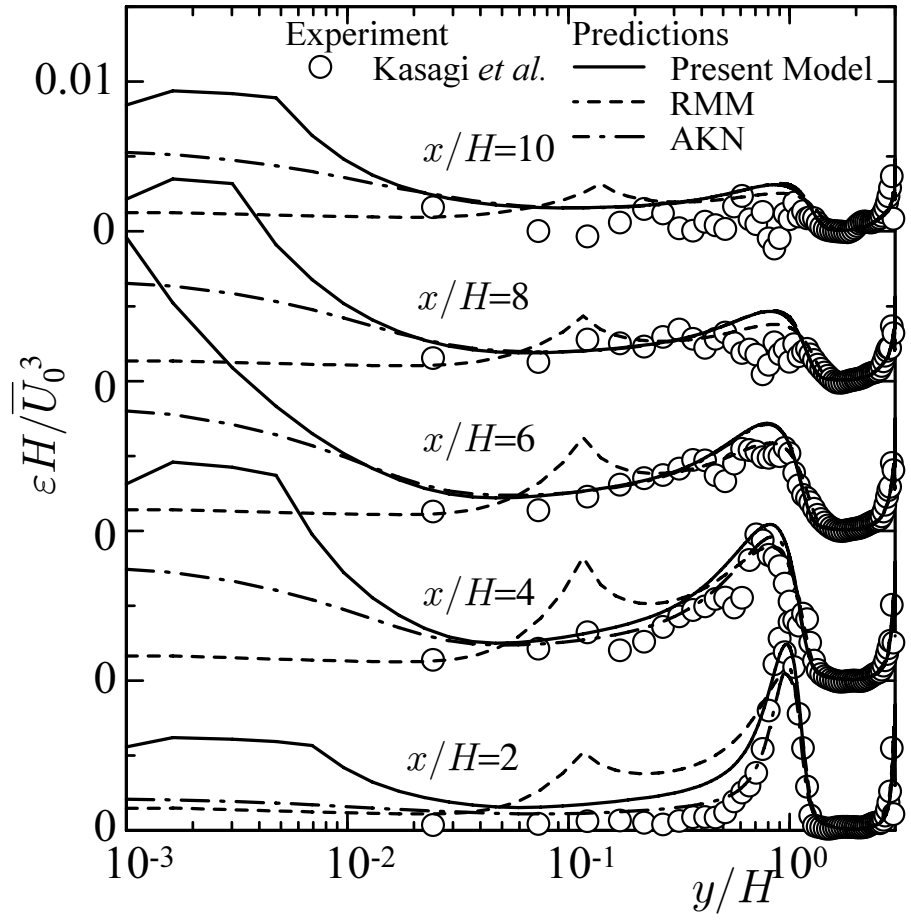

Figure 6.29: Distributions of dissipation rates in backward-facing step flow

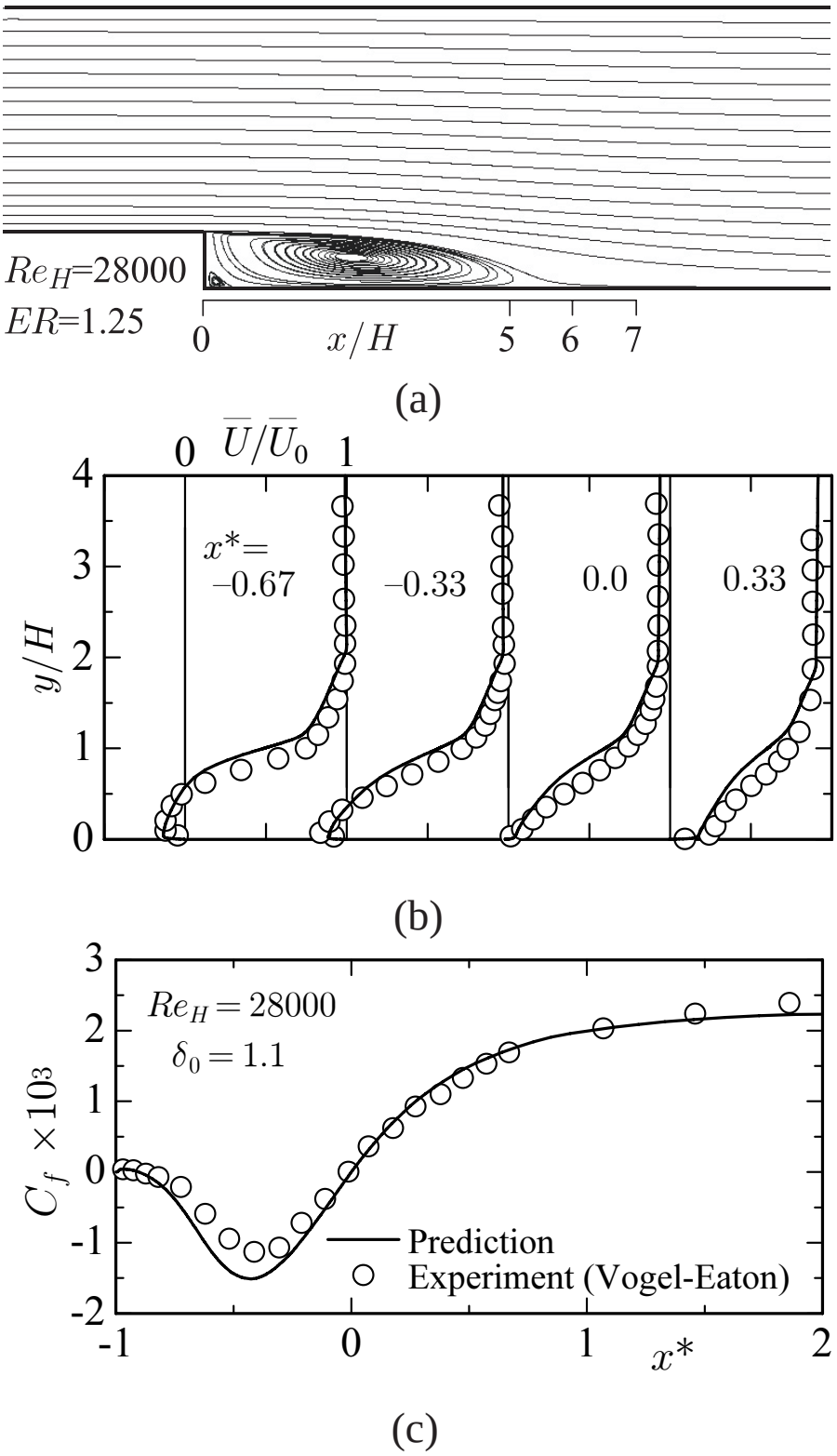

Figure 6.30: Computational results for velocity field in backward-step flow of Vogel & Eaton (1985): (a) streamline; (b) mean velocity; (c) skin friction coefficient

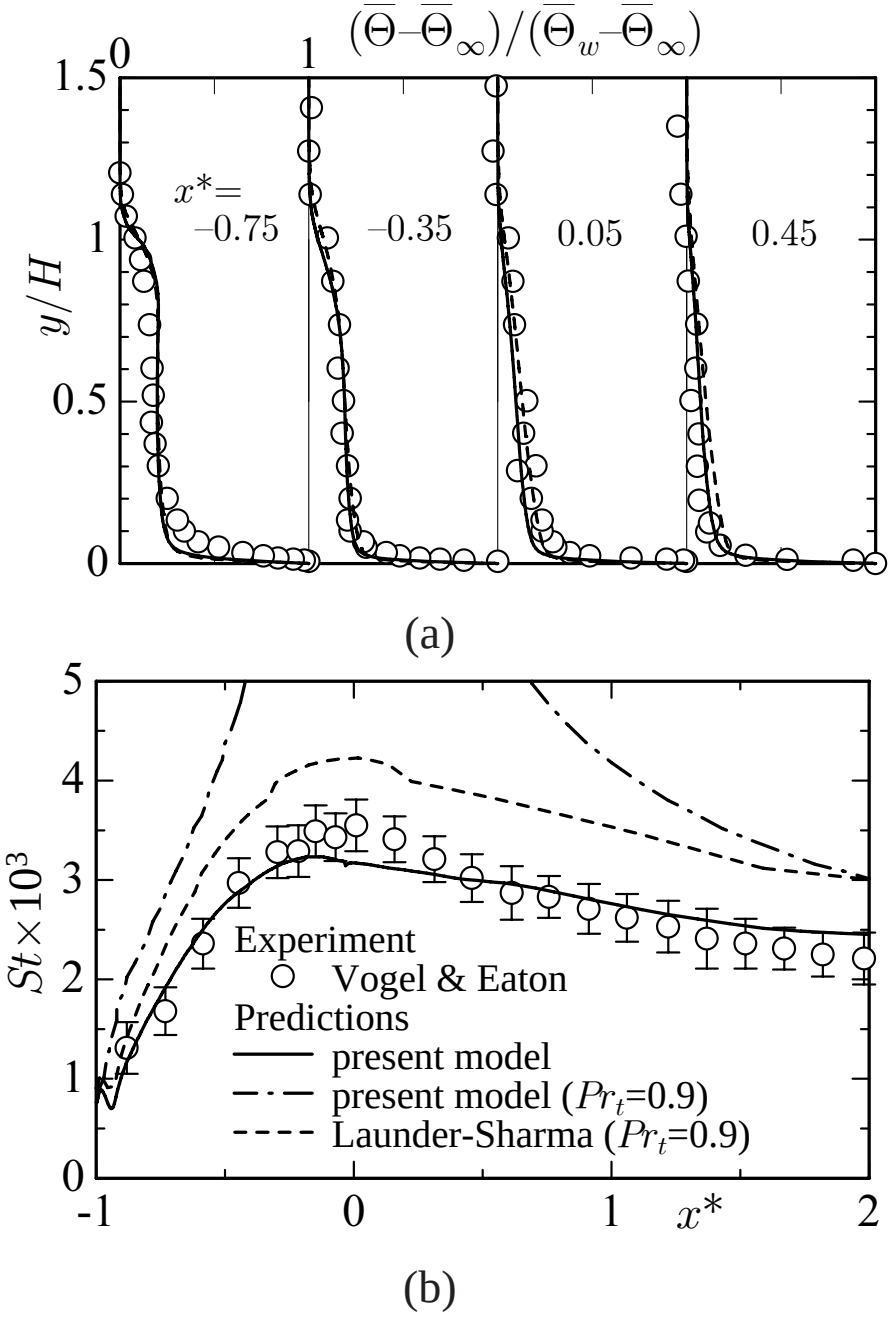

Figure 6.31: Comparison with experiment of Vogel & Eaton (1985) for thermal field: (a) mean temperature; (b) Stanton number on step side wall

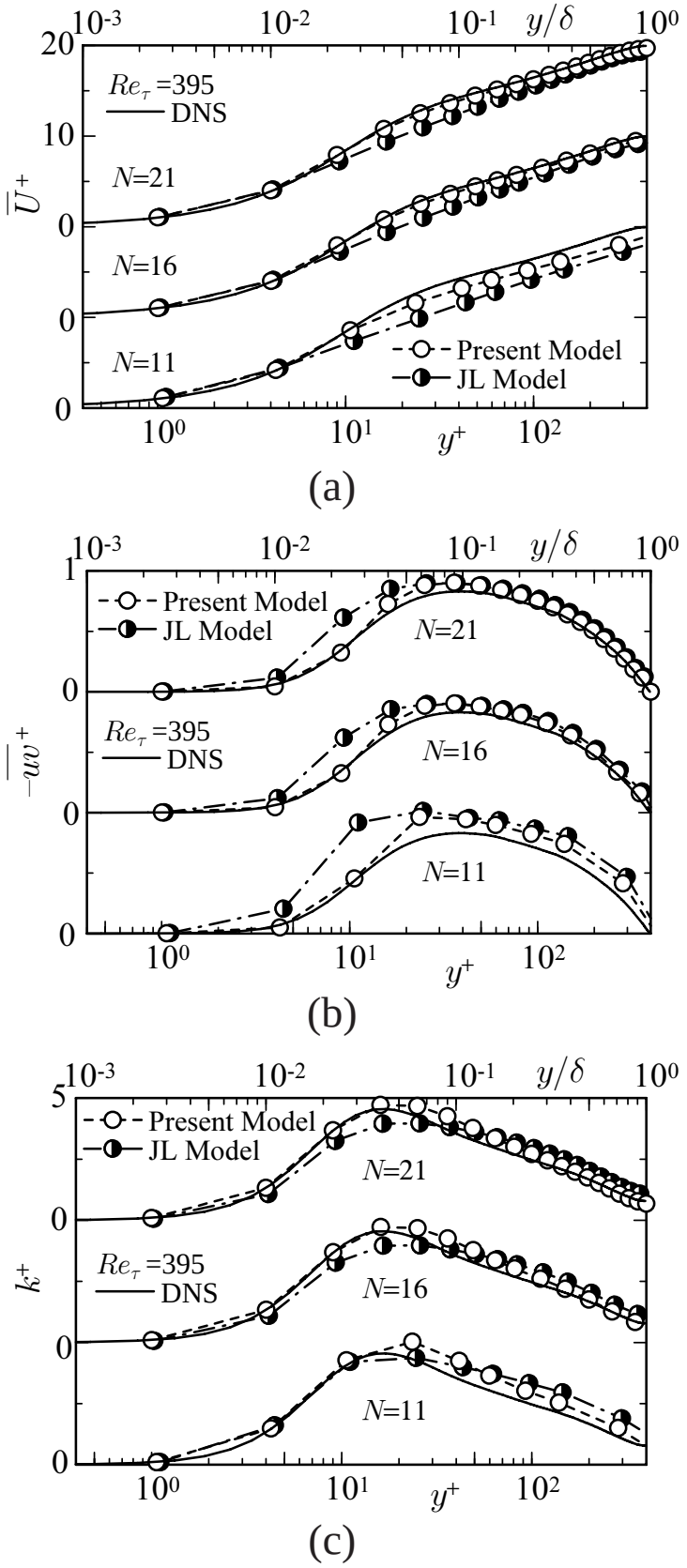

Figure 6.32: Grid dependence of mean velocity profiles in channel flow: (a) mean velcotiy; (b) Reynolds shear stress; (c) turbulence energy

CHAPTER 7

Nonlinear two-equation model taking into account the wall-limiting behaviour and redistribution of stress components

Nonlinear k–ε models have been extensively used in many technological applications (Abe *et al. 1997*; Myong & Kasagi 1990b; Craft *et al.* 1997; Apsley & Leschziner 1998; Suga & Abe 2000). The existing low-Reynolds-number nonlinear k–ε models, however, can not satisfy the requirement for the wall-limiting behaviour of the Reynolds stress component, $\overline{u_2^2}$, in the wall-normal direction, x_2, which should be proportional to x_2^4 near the wall. Since the wall-limiting behaviour of Reynolds normal stress components expressed in the nonlinear k–ε model are determined by the turbulence energy, k, which appears in the lowest order term in the model, the Reynolds stress components, $\overline{u_1^2}$, $\overline{u_2^2}$ and $\overline{u_3^2}$ are proportional to x_2. Especially in the prediction of turbulent heat-transfer phenomena of a wall-bounded flow, the Reynolds normal stress component of the wall-normal direction, $\overline{u_2^2}$, is the most important turbulent quantity. This is because $\overline{u_2^2}$ is included in the production of turbulent heat-flux (Launder 1988), and also in the turbulent diffusion term modeled using the generalized gradient diffusion hypothesis (GGDH) (Launder 1988; Daly & Harlow 1970) in the wall-bounded flow. Therefore, the modeled $\overline{u_2^2}$ should be satisfied the wall-limiting behaviour vicinity of the wall for the requirement of a quantitative prediction of heat transfer phenomena in the wall-bounded flow. Moreover, in order to satisfy the mathematical requirement of a turbulence model in the wall-bounded flow, exactly reproducing the wall-limiting behaviour of the Reynolds stress components should be needed. On the other hand, regarding the redistribution of the Reynolds stress components (i.e., anisotropy in Reynolds normal stress components near the wall which is also essential for of a

prediction of a turbulent flow), the current nonlinear k–ε models are not sufficient to reproduce proper anisotropy in Reynolds normal stress components near the wall.

In this Chapter, in order to explore typical problems for the existing low-Reynolds-number nonlinear k–ε models, we have assessed the nonlinear models by using the direct numerical simulation (DNS) database in the inertial (Kasagi *et al.* 1992; Moser *et al.* 1999) and noninertial frame (Nishimura & Kasagi 1996) (here the rotating channel flow, which is the typical noninertial frame, is adopted). Then, on the basis of the assessment result, we have proposed a new expression of Reynolds stress in a low-Reynolds-number nonlinear k–ε model which exactly satisfies the wall-limiting behaviour of Reynolds normal stress components and predicts the anisotropy near the wall in both the inertial and noninertial frames.

7.1 Assessment of nonlinear two-equation models

In order to clarify the performance and underlying problems of the existing nonlinear k–ε models, we have evaluated them using DNS databases in the fully developed two-dimensional channel flow of Kasagi *et al.* (1992) ($Re_\tau = 150$) and Moser *et al.* (1999) (Re_τ=590 where $Re_\tau = u_\tau \delta/\nu$ is the Reynolds number based on the friction velocity, u_τ, and the channel half width, δ) for the inertial frame, and in the fully developed channel flow with spanwise rotation ($Re^*_\tau = 150$ and $Ro_\tau = 2.5$ where $Re^*_\tau = u^*_\tau \delta/\nu$ is the Reynolds number based on the averaged friction velocity of both walls, u^*_τ, and the channel half width, δ; and $Ro_\tau = 2\Omega\delta/u^*_\tau$ is the rotation number based on u^*_τ, δ and the angular velocity, Ω) (Nishimura & Kasagi 1996) for the noninertial frame as shown in Fig. 7.1. In the evaluation, the DNS data are given to the model expression of Reynolds stress except for $\overline{u_i u_j}$, i.e., the correct mean velocity, turbulence energy and dissipation rate of turbulence energy are specified. Therefore, we can obtain the exact behaviour of the model expression of Reynolds stress. We have evaluated five low-Reynolds-number nonlinear k–ε models, which are the quadratic type models of the kind proposed by Abe, Kondoh and Nagano (1997) (hereinafter referred to as the NLAKN model) and Myong and Kasagi (1990b) (NLMK), and the cubic type model proposed by Craft, Launder and Suga (1997) (NLCLS), Apsley and Leschziner (1998) (NLAL) and Suga and Abe (2000) (NLSA). These model functions and constants in Eq. (2.6) are listed in Table 7.1.

Figures 7.2–7.5 show the assessment results for the Reynolds stress expressions $\overline{u_2^2}$, $\overline{u_1^2}$, $\overline{u_3^2}$

Table 7.1: Model constants and functions of nonlinear models

Model	C_0	C_1	C_2	C_3	C_4
NLAKN (quadratic)	$\frac{1}{f_R}$	$\frac{4C_D}{f_R}$	$\frac{4C_D}{f_R}$	0	0
NLMK (quadratic)	1	$0.95C_\mu f_\mu$	$1.1C_\mu f_\mu$	$0.2C_\mu f_\mu$	0
NLCLS (cubic)	1	$0.44C_\mu \frac{f_q}{f_r}$	$-0.2C_\mu \frac{f_q}{f_r}$	$0.84C_\mu \frac{f_q \tilde{S}}{f_r(\tilde{S}+\tilde{\Omega})/2}$	$-6.4C_\mu f_c$
NLAL (cubic)	$\frac{1}{f_c}$	$\frac{(\tilde{a}_{11}-\tilde{a}_{22})}{\tilde{\sigma}^2} f_p^2$	$\frac{6\,(\tilde{a}_{11}+\tilde{a}_{22})}{\tilde{\sigma}^2} f_p^2$	0	$6\frac{C_\mu}{f_c}\left(\frac{\bar{\beta}}{\tilde{\sigma}}\right)\left(\frac{\bar{\gamma}}{\tilde{\sigma}}\right) f_p^2$
NLSA (cubic)	1	$0.44 f_q$	$-0.2 f_q$	$1.68 f_q \frac{\tilde{S}}{\tilde{S}+\tilde{\Omega}}$	$-3.2 f_c$

Model	C_5	C_6	C_7	A_{ij}	τ_R
NLAKN	0	0	0	0	$\frac{\nu_t}{k}$
NLMK	0	0	0	$\frac{2}{3}\nu\frac{k}{\varepsilon}A_{ij}(n,m)\left(\frac{\partial\sqrt{k}}{\partial x_n}\right)^2$	$\frac{k}{\varepsilon}$
NLCLS	0	$-4C_\mu f_c$	$4C_\mu f_c$	0	$\frac{k}{\tilde{\varepsilon}}$
NLAL	$-6\frac{C_\mu}{f_c}\left(\frac{\bar{\gamma}}{\tilde{\sigma}}\right)^2 f_p^2$	$-\frac{4}{3}\frac{C_\mu}{f_c}\left(\frac{\bar{\beta}}{\tilde{\sigma}}\right)^2 f_p^2$	$-2\frac{C_\mu}{f_c}\left(\frac{\bar{\gamma}}{\tilde{\sigma}}\right)^2 f_p^2$	0	$\frac{k}{\varepsilon}$
NLSA	0	$-4f_c$	$4f_c$	$c_a k A_{ij}$	$\frac{k}{\tilde{\varepsilon}}$

Model	C_μ	f_μ
NLAKN	0.12	$[1-f_w(26)]\left[1+\left(\frac{35}{R_t^{\frac{3}{4}}}\right) f_d\right]$
NLMK	0.09	$\left(1+\frac{3.45}{\sqrt{R_t}}\right)\left[1-\exp\left(-\frac{y^+}{70}\right)\right]$
NLCLS	$\frac{0.667 r_\eta\left\{1-\exp\left[-0.415\exp\left(1.3\eta^{\frac{5}{6}}\right)\right]\right\}}{1+1.8\eta}$	1
NLAL	$\frac{-\tilde{a}_{12}}{\tilde{\sigma}} f_p$	1
NLSA	$0.09 C_{\mu_A} C_{\mu_{R_t}} C_{\mu_S}$	1

Table 7.1: (continued)

NLAKN	$f_B = 1 + C_\eta \left(C_D \nu_t/k\right)^2 \left(\Omega^2 - S^2\right), \quad f_d = \exp\left[-\left(R_t/30\right)^{\frac{3}{4}}\right]$
	$f_R = 1 + \left(C_D \nu_t/k\right)^2 \left[(22/3)\Omega^2 + (2/3)\left(\Omega^2 - S^2\right) f_B\right], \quad f_w(\xi) = \exp[-(n^*/\xi)^2]$
	$n^* = u_\varepsilon n/\nu, \;\; u_\varepsilon = (\nu\varepsilon)^{\frac{1}{4}}, \quad S^2 = S_{ij}S_{ij}, \;\; \Omega^2 = \Omega_{ij}\Omega_{ij}, \quad C_\eta = 5.0, \;\; C_D = 0.8$
NLMK	$A_{ij}(n,m) = -\delta_{ij} - \delta_{in}\delta_{jn} + 4\delta_{im}\delta_{jm}$; n : wall-normal direction, m : streamwise direction
NLCLS	$A_2 = a_{ij}a_{ji}, \quad a_{ij} = \overline{u_i u_j}/k - 2\delta_{ij}/3, \quad \tilde{S} = (k/\tilde{\varepsilon})\sqrt{2S_{ij}S_{ij}}, \quad \tilde{\Omega} = (k/\tilde{\varepsilon})\sqrt{2\Omega_{ij}\Omega_{ij}}$
	$f_c = r_\eta^2 / \left(1 + 0.45\eta^{2.5}\right)$
	$f_r = \left\{1.1\sqrt{\tilde{\varepsilon}/\varepsilon}\left[1 - 0.8\exp\left(-\tilde{R}_t/30\right)\right]\right\} / \left(1 + 0.6A_2 + 0.2A_2^{3.5}\right)$
	$f_q = r_\eta / \sqrt{1 + 0.0086\eta^2}, \quad r_\eta = 1 + \left\{1 - \exp\left[-(2A_2)^3\right]\right\}\left[1 + 4\sqrt{\exp\left(-\tilde{R}_t/20\right)}\;\right]$
	$\tilde{R}_t = k/(\nu\tilde{\varepsilon}), \quad \tilde{\varepsilon} = \varepsilon - 2\nu\left(\partial\sqrt{k}/\partial x_j\right)^2, \quad \eta = r_\eta \max(\tilde{S}, \tilde{\Omega})$
NLAL	$\tilde{a}_{11} = 1 + 0.42\exp\left(0.296 x_2^{*\frac{1}{2}} - 0.040 y^*\right) - 2/3$
	$\tilde{a}_{22} = 0.404\left[1 - \exp\left(-0.001x_2^* - 0.000147x_2^{*2}\right)\right] - 2/3$
	$\tilde{a}_{12} = 0.3\left[1 - \exp\left(-0.00443 x_2^{*\frac{1}{2}} - 0.0189 x_2^*\right)\right]$
	$f_0 = 1 + 1.25\max\left(0.09\tilde{\sigma}^2, 1.0\right), \quad f_c = \left[1 + (1/3)\bar{\beta}^2 - \bar{\gamma}^2\right]$
	$f_p = 2f_0 / \left[1 + \sqrt{1 + 4f_0(f_0 - 1)(\sigma/\tilde{\sigma})^2}\right], \quad x_2^* = x_2\sqrt{k}/\nu$
	$\sigma = (k/\varepsilon)\sqrt{\left(\partial\bar{U}_i/\partial x_j\right)^2}$
	$\tilde{\sigma} = 3.33\left[1 - \exp\left(-0.45x_2^*\right)\right]\left[1 + 0.277 x_2^{*\frac{3}{2}}\exp\left(-0.088x_2^*\right)\right]$
	$\bar{\beta} = 0.22, \quad \bar{\gamma} = 0.62$
NLSA	$A = 1 - (9/8)(A_2 - A_3), \quad A_2 = a_{ij}a_{ji}, \quad A_3 = a_{ij}a_{jk}a_{ki}, a_{ij} = \overline{u_i u_j}/k - 2\delta_{ij}/3$
	$A_{ij} = c_a' \left(k/\tilde{\varepsilon}\right)^2 \left[\left(\partial\sqrt{Ak}/\partial x_i\right)\left(\partial\sqrt{Ak}/\partial x_j\right) - \delta_{ij}\left(\partial\sqrt{Ak}/\partial x_k\right)\left(\partial\sqrt{Ak}/\partial x_k\right)/3\right]$
	$c_a = -\left[(8/3)^{\frac{1}{2}} f_a\right] / \left[1 + 2\left(A_{ij}A_{ij}\right)^{\frac{1}{2}}\right], \quad c_a' = 1/\left[1 - \exp\left(-\tilde{R}_t/30\right)\right]$
	$C_{\mu A} = \min\left[1.05, 1.2\left\{1 - \exp\left[-A - (A/0.6)^\alpha\right]\right\} + 0.18\left[1 - \exp(-10A)\right]^{\frac{1}{2}}\right]$
	$C_{\mu R_t} = 1 + 2A\exp\left(-R_t^2/8100\right), \quad C_{\mu S} = \min\left[1, 1.2/(1 + 0.06\eta)\right]$
	$f_a = \exp\left[-\left(\tilde{S}/2.2\right)^2\right], \quad f_c = \left[(2/3)r_\eta^3\right] / \left[(1 + 1.8\eta)(1 + 0.45\eta^{2.5})\right]$
	$f_q = \left[(2/3)r_\eta^2(1 - f_a)\right] / \left[(1 + 1.8\eta)(1 + 0.0086\eta^2)^{\frac{1}{2}}\right]$
	$r_\eta = 1 + 0.9\left[1 + 0.4\beta\exp\left(-R_t/5\right)^{\frac{1}{4}}\right]\exp\left[-\left(A/0.7\right)^2\right], \quad \tilde{R}_t = k/(\nu\tilde{\varepsilon})$
	$\tilde{S} = (k/\tilde{\varepsilon})\sqrt{2S_{ij}S_{ij}}, \quad \tilde{\Omega} = (k/\tilde{\varepsilon})\sqrt{2\Omega_{ij}\Omega_{ij}}$
	$\alpha = 1 + 2.6\min\left[1, R_t/200\right], \quad \beta = \min\left[10, \max(0, \tilde{S} - 5)\right],$
	$\tilde{\varepsilon} = \varepsilon - 2\nu\left(\partial\sqrt{k}/\partial x_j\right)^2, \quad \eta = r_\eta \max(\tilde{S}, \tilde{\Omega})$

and $\overline{u_1u_2}$ near the wall in the channel flows. Note that the Reynolds normal stresses of the all models are expressed to include the quadratic mean velocity gradients in such cases as follows:

$$\begin{aligned}\overline{u_1^2} &= \frac{2}{3}k + C_1k\tau_R^2\left(\Omega_{12}S_{21}+\Omega_{12}S_{21}\right)\\ &\quad + C_2k\tau_R^2\left(S_{12}S_{21}-\frac{S^2}{3}\right)+C_3k\tau_R^2\left(\Omega_{12}\Omega_{21}-\frac{\Omega^2}{3}\right)+A_{11}, \qquad (7.1)\\ \overline{u_2^2} &= \frac{2}{3}k + C_1k\tau_R^2\left(\Omega_{21}S_{12}+\Omega_{21}S_{12}\right)\\ &\quad + C_2k\tau_R^2\left(S_{21}S_{12}-\frac{S^2}{3}\right)+C_3k\tau_R^2\left(\Omega_{21}\Omega_{12}-\frac{\Omega^2}{3}\right)+A_{22}, \qquad (7.2)\\ \overline{u_3^2} &= \frac{2}{3}k + C_2k\tau_R^2\left(-\frac{S^2}{3}\right)+C_3k\tau_R^2\left(-\frac{\Omega^2}{3}\right)+A_{33}, \qquad (7.3)\end{aligned}$$

where $S^2 = S_{mn}S_{mn}$ and $\Omega^2 = \Omega_{mn}\Omega_{mn}$. Therefore, the both quadratic and cubic models are of an identical expression for the Reynolds normal stress components.

The NLAKN model can not reproduce anisotropy adequately near the wall, while the NLMK and NLCLS models give negative values for the Reynolds normal stress components $\overline{u_2^2}$ and $\overline{u_3^2}$ as shown in Figs. 7.2(b)(c) and 7.4(b)(c). Thus, these models do not satisfy the realizability constraint for the Reynolds normal stress. Evaluations of the modeled Reynolds shear stress are shown in Figs. 7.2(d) and 7.3(d). Note that the cubic type models include the cubic mean velocity gradients in the expression, and the quadratic type models do not:

$$\begin{aligned}\overline{u_1u_2} = &-2C_0\nu_tS_{12}\\ &\text{—— quadratic model ——}\\ &+C_5k\tau_R^3\left(\Omega_{12}\Omega_{21}S_{12}+S_{12}\Omega_{21}\Omega_{12}\right)+C_6k\tau_R^3S_{12}S^2+C_7k\tau_R^3S_{12}\Omega^2\\ &\text{—— cubic model ——}. \qquad (7.4)\end{aligned}$$

In Figs. 7.2(d) and 7.4(d), it can be seen that the NLMK, NLCLS and NLAL overpredict the Reynolds shear stress near the wall for an insufficient reflection of wall effects.

The wall-limiting behaviour of turbulence is given by the Taylor-series expansion of turbulent quantities near the wall as: $\overline{u_1^2} \propto x_2^2$, $\overline{u_2^2} \propto x_2^4$, $\overline{u_3^2} \propto x_2^2$, $\overline{u_1u_2} \propto x^3$, $k \propto x_2^2$ and $\varepsilon \propto x_2^0$. It is confirmed from Figs. 7.3(b) and 7.5(b) that only the NLMK model satisfies the wall-limiting behaviour of $\overline{u_2^2}$ though it does not fulfill the realizability conditions. The wall-limiting behaviour of the Reynolds shear stress is indicated in Figs. 7.3(d) and 7.5(d). Since the NLCLS and NLSA models adopt the quasi dissipation-rate, i.e., $\widetilde{\varepsilon}\,[=\varepsilon - 2\nu(\partial\sqrt{k}/\partial x_j)^2]$ which is exactly proportional to x_2^2 in the definition itself, but often it is proportional to x_2^1 with the solved

equations (Nagano & Hishida 1987), the models do not satisfy the wall-limiting behaviour of $\overline{u_1 u_2}$.

In the rotating channel flow (noninertial frame), the evaluations of the Reynolds stress component expressions are shown in Figs. 7.6–7.9, in which the results are indicated on both the pressure and suction sides. Moreover, no models satisfying both the wall-limiting behaviour and the anisotropy of the normal stress components are observed from the figures. Obviously, the flow tends to laminarize on the suction side, and though the NLAL model retains the realizability constraint for the Reynolds normal stress in the assessments of the inertial frame, the model can not fulfill the realizability conditions on the suction side in the noninertial frame. Regarding the prediction of the Reynolds shear stress, it can be seen that all models give insufficient predictions as shown in Figs. 7.6(d) and 7.7(d).

From these evaluations of the Reynolds stress expressions in the low-Reynolds-number nonlinear k–ε models, it is evident that models satisfying both the wall-limiting behaviour and anisotropy of the Reynolds normal stress components do not exist.

7.2 Proposal of nonlinear eddy viscosity model

From the results of model assessment, we have confirmed that the NLMK model (Myong & Kasagi 1990b) satisfies the wall-limiting behaviour, but that it gives a negative value of $\overline{u_2^2}$ near the wall. Since the additional term proposed by Myong and Kasagi (1990b) includes the unit tensors which determine the streamwise and wall-normal directions, the model may be difficult to handle for an analysis of fluid flows along complex shapes. In this study, on the basis of the physical consideration of turbulence, we have improved the NLAKN model (Abe *et al.* 1997) to reproduce the wall-limiting behaviour and anisotropy of the Reynolds normal stress components near the wall.

The Reynolds stress expression is modified to represent the original part as well as the wall reflection part, similar to a wall-reflection term for the pressure-strain correlation in the Reynolds stress model, as follows:

$$\overline{u_i u_j} = \frac{2}{3} k \delta_{ij} - 2 C_0 \nu_t S_{ij} + Q_o + Q_w, \tag{7.5}$$

where

$$Q_o = C_1 k\tau_{Ro}^2(W_{jk}S_{ki}+W_{ik}S_{kj}) + C_2 k\tau_{Ro}^2\left(S_{ik}S_{kj}-\frac{\delta_{ij}}{3}S_{mn}S_{mn}\right), \tag{7.6}$$

$$Q_w = C_1' k\tau_{Rw}^2(W_{jk}S_{ki}+W_{ik}S_{kj}) + C_2' k\tau_{Rw}^2\left(S_{ik}S_{kj}-\frac{\delta_{ij}}{3}S_{mn}S_{mn}\right), \tag{7.7}$$

where C_1' and C_2' are the model constants for the wall-reflection term, and $W_{ij}=\Omega_{ij}+\epsilon_{mji}\Omega_m$ is used for satisfying the MFI in the noninertial frame (Speziale *et al.* 1997). The quantity $\tau_{Ro}(=\nu_t/k)$ is the characteristic time-scale defined in the original model (Abe *et al.* 1997), and the time-scale τ_{Rw} in the wall-reflection part, Q_w, should be modeled to improve the near-wall behaviour. We have considered typical wall shear flows with/without the spanwise rotation, in which the mean shear $\partial\bar{U}_1/\partial x_2$ is the dominant parameter. Thus, in the wall-normal direction, the Reynolds stress component should satisfy the following equation from the relation between the model expression for $\overline{u_2^2}$ in Eq. (7.5) and the Taylor-series expansion in Eqs. (2.4)–(2.22).

$$\begin{aligned}\overline{u_2^2} = \frac{2}{3}k + k\tau_{Ro}^2\left[C_1(-2S_{12}W_{12})+C_2\frac{S_{12}S_{12}}{3}\right]\\ + k\tau_{Rw}^2\left[C_1'(-2S_{12}W_{12})+C_2'\frac{S_{12}S_{12}}{3}\right],\end{aligned} \tag{7.8}$$

where we have set the model constants $C_1'=C_1$ and $C_2'=C_2$, respectively, and $C_1=C_2=4C_D/f_R$ in the original model (Abe *et al.* 1997), thus,

$$\begin{aligned}\alpha_v x_2^4+\cdots =& \frac{2}{3}\beta_v x_2^2 - \beta_v x_2^2(\tau_{Ro}^2+\tau_{Rw}^2)\left[2C_1\left(C_{S0}+C_{S1}x_2\right)\left(C_{S0}+C_{\Omega1}x_2-\Omega_3\right)\right.\\ & \left.-C_2(C_{S0}+C_{S1}x_2)^2/3\right]+\cdots,\end{aligned} \tag{7.9}$$

here α_v, β_v and γ_v are the coefficients which occur in the Taylor-series expansion of turbulent quantities as follows:

$$\alpha_v = \overline{c_2^2} = (1/4)\overline{(\partial^2 u_2/\partial x_2^2)^2}, \tag{7.10}$$

$$\beta_v = (\overline{b_1^2}+\overline{b_3^2})/2, \tag{7.11}$$

$$\gamma_v = 2(C_{S0}+C_{S1}x_2)(5C_{S0}/6+C_{\Omega1}x_2-C_{S1}x_2/6-\Omega_3). \tag{7.12}$$

Therefore, the following relation should hold:

$$\alpha_v x_2^4+\cdots = \frac{2}{3}\beta_v x_2^2 - C_1\beta_v x_2^2\tau_{Rw}^2\gamma_v - C_1\beta_v x_2^2\tau_{Ro}^2\gamma_v+\cdots. \tag{7.13}$$

Consequently, to balance the above equation in the order of x_2^4, the characteristic time-scale τ_{Rw} should satisfy the following relation.

$$\tau_{Rw} = \sqrt{\frac{1}{C_1}\left(\frac{2}{3} - \frac{\alpha_v}{\beta_v}x_2^2\right)\frac{1}{\gamma_v}}. \tag{7.14}$$

where α_v, β_v and γ_v should be modeled.

First, we have modeled α_v in Eq. (7.14) with x_2^2 using the velocity scale $\sqrt{k}$ and a length scale ℓ as follows:

$$\alpha_v x_2^2 = \overline{c_2^2}x_2^2 = \frac{1}{4}\overline{\left(\frac{\partial^2 v}{\partial x_2^2}\right)^2}x_2^2 \simeq \frac{1}{4}C_v\frac{k}{\ell^2}, \tag{7.15}$$

where C_v is the model constant, and the length scale ℓ is represented as the Kolmogorov micro scale, $\nu^{\frac{3}{4}}/\varepsilon^{\frac{1}{4}}$, we obtain:

$$\frac{1}{4}C_v\frac{k}{\ell^2} = \frac{1}{4}C_v\frac{k}{\nu^{\frac{3}{2}}/\varepsilon^{\frac{1}{2}}}. \tag{7.16}$$

The following relation is obtained with Eqs. (2.13) and (2.14) for the coefficient β in Eq. (7.14):

$$\beta_v = \frac{\overline{b_1^2} + \overline{b_3^2}}{2} \simeq \frac{\varepsilon}{2\nu}. \tag{7.17}$$

Therefore, $(\alpha_v/\beta_v)x_2^2$ in Eq. (7.14) is modeled as follows:

$$\frac{\alpha_v}{\beta_v}x_2^2 \simeq \frac{1}{4}C_v\frac{k}{\nu^{\frac{3}{2}}/\varepsilon^{\frac{1}{2}}}\frac{2\nu}{\varepsilon} = \frac{1}{2}C_v\sqrt{R_t}, \tag{7.18}$$

where $R_t = k^2/(\nu\varepsilon)$ is the turbulent Reynolds number.

On the other hand, regarding the coefficient of Taylor series expansion for the mean velocity gradient, the following relations hold:

$$S^2 = S_{ij}S_{ij} \simeq 2(C_{S0} + C_{S1}x_2)^2, \tag{7.19}$$

$$W^2 = W_{ij}W_{ij} \simeq 2(C_{S0} + C_{\Omega 1}x_2 - \Omega_3)^2. \tag{7.20}$$

By this relation, the coefficient γ in Eq. (7.14) can be represented as follows:

$$\gamma_v \simeq \frac{W^2}{2} + \frac{S^2}{3} - \left(\sqrt{\frac{S^2}{2}} - \sqrt{\frac{W^2}{2}}\right)^2, \tag{7.21}$$

where in order to avoid a negative value of the equation (7.21), we have adopted the model function f_{v1} which goes to 0 away from the wall, when the mean velocity gradient $\partial\bar{U}_1/\partial x_2$ goes to 0.

$$\gamma_v \simeq f_{SW} = \frac{W^2}{2} + \frac{S^2}{3} - \left(\sqrt{\frac{S^2}{2}} - \sqrt{\frac{W^2}{2}}\right)^2 f_{v1}. \tag{7.22}$$

Consequently, the characteristic time-scale τ_{Rw} is modeled as follows:

$$\tau_{Rw} = \sqrt{\frac{2}{3}\frac{1}{C_1 f_{SW}}}\left(1 - \frac{3C_v\sqrt{R_t}}{8}\right). \tag{7.23}$$

Moreover, the characteristic time-scale τ_{Rw} should be a positive. However, the above model may give a negative value when R_t goes to infinity. Thus, in order to avoid a negative value of the τ_{Rw}, we have finally adopted the following formulation for the τ_{Rw}.

$$\tau_{Rw} = \sqrt{\frac{2}{3}\frac{1}{C_1 f_{SW}}}\left(1 - \frac{3C_{v1}f_{v2}}{8}\right) f_{v1}^2, \tag{7.24}$$

where $f_{v2} = 1 - \exp\left(-\sqrt{R_t}/C_{v2}\right)$ and $f_{v1} = f_w(40)$. Since f_{v2} becomes 1 at $R_t \to \infty$, the model constant C_{v1} should satisfy the inequality $3C_{v1}/8 < 1$ at this condition in order to avoid the negative value of τ_{Rw}. Near the wall, since $3C_{v1}f_{v2}/8 \simeq 3C_{v1}(\sqrt{R_t}/C_{v2})$ holds, the relation between Eq. (7.23) and Eq. (7.24) gives $C_v = C_{v1}/C_{v2}$. Thus, referring to substituting DNS data (Moser *et al.* 1999) for Eq. (7.18), we have set the model constants $C_{v1} = 0.4$ and $C_{v2} = 2 \times 10^3$ on the basis of the numerical optimization in various flows.

The model function $f_w(\xi)$ is the wall-reflection function proposed by Abe *et al.* (1994) as follows:

$$f_w(\xi) = \exp\left[-\left(\frac{n^*}{\xi}\right)^2\right], \tag{7.25}$$

where n^* is the dimensionless distance defined as $n^* = (\nu\varepsilon)^{\frac{1}{4}}n/\nu$, and $f_w(40) = f_{v1}$ means $\exp\left[-(n^*/40)^2\right]$. Note that the wall distance n is defined as "the distance between that point and the nearest point on the whole surface in a flow field" (Abe *et al.* 1997).

The model constants and functions in the proposed model are listed in Table 7.2.

7.3 Results and discussion of proposed model

The evaluations for the proposed model are shown in Figs. 7.10 and 7.11 in the inertial frame. In Fig. 7.10, the proposed model can reproduce the rational anisotropy of a Reynolds

Table 7.2: Model constants and functions of the proposed model

C_0	C_1	C_2	C_1'	C_2'	C_D	C_v	C_{v1}	C_{v2}	C_μ	C_η
$\frac{1}{f_R}$	$\frac{4C_D}{f_R}$	$\frac{4C_D}{f_R}$	C_1	C_2	0.8	$\frac{C_{v1}}{C_{v2}}$	0.4	2×10^3	0.12	5.0

f_B	f_R
$1+C_\eta\left(C_D\tau_{Ro}\right)^2\left(W^2-S^2\right)$	$1+\left(C_D\tau_{Ro}\right)^2\left[\frac{22}{3}W^2+\frac{2}{3}\left(W^2-S^2\right)f_B\right]$

f_{SW}	f_{v1}	f_{v2}	$f_w(\xi)$
$\frac{W^2}{2}+\frac{S^2}{3}-\left(\sqrt{\frac{S^2}{2}}-\sqrt{\frac{W^2}{2}}\right)^2 f_{v1}$	$f_w(40)$	$1-\exp\left(-\frac{\sqrt{R_t}}{C_{v2}}\right)$	$\exp\left[-\left(\frac{n^*}{\xi}\right)\right]$

f_μ	τ_{Ro}	τ_{Rw}
$[1-f_w(26)]\left\{1+\left(\frac{35}{R_t^{\frac{3}{4}}}\right)\exp\left[-\left(\frac{R_t}{30}\right)^{\frac{3}{4}}\right]\right\}$	$\frac{\nu_t}{k}$	$\sqrt{\frac{2}{3}\frac{1}{C_1 f_{SW}}}\left(1-\frac{3C_{v1}f_{v2}}{8}\right)f_{v1}^2$

normal stress component in comparison with the original model (Abe *et al.* 1997). Moreover, in comparison with DNS (Kasagi *et al.* 1992; Moser *et al.* 1999), it can be seen that the proposed model reproduces the rational anisotropy of the Reynolds normal stress components and exactly satisfies their wall-limiting behaviour. Distributions of the proposed characteristic time-scale τ_{Rw} are shown in Fig. 7.12. On the wall-affected region, it can be seen that the Reynolds normal stresses are subject to the proposed time-scale. In particular, the wall-normal stress component, $\overline{u_2^2}$, is suppressed with τ_{Rw} for the balance of the equation. Thus, the proper anisotropy of the Reynolds normal stress component near the wall can be reproduced by the proposed model.

Next, we have performed an *a priori* test for the proposed model in the rotating channel flow ($Re_\tau = 150$ and $Ro_\tau = 2.5$) which is typical case of the noninertial frame. Figure 7.13(a) shows the rms velocity fluctuations predicted by proposed model. That model gives the appro-

priate Reynolds normal stress components on both the pressure and suction sides in comparison with the DNS (Nishimura & Kasagi 1996). The characteristic time-scales in the rotating channel flow are shown in Fig. 7.13(b). On the suction side, since the flow tends to laminarization, a time scale of turbulence becomes shorter than on the pressure side. It can be seen that these time scales of the proposed model capture this tendency. Therefore, the proposed model yields proper prediction on the both pressure and suction sides. The wall-limiting behaviour of Reynolds normal stress components on both sides is indicated in Figs. 7.13(c) and (d). Obviously, the proposed model exactly reproduces them.

Though it is clear in the previous section that the existing nonlinear turbulence models can not satisfy the wall-limiting behaviour and anisotropy of the Reynolds normal stress components near the wall in both the inertial and noninertial frames, the present model can reproduce adequately these in the both frames. This confirms that the proper modelling was achieved for the Reynolds stress expression of the nonlinear model, in which we have adopted the wall-reflection term, Q_w in Eq. (7.5), and for the new characteristic time-scale, τ_{Rw}.

In addition, in order to explore the performance of the proposed model, we have applied it to a Couette-Poiseuille channel and backward-facing step flows as shown in Fig 7.14. For a Couette-Poiseuille channel flow, the DNS database (Kuroda *et al.* 1994) is available to provide the Reynolds number based on the moving wall velocity, $\bar{U}_w$, is $Re_w = \bar{U}_w\delta/\nu = 3000$. Figure 7.15 shows the assessment result of the proposed model in the Couette-Poiseuille channel flow. Since the weak mean velocity gradient exists on the moving-wall side, turbulence decreases on that side. It can be seen that the predicted Reynolds normal stress components are good agreement with the DNS data on both the moving-wall and stationary sides. In addition, the wall-limiting behaviour of the Reynolds normal stress components are satisfied exactly on the both sides.

Finally, we have tried to assess the proposed model in the backward-facing step flow. Since the proposed model does not contain the unit tensors to indicate flow directions, the wall-limiting behaviour of wall-normal Reynolds stress component, which is proportional to the fourth power of wall-normal direction, must be obtained automatically by determining merely the distance from the wall for the wall-reflection function in Eq. (7.25). Therefore, we have confirmed the performance of the proposed model in the flow which has two walls in different directions, i.e., a backward-facing step flow as shown in Fig. 7.14(b). Although the database

of the backward-facing step flow has been presented (e.g. Kasagi & Matsunaga 1995), the data toward the streamwise direction from the perpendicular wall has never been supplied. Thus, we have employed the prediction of the trustworthiest turbulence model proposed by Abe *et al.* (1994) for the assessment. The flow condition of the assessment is identical with the experiment (Kasagi & Matsunaga 1995). Figure 7.16 shows the wall-limiting behaviour of the proposed model near two-direction walls, i.e., one is parallel to the streamwise direction, x_1, and the other is perpendicular to the x_1 axis. On the parallel wall, the Reynolds stress component of wall-normal direction is $\overline{u_2^2}$, and on the perpendicular wall it is $\overline{u_1^2}$. Obviously, the proposed model automatically reproduces the Reynolds stress component in the wall-normal direction, with $\overline{u_2^2} \propto (x_2/h)^4$ on the parallel wall and $\overline{u_1^2} \propto (x_1/h)^4$ on the perpendicular wall.

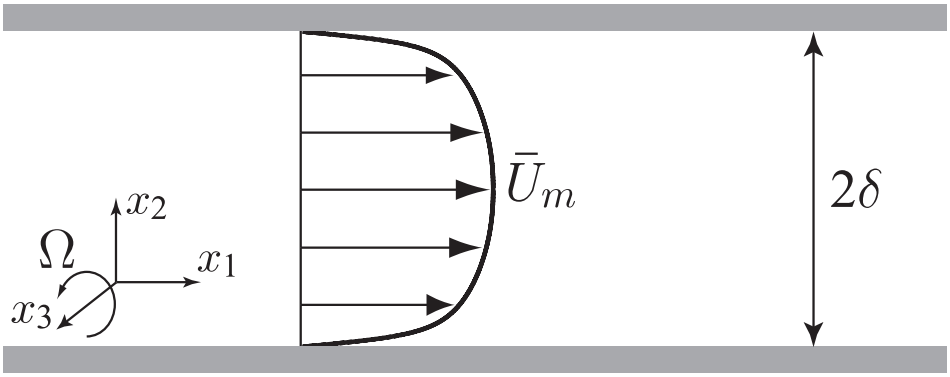

Figure 7.1: Flow geometry in a channel flow with/without rotation.

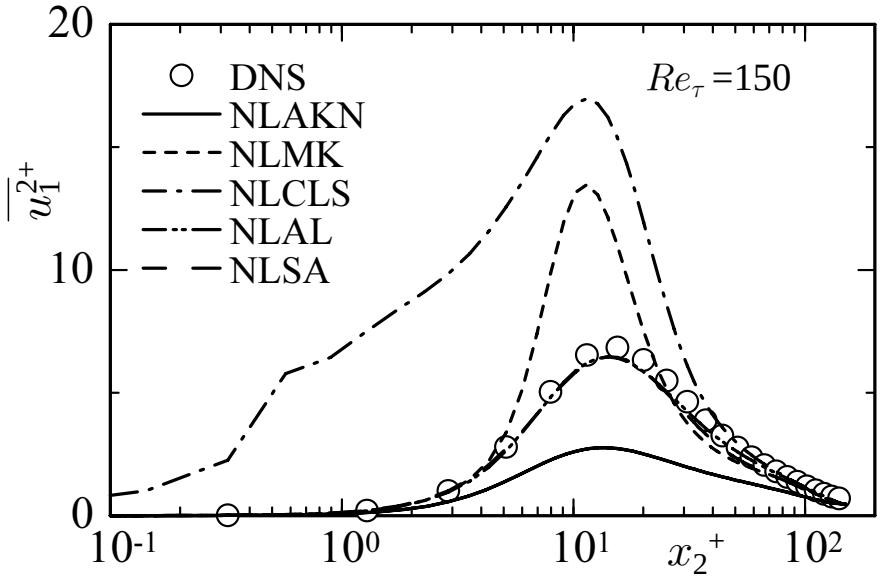

(a)

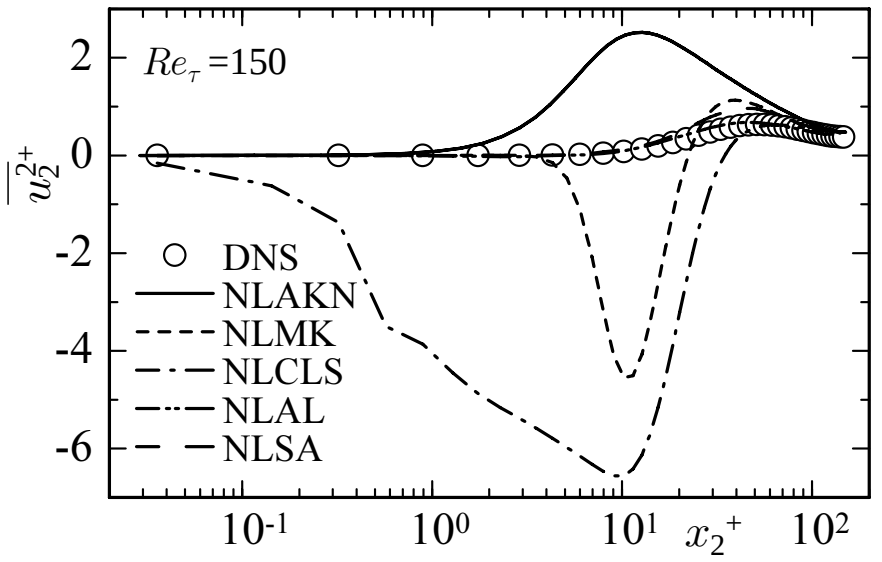

(b)

Figure 7.2: *A priori* test for Reynolds stress expressions near wall ($Re_\tau = 150$); (a) $\overline{u_1^2}$, (b) $\overline{u_2^2}$, (c) $\overline{u_3^2}$, (d) $-\overline{u_1 u_2}$.

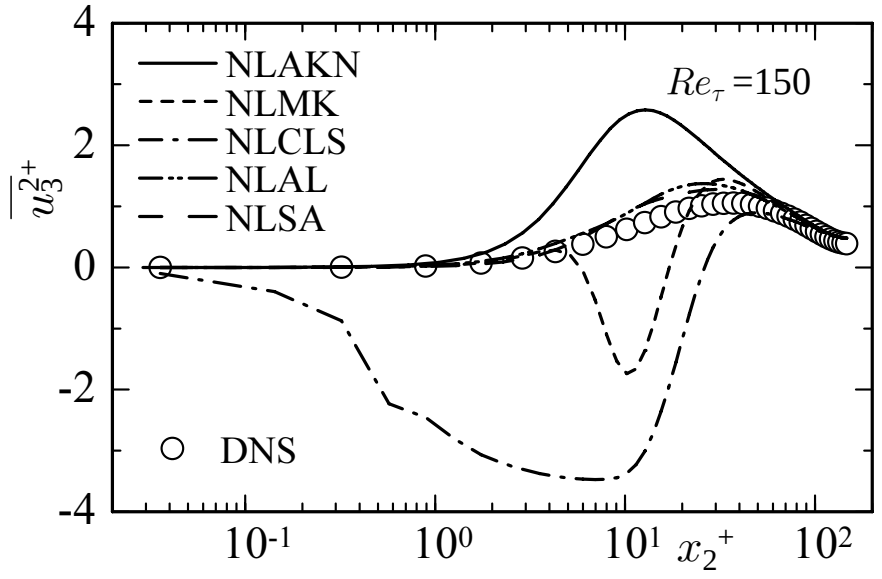

(c)

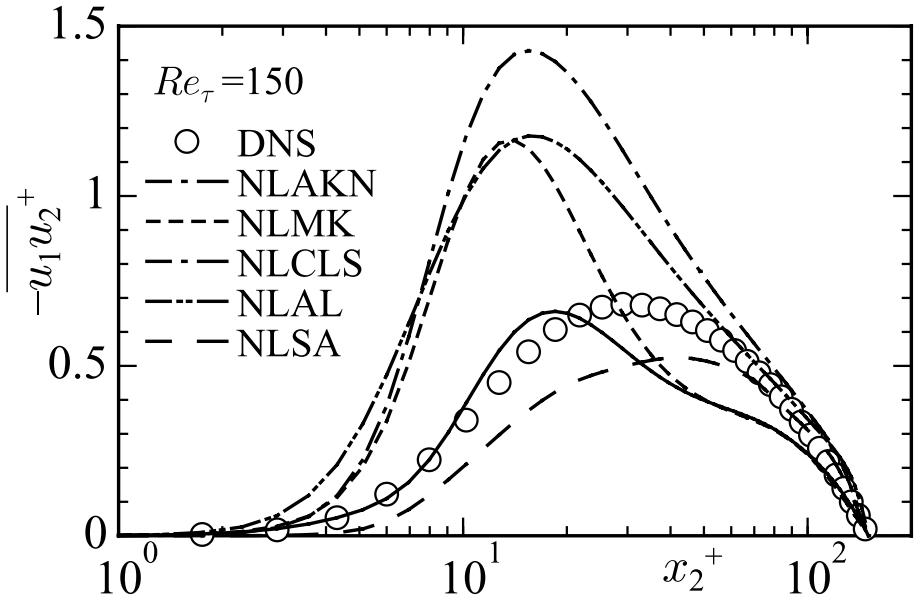

(d)

Figure 7.2: (continued)

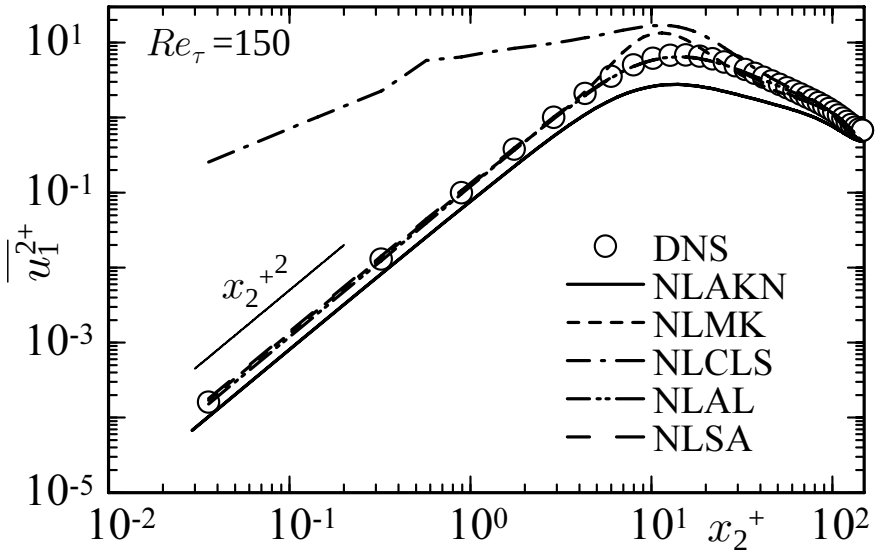

(a)

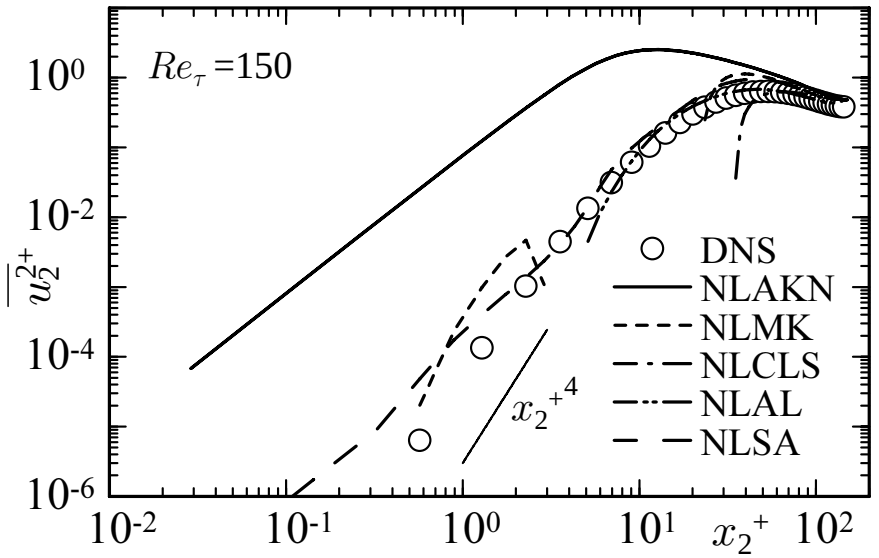

(b)

Figure 7.3: *A priori* test for wall-limiting behaviour of Reynolds stress expressions ($Re_\tau = 150$); (a) $\overline{u_1^2}$, (b) $\overline{u_2^2}$, (c) $\overline{u_3^2}$, (d) $-\overline{u_1 u_2}$.

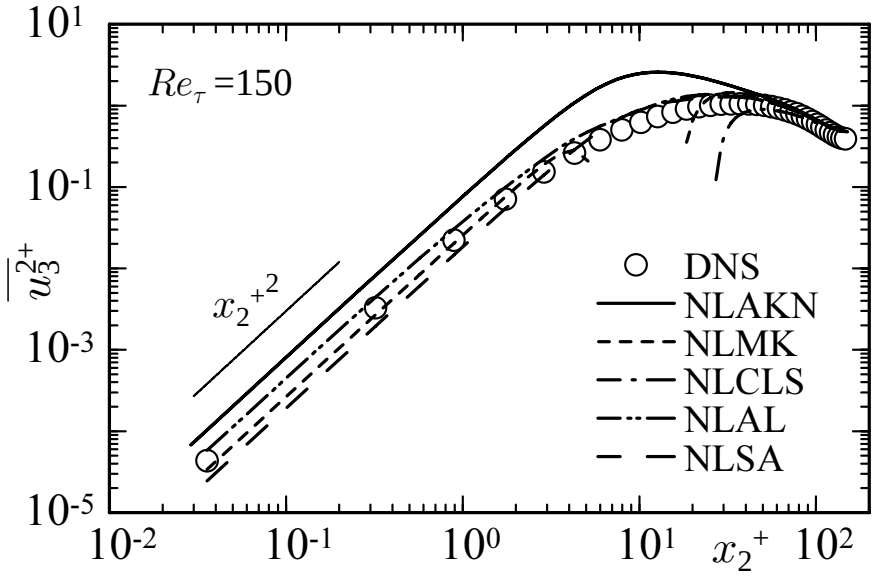

(c)

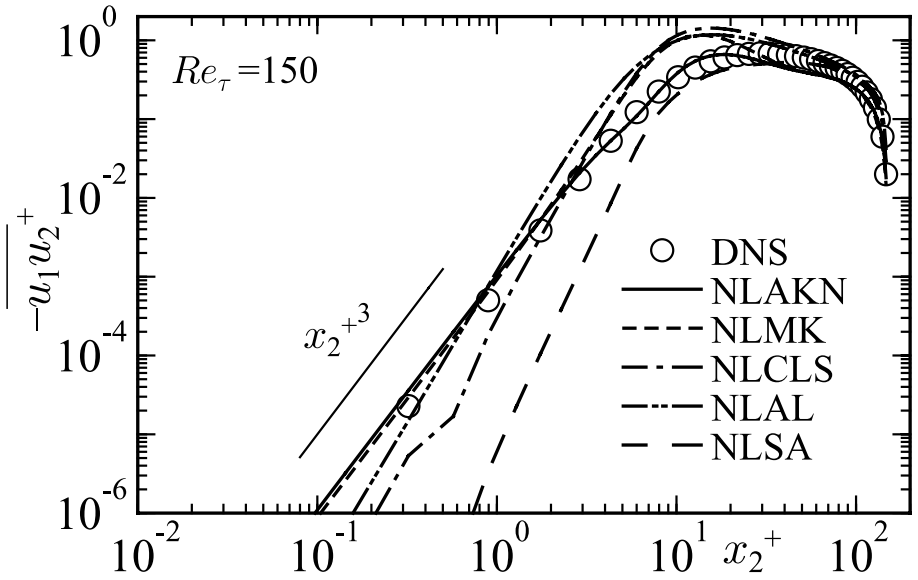

(d)

Figure 7.3: (continued)

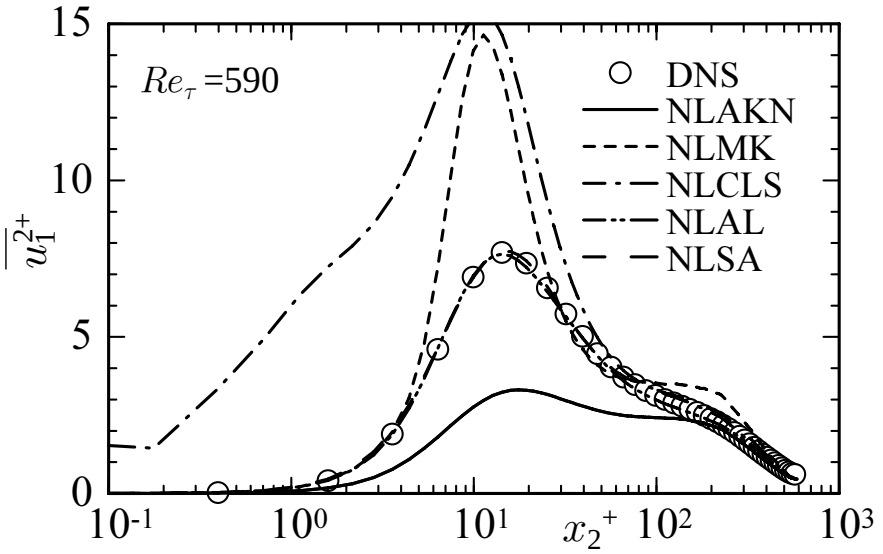

(a)

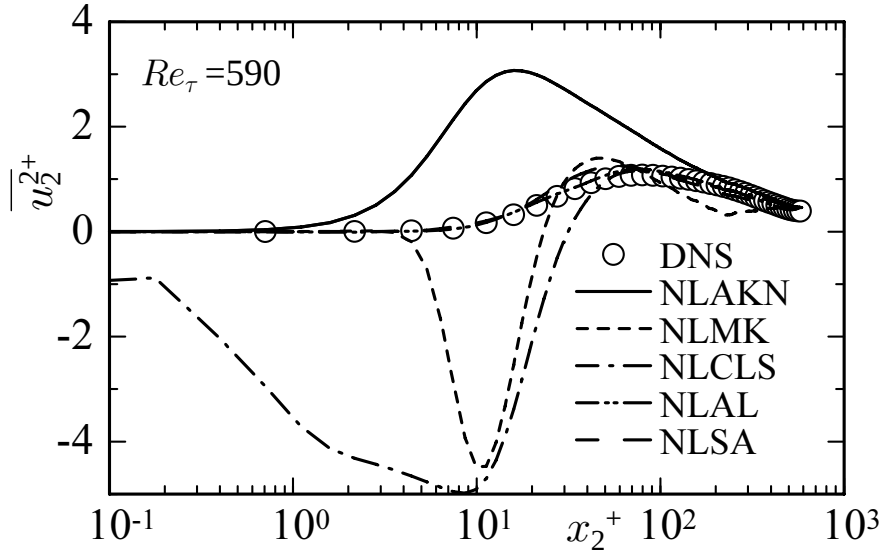

(b)

Figure 7.4: *A priori* test for Reynolds stress expressions near wall in channel flow ($Re_\tau = 590$); (a) $\overline{u_1^2}$, (b) $\overline{u_2^2}$, (c) $\overline{u_3^2}$, (d) $-\overline{u_1 u_2}$.

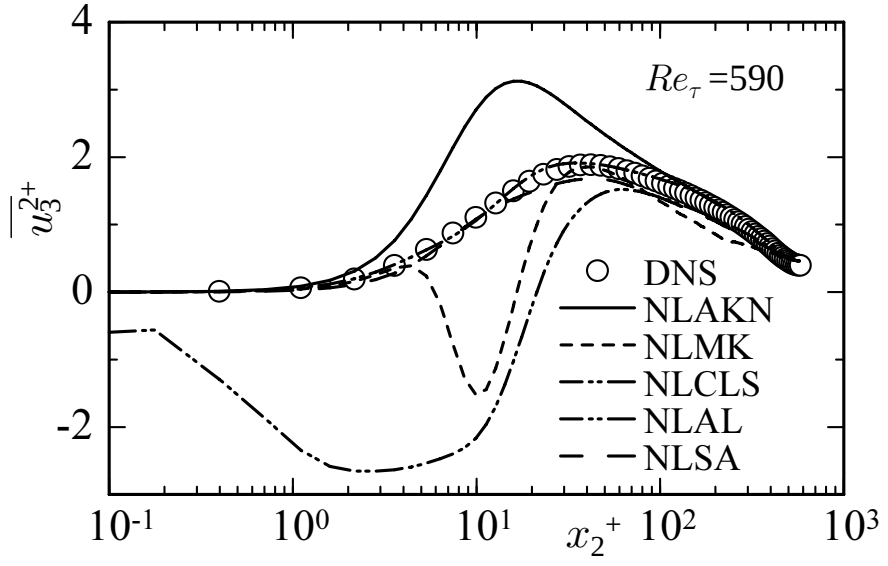

(c)

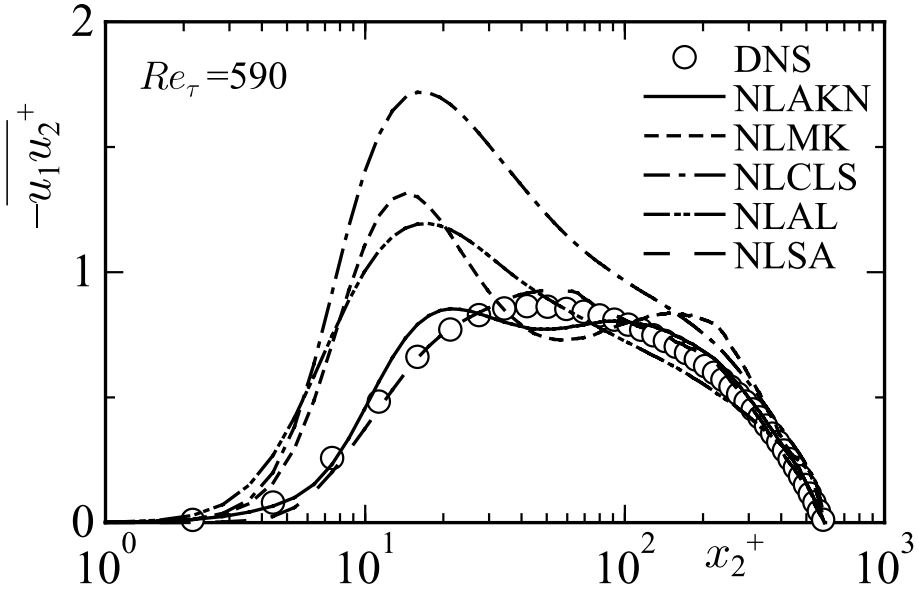

(d)

Figure 7.4: (continued)

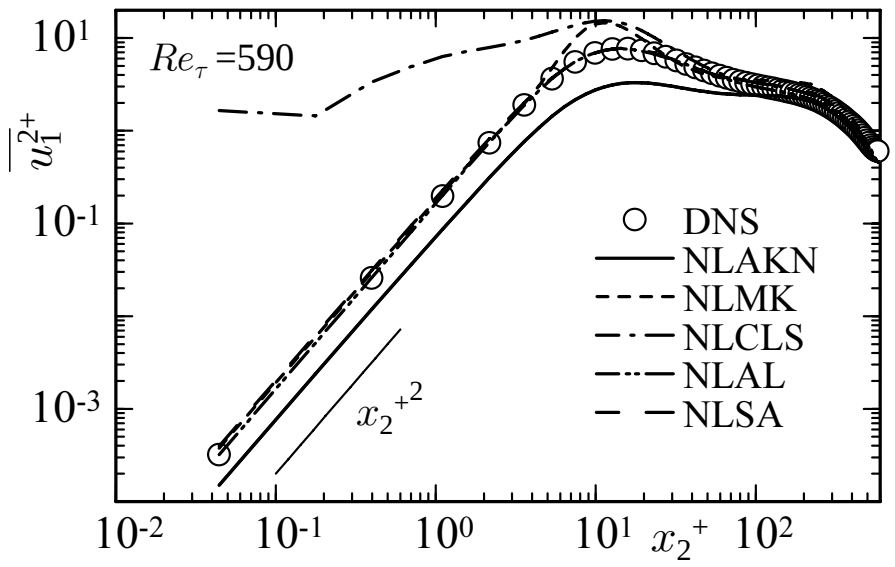

(a)

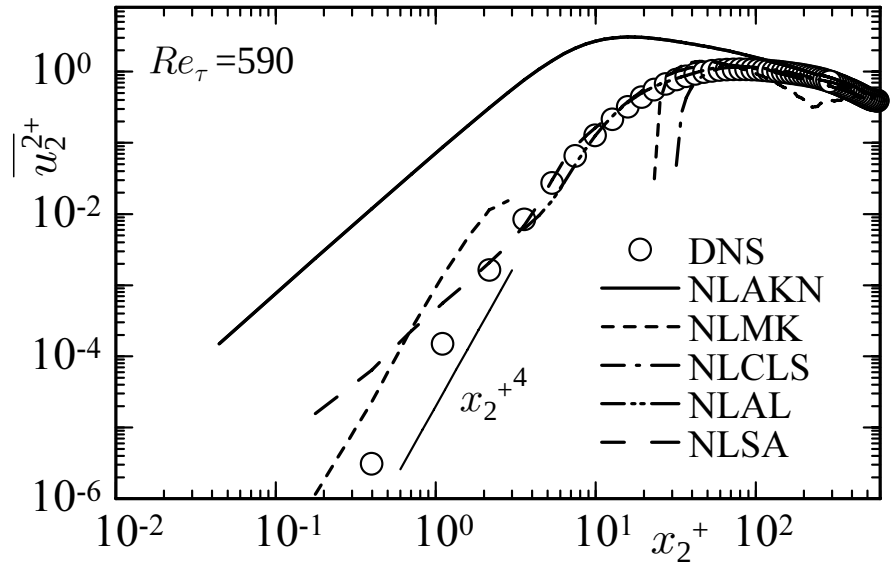

(b)

Figure 7.5: *A priori* test for wall-limiting behaviour of Reynolds stress expressions in channel flow ($Re_\tau = 590$); (a) $\overline{u_1^2}$, (b) $\overline{u_2^2}$, (c) $\overline{u_3^2}$, (d) $-\overline{u_1 u_2}$.

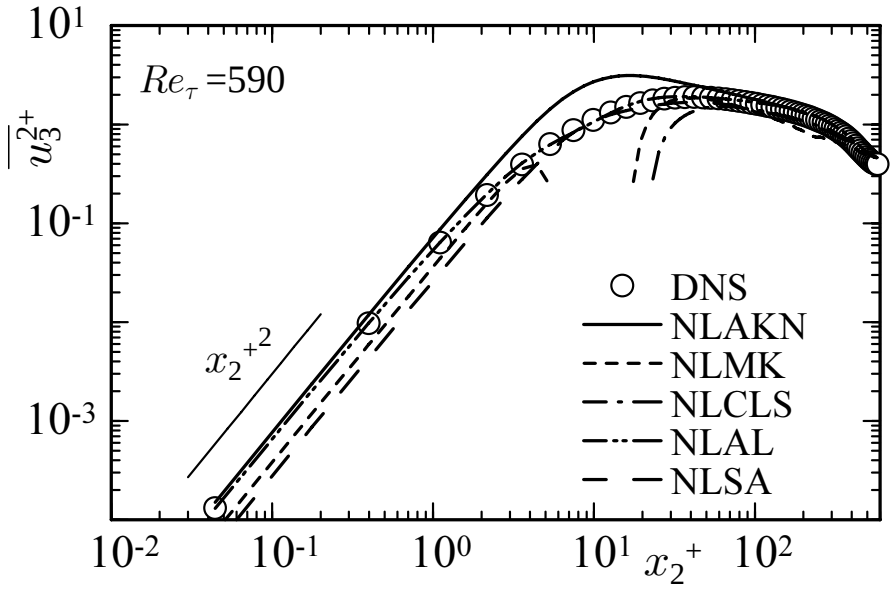

(c)

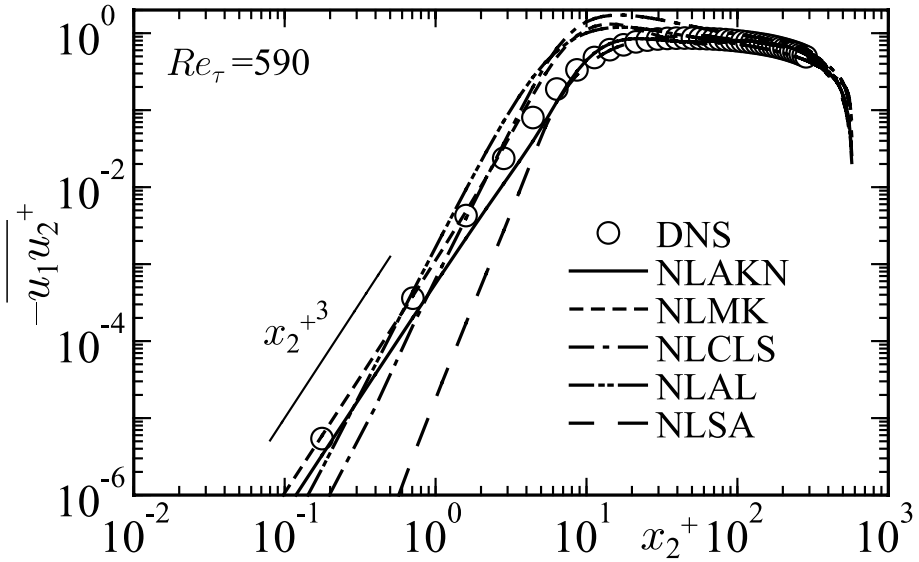

(d)

Figure 7.5: (continued)

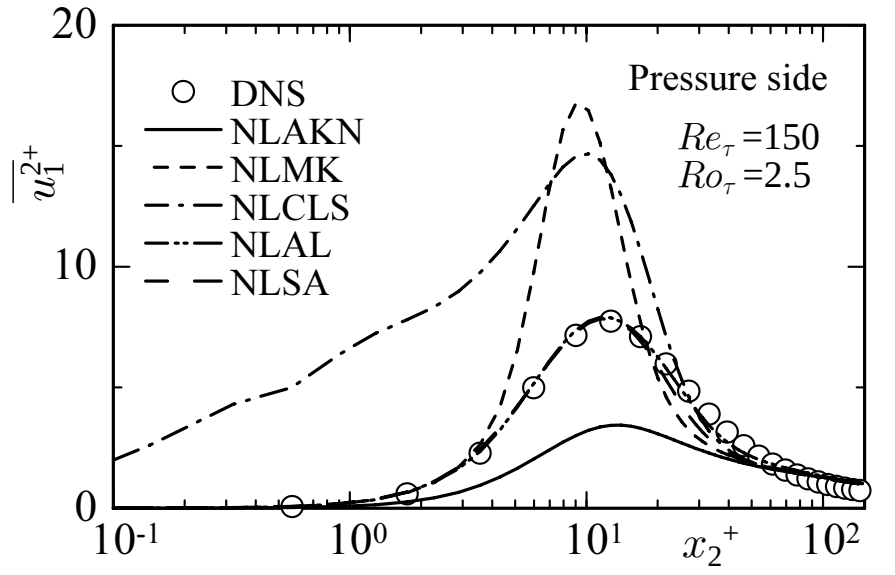

(a)

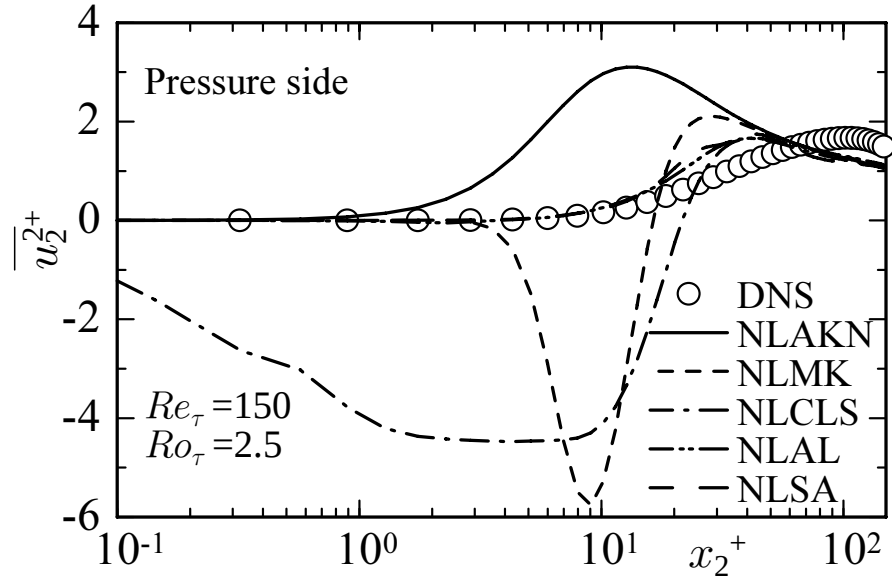

(b)

Figure 7.6: *A priori* test for Reynolds stress expressions in rotating channel flow on pressure side ($Re_\tau = 150, Ro_\tau = 2.5$); (a) $\overline{u_1^2}$, (b) $\overline{u_2^2}$, (c) $\overline{u_3^2}$, (d)$-\overline{u_1 u_2}$.

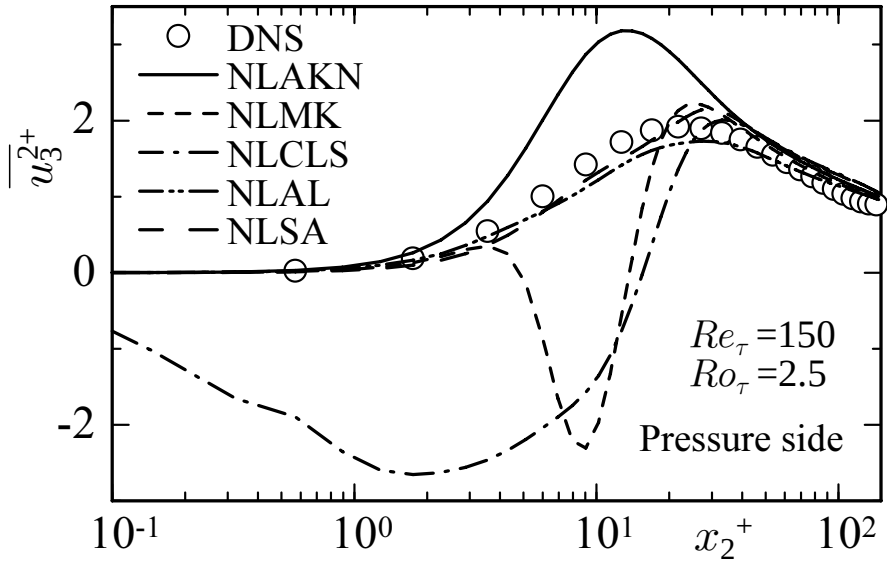

(c)

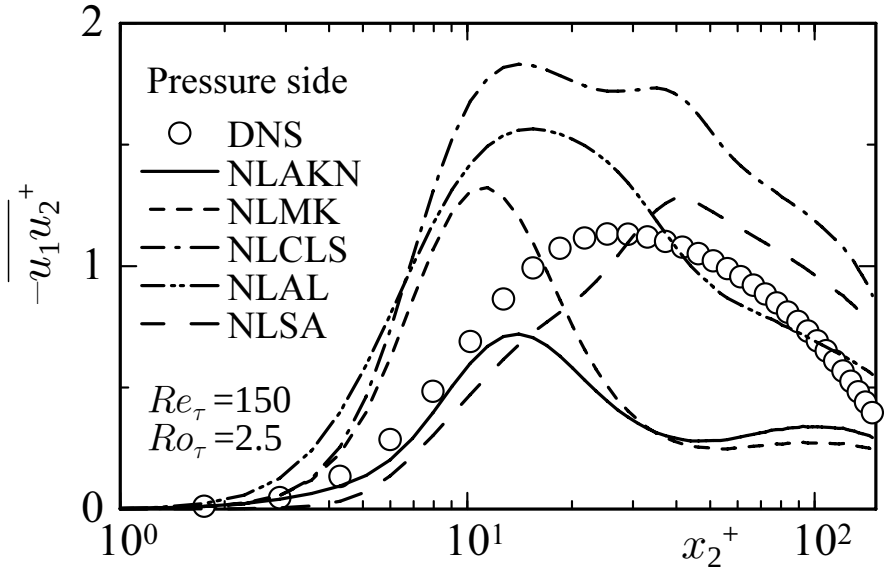

(d)

Figure 7.6: (continued)

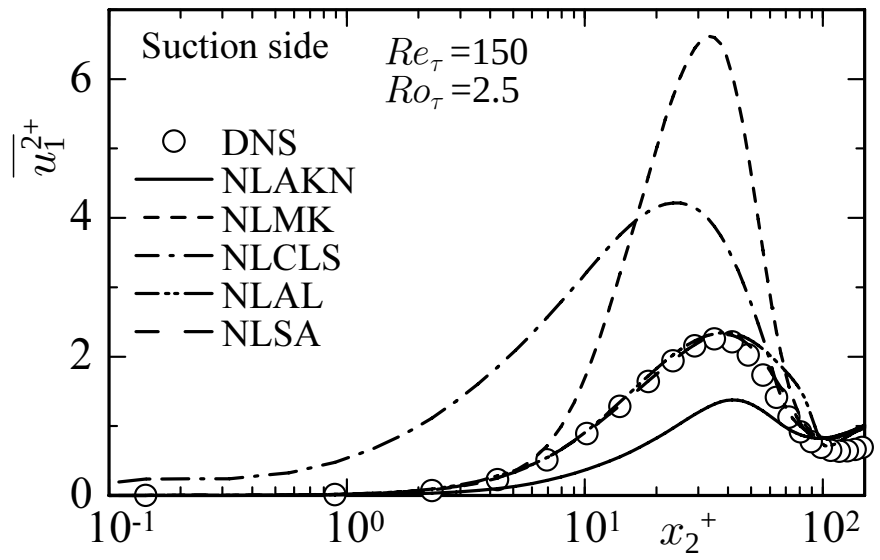

(a)

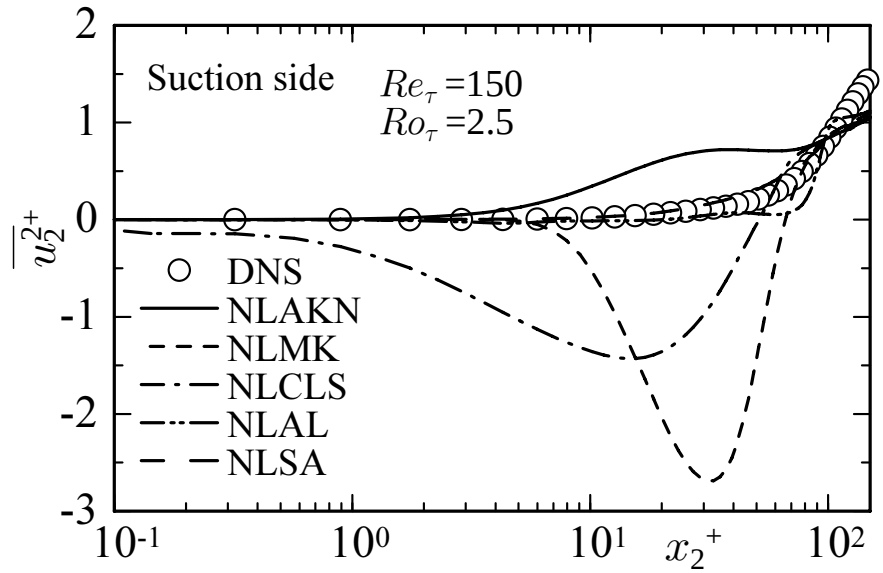

(b)

Figure 7.7: *A priori* test for Reynolds stress expressions in rotating channel flow on suction side ($Re_\tau = 150, Ro_\tau = 2.5$); (a) $\overline{u_1^2}$, (b) $\overline{u_2^2}$, (c) $\overline{u_3^2}$, (d)$\overline{u_1 u_2}$.

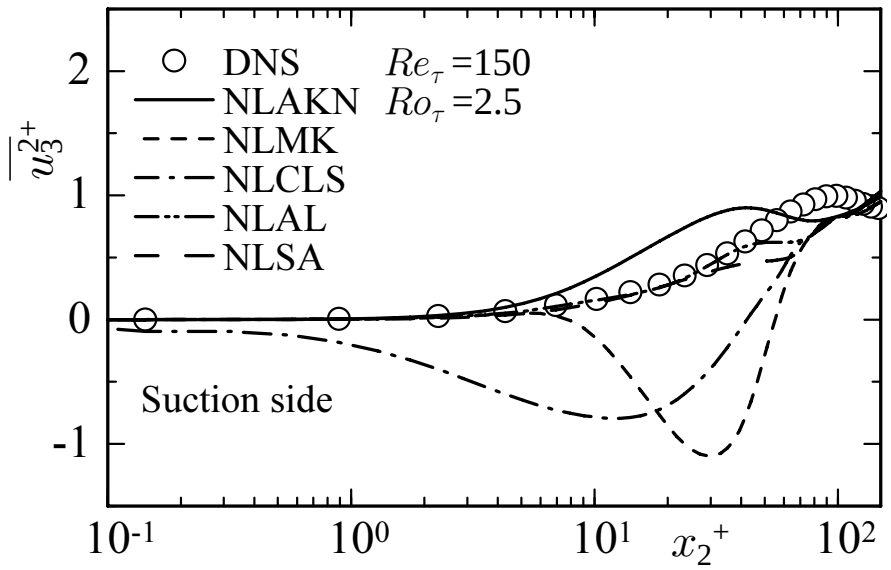

(c)

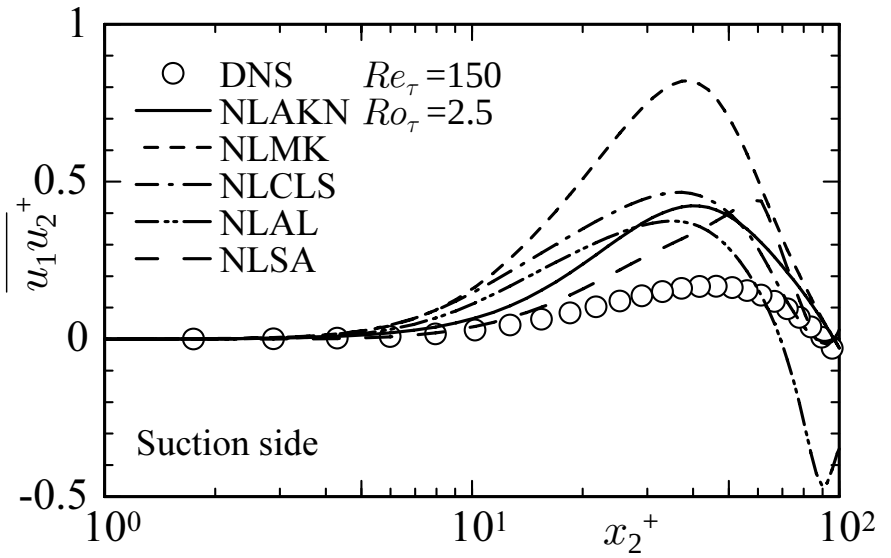

(d)

Figure 7.7: (continued)

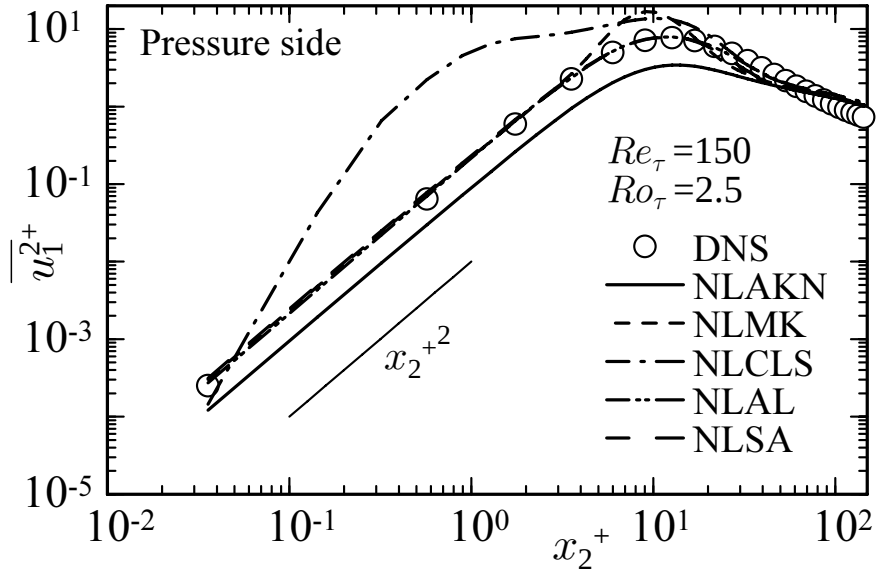

(a)

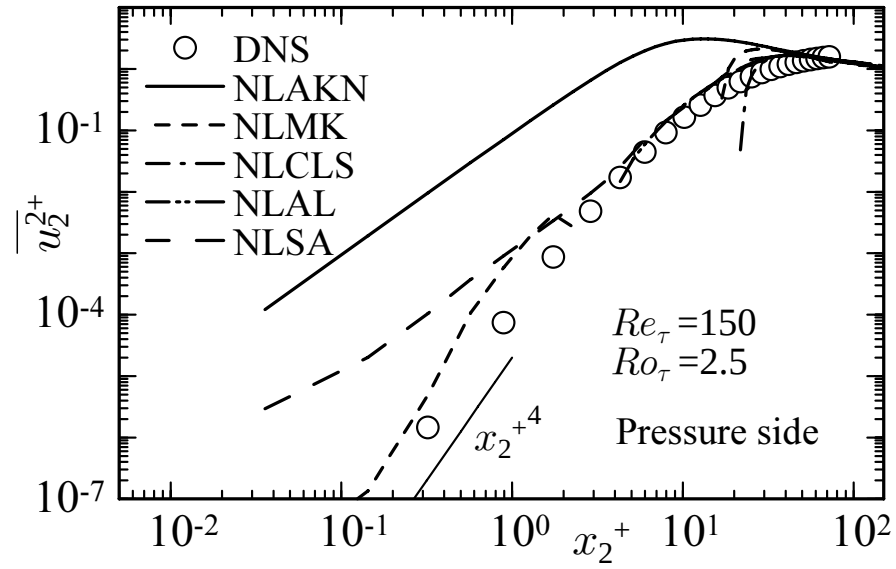

(b)

Figure 7.8: *A priori* test for wall-limiting behaviour of Reynolds stress expressions in rotating channel flow on pressure side ($Re_\tau = 150, Ro_\tau = 2.5$); (a) $\overline{u_1^2}$, (b) $\overline{u_2^2}$, (c) $\overline{u_3^2}$, (d)$-\overline{u_1 u_2}$.

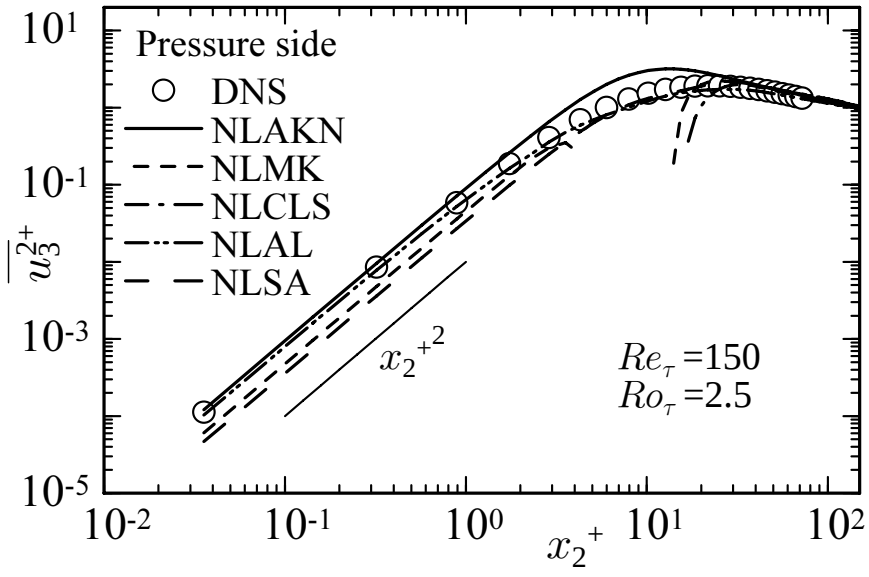

(c)

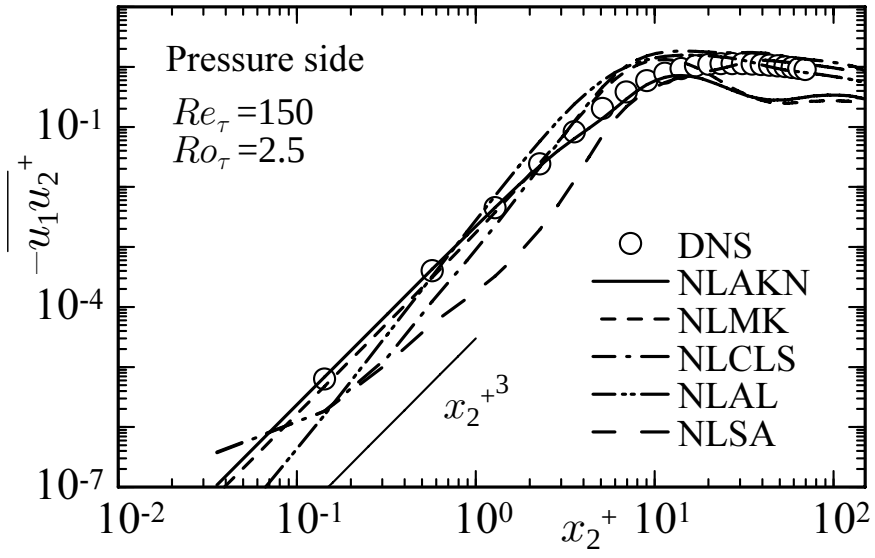

(d)

Figure 7.8: (continued)

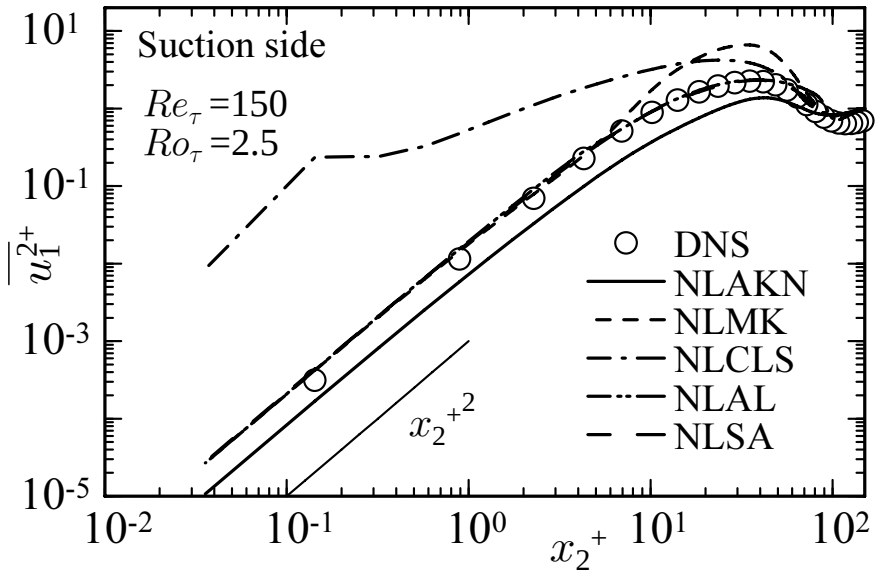

(a)

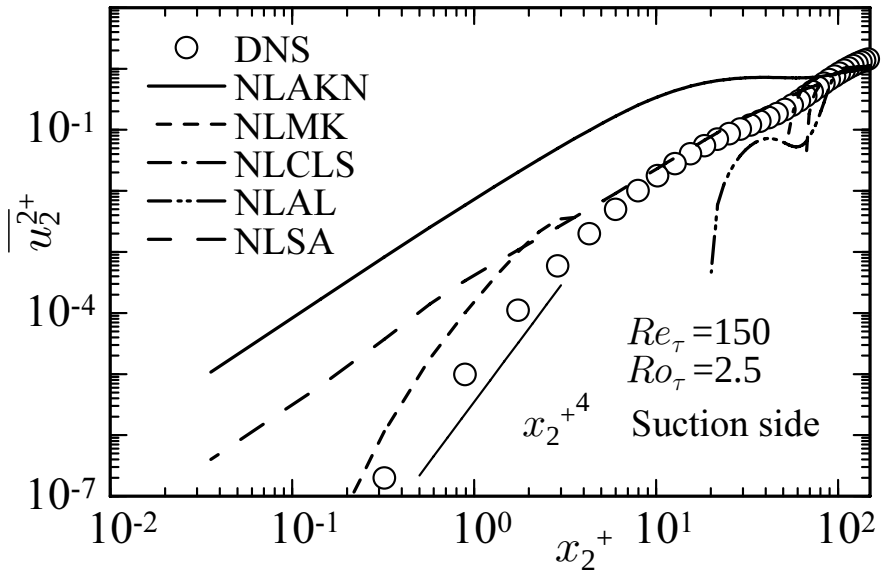

(b)

Figure 7.9: *A priori* test for wall-limiting behaviour of Reynolds stress expressions in rotating channel flow on suction side ($Re_\tau = 150, Ro_\tau = 2.5$); (a) $\overline{u_1^2}$, (b) $\overline{u_2^2}$, (c) $\overline{u_3^2}$, (d)$\overline{u_1 u_2}$.

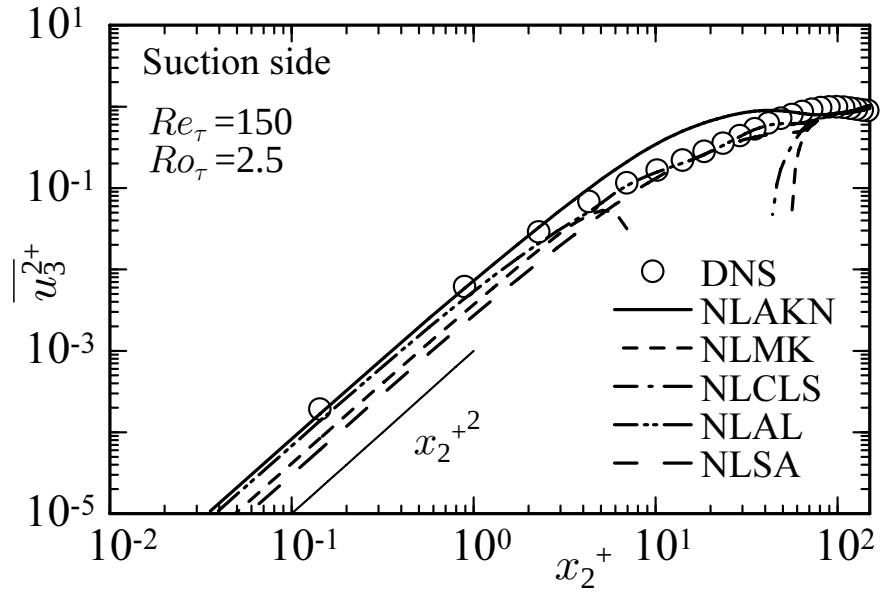

(c)

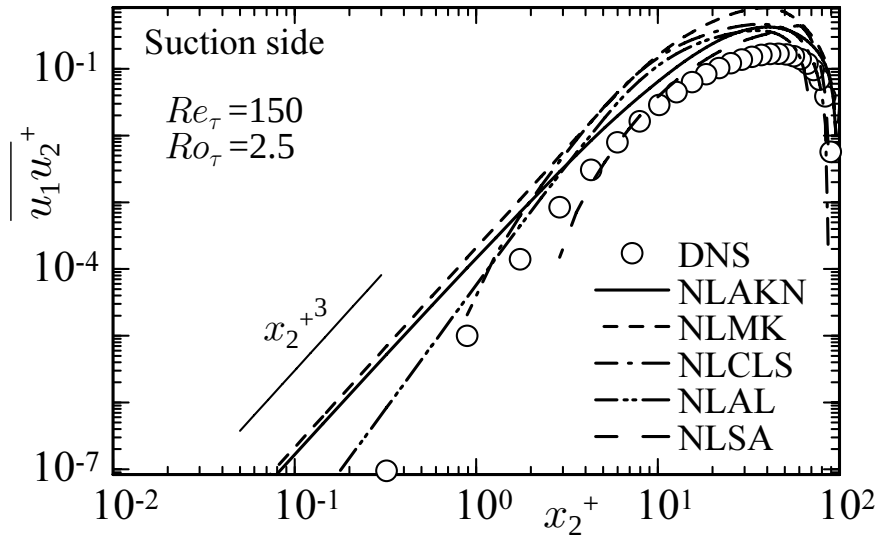

(d)

Figure 7.9: (continued)

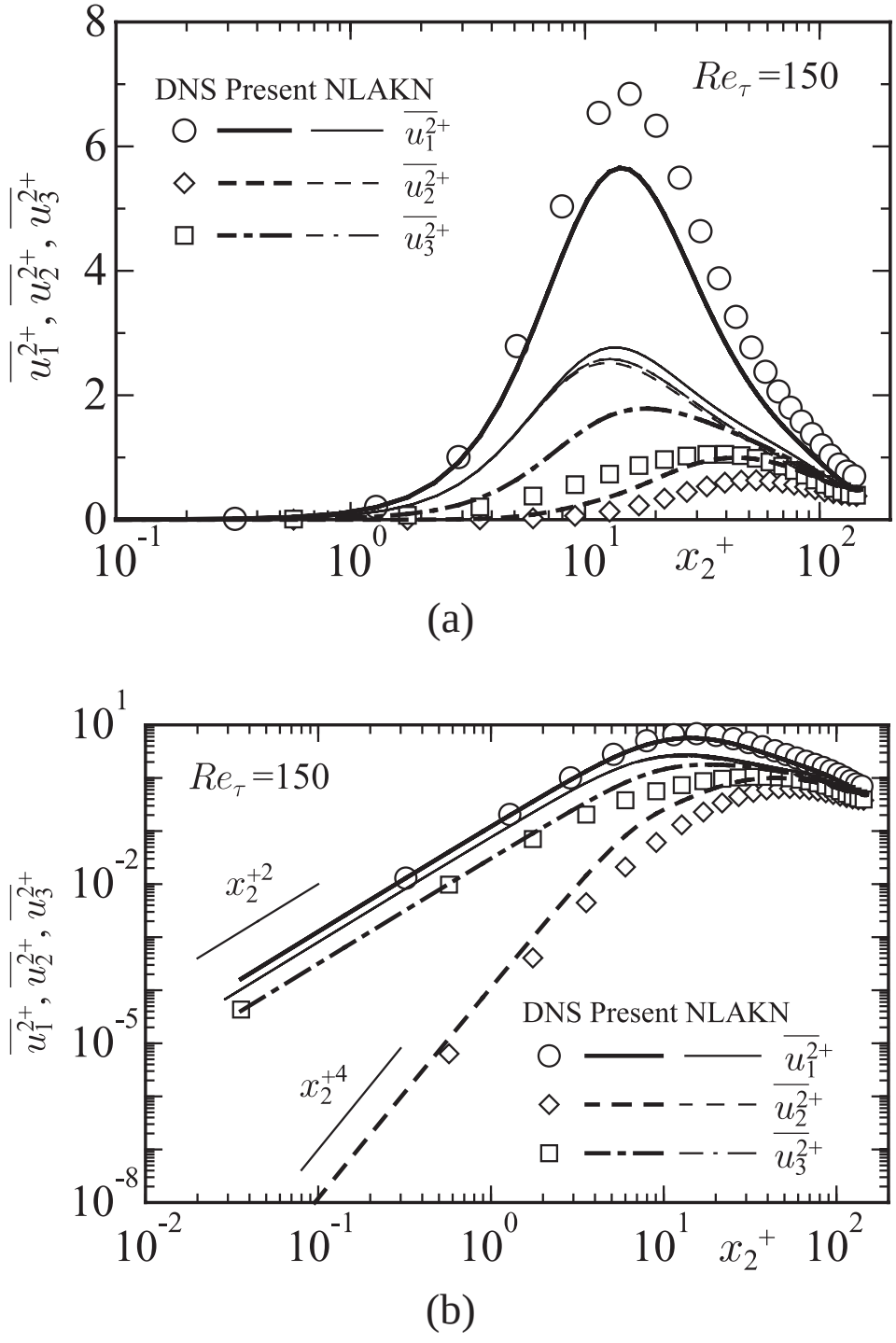

Figure 7.10: *A priori* test for the proposed Reynolds stress expression in channel flow ($Re_\tau = 150$); (a) velocity fluctuations near wall, (b) wall-limiting behaviour.

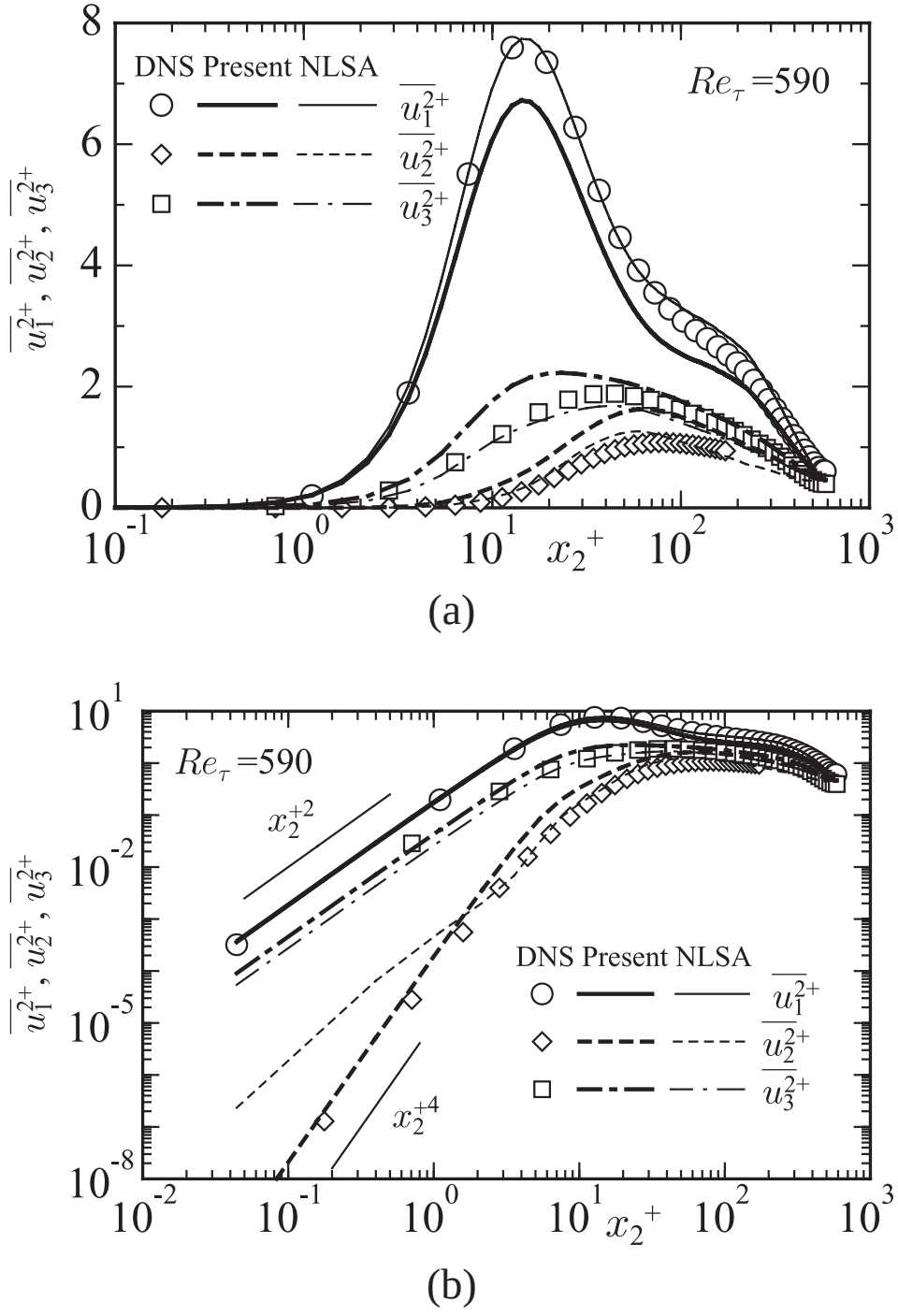

Figure 7.11: *A priori* test for the proposed Reynolds stress expression in channel flow ($Re_\tau = 590$); (a) velocity fluctuations near wall, (b) wall-limiting behaviour.

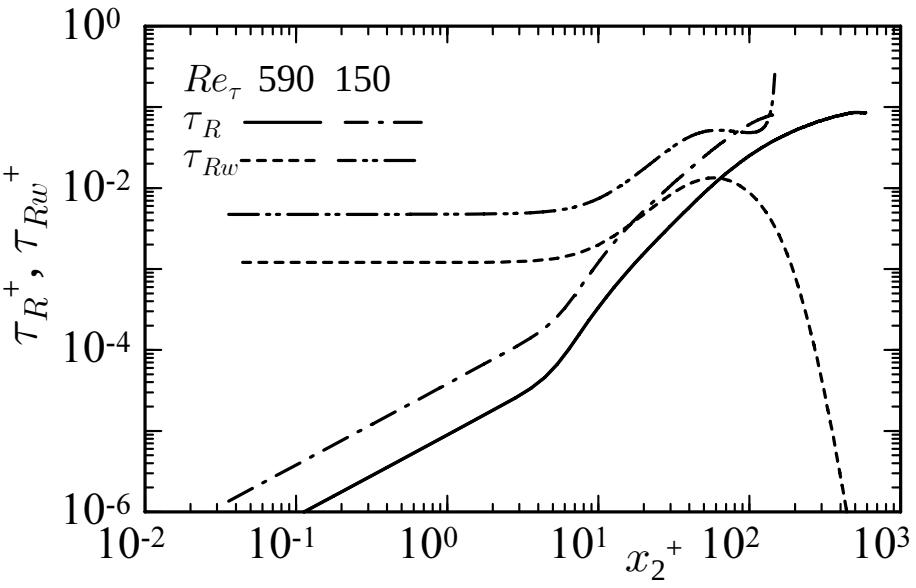

Figure 7.12: Distributions of time scale of the proposed model in channel flows

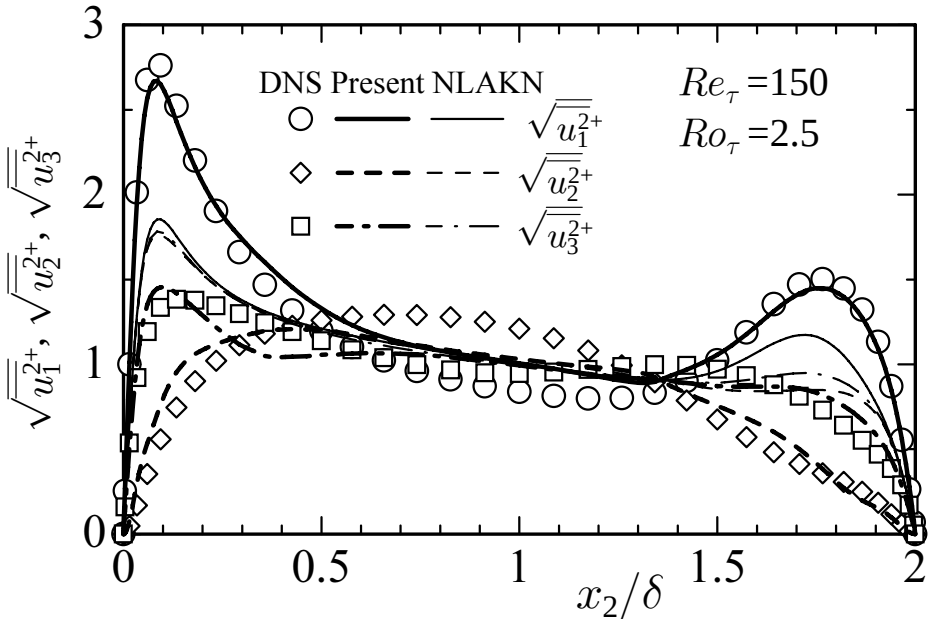

(a)

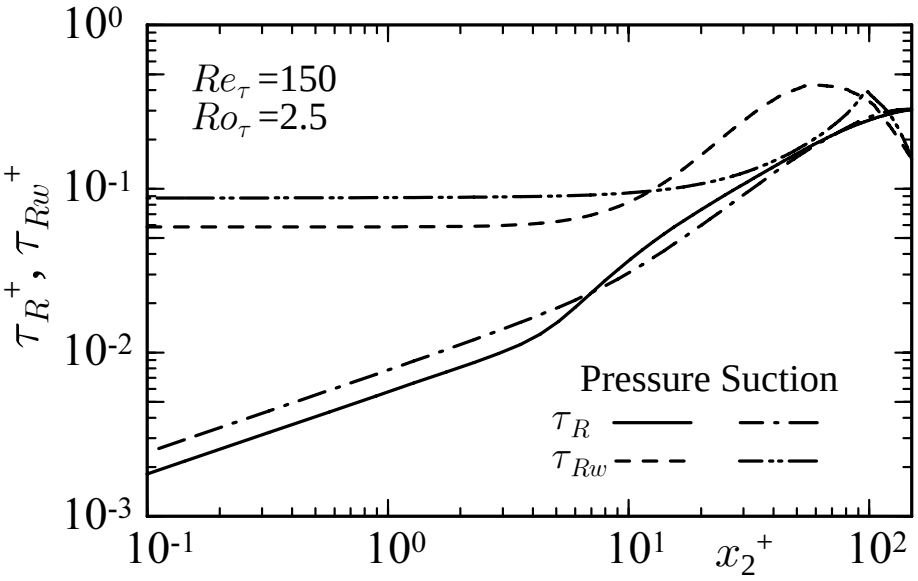

(b)

Figure 7.13: *A priori* test for the proposed model in rotating channel flow ($Re_\tau = 150$, $Ro_\tau = 2.5$); (a) rms velocity fluctuations, (b) time scales, (c) wall-limiting behaviour of normal stress components (pressure side), (d) wall-limiting behaviour normal stress components (suction side).

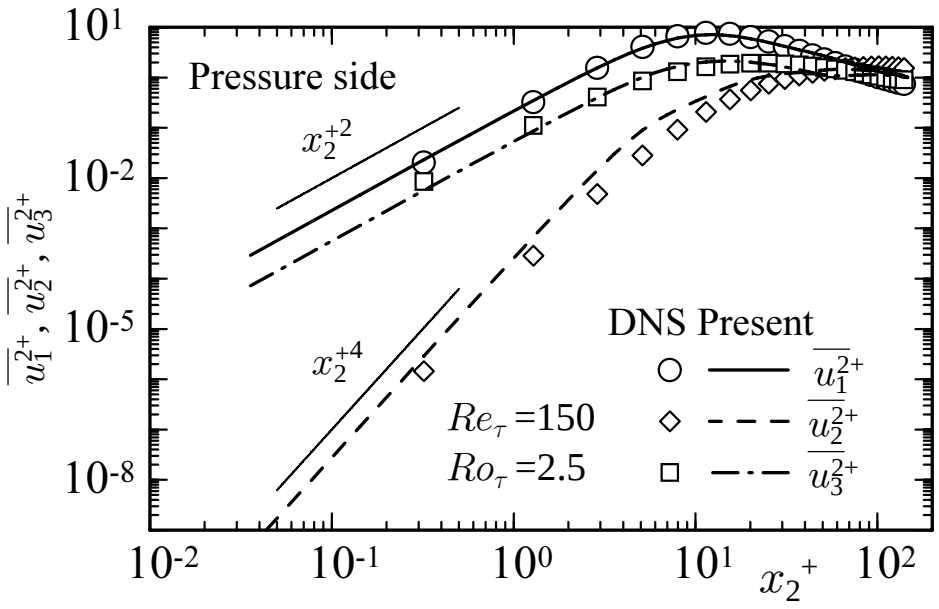

(c)

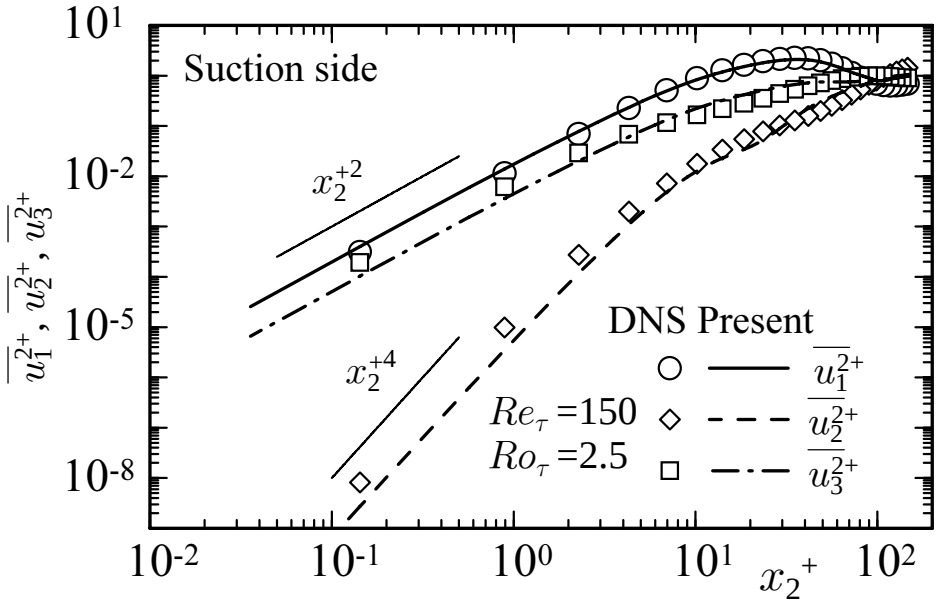

(d)

Figure 7.13: (continued)

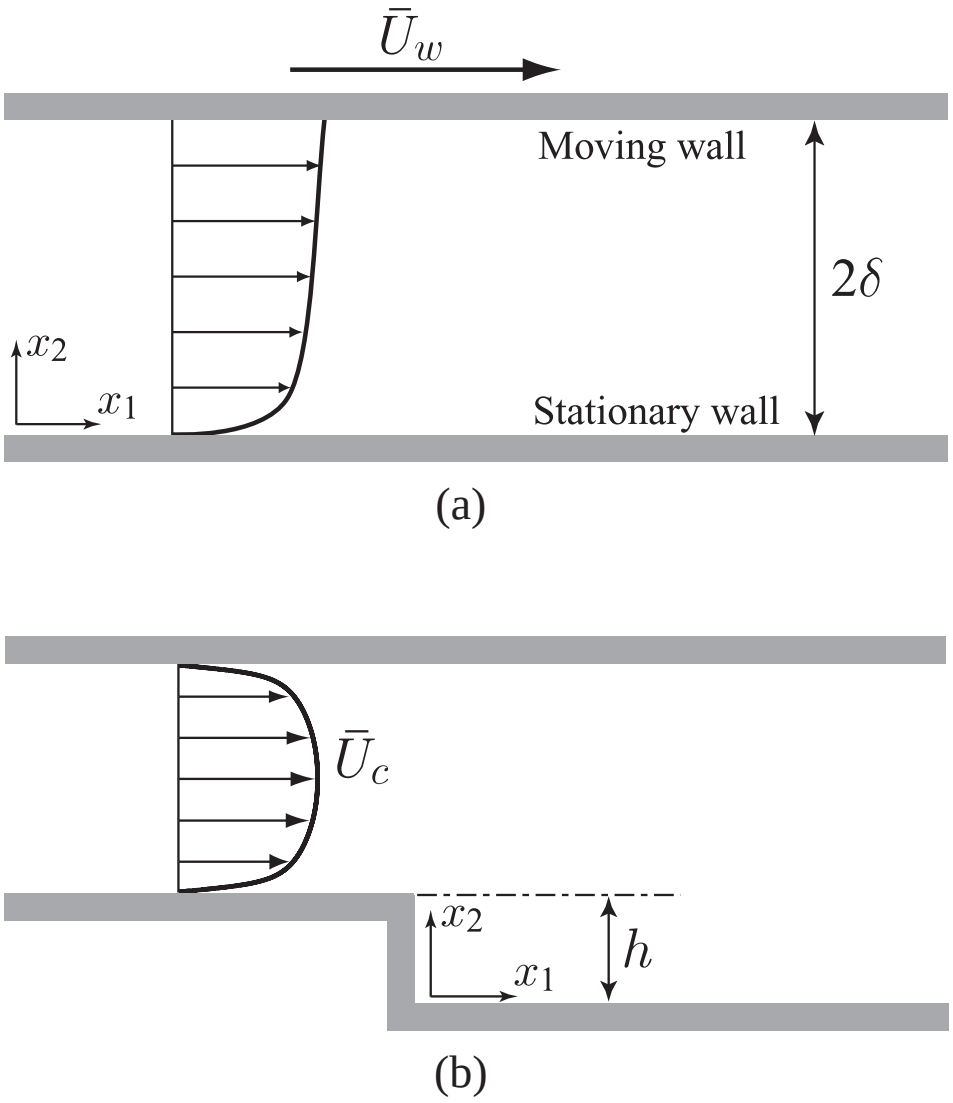

Figure 7.14: Flow geometries; (a) Couette-Poiseuille channel flow, (b) backward-facing step flow.

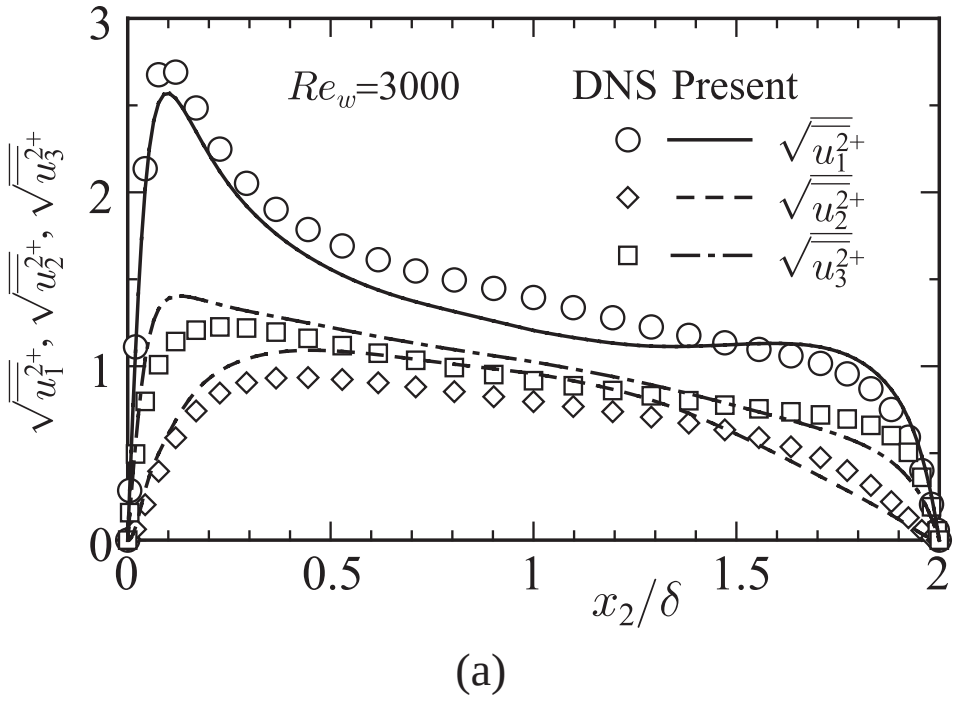

(a)

Figure 7.15: *A priori* test for the proposed Reynolds stress expression in Couette-Poiseuille channel flow ($Re_w = 3000$); (a) Reynolds stress components, (b) wall-limiting behaviour (moving-wall side), (c) wall-limiting behaviour (stationary-wall side).

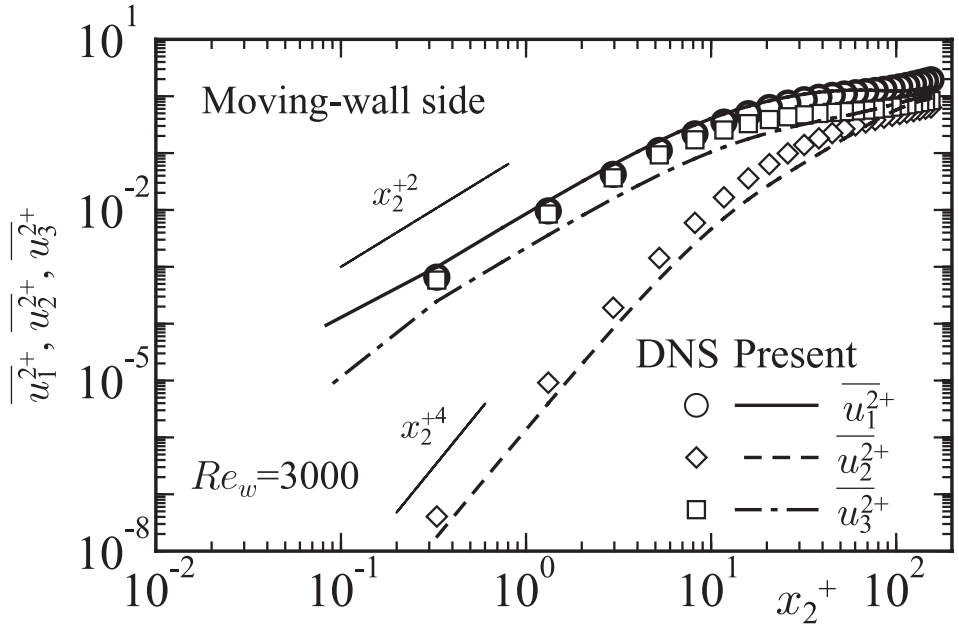

(b)

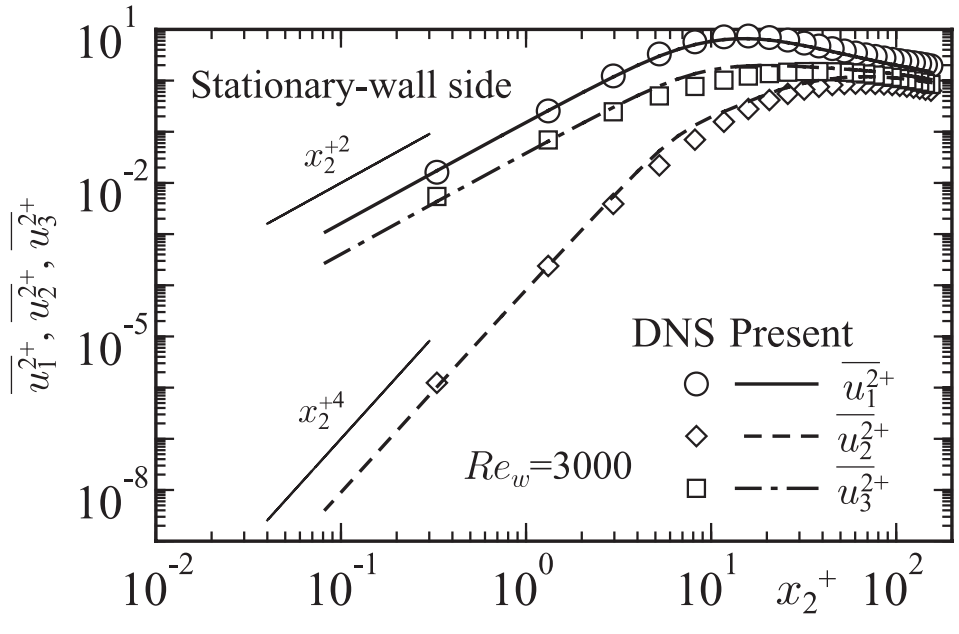

(c)

Figure 7.15: (continued)

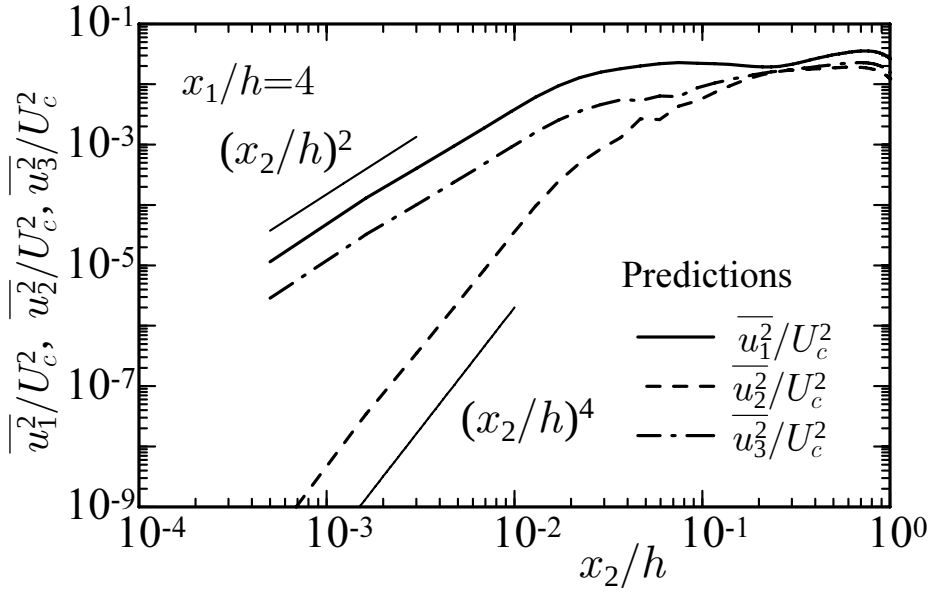

(a)

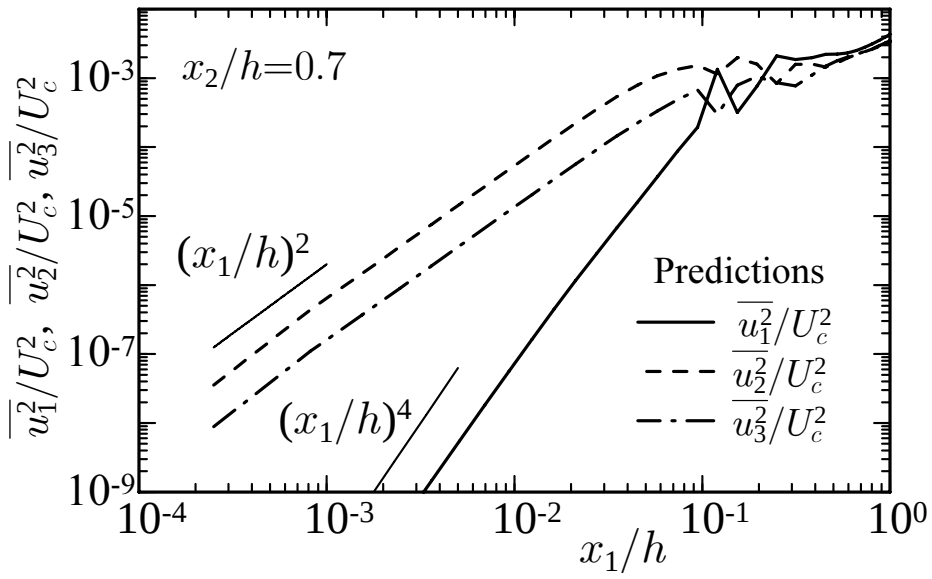

(b)

Figure 7.16: *A priori* test for the proposed Reynolds stress expression in backward-facing step flow ($Re_h = 5500$); wall-limiting behaviour (a) on parallel wall (b) on perpendicular wall.

CHAPTER 8

An improved turbulence model for rotating shear flows

Rotating shear flows are encountered in many technological applications such as turbomachinery. Therefore, it is important to know the mechanism and detail of the flow with rotation for the relevant applications. However, it is extremely difficult to measure a rotating flow, so direct numerical simulation (DNS) is utilized for examining a typical rotating flow, and a turbulence model is useful for predicting realistic rotating flows. Especially, two-equation models, in particular the non-linear k–ε model, are very effective for solving various flow problems encountered in technological applications. In channel flows with rotation, however, the explicit effects of rotation only appear in the Reynolds stress components. The exact equations for k and ε do not have any explicit terms concerned with the rotating effects. Moreover, a Coriolis force vanishes in the momentum equation for a fully developed channel flow with spanwise rotation. Consequently, in order to predict rotating channel flows, after proper revision the Reynolds stress equation model (RSM) or the non-linear eddy viscosity model (NLEVM) should be used.

In this Chapter, we improve the non-linear k–ε model so as to predict rotating channel flows. In the modelling, the wall-limiting behaviour of turbulence is also considered. First, we evaluated the non-linear k–ε model using the DNS database for a fully developed rotating turbulent channel flow. Next, we assessed the non-linear k–ε model at various rotation numbers. Finally, based on these assessments, we reconstruct the non-linear k–ε model to calculate rotating shear flows, and the proposed model is tested in various rotating shear flows.

8.1 Evaluation of modeled equations in rotating channel flows

First, we evaluate the modeled ε–equations of importance for determining the time-scale, and the modeled expressions for Reynolds shear stress by using the trustworthy DNS data of Nishimura and Kasagi (1996) in the fully developed channel flow with spanwise rotation as shown in figure 8.1. Figure 8.2 shows the results of assessment for ε-equations in the rotating channel flow. The AKN model (Abe *et al.* 1994), which is a linear eddy viscosity model, is included for comparison. It can be seen that the NLAKN slightly overpredicts the ε near the wall on the pressure side. On the suction side, however, none of the ε models give quantitative agreement with the DNS.

Next, we explore the rotation number dependence of the model prediction with the aid of the DNS data from Kristoffersen & Andersson (1993). The evaluation has been performed at different rotation numbers ($Ro_\tau = 2\Omega\delta/u_\tau$; δ is the channel half width and u_τ is the friction velocity) from 3.05 to 7.63. Figure 8.3 shows the predictions of the NLAKN model at various rotation numbers in comparison with the DNS. It is well known that a region exists in a rotating channel where the vorticity ratio, $S = -2\Omega/(d\bar{U}/dy)$, becomes $S = -1$, which represents neutral stability (Kristoffersen & Andersson 1993; Johnston *et al.* 1972). This relation yields the following equation:

$$\overline{U}^+ = Ro_\tau \left(\frac{y}{\delta}\right) + C. \tag{8.1}$$

The mean velocity profile with the gradient Ro_τ indeed exists in the region of neutral stability in the DNS. However, in order to satisfy the DNS-based relation with the NLAKN model, a rotation number about three times as large as the DNS has to be provided in the calculation, thus indicating the weak rotation number dependence of the NLAKN model.

We have also assessed the model performance at a much higher rotation number (Lamballais *et al.* 1996). The rotation number based on the mean velocity, the channel half width and the angular velocity ($= 2\Omega\delta/U_m$) is 1.5, which is larger than the maximum value ($Ro = 0.5$) of the above DNS (Kristoffersen & Andersson 1993), and the corresponding Reynolds number ($= 2\bar{U}_m\delta/\nu$) is 3750. However, in the calculations using the NLAKN model, the rotation number 4.2 is used for the above-mentioned reason. From figure 8.4, it can be seen that the model can not represent laminarization phenomena on the suction side, i.e., no observable vanishing of either the turbulence energy or the Reynolds shear stress. From these results, it can be

concluded that predictions from the existing non-linear k–ε model indicate weak dependence on the rotation number.

On the other hand, the expressions for Reynolds shear stress of several nonlinear models are evaluated as shown in the previous Chapter (see Chapter 7).

As demonstrated in the foregoing, there are crucial weak points in the NLAKN model for the prediction of rotating flows, which should be amended.

8.2 Reconstruction of turbulence model

In this section, we reconstruct the NLAKN model based on the above-mentioned evaluation. In order to satisfy the wall-limiting behaviour of normal stress components in the NLEVM, the Reynolds stress expression is modified to represent the original part and the wall-reflection part, similar to a wall-reflection term for the pressure-strain correlation in the Reynolds stress model referred to by Hattori *et al.* (2002), as follows

$$\overline{u_i u_j} = \frac{2}{3}k\delta_{ij} - 2\nu_t S_{ij} + Q_o + Q_w, \tag{8.2}$$

where

$$Q_o = \frac{4C_D}{f_R}k\tau_{Ro}^2\left[(S_{ik}\Omega_{kj} - \Omega_{ik}S_{kj}) - \left(S_{ik}S_{kj} - \frac{\delta_{ij}}{3}S_{mn}S_{mn}\right)\right], \tag{8.3}$$

$$Q_w = \frac{4C_D}{f_R}k\tau_{Rw}^2\left[(S_{ik}\Omega_{kj} - \Omega_{ik}S_{kj}) - \left(S_{ik}S_{kj} - \frac{\delta_{ij}}{3}S_{mn}S_{mn}\right)\right]. \tag{8.4}$$

Here $\tau_{Ro}(=\nu_t/k)$ is the original part of the time scale defined by NLAKN (Abe *et al.* 1997), and τ_{Rw} is introduced to satisfy the wall-limiting behaviour. The time scale τ_{Rw} is modelled in consideration of the wall-limiting behaviour of the normal stress components as follows:

$$\tau_{Rw} = \sqrt{\frac{2}{3}\frac{1}{C_1 f_{SW}}}\left(1 - \frac{3C_{v1}f_{v2}}{8}\right)f_{v1}^2, \tag{8.5}$$

where the model functions $f_{v1} = \exp\left[-\left(R_{tm}/45\right)^2\right]$ and $f_{v2} = 1 - \exp\left(-\sqrt{R_t}/C_{v2}\right)$ and the model constants $C_1 = 4C_D/f_R$, $C_{v1} = 0.4$ and $C_{v2} = 2 \times 10^3$ are introduced to avoid the negative value of Eq. (8.5), when $R_t \to \infty$ (if $R_t \to \infty$, f_{v2} becomes 1. Thus, the proposed model constant C_{v1} satisfies the inequality $3C_{v1}/8 < 1$). The formulation f_{SW} in Eq. (8.5) is given by:

$$f_{SW} = \frac{W^2}{2} + \frac{S^2}{3} - f_{SW}^{\Omega}. \tag{8.6}$$

f_{SW}^{Ω} is related with the rotation number defined as follows:

$$f_{SW}^{\Omega} = \left[\left(\sqrt{\frac{S^2}{2}} - \sqrt{\frac{W^2}{2}} \right) f_w(1) \right]^2 . \tag{8.7}$$

This represents Ω_k^2 implicitly in the rotating channel flows. By introduction of the time scale τ_{Rw}, the wall-limiting behaviour of normal stress components is satisfied, i.e., $\overline{u^2} \propto y^2$, $\overline{v^2} \propto y^4$ and $\overline{w^2} \propto y^2$.

The modified turbulence Reynolds number R_{tm} is proposed in Eq. (8.5) for capturing the laminarization phenomena on the suction side as follows:

$$R_{tm} = \frac{C_{tm} n^* R_t^{1/4}}{C_{tm} R_t^{1/4} + n^*}, \tag{8.8}$$

where C_{tm} is the model constant set at 1.3×10^2.

Next, in order to modify the rotation number dependence of the model, we adopt the rotation-influenced additional term of Shimomura (1989) in the ε–equation, which can represent the asymmetry in turbulence quantities of rotating channel flows:

$$R = C_\Omega f_\Omega k \epsilon_{ij\ell} W_{ij} \Omega_\ell . \tag{8.9}$$

where $C_\Omega = -0.045$, and the following model function f_Ω is newly introduced to reflect the low-Reynolds-number and rotation number effects:

$$f_\Omega = C_{f_\Omega} \exp \left[- \left(\frac{R_\Omega}{10} \right)^{0.2} \right], \tag{8.10}$$

where $C_{f_\Omega} = 6.0$ is the model constant, and R_Ω is a parameter defined as follows:

$$R_\Omega = \eta_t \sqrt{f_{SW}^{\Omega}}, \tag{8.11}$$

where $\eta_t (= \sqrt{\nu/\varepsilon})$ is the Kolmogorov time scale. η_t is sensitive to the low-Reynolds-number effect, and thus we introduce this parameter into f_Ω.

Considering information obtained previously (Abe *et al.* 1994; Nagano & Shimada1996), the following revised model functions are employed in the proposed model:

$$f_\mu = \left\{ 1 + \left(\frac{40}{R_t^{3/4}} \right) \exp \left[- \left(\frac{R_t}{35} \right)^{3/4} \right] \right\} \left[1 - f_w(32) \right], \tag{8.12}$$

$$f_\varepsilon = \left\{ 1 - 0.3 \exp \left[- \left(\frac{R_t}{6.5} \right) \right] \right\} \left[1 - f_w(3.7) \right], \tag{8.13}$$

$$f_w(\xi) = \exp \left[- \left(\frac{R_{tm}}{\xi} \right)^2 \right]. \tag{8.14}$$

The turbulent diffusion terms in k– and ε–equations are modeled with the GGDH similar to the NLAKN model:

$$T_k = \frac{\partial}{\partial x_j}\left(C_s f_{t1}\frac{\nu_t}{k}\overline{u_j u_\ell}\frac{\partial k}{\partial x_\ell}\right), \tag{8.15}$$

$$T_\varepsilon = \frac{\partial}{\partial x_j}\left(C_\varepsilon f_{t2}\frac{\nu_t}{k}\overline{u_j u_\ell}\frac{\partial \varepsilon}{\partial x_\ell}\right), \tag{8.16}$$

where $C_s = C_\varepsilon = 1.4$. The model functions in Eq. (8.16) are modified for introduction of τ_{Rw} as follows:

$$\left.\begin{aligned} f_{t1} &= [1 + 9.0 f_w(8)]/[1 - f_w(32)]^{\frac{1}{2}} \\ f_{t2} &= [1 + 5.0 f_w(8)]/[1 - f_w(32)]^{\frac{1}{2}} \end{aligned}\right\}. \tag{8.17}$$

The pressure diffusion terms in k– and ε–equations, which are often ignored in conventional modeling, are introduced to satisfy exactly the wall-limiting behaviour, and the same extra production term is also added to the ε–equation as in the NS model (Nagano & Shimada 1995a) as follows:

$$\Pi_k = \max\left\{-0.5\nu\frac{\partial}{\partial x_j}\left[\frac{k}{\varepsilon}\frac{\partial \varepsilon}{\partial x_j}f_w(1)\right], 0\right\}, \tag{8.18}$$

$$\Pi_\varepsilon = C_{\varepsilon 4}\frac{\partial}{\partial x_j}\left\{[1 - f_w(5)]\,\frac{\varepsilon}{k}\frac{\partial k}{\partial x_j}f_w(5)\right\}, \tag{8.19}$$

$$E = C_{\varepsilon 3}\nu\frac{k}{\varepsilon}\overline{u_j u_\ell}\frac{\partial^2 \bar{U}_i}{\partial x_\ell \partial x_k}\frac{\partial^2 \bar{U}_i}{\partial x_j \partial x_k} + C_{\varepsilon 5}\nu\frac{k}{\varepsilon}\frac{\partial \overline{u_j u_k}}{\partial x_j}\frac{\partial \bar{U}_i}{\partial x_k}\frac{\partial^2 \bar{U}_i}{\partial x_j \partial x_k}, \tag{8.20}$$

where $C_{\varepsilon 3} = 0.02$, $C_{\varepsilon 4} = 0.5$ and $C_{\varepsilon 5} = 0.015$. The other model constants are the same as those of the original NLAKN model.

8.3 Results and discussion

In order to demonstrate the performance of the improved NLAKN model, various rotation and Reynolds number flows have been calculated using the proposed model. Figure 8.5 shows the distributions of mean velocity and Reynolds shear stress in comparison with the original model predictions and the DNS data (Nishimura & Kasagi 1996) ($Re_\tau = 150$, $Ro_\tau = 2.5$). The turbulence energy and its dissipation rate are indicated in figure 8.6. It can be seen that predictions with the improved model agree with the DNS data. Obviously, the proposed model adequately captures turbulent quantities on the suction side, and the introduced model functions

are found to work effectively. The predicted normal stress components are shown in figure 8.7. Since the introduced time scale τ_{Rw} functions effectively near the wall like a wall-reflection term of a pressure strain term in the RSM, the proposed model reproduces exactly the normal stress components in the rotating channel flow. Figure 8.8 shows the wall-limiting behaviour of normal stress components, while indicating that the proposed model can predict the wall-limiting behaviour of normal stress components. Especially, the wall-normal component, $\overline{v^2}$, which is an important quantity for the turbulent diffusion term, is reproduced appropriately in the present model.

Secondly, we appraised the rotation number dependence of the improved model. Figures 8.9, 8.10 and 8.11 show the mean velocity, Reynolds shear stress and turbulence energy profiles in various rotation number flows together with the related DNS data (Kristoffersen & Andersson 1993) ($Re_\tau = 194$, $Ro_\tau = 0 \sim 7.63$). In figure 8.9, it can be seen that the calculated mean velocities are considerably refined in comparison with figure 8.3. Also, the Reynolds shear stresses and the turbulence energy predicted by the present model are in good agreement with the DNS data in various rotation number flows. The rms velocity fluctuations are indicated in figure 8.12. It can be seen that the present non-linear model predicts properly the normal stress components as well as the previous test case.

Next, we have applied the proposed model for the rotating channel flows measured by Jonston *et al.* (1972), in which the Reynolds numbers are set higher than the DNS shown previously. [The highest Reynolds number ($Re = 2\bar{U}_m\delta/\nu$) of the DNS is 5800 (Kristoffersen & Andersson 1993).] The experimental conditions $Re = 11500, 35000$ and $Ro = 0.21, 0.068$, respectively are given. Figures 8.13 and 8.14 show the mean velocity profiles in comparison with the experimental data (Johnston *et al.* 1972), and the results of the Reynolds stress model (Shima 1993) also are included in figures for comparison. Obviously, the proposed model reproduces the high Reynolds number rotating channel flows.

Finally, we have calculated a high rotation-number flow ($Ro = 1.5$). In the foregoing calculations corresponding to the DNS of Kristoffersen and Andersson (1993), the maximum rotation number is $Ro = 0.5$. Thus, the DNS data for $Ro = 1.5$ (Lamballais *et al.* 1996) used here significantly increase the validation range for the proposed model. In figure 8.15, predictions for mean velocity are presented; in figure 8.16, corresponding predictions for turbulence energy and Reynolds shear stress are shown in comparison with the original model predictions and

DNS data. In the present case, the laminar region (or no turbulence) in the channel poses one of the most difficult problems for evaluation of a turbulence model. The proposed model predicts the laminar region on the suction side, but the original model produces turbulence there. Hence, the mean velocity profile predicted by the improved model comes to show good agreement with the DNS data.

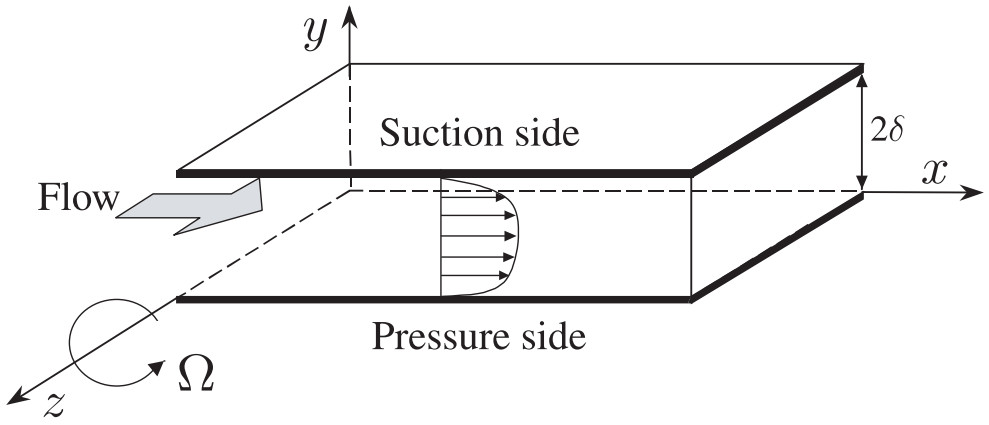

Figure 8.1: Rotating channel flow and coordinate system

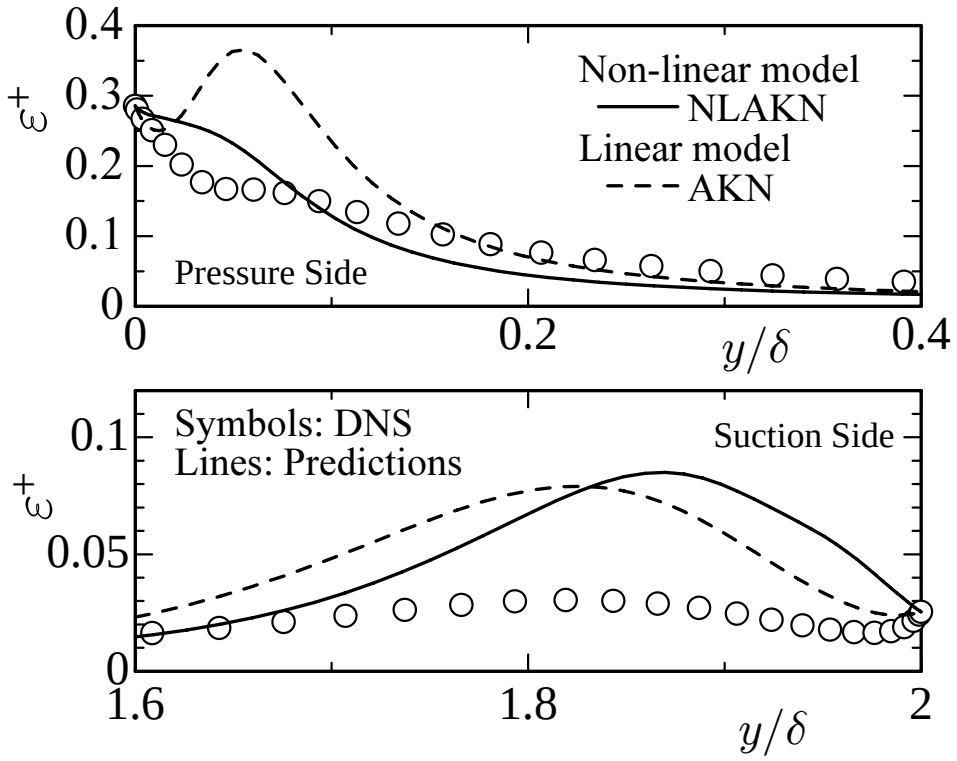

Figure 8.2: *A priori* test for ε–equations in rotating channel flow

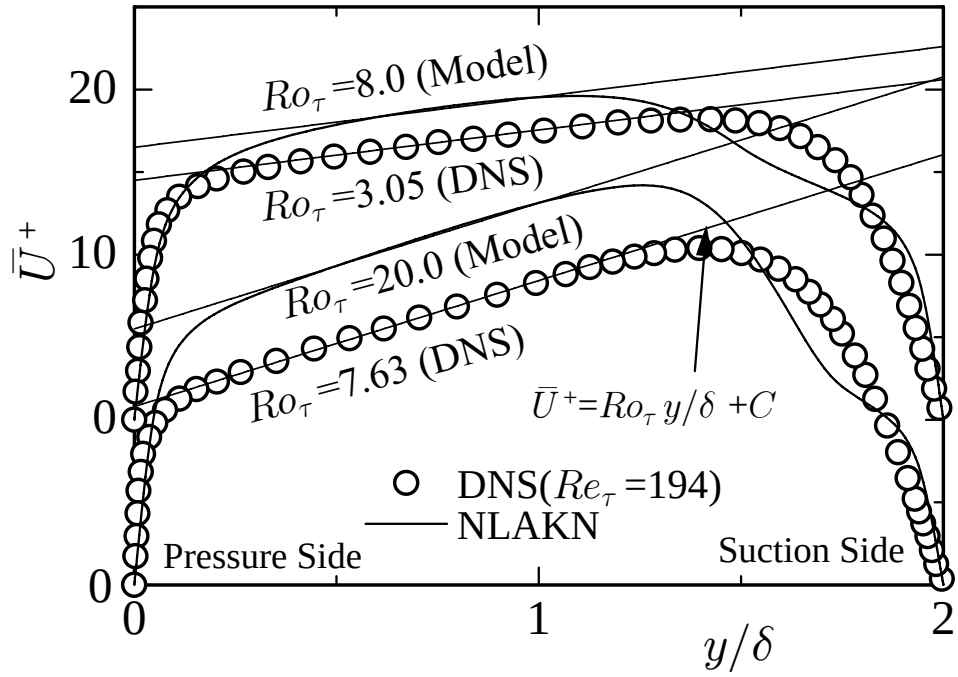

Figure 8.3: Predicted mean velocity profiles at various rotation numbers

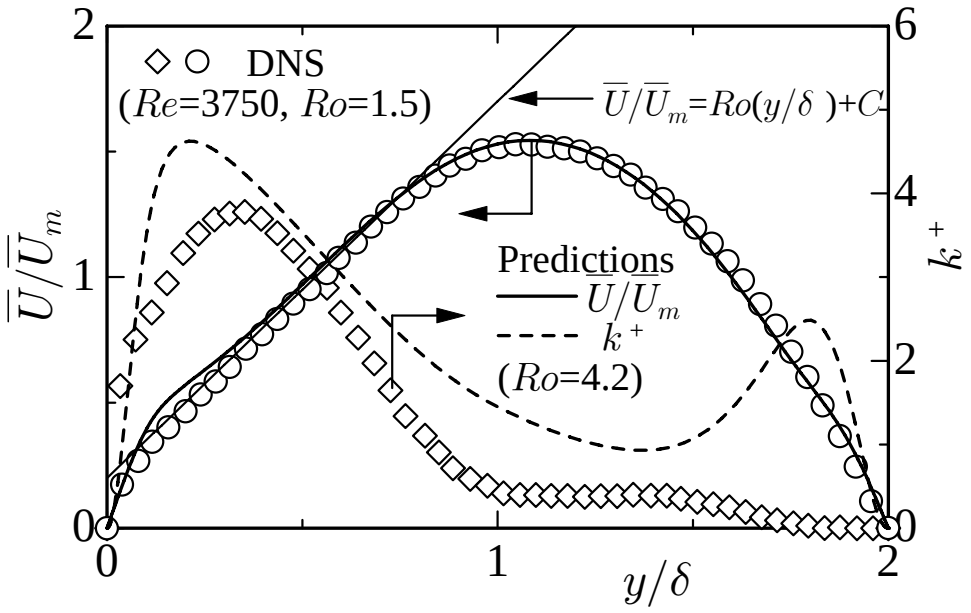

Figure 8.4: Profiles of turbulent quantities at high rotating number $(Ro = 1.5)$

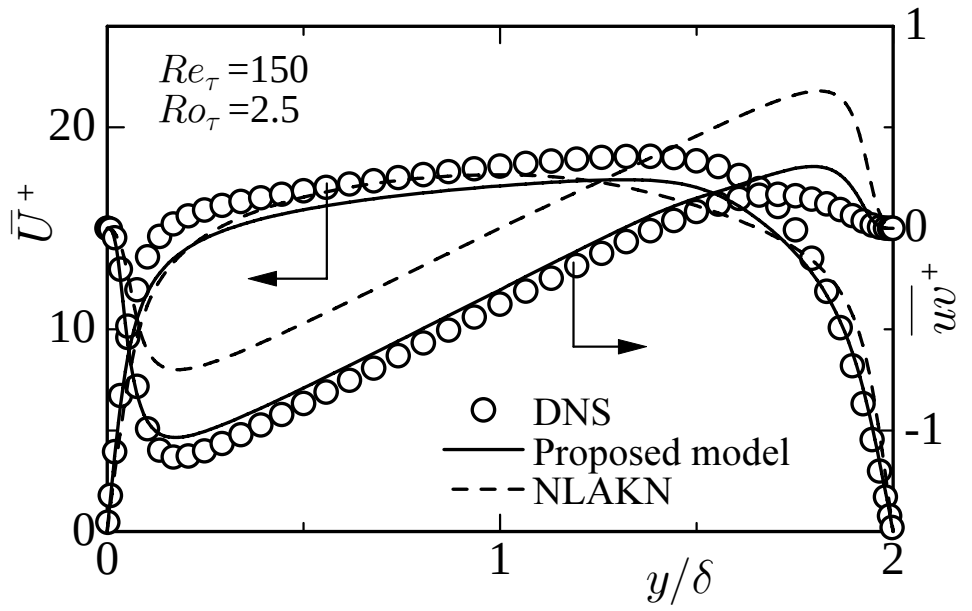

Figure 8.5: Distributions of mean velocity and Reynolds shear stress in rotating channel flow ($Ro_\tau = 2.5$)

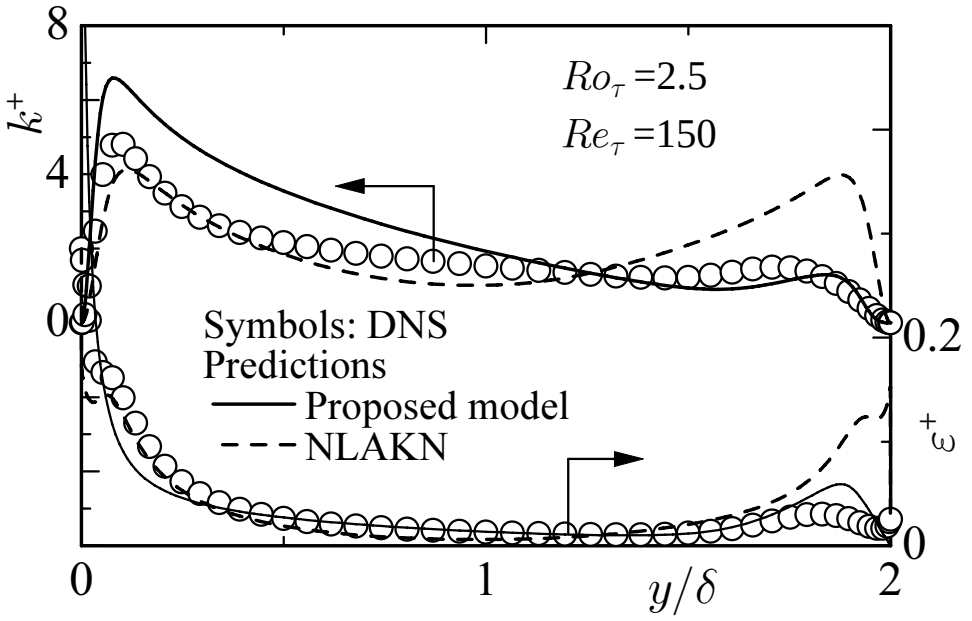

Figure 8.6: Distributions of turbulence energy and its dissipation rate in rotating channel flow ($Ro_\tau = 2.5$)

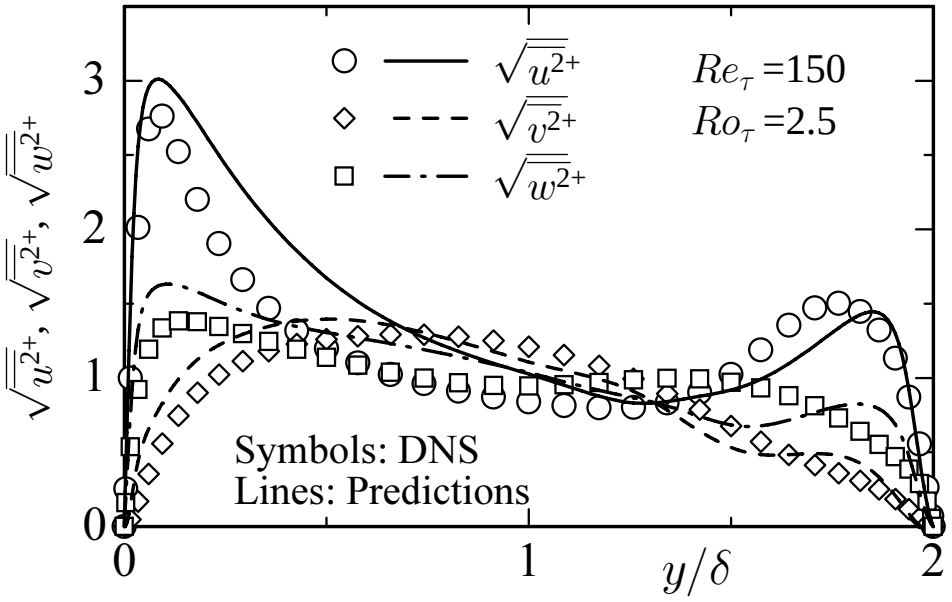

Figure 8.7: Distributions of normal stress components in rotating channel flow ($Ro_\tau = 2.5$)

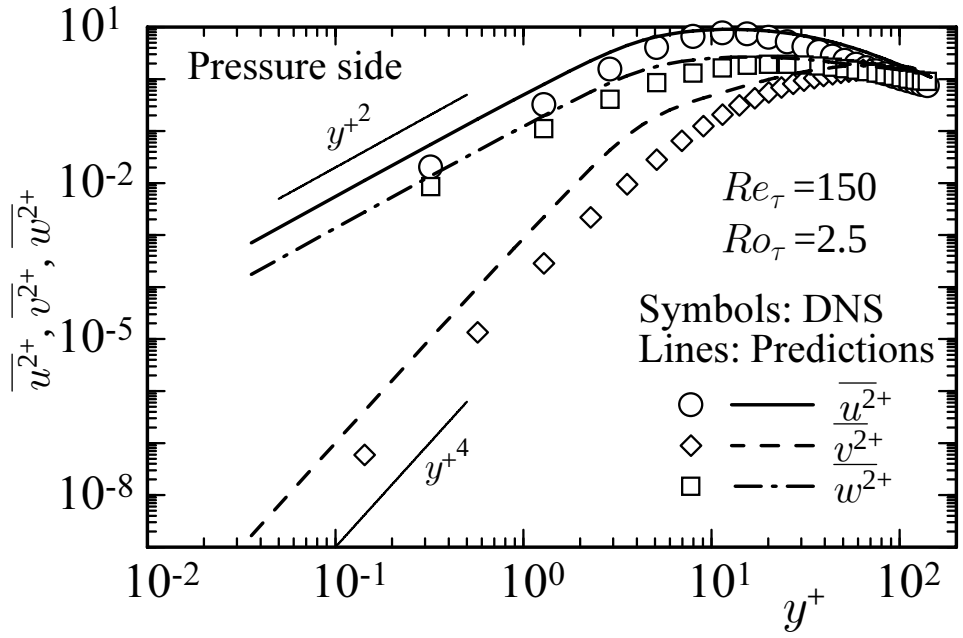

Figure 8.8: Wall-limiting behaviour of normal stress components in rotating channel flow ($Ro_\tau = 2.5$)

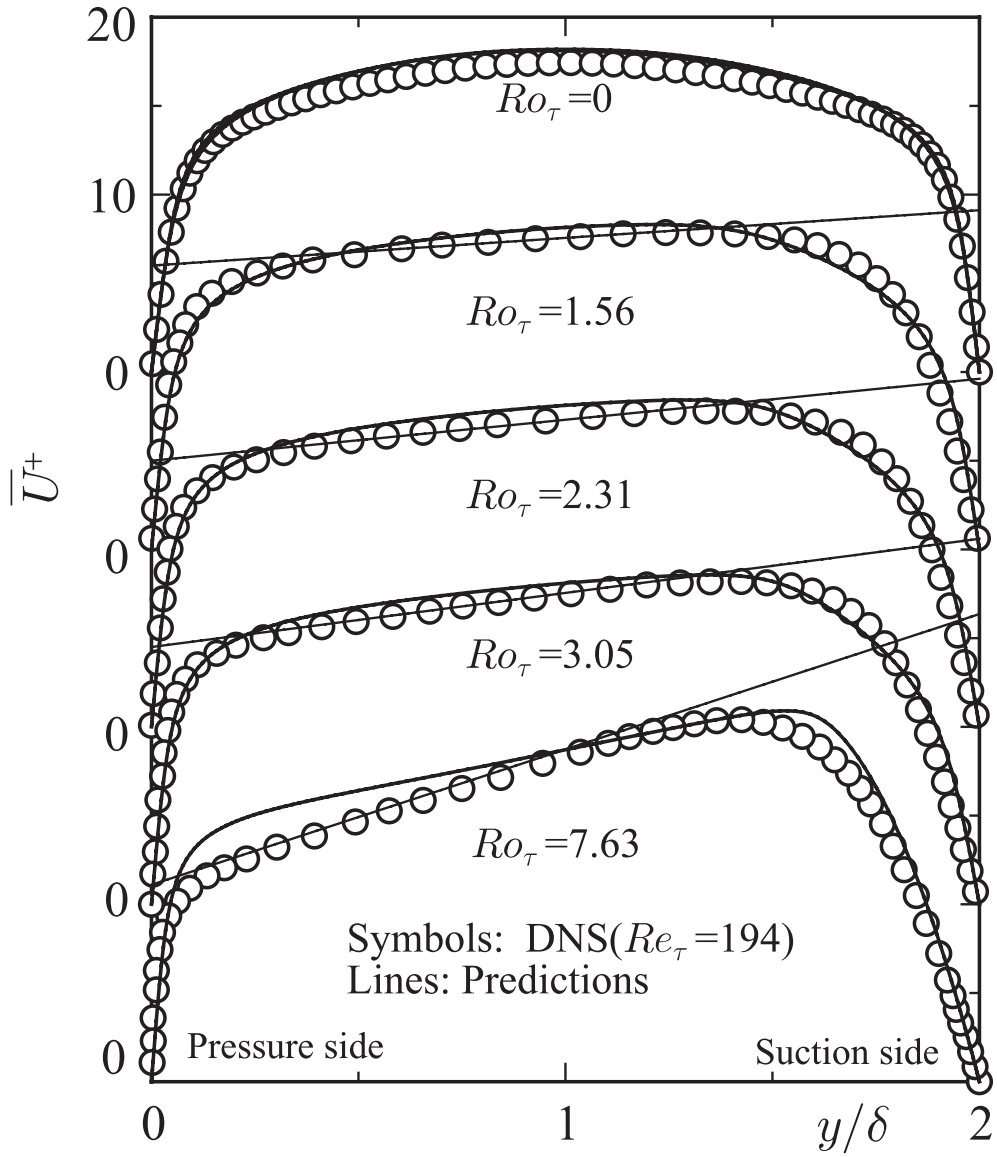

Figure 8.9: Mean velocity profiles in various rotation number flows

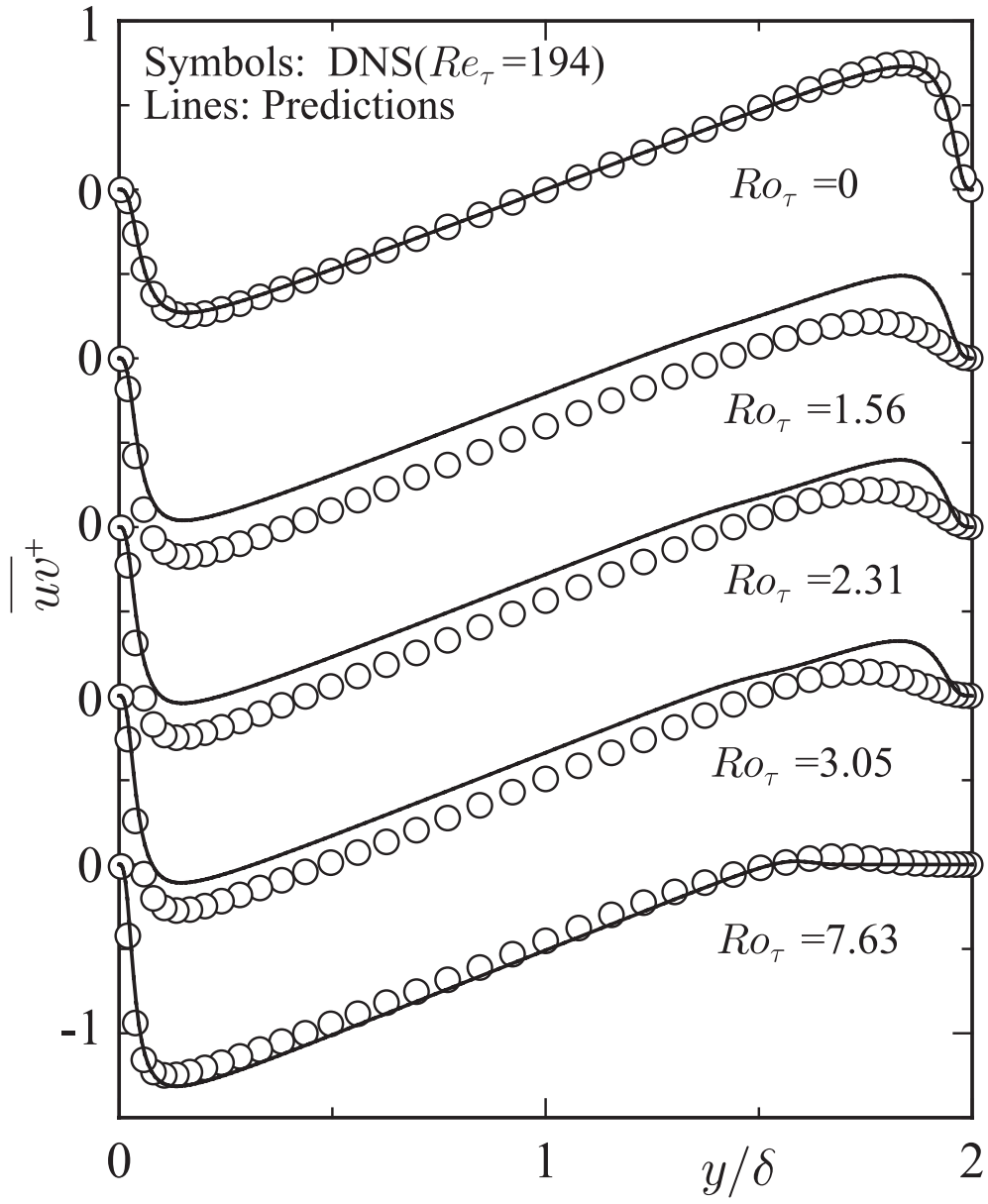

Figure 8.10: Distributions of Reynolds shear stress in various rotation number flows

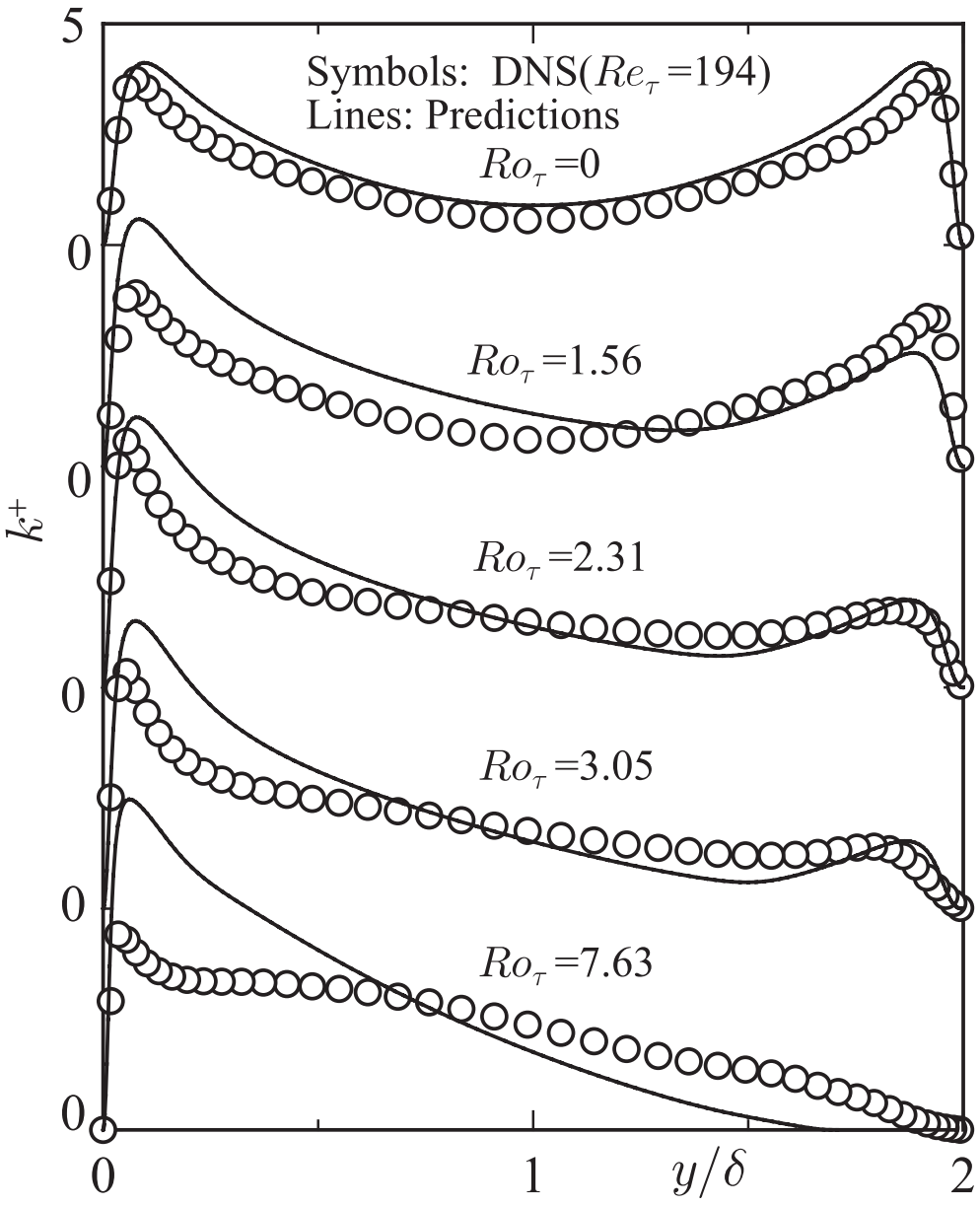

Figure 8.11: Distributions of turbulence energy in various rotation number flows

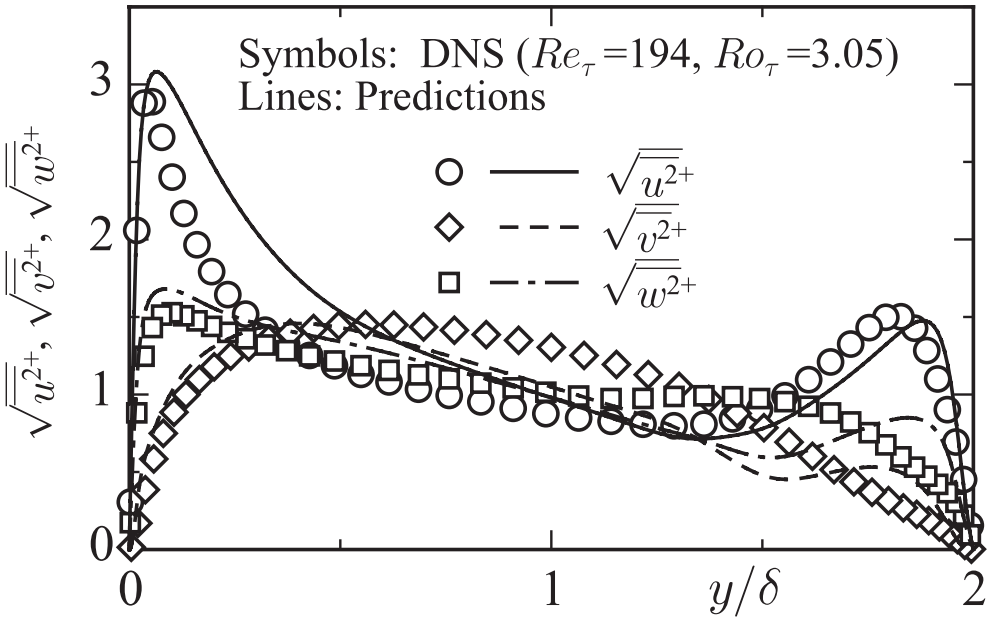

Figure 8.12: Rms velocity fluctuations in rotating channel flow ($Ro_\tau = 3.05$)

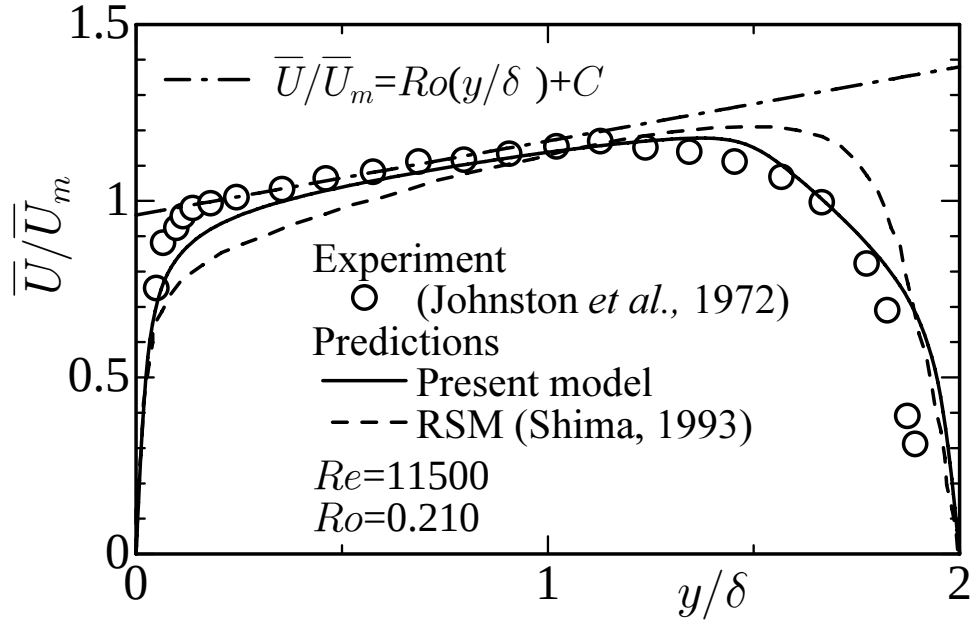

Figure 8.13: Mean velocity profiles in high Reynolds number flow ($Re = 11500$, $Ro = 0.21$)

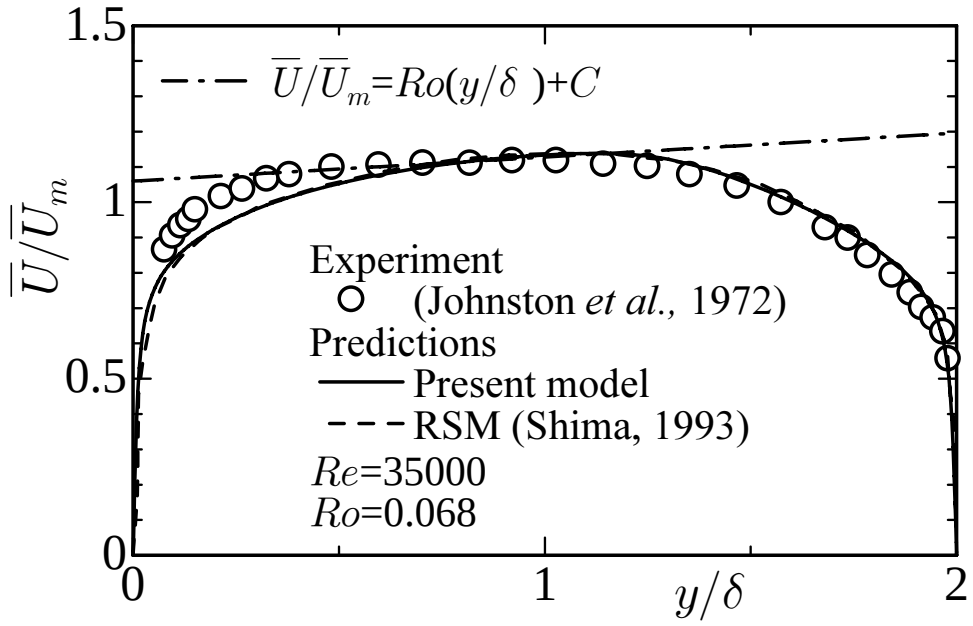

Figure 8.14: Mean velocity profiles in high Reynolds number flow ($Re = 35000$, $Ro = 0.068$)

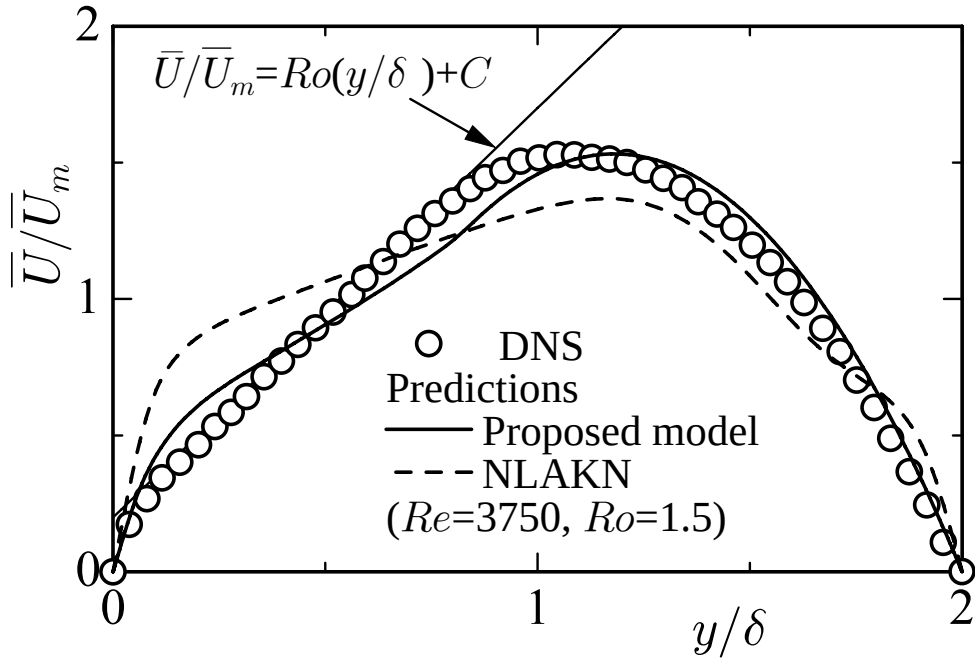

Figure 8.15: Mean velocity profiles in high rotation number flow ($Ro = 1.5$)

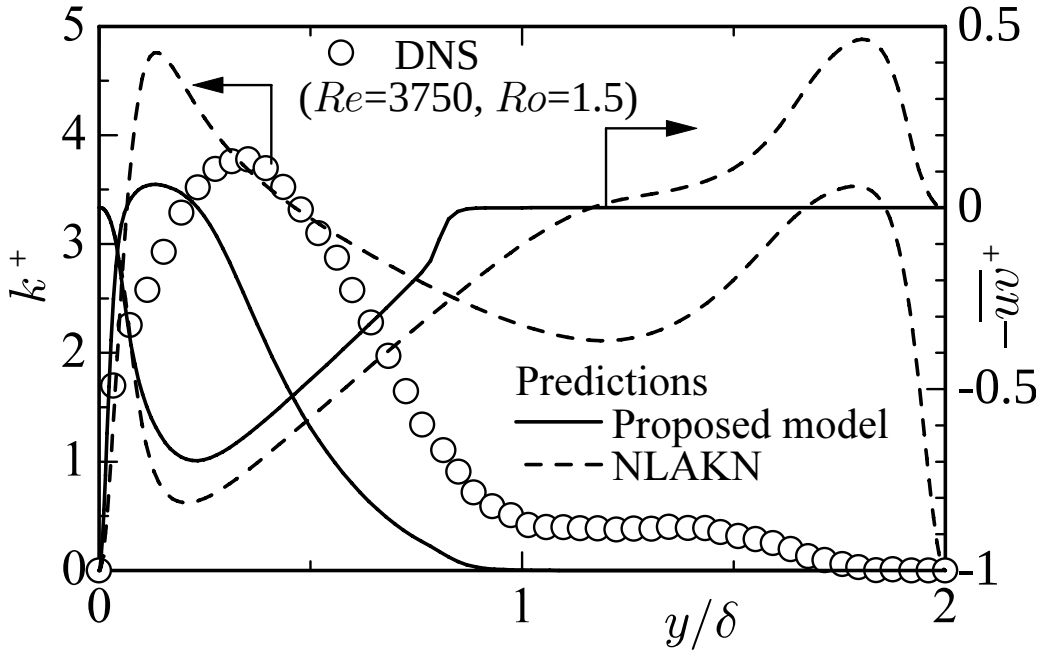

Figure 8.16: Distributions of turbulence energy and Reynolds shear stress in high rotation number flow ($Ro = 1.5$)

CHAPTER 9

Conclusions

To analyize turblent flow with heat transfer, six turbulence model have been developed. The conclusion obtained from the present study are summarized as follows.

In Chapter 3, a convenient but rigorous turbulence model is developed to calculate flows in the presence of pressure gradients. In the present model, we can make the dissipation rate $\widetilde{\varepsilon}$ of turbulent energy zero at a wall, though the wall limiting behavior of velocity fluctuations is reproduced exactly. Thus, the model assures computational expediency and stability. The model predictions show that agreement with the experiments and the DNS data is, in general, very good. It is also shown that the present model works very well for calculating the boundary layer under arbitrary pressure gradient conditions.

In Chapter 4, advanced turbulence models are developed to calculate flows in the presence of pressure gradients and complex turbulent heat transfer. In the present models, we can make the apparent dissipation rates of both turbulent energy and temperature variance zero at walls, though the wall limiting behavior of turbulence in the velocity and thermal fields is reproduced exactly. Thus, the models assure computational expediency and stability. The model predictions indicate that agreement with the experiments and the DNS data is generally very good. It is also shown that the present model works very well for calculating the heat transfer under different wall thermal conditions.

In Chapter 5, using the DNS data for wall turbulent shear flows with heat transfer, we have constructed a rigorous near-wall model for the temperature variance and its dissipation-rate equations. In the k_θ– and ε_θ–equations, the turbulent diffusion terms are represented with the gradient-type diffusion plus convection by large-scale motions. In the ε_θ–equation, all of the production and destruction terms are modeled to reproduce the correct behaviour of ε_θ near the wall. It should be noted that the wall limiting behaviour of ε_θ does not follow the strict one, if

the correct profile of k_θ could not be obtained. It is also shown that the present model works very well for calculating the heat transfer under different thermal conditions. Furthermore, the present model reproduces the budget profiles of turbulence quantities as accurately as DNS. Thus, we anticipate a practical application of the present model to disclosing the underlying physics of turbulent heat transfer in the complex flows of technological interest.

In Chapter 6, the two-layer two-equation heat transfer models are constructed for various flow conditions with heat transfer including Prandtl number effects. In this study, a new approach for the two-layer models is made on the basis of the time-scale modeling, which differs from the traditional approach based on the length-scale modeling. Thereby, both dissipation-rates of turbulent energy and of temperature variance are only modeled algebraically near the wall. Also, criterion functions to link the between algebraic formulas to equations are proposed. These criterion functions serve for connection between the algebraic formulas and equations near the wall in various flows with heat transfer including Prandtl number effects. The model predictions indicate that the agreement with the experiments and DNS data is generally very good, and the calculation stability achieved is remarkably high.

In Chapter 7, major problems in the behaviour of the existing nonlinear k–ε models near the wall are clarified by the assessment using the DNS database in fully developed two-dimensional channel flows of the inertial frame and in a fully developed two-dimensional rotating channel flow of the noninertial frame. It is clear from the assessment that the existing nonlinear models can not reproduce the wall-limiting behaviour and anisotropy of the Reynolds normal stress components either quantitatively or qualitatively in such flows. Considering the assessment results, we have proposed the nonlinear k–ε model satisfying the wall-limiting behaviour and anisotropy of the Reynolds normal stress components exactly near the wall in both the inertial and noninertial frames. We have improved the quadratic nonlinear k–ε model, in which the wall-reflection term and the new characteristic time-scale are introduced. Since no unit tensors determining the direction are contained in the proposed model, the Reynolds stress component of wall-normal direction and its wall-limiting behaviour which is proportional to the fourth power of wall-normal direction must be obtained automatically, though the distance from the wall must be determined merely for the wall-reflection function. The proposed model has been evaluated in the three flows of the inertial frame and in the rotating channel flow of the non-inertial frame. From the assessment results of the present model, it was demonstrated that the

proposed model gives the proper anisotropy of the Reynolds normal stress component, and satisfies the wall-limiting behaviour of the Reynolds normal stress component near the wall on both the inertial and noninertial frames.

In Chapter 8, we have developed a non-linear two-equation turbulence model to predict rotating channel flows, in which the wall-limiting behaviour and redistribution of normal stress components are also considered. The predictions with the proposed quadratic model give good agreement with the DNS data for various rotation number flows. The proposed model also satisfies the wall-limiting behaviour of the normal stress components exactly, and can adequately predict redistribution of the normal stress components.

Appendix A

Summary of the proposed two-equation models

A.1 k–$\widetilde{\varepsilon}$ model in Chapter 3

The k–$\widetilde{\varepsilon}$ model in Chapter 3 is summarized as follows:

Reynolds stress

$$\overline{u_i u_j} = \frac{2}{3}\delta_{ij}k - \nu_t\left(\frac{\partial \bar{U}_i}{\partial x_j} + \frac{\partial \bar{U}_j}{\partial x_i}\right).$$

Eddy viscotiy

$$\nu_t = C_\mu f_\mu \frac{k^2}{(\widetilde{\varepsilon} + D)} = C_\mu f_\mu \frac{k^2}{\varepsilon},$$

where

$$f_\mu = \left[1 - \exp\left(-\frac{y^+}{A^+}\right)\right]^2 \left\{1 + \left(\frac{20}{R_t{}^{\frac{3}{4}}}\right)\exp\left[-\left(\frac{R_t}{120}\right)^2\right]\right\},$$

$$R_t = \frac{k^2}{\nu(\widetilde{\varepsilon} + D)} = \frac{k^2}{\nu\varepsilon}, \quad A^+ = \frac{30}{1 + 11.8P^+},$$

$$\varepsilon = \widetilde{\varepsilon} + D, \quad D = 2\nu\left(\frac{\partial\sqrt{k}}{\partial y}\right)^2, \quad \frac{\partial\sqrt{k}}{\partial y} \geq 0,$$

$$C_\mu = 0.09.$$

k-equation

$$\frac{Dk}{Dt} = \frac{\partial}{\partial x_j}\left[\left(\nu + \frac{\nu_t}{\sigma_k}\right)\frac{\partial k}{\partial x_j}\right] - \overline{u_i u_j}\frac{\partial \bar{U}_i}{\partial x_j} - (\widetilde{\varepsilon} + D),$$

where $\sigma_k = 1.4$.

$\widetilde{\varepsilon}$-equation

$$\frac{D\widetilde{\varepsilon}}{Dt} = \frac{\partial}{\partial x_j}\left[\left(\nu + \frac{\nu_t}{\sigma_\varepsilon}\right)\frac{\partial \widetilde{\varepsilon}}{\partial x_j}\right] - \frac{\widetilde{\varepsilon}}{k}\left(C_{\varepsilon 1}\overline{u_i u_j}\frac{\partial \bar{U}_i}{\partial x_j} + C_{\varepsilon 2} f_\varepsilon \widetilde{\varepsilon}\right) + \nu\nu_t\left(1 - f_w\right)\left(\frac{\partial^2 \bar{U}_i}{\partial x_j \partial x_k}\right)^2,$$

where

$$\sigma_\varepsilon = 1.3, \quad C_{\varepsilon 1} = 1.45, \quad C_{\varepsilon 2} = 1.9,$$

$$f_\varepsilon = 1 - 0.3\exp\left(-{R_t}^2\right), \quad f_w = \left[1 - \exp\left(-\frac{y^+}{30}\right)\right]^2.$$

The ASM used for solving the additional production term due to irrotational strains in the $\widetilde{\varepsilon}$-equation is given as follows:

$$\overline{u_i u_j} = \left(P_{ij} + \Phi_{ij} - \varepsilon_{ij}\right)\left(\frac{k}{P_k - \varepsilon}\right),$$

where

$$\begin{aligned}
P_{ij} &= -\overline{u_i u_k}\frac{\partial \bar{U}_j}{\partial x_k} - \overline{u_j u_k}\frac{\partial \bar{U}_i}{\partial x_k}, \\
\Phi_{ij} &= \Phi_{ij1} + \Phi_{ij2} + \Phi_{ijw}, \\
\Phi_{ij1} &= -C_1\left(\frac{\varepsilon}{k}\right)\left(\overline{u_i u_j} - \frac{3}{2}\delta_{ij}k\right), \\
\Phi_{ij2} &= -C_2\left(P_{ij} - \frac{3}{2}\delta_{ij}P_k\right), \\
\Phi_{ijw} &= \Phi'_{ij1} + \Phi'_{ij2}, \\
\Phi'_{ij1} &= C'_1\left(\frac{\varepsilon}{k}\right)\left(\overline{u_k u_m}n_k n_m \delta_{ij} - \frac{3}{2}\overline{u_k u_i}n_k n_j - \frac{3}{2}\overline{u_k u_j}n_k n_i\right) f_y, \\
\Phi'_{ij2} &= C_2\left(\Phi_{km2}n_k n_m \delta_{ij} - \frac{3}{2}\Phi_{ik2}n_k n_j - \frac{3}{2}\Phi_{jk2}n_k n_i\right) f_y, \\
f_y &= \frac{k^{\frac{3}{2}} C_\mu^{\frac{3}{4}}}{\varepsilon y \kappa}, \\
& C_1 = 3.0, \quad C_2 = 0.3, \quad C'_1 = 0.75, \quad C'_2 = 0.5, \quad \kappa = 0.4, \\
\varepsilon_{ij} &= \frac{2}{3}\delta_{ij}\varepsilon,
\end{aligned}$$

here $n_i = 1$ (in the direction normal to the wall) and $n_i = 0$ (otherwise). The additional production term can be written in the 2-dimensional flow as follows:

$$-C'_{\varepsilon 1}\frac{\widetilde{\varepsilon}}{k}\left(\overline{u^2} - \overline{v^2}\right)\frac{\partial \bar{U}}{\partial x},$$

$$C'_{\varepsilon 1} = 2.5 C_{\varepsilon 1}.$$

A.2 Nonlinear k–$\widetilde{\varepsilon}$ model and k_θ–$\widetilde{\varepsilon}_\theta$ model in Chapter 4

The proposed nonlinear k–$\widetilde{\varepsilon}$ model and k_θ–$\widetilde{\varepsilon}_\theta$ model in Chapter 4 are summarized. The equations for the velocity field can be written as follows:

Reynolds stress

$$\begin{aligned}\overline{u_i u_j} =& \frac{2}{3}k\delta_{ij} - \frac{1}{f_R}2\nu_t S_{ij} \\ &+ \frac{4C_D}{f_R}k\tau_R^2\left[\left(S_{ik}\Omega_{kj} - \Omega_{ik}S_{kj}\right) - \left(S_{ik}S_{kj} - \frac{\delta_{ij}}{3}S_{mn}S_{mn}\right)\right],\end{aligned}$$

where

$$\begin{aligned}f_R =& 1 + \left(C_D\tau_R\right)^2\left[\frac{22}{3}\Omega^2 + \frac{2}{3}\left(\Omega^2 - S^2\right)f_B\right], \quad C_D = 0.8, \quad \tau_R = \frac{\nu_t}{k} \\ f_B =& 1 + C_\eta\left(\Omega^2 - S^2\right), \quad C_\eta = 5.0.\end{aligned}$$

Eddy viscotiy

$$\nu_t = C_\mu f_\mu \frac{k^2}{(\widetilde{\varepsilon} + D)} = C_\mu f_\mu \frac{k^2}{\varepsilon},$$

where

$$\begin{aligned}f_\mu =& \left[1 - f_w\,(28)\right]\left\{1 + \left(\frac{23}{R_t^{\frac{3}{4}}}\right)\exp\left[-\left(\frac{R_t}{150}\right)^2\right]\right\}, \\ f_w(\xi) =& \exp\left[-\left(\frac{y^*}{\xi}\right)^2\right], \\ \varepsilon =& \widetilde{\varepsilon} + D, \quad D = 2\nu\left(\frac{\partial\sqrt{k}}{\partial y}\right)^2, \quad \frac{\partial\sqrt{k}}{\partial y} \geq 0, \\ R_t =& \frac{k^2}{\nu(\widetilde{\varepsilon} + D)} = \frac{k^2}{\nu\varepsilon}, \\ C_\mu =& 0.12.\end{aligned}$$

k-equation

$$\frac{Dk}{Dt} = \frac{\partial}{\partial x_j}\left[\left(\nu\delta_{j\ell} + C_s f_{t1}\frac{\nu_t}{k}\overline{u_j u_\ell}\right)\frac{\partial k}{\partial x_\ell}\right] - \overline{u_i u_j}\frac{\partial \bar{U}_i}{\partial x_j} - \left(\widetilde{\varepsilon} + D\right),$$

where

$$C_s = 1.4, \quad f_{t1} = 1 + 6.0 f_w(5).$$

$\widetilde{\varepsilon}$-equation

$$\begin{aligned}\frac{D\widetilde{\varepsilon}}{Dt} =& \frac{\partial}{\partial x_j}\left[\left(\nu\delta_{j\ell} + C_\varepsilon f_{t2}\frac{\nu_t}{k}\overline{u_j u_\ell}\right)\frac{\partial\widetilde{\varepsilon}}{\partial x_\ell}\right] - \frac{\widetilde{\varepsilon}}{k}\left(C_{\varepsilon 1}\overline{u_i u_j}\frac{\partial \bar{U}_i}{\partial x_j} + C_{\varepsilon 2} f_\varepsilon \widetilde{\varepsilon}\right) \\ &+ 0.01 f_w(28)\nu\frac{k}{\widetilde{\varepsilon}}\overline{u_\ell u_k}\left(\frac{\partial^2 \bar{U}_i}{\partial x_\ell \partial x_k}\right)\left(\frac{\partial^2 \bar{U}_i}{\partial x_j \partial x_k}\right),\end{aligned}$$

where

$$\begin{aligned}C_\varepsilon =& 1.4, \quad f_{t2} = 1 + 5.0 f_w(5), \\ C_{\varepsilon 1} =& 1.45, \quad C_{\varepsilon 2} = 1.9, \\ f_\varepsilon =& 1 - 0.3\exp\left[-\left(\frac{R_t}{6.5}\right)^2\right].\end{aligned}$$

The equations for the thermal field can be written as follows:

Turbulent heat flux

$$\overline{u_j\theta} = -\alpha_t\frac{\partial\bar{\Theta}}{\partial x_j}.$$

Eddy diffusivity for heat

$$\alpha_t = C_\lambda f_\lambda k \tau_m,$$

where

$$\begin{aligned}f_\lambda =& \left[1 - f_w(26)\right]^{\frac{1}{2}}\left[1 - f_w\left(\frac{26}{Pr^{\frac{1}{3}}}\right)\right]^{\frac{1}{2}}, \\ \tau_m =& \frac{k}{\varepsilon}\left\{\frac{2R}{0.5+R} + \left(\frac{23\sqrt{2R}/Pr^{\frac{4}{3}}}{R_t^{\frac{3}{4}}}\right)\exp\left[-\left(\frac{R_t}{150}\right)^2\right]\right\}, \\ R =& \frac{k_\theta/\varepsilon_\theta}{k/\varepsilon}, \\ \varepsilon_\theta =& \widetilde{\varepsilon}_\theta + D_\theta, \quad D_\theta = 2\alpha\left(\frac{\partial\sqrt{\Delta k_\theta}}{\partial y}\right)^2, \quad \frac{\partial\sqrt{\Delta k_\theta}}{\partial y} \geq 0, \\ C_\lambda =& 0.1.\end{aligned}$$

k_θ-equation

$$\frac{Dk_\theta}{Dt} = \frac{\partial}{\partial x_j}\left[\left(\alpha + f_{t3}\frac{\alpha_t}{\sigma_h}\right)\frac{\partial k_\theta}{\partial x_j}\right] - \overline{u_j\theta}\frac{\partial \bar{\Theta}}{\partial x_j} - \left(\widetilde{\varepsilon}_\theta + D_\theta\right),$$

where

$$\sigma_h = 1.4, \quad f_{t3} = 1 + 9.0 f_w(5),$$

$\widetilde{\varepsilon}_\theta$-equation

$$\begin{aligned}\frac{D\widetilde{\varepsilon}_\theta}{Dt} =& \frac{\partial}{\partial x_j}\left[\left(\alpha + f_{t4}\frac{\alpha_t}{\sigma_\phi}\right)\frac{\partial \widetilde{\varepsilon}_\theta}{\partial x_j}\right] \\ &- \frac{\widetilde{\varepsilon}_\theta}{k_\theta}\left(C_{P1} f_{P1}\overline{u_j\theta}\frac{\partial \bar{\Theta}}{\partial x_j} + C_{D1} f_{D1}\widetilde{\varepsilon}_\theta\right) - \frac{\widetilde{\varepsilon}_\theta}{k}\left(C_{P2} f_{P2}\overline{u_i u_j}\frac{\partial \bar{U}_i}{\partial x_j} + C_{D2} f_{D2}\widetilde{\varepsilon}\right) \\ &+ \alpha\alpha_t f_w(26)\left(\frac{\partial^2 \bar{\Theta}}{\partial x_j \partial x_k}\right)^2,\end{aligned}$$

where

$$\begin{aligned}\sigma_\phi =& 1.0, \quad f_{t4} = 1 + 1.0 f_w(5), \\ C_{P1} =& 0.85, \quad C_{P2} = 0.64, \quad C_{D1} = 1.0, \quad C_{D2} = 0.9, \\ f_{D1} =& f_{P1} = f_{P2} = 1.0, \quad f_{D2} = \frac{1}{C_{D2}}\left(C_{\varepsilon 2} f_\varepsilon - 1\right).\end{aligned}$$

A.3 k_θ–ε_θ and k–ε models in Chapter 5

The rigorous k_θ–ε_θ model and modified k–ε model (Nagano & Shimada 1995) in Chapter 5 are summarized. The proposed k_θ–ε_θ model is given as follows:

Turbulent heat flux

$$\overline{u_j\theta} = -\alpha_t \frac{\partial \bar{\Theta}}{\partial x_j}.$$

Eddy diffusivity for heat

$$\alpha_t = C_\lambda f_\lambda k \tau_m,$$

where

$$\begin{aligned}
f_\lambda &= \left[1 - f_w\left(28\right)\right]^{\frac{1}{2}} \left[1 - f_w\left(\frac{28}{Pr^{\frac{1}{3}}}\right)\right]^{\frac{1}{2}}, \\
\tau_m &= \frac{k}{\varepsilon}\left[\frac{2R}{0.5+R} + \left(\frac{26\sqrt{2R}/Pr^{\frac{4}{3}}}{R_t^{\frac{3}{4}}}\right)\exp\left(-\frac{R_h}{220}\right)\right], \\
R &= \frac{k_\theta/\varepsilon_\theta}{k/\varepsilon}, \quad R_h = R_t\left(\frac{2R}{0.5+R}\right), \\
C_\lambda &= 0.1, \\
f_w(\xi) &= \exp\left[-\left(\frac{y^*}{\xi}\right)^2\right].
\end{aligned}$$

k_θ-equation

$$\frac{Dk_\theta}{Dt} = \frac{\partial}{\partial x_j}\left[\left(\alpha + \frac{\alpha_t}{\sigma_h^*}\right)\frac{\partial k_\theta}{\partial x_j} + C_\theta\left(\sigma_{\overline{u_k u_\ell}} d_k n_\ell e_j f_{w\theta}\sqrt{k}\, k_\theta\right)\right] - \overline{u_j\theta}\frac{\partial \bar{\Theta}}{\partial x_j} - \varepsilon_\theta,$$

where

$$\begin{aligned}
\sigma_h^* &= \frac{1.8}{1 + 0.5 f_w(28)}, \quad C_\theta = 0.1, \\
f_{w\theta} &= [1 - f_w(28)]^{\frac{1}{2}}[f_w(28)]^{\frac{1}{2}},
\end{aligned}$$

here d_k, n_ℓ and e_j are unit vectors in the streamwise, wall-normal and x_j directions, respectively and the sign function $\sigma_{\overline{u_k u_\ell}}$ is given as follows:

$$\sigma_{\overline{u_k u_\ell}} = \begin{cases} 1 & (x \geq 0), \\ -1 & (x < 0). \end{cases}$$

$\widetilde{\varepsilon}_\theta$-equation

$$\begin{aligned}\frac{D\varepsilon_\theta}{Dt} =&\frac{\partial}{\partial x_j}\left[\left(\alpha+\frac{\alpha_t}{\sigma_\phi}\right)\frac{\partial\varepsilon_\theta}{\partial x_j}+C_{\varepsilon_\theta}\alpha\left(f_{w\varepsilon_\theta}\frac{\varepsilon}{k}\frac{\partial k_\theta}{\partial x_j}\right)\right]\\ &-\frac{\varepsilon_\theta}{k_\theta}\left(C_{P1}f_{P1}\overline{u_j\theta}\frac{\partial\bar{\Theta}}{\partial x_j}+C_{D1}f_{D1}\varepsilon_\theta\right)-\frac{\varepsilon_\theta}{k}\left(C_{P2}f_{P2}\overline{u_iu_j}\frac{\partial\bar{U}_i}{\partial x_j}+C_{D2}f_{D2}\varepsilon\right)\\ &+\alpha\alpha_t f_w(12)\left(\frac{\partial^2\bar{\Theta}}{\partial x_j\partial x_k}\right)^2+C_{P3}\alpha\frac{k}{\varepsilon}f(R)\frac{\partial k}{\partial x_k}\frac{\partial\bar{\Theta}}{\partial x_j}\frac{\partial^2\bar{\Theta}}{\partial x_j\partial x_k}\end{aligned}$$

where

$$\begin{aligned}\sigma_\phi =&1.0,\\ f_{w\varepsilon_\theta} =&[1-f_w(3)]^{\frac{3}{2}}f_w(3),\quad f(R)=\frac{2R}{0.5+R},\\ C_{P1} =&0.85,\quad C_{P2}=0.77,\quad C_{P3}=0.05,\quad C_{D1}=1.0,\quad C_{D2}=0.9,\quad C_{\varepsilon_\theta}=1.6,\\ f_{P1} =&\left(1-f'_{P1}\right)f_p\left[1-f_w(12)\right],\\ f_{P2} =&\left(1-f'_{P2}\right)f_p,\\ f_{D1} =&1-f_w(12),\\ f_{D2} =&\frac{1}{C_{D2}}\left(C_{\varepsilon 2}f_\varepsilon-1\right)\left[1-f_w(12)\right],\\ f_\varepsilon =&1-0.3\exp\left[-\left(\frac{R_t}{6.5}\right)^2\right],\\ f'_{P1} =&\exp\left(-7\times10^{-5}R_T^{10}\right)\left[1-\exp(-2.2R_T^{\frac{1}{2}})\right],\\ f'_{P2} =&\exp\left(-7\times10^{-5}R_U^{10}\right)\left[1-\exp(-2.2R_U^{\frac{1}{2}})\right],\\ f_p =&1+0.75\exp\left[-\left(\frac{R_h}{40}\right)^{\frac{1}{2}}\right],\\ R_T =&f_w(6)\frac{u_\tau\theta_\tau}{(\alpha+\alpha_t)(\varepsilon_\theta/\alpha)^{\frac{1}{2}}},\quad R_U=f_w(6)\frac{{u_\tau}^2}{(\nu+\nu_t)(\varepsilon/\nu)^{\frac{1}{2}}}.\end{aligned}$$

In the velocity field, the modified k–ε model is given as follows:

Reynolds stress

$$-\overline{u_i u_j} = \nu_t \left(\frac{\partial \bar{U}_i}{\partial x_j} + \frac{\partial \bar{U}_j}{\partial x_i} \right) - \frac{2}{3}\delta_{ij} k.$$

Eddy viscotiy

$$\nu_t = C_\mu f_\mu \frac{k^2}{\varepsilon}$$

where

$$f_\mu = (1 - f_{w2}) \left\{ 1 + \left(\frac{60}{R_t{}^{\frac{3}{4}}} \right) \exp \left[- \left(\frac{R_t}{55} \right)^{\frac{1}{2}} \right] \right\}, \quad f_{w2} = f_w(26).$$

k-equation

$$\frac{Dk}{D\tau} = \frac{\partial}{\partial y} \left[\left(\nu + \frac{\nu_t}{\sigma_k^*} \right) \frac{\partial k}{\partial y} \right] - \overline{uv} \frac{\partial \bar{U}}{\partial y} - \varepsilon + \max \left[-0.5\nu \frac{\partial}{\partial y} \left(\frac{k}{\varepsilon} \frac{\partial \varepsilon}{\partial y} f_{w1} \right), 0 \right],$$

where

$$\sigma_k^* = \frac{1.4}{f_t}, \quad f_t = 1 + 6 f_{w1}, \quad f_{w1} = f_w(4).$$

ε-equation

$$\begin{aligned} \frac{D\varepsilon}{D\tau} = & \frac{\partial}{\partial y} \left[\left(\nu + \frac{\nu_t}{\sigma_\varepsilon^*} \right) \frac{\partial \varepsilon}{\partial y} \right] - C_{\varepsilon 1} \frac{\varepsilon}{k} \overline{uv} \frac{\partial \bar{U}}{\partial y} - C_{\varepsilon 2} f_2 \frac{\varepsilon^2}{k} + f_{w2} \nu \nu_t \left(\frac{\partial^2 \bar{U}}{\partial y^2} \right)^2 \\ & + C_{\varepsilon 3} \nu \frac{k}{\varepsilon} \frac{\partial k}{\partial y} \frac{\partial \bar{U}}{\partial y} \frac{\partial^2 \bar{U}}{\partial y^2} + C_{\varepsilon 4} \nu \frac{\partial}{\partial y} \left[(1 - f_{w1}) \frac{\varepsilon}{k} \frac{\partial k}{\partial y} f_{w1} \right], \end{aligned}$$

where

$$\begin{aligned} \sigma_\varepsilon^* &= \frac{1.3}{f_t}, \\ C_{\varepsilon 1} &= 1.45, \quad C_{\varepsilon 2} = 1.9, \quad C_{\varepsilon 3} = 0.005, \quad C_{\varepsilon 4} = 0.5, \\ f_2 &= (1 + f_2')(1 - f_{w1}) \left\{ 1 - 0.6 \exp \left[- \left(\frac{R_t}{45} \right)^{\frac{1}{2}} \right] \right\}, \\ f_2' &= \exp \left(-2 \times 10^{-4} R_v^{13} \right) \left[1 - \exp \left(-2.2 R_v^{0.5} \right) \right], \\ R_v &= \left(\frac{k}{\varepsilon} \right) \frac{1}{1 + \nu_t / \nu} \left(\frac{1}{R_t{}^{\frac{1}{2}}} \right) f_{w1}. \end{aligned}$$

A.4 Two-layer k–ε and k_θ–ε_θ models in Chapter 6

The proposed two-layer k–$\widetilde{\varepsilon}$ and k_θ–$\widetilde{\varepsilon}_\theta$ models in Chapter 6 are summarized. The equations for the velocity field can be written as follows:

Reynolds stress

$$-\overline{u_i u_j} = \nu_t \left(\frac{\partial \bar{U}_i}{\partial x_j} + \frac{\partial \bar{U}_j}{\partial x_i} \right) - \frac{2}{3}\delta_{ij} k.$$

Eddy viscotiy

$$\nu_t = C_\mu f_\mu \frac{k^2}{\varepsilon} \left\{ 1 + \left(\frac{40}{R_t^{3/4}} \right) \exp \left[- \left(\frac{R_t}{25} \right)^{1/2} \right] \right\},$$

where

$$f_\mu = 1 - \exp \left[- \left(\frac{n^*}{24} \right)^2 \right], \quad n^* = \frac{u_\varepsilon n}{\nu}.$$

k-equation

$$\frac{Dk}{Dt} = \frac{\partial}{\partial x_j} \left[\left(\nu + \frac{\nu_t}{\sigma_k^*} \right) \frac{\partial k}{\partial x_j} \right] - \overline{u_i u_j} \frac{\partial \bar{U}_i}{\partial x_j} - \varepsilon,$$

where

$$\sigma_k^* = \frac{\sigma_k}{f_k} = \frac{\sigma_k}{1 + 5 f_w}, \quad f_w = \exp \left[- \left(\frac{n^*}{10} \right)^2 \right].$$

Algebraic ε-equation and ε-equation

ε is given as follows:

$$\varepsilon = \begin{cases} \text{algebraic equation} = \widetilde{\varepsilon}_a + D & \text{for } f_c \geq 1 \\ \text{transport equation} & \text{for } f_c < 1 \end{cases},$$

where

$$f_c = \left(\frac{0.5}{R_c} \right) \left\{ 1 - \exp \left[-1 \times 10^4 \left(\frac{S\nu}{\bar{U}_i^2} \right) \right] \right\}, \quad R_c = \frac{\tau_b k}{\nu}, \quad \tau_b = \frac{\nu}{\nu S + k}, \quad S = 2 S_{ij} S_{ij}{}^{\frac{1}{2}},$$

$$\widetilde{\varepsilon}_a = \left(\frac{k}{\tau_b} \right) f_b, \quad D = 2\nu \left(\frac{\partial \sqrt{k}}{\partial x_j} \right) \left(\frac{\partial \sqrt{k}}{\partial x_j} \right), \quad f_b = \left(\frac{1}{90} \right) \exp \left[- \left(1.0 \times 10^{-4} R_s \right)^{\frac{1}{2}} \right],$$

here transport equation can be written as follows:

$$\frac{D\varepsilon}{Dt} = \frac{\partial}{\partial x_j}\left[\left(\nu + \frac{\nu_t}{\sigma_\varepsilon}\right)\frac{\partial \varepsilon}{\partial x_j}\right] - \frac{\varepsilon}{k}\left(C_{\varepsilon 1}\overline{u_i u_j}\frac{\partial \bar{U}_i}{\partial x_j} + C_{\varepsilon 2} f_\varepsilon \varepsilon\right),$$

where

$$\begin{aligned}\sigma_\varepsilon &= 1.4, \quad C_{\varepsilon 1} = 1.5, \quad C_{\varepsilon 2} = 1.9,\\ f_\varepsilon &= 1 - 0.3\exp\left[-\left(\frac{R_t}{6.5}\right)^2\right].\end{aligned}$$

The equations for the themal field can be written as follows:

Turbulent heat flux

$$\overline{u_j\theta} = -\alpha_t \frac{\partial \bar{\Theta}}{\partial x_j}.$$

Eddy diffusivity for heat

$$\alpha_t = C_\lambda f_\lambda \frac{k^2}{\varepsilon}\left\{f(R) + \sqrt{\frac{2R}{Pr}}\frac{55}{\left(1+2\sqrt{Pr}\right)^{\frac{1}{4}}}\frac{1}{R_t^{\frac{3}{4}}}\exp\left[-\left(\frac{R_t f(R)}{12}\right)^{\frac{1}{2}}\right]\right\}$$

where

$$f_\lambda = 1 - \exp\left(-7.5\times 10^{-4} {n^*}^{\frac{7}{4}} {n_\theta^*}^{\frac{1}{4}}\right), \quad f(R) = \frac{2R}{R + 0.2/Pr^{\frac{1}{4}}}, \quad n_\theta^* = \left(1+2\sqrt{Pr}\right)n^*.$$

k_θ-equation

$$\frac{Dk_\theta}{Dt} = \frac{\partial}{\partial x_j}\left[\left(\alpha + \frac{\alpha_t}{\sigma_h^*}\right)\frac{\partial k_\theta}{\partial x_j} + C_\theta\left(\sigma_{\overline{u_k u_\ell}} d_k n_\ell e_j f_{w\theta}\sqrt{k}\, k_\theta\right)\right] - \overline{u_j\theta}\frac{\partial \bar{\Theta}}{\partial x_j} - \varepsilon_\theta,$$

where

$$\begin{aligned}\sigma_h^* &= \frac{1.8}{1+9f_w}, \quad C_\theta = 0.05,\\ f_{w\theta} &= \sqrt{f_\lambda\left(1-f_\lambda\right)},\end{aligned}$$

here d_k, n_ℓ and e_j are unit vectors in the streamwise, wall-normal and x_j directions, respectively and the sign function $\sigma_{\overline{u_k u_\ell}}$ is given as follows:

$$\sigma_{\overline{u_k u_\ell}} = \begin{cases} 1 & (x \geq 0),\\ -1 & (x < 0).\end{cases}$$

Algebraic ε_θ-equation and ε_θ-equation

ε_θ is given as follows:

$$\varepsilon_\theta = \begin{cases} \text{algebraic equation} = \widetilde{\varepsilon}_{\theta a} + D_\theta & \text{for } f_{c\theta} \geq 1 \\ \text{transport equation} & \text{for } f_{c\theta} < 1 \end{cases},$$

where

$$f_{c\theta} = \left(\frac{1.0}{R_{c\theta}}\right)\left\{1 - \exp\left[-1 \times 10^4 \left(\frac{S\nu}{\bar{U}_i^2}\right)\right]\right\} \exp\left(-\sqrt{\frac{R_{c\theta}}{10}}\right),$$

$$R_{c\theta} = \frac{\tau_{b\theta} k}{\nu}, \quad \tau_{b\theta} = \frac{\nu}{k + \nu S + \nu G\sqrt{k/k_\theta}}, \quad G = \sqrt{\left(\frac{\partial\bar{\Theta}}{\partial x_j}\right)\left(\frac{\partial\bar{\Theta}}{\partial x_j}\right)},$$

$$\widetilde{\varepsilon}_{\theta_a} = \left(\frac{k_\theta}{\tau_{b\theta}}\right), \quad D_\theta = 2\alpha\left(\frac{\partial\sqrt{\Delta k_\theta}}{\partial x_j}\right)\left(\frac{\partial\sqrt{\Delta k_\theta}}{\partial x_j}\right), \quad f_{b\theta} = \frac{1}{130\sqrt{Pr}} \exp\left[-\left(\frac{R_{c\theta}}{13}\right)^{\frac{1}{2}}\right],$$

here transport equation for ε_θ can be written as follows:

$$\begin{aligned} \frac{D\varepsilon_\theta}{Dt} =& \frac{\partial}{\partial x_j}\left[\left(\alpha + \frac{\alpha_t}{\sigma_\phi}\right)\frac{\partial\varepsilon_\theta}{\partial x_j}\right] \\ & - \frac{\varepsilon_\theta}{k_\theta}\left(C_{P1} f_{P1} \overline{u_j\theta}\frac{\partial\bar{\Theta}}{\partial x_j} + C_{D1} f_{D1}\varepsilon_\theta\right) - \frac{\varepsilon_\theta}{k}\left(C_{P2} f_{P2}\overline{u_i u_j}\frac{\partial\bar{U}_i}{\partial x_j} + C_{D2} f_{D2}\varepsilon\right), \end{aligned}$$

where

$$\begin{aligned} \sigma_\phi =& 1.8, \\ C_{P1} =& 0.9, \quad C_{P2} = 0.77, \quad C_{D1} = 1.0, \quad C_{D2} = 0.9, \\ f_{D1} =& f_{P1} = f_{P2} = 1.0, \quad f_{D2} = \frac{1}{C_{D2}}\left(1.9 f_\varepsilon - 1\right), \\ f_\varepsilon =& 1 - 0.3\exp\left[-\left(\frac{R_t}{6.5}\right)^2\right]. \end{aligned}$$

A.5 Reynolds stress expression for nonlinear k–ε model in Chapter 7

The proposed Reynolds stress expression for nonlinear k–ε model in Chapter 7 is given as follows:

$$\overline{u_i u_j} = \frac{2}{3}k\delta_{ij} - 2C_0\nu_t S_{ij} + Q_o + Q_w,$$

where

$$\begin{aligned}
\nu_t =& = C_\mu f_\mu \frac{k^2}{\varepsilon},\\
Q_o =& C_1 k\tau_{Ro}^2(W_{jk}S_{ki} + W_{ik}S_{kj}) + C_2 k\tau_{Ro}^2\left(S_{ik}S_{kj} - \frac{\delta_{ij}}{3}S_{mn}S_{mn}\right),\\
Q_w =& C_1' k\tau_{Rw}^2(W_{jk}S_{ki} + W_{ik}S_{kj}) + C_2' k\tau_{Rw}^2\left(S_{ik}S_{kj} - \frac{\delta_{ij}}{3}S_{mn}S_{mn}\right),
\end{aligned}$$

here

$$\begin{aligned}
\tau_{Ro} =& \frac{\nu_t}{k}, \quad \tau_{Rw} = \sqrt{\frac{2}{3}\frac{1}{C_1 f_{SW}}}\left(1 - \frac{3C_{v1}f_{v2}}{8}\right)f_{v1}^2,\\
C_0 =& \frac{1}{f_R}, \quad C_1 = \frac{4C_D}{f_R}, \quad C_2 = \frac{4C_D}{f_R}, \quad C_1' = C_1, \quad C_2' = C_2,\\
C_D =& 0.8, \quad C_v = \frac{C_{v1}}{C_{v2}}, \quad C_{v1} = 0.4, \quad C_{v2} = 2\times 10^3, \quad C_\mu = 0.12, \quad C_\eta = 5.0,\\
f_B =& 1 + C_\eta\left(C_D\tau_{Ro}\right)^2\left(W^2 - S^2\right),\\
f_R =& 1 + \left(C_D\tau_{Ro}\right)^2\left[\frac{22}{3}W^2 + \frac{2}{3}\left(W^2 - S^2\right)f_B\right],\\
f_{SW} =& \frac{W^2}{2} + \frac{S^2}{3} - \left(\sqrt{\frac{S^2}{2}} - \sqrt{\frac{W^2}{2}}\right)^2 f_{v1},\\
f_{v1} =& f_w(40), \quad f_{v2} = 1 - \exp\left(-\frac{\sqrt{R_t}}{C_{v2}}\right), \quad f_w(\xi) = \exp\left[-\left(\frac{n^*}{\xi}\right)\right],\\
f_\mu =& \left[1 - f_w(26)\right]\left\{1 + \left(\frac{35}{R_t^{\frac{3}{4}}}\right)\exp\left[-\left(\frac{R_t}{30}\right)^{\frac{3}{4}}\right]\right\},\\
S^2 =& S_{ij}S_{ij}, \quad W^2 = W_{ij}W_{ij}.
\end{aligned}$$

A.6 Nonlinear k–ε model in Chapter 8

The proposed nonlinear k–ε model in Chapter 8 is given as follows:

Reynolds stress

$$\overline{u_i u_j} = \frac{2}{3}k\delta_{ij} - 2C_0\nu_t S_{ij} + Q_o + Q_w,$$

where

$$\begin{aligned} Q_o =& C_1 k\tau_{Ro}^2(W_{jk}S_{ki} + W_{ik}S_{kj}) + C_2 k\tau_{Ro}^2\left(S_{ik}S_{kj} - \frac{\delta_{ij}}{3}S_{mn}S_{mn}\right), \\ Q_w =& C_1' k\tau_{Rw}^2(W_{jk}S_{ki} + W_{ik}S_{kj}) + C_2' k\tau_{Rw}^2\left(S_{ik}S_{kj} - \frac{\delta_{ij}}{3}S_{mn}S_{mn}\right), \end{aligned}$$

here

$$\begin{aligned} \tau_{Ro} =& \frac{\nu_t}{k}, \quad \tau_{Rw} = \sqrt{\frac{2}{3}\frac{1}{C_1 f_{SW}}}\left(1 - \frac{3C_{v1}f_{v2}}{8}\right)f_{v1}^2, \\ C_0 =& \frac{1}{f_R}, \quad C_1 = \frac{4C_D}{f_R}, \quad C_2 = \frac{4C_D}{f_R}, \quad C_1' = C_1, \quad C_2' = C_2, \\ C_D =& 0.8, \quad C_v = \frac{C_{v1}}{C_{v2}}, \quad C_{v1} = 0.4, \quad C_{v2} = 2\times 10^3, \quad C_\mu = 0.12, \quad C_\eta = 5.0, \\ f_B =& 1 + C_\eta\left(C_D\tau_{Ro}\right)^2\left(W^2 - S^2\right), \\ f_R =& 1 + \left(C_D\tau_{Ro}\right)^2\left[\frac{22}{3}W^2 + \frac{2}{3}\left(W^2 - S^2\right)f_B\right], \\ f_{SW} =& \frac{W^2}{2} + \frac{S^2}{3} - f_{SW}^\Omega, \quad f_{SW}^\Omega = \left[\left(\sqrt{\frac{S^2}{2}} - \sqrt{\frac{W^2}{2}}\right)^2 f_w(1)\right]^2, \\ f_{v1} =& \exp\left[-\left(\frac{R_{tm}}{45}\right)^2\right], \quad f_{v2} = 1 - \exp\left(-\frac{\sqrt{R_t}}{C_{v2}}\right), \\ S^2 =& S_{ij}S_{ij}, \quad W^2 = W_{ij}W_{ij}. \end{aligned}$$

Eddy viscotiy

$$\begin{aligned} \nu_t =& C_\mu f_\mu \frac{k^2}{\varepsilon}, \\ f_\mu =& \left\{1 + \left(\frac{40}{R_t^{3/4}}\right)\exp\left[-\left(\frac{R_t}{35}\right)^{3/4}\right]\right\}\left[1 - f_w(32)\right], \\ f_w(\xi) =& \exp\left[-\left(\frac{R_{tm}}{\xi}\right)^2\right], \quad R_{tm} = \frac{C_{tm}n^* R_t^{1/4}}{C_{tm}R_t^{1/4} + n^*}, \quad C_{tm} = 1.3\times 10^2, \end{aligned}$$

k-equation

$$\frac{Dk}{Dt} = \frac{\partial}{\partial x_j}\left[\left(\nu\delta_{j\ell} + C_s f_{t1}\frac{k}{\varepsilon}\overline{u_j u_\ell}\right)\frac{\partial k}{\partial x_\ell}\right] - \overline{u_i u_j}\frac{\partial \bar{U}_i}{\partial x_j} - \varepsilon + \max\left\{-0.5\nu\frac{\partial}{\partial x_j}\left[\frac{k}{\varepsilon}\frac{\partial \varepsilon}{\partial x_j}f_w(1)\right], 0\right\},$$

where

$$C_s = 1.4, \quad f_{t1} = \frac{1 + 9.0 f_w(8)}{[1 - f_w(32)]^{\frac{1}{2}}}.$$

ε-equation

$$\begin{aligned}\frac{D\varepsilon}{Dt} =& \frac{\partial}{\partial x_j}\left[\left(\nu\delta_{j\ell} + C_\varepsilon f_{t2}\frac{k}{\varepsilon}\overline{u_j u_\ell}\right)\frac{\partial \varepsilon}{\partial x_\ell}\right] - \frac{\varepsilon}{k}\left(C_{\varepsilon 1}\overline{u_i u_j}\frac{\partial \bar{U}_i}{\partial x_j} + C_{\varepsilon 2} f_\varepsilon \varepsilon\right) \\ &+ C_{\varepsilon 4}\frac{\partial}{\partial x_j}\left\{[1 - f_w(5)]\frac{\varepsilon}{k}\frac{\partial k}{\partial x_j}f_w(5)\right\} \\ &+ C_{\varepsilon 3}\nu\frac{k}{\varepsilon}\overline{u_j u_\ell}\frac{\partial^2 \bar{U}_i}{\partial x_\ell \partial x_k}\frac{\partial^2 \bar{U}_i}{\partial x_j \partial x_k} + C_{\varepsilon 5}\nu\frac{k}{\varepsilon}\frac{\partial \overline{u_j u_k}}{\partial x_j}\frac{\partial \bar{U}_i}{\partial x_k}\frac{\partial^2 \bar{U}_i}{\partial x_j \partial x_k} + C_\Omega f_\Omega k \epsilon_{ij\ell} W_{ij}\Omega_\ell,\end{aligned}$$

where

$$\begin{aligned} C_\varepsilon =& 1.4, \quad f_{t2} = \frac{1 + 5.0 f_w(8)}{[1 - f_w(32)]^{\frac{1}{2}}}, \\ C_{\varepsilon 1} =& 1.45, \quad C_{\varepsilon 2} = 1.9, \quad C_{\varepsilon 3} = 0.02, \quad C_{\varepsilon 4} = 0.5, \quad C_{\varepsilon 5} = 0.015, \\ f_\varepsilon =& 1 - 0.3\exp\left[-\left(\frac{R_t}{6.5}\right)^2\right], \\ f_\Omega =& C_{f_\Omega}\exp\left[-\left(\frac{R_\Omega}{10}\right)^{0.2}\right], \quad R_\Omega = \eta_t\sqrt{f_{SW}^\Omega}, \\ C_\Omega =& -0.045, \quad C_{f_\Omega} = 6.0, \quad \eta_t = \sqrt{\frac{\nu}{\varepsilon}}. \end{aligned}$$

Appendix B

Wall-limiting behaviour of terms in transport equations

B.1 Transport equation for the turbulence energy

Transport equation for the turbulence energy in Eq. (2.7) is given as follows:

$$\frac{Dk}{Dt} = D_k + T_k + \Pi_k + P_k - \varepsilon, \tag{B.1}$$

where

$$\begin{aligned}
D_k =& \nu \frac{\partial^2 k}{\partial x_j \partial x_j} && \text{: Molecular diffusion,} \\
T_k =& -\frac{\partial \overline{u_j k'}}{\partial x_j} && \text{: Turbulent diffusion,} \\
\Pi_k =& -\frac{\partial}{\partial x_j} \overline{\left(u_j \frac{p}{\rho} \right)} && \text{: Pressure diffusion,} \\
P_k =& -\overline{u_i u_j} \frac{\partial \bar{U}_i}{\partial x_j} && \text{: Production,} \\
\varepsilon =& \nu \overline{\frac{\partial u_i}{\partial x_j} \frac{\partial u_i}{\partial x_j}} && \text{: Dissipation,}
\end{aligned}$$

here $k' = u_i u_i / 2$.

The wall-limiting behaviour of individual terms are obtained with Eqs. (2.20)$\sim$(2.26) and the fluctuating pressure given as follows:

$$p = a_p + b_p x_2 + c_p x_2^2 + d_p x_2^3 + \cdots . \tag{B.2}$$

The wall-normal component of individual terms should be considered for the wall-limiting

behaviour, thus the following wall-limiting behaviour for individual terms are obtained.

$$D_k \simeq \nu \frac{\partial^2 k}{\partial x_2^2} = \nu \left(\overline{b_1^2} + \overline{b_3^2} \right) + 6\nu \left(\overline{b_1 c_1} + \overline{b_3 c_3} \right) x_2 + \cdots \propto x_2^0, \tag{B.3}$$

$$T_k \simeq - \frac{\partial \overline{u_2 k'}}{\partial x_2} = - \left(\overline{b_1^2 c_2} + \overline{b_3^2 c_2} \right) x_2^3 + \cdots \propto x_2^3, \tag{B.4}$$

$$\Pi_k \simeq - \frac{1}{\rho} \frac{\partial}{\partial x_2} \overline{u_2 p} = - \frac{2}{\rho} \overline{a_p c_2} x_2 - \frac{3}{\rho} \left(\overline{a_p d_2} + \overline{b_p c_2} \right) x_2^2 + \cdots \propto x_2^1, \tag{B.5}$$

$$\begin{aligned} P_k \simeq & - \overline{u_1 u_2} \frac{\partial \bar{U}_1}{\partial x_2} - \overline{u_2^2} \frac{\partial \bar{U}_2}{\partial x_2} - \overline{u_2 u_3} \frac{\partial \bar{U}_3}{\partial x_2} \\ = & - \left(\overline{b_1 c_2} B_1 + \overline{b_3 c_2} B_3 \right) x_2^3 - 2 \overline{c_2^2} C_2 x_2^5 + \cdots \propto x_2^3, \end{aligned} \tag{B.6}$$

$$\begin{aligned} \varepsilon \simeq & \nu \left[\overline{\left(\frac{\partial u_1}{\partial x_2} \right)^2} + \overline{\left(\frac{\partial u_2}{\partial x_2} \right)^2} + \overline{\left(\frac{\partial u_3}{\partial x_2} \right)^2} \right] \\ = & \nu \left(\overline{b_1^2} + \overline{b_3^2} \right) + 4\nu \left(\overline{b_1 c_1} + \overline{b_3 c_3} \right) x_2 \\ & + 4\nu \left[\overline{c_1^2} + \overline{c_2^2} + \overline{c_3^2} + (3/2) \overline{b_1 d_1} + (3/2) \overline{b_3 d_3} \right] x_2^2 + \cdots \propto x_2^0. \end{aligned} \tag{B.7}$$

Note that the molecular diffusion term balances with the dissipation term near the wall in order of x_2^0. However, the difference between Eqs. (B.3) and (B.7) is $2\nu \left(\overline{b_1 c_1} + \overline{b_3 c_3} \right) x_2^1$ in order of x_2^1. Therefore, if the modeled k-equation does not have the term of $2\nu \left(\overline{b_1 c_1} + \overline{b_3 c_3} \right) x_2$, the coefficient $\nu \left(\overline{b_1 c_1} + \overline{b_3 c_3} \right)$ should be zero on the wall, and $\nu \left(\overline{b_1 c_1} + \overline{b_3 c_3} \right)$ equals the gradient of ε on the wall, i.e., $\partial \varepsilon / \partial x_2 |_w = 0$ holds.

To satisfy the wall-limiting behaviour of dissipation term in the modeled k-equation, the pressure diffusion term in Eq. (B.5) should be modeled.

B.2 Transport equation for the dissipation rate of turbulence energy

Transport equation for he dissipation rate of turbulence energy in Eq. (2.8) is given as follows:

$$\frac{D\varepsilon}{Dt} = D_\varepsilon + T_\varepsilon + \Pi_\varepsilon + P_\varepsilon^1 + P_\varepsilon^2 + P_\varepsilon^3 + P_\varepsilon^4 - \Upsilon, \tag{B.8}$$

where

$$D_\varepsilon = \nu \frac{\partial^2 \varepsilon}{\partial x_j \partial x_j} \qquad : \text{Molecular diffusion,}$$

$$
\begin{aligned}
T_\varepsilon =& -\frac{\partial\overline{u_j\varepsilon'}}{\partial x_j} && \text{: Turbulent diffusion,}\\
\Pi_\varepsilon =& -2\nu\frac{\partial}{\partial x_j}\left[\overline{\frac{\partial(p/\rho)}{\partial x_m}\frac{\partial u_j}{\partial x_m}}\right] && \text{: Pressure diffusion,}\\
P_\varepsilon^1 =& -2\nu\overline{\frac{\partial u_i}{\partial x_j}\frac{\partial u_k}{\partial x_j}}\frac{\partial\bar{U}_i}{\partial x_k} && \text{: Mixed production,}\\
P_\varepsilon^2 =& -2\nu\overline{\frac{\partial u_i}{\partial x_k}\frac{\partial u_i}{\partial x_m}}\frac{\partial\bar{U}_k}{\partial x_m} && \text{: Production by mean velocity gradient,}\\
P_\varepsilon^3 =& -2\nu\overline{u_k\frac{\partial u_i}{\partial x_m}}\frac{\partial^2\bar{U}_i}{\partial x_k\partial x_m} && \text{: Gradient production,}\\
P_\varepsilon^4 =& -2\nu\overline{\frac{\partial u_i}{\partial x_k}\frac{\partial u_i}{\partial x_m}\frac{\partial u_k}{\partial x_m}} && \text{: Turbulent production,}\\
\Upsilon =& 2\nu^2\overline{\frac{\partial^2 u_i}{\partial x_k\partial x_m}\frac{\partial^2 u_i}{\partial x_k\partial x_m}} && \text{: Destruction,}
\end{aligned}
$$

here $\varepsilon' = \nu(\partial u_i/\partial x_m)(\partial u_i/\partial x_m)$.

Similarly, the wall-limiting behaviour of individual terms are given as follows:

$$D_\varepsilon \simeq \nu\frac{\partial^2\varepsilon}{\partial x_2^2} = 8\nu^2\left[\overline{c_1^2}+\overline{c_2^2}+\overline{c_3^2}+(3/2)\overline{b_1d_1}+(3/2)\overline{b_3d_3}\right]+\cdots\propto x_2^0, \tag{B.9}$$

$$T_\varepsilon \simeq -\frac{\partial\overline{u_2\varepsilon'}}{\partial x_2} = -2\nu\left(\overline{b_1^2c_2}+\overline{b_3^2c_2}\right)x_2+\cdots\propto x_2^1, \tag{B.10}$$

$$\Pi_\varepsilon \simeq -2\frac{\nu}{\rho}\frac{\partial}{\partial x_2}\left(\overline{\frac{\partial p}{\partial x_2}\frac{\partial u_2}{\partial x_2}}\right) = -4\frac{\nu}{\rho}\overline{c_2b_p}+\cdots\propto x_2^0, \tag{B.11}$$

$$
\begin{aligned}
P_\varepsilon^1 \simeq& -2\nu\left(\overline{\frac{\partial u_1}{\partial x_2}\frac{\partial u_2}{\partial x_2}}\frac{\partial\bar{U}_1}{\partial x_2}+\overline{\frac{\partial u_2}{\partial x_2}\frac{\partial u_2}{\partial x_2}}\frac{\partial\bar{U}_2}{\partial x_2}+\overline{\frac{\partial u_3}{\partial x_2}\frac{\partial u_2}{\partial x_2}}\frac{\partial\bar{U}_3}{\partial x_2}\right)\\
=& -4\nu\left(\overline{b_1c_2}B_1+\overline{b_3c_2}B_3\right)x_2+\cdots\propto x_2^1,
\end{aligned} \tag{B.12}
$$

$$
\begin{aligned}
P_\varepsilon^2 \simeq& -2\nu\left(\overline{\frac{\partial u_1}{\partial x_2}\frac{\partial u_1}{\partial x_2}}\frac{\partial\bar{U}_2}{\partial x_2}+\overline{\frac{\partial u_2}{\partial x_2}\frac{\partial u_2}{\partial x_2}}\frac{\partial\bar{U}_2}{\partial x_2}+\overline{\frac{\partial u_3}{\partial x_2}\frac{\partial u_3}{\partial x_2}}\frac{\partial\bar{U}_2}{\partial x_2}\right)\\
=& -4\nu\left(\overline{b_1^2}+\overline{b_3^2}\right)C_2x_2+\cdots\propto x_2^1,
\end{aligned} \tag{B.13}
$$

$$
\begin{aligned}
P_\varepsilon^3 \simeq& -2\nu\left(\overline{u_2\frac{\partial u_1}{\partial x_2}}\frac{\partial^2\bar{U}_1}{\partial x_2^2}+\overline{u_2\frac{\partial u_2}{\partial x_2}}\frac{\partial^2\bar{U}_2}{\partial x_2^2}+\overline{u_2\frac{\partial u_3}{\partial x_2}}\frac{\partial^2\bar{U}_3}{\partial x_2^2}\right)\\
=& -4\nu\left(\overline{b_1c_2}C_1+\overline{b_3c_2}C_3\right)x_2^2+\cdots\propto x_2^2,
\end{aligned} \tag{B.14}
$$

$$
\begin{aligned}
P_\varepsilon^4 \simeq& -2\nu\left(\overline{\frac{\partial u_1}{\partial x_2}\frac{\partial u_1}{\partial x_2}\frac{\partial u_2}{\partial x_2}}+\overline{\frac{\partial u_2}{\partial x_2}\frac{\partial u_2}{\partial x_2}\frac{\partial u_2}{\partial x_2}}+\overline{\frac{\partial u_3}{\partial x_2}\frac{\partial u_3}{\partial x_2}\frac{\partial u_2}{\partial x_2}}\right)\\
=& -4\nu\left(\overline{b_1^2c_2}+\overline{b_3^2c_2}\right)x_2+\cdots\propto x_2^1,
\end{aligned} \tag{B.15}
$$

$$\Upsilon \simeq 2\nu^2\left[\overline{\left(\frac{\partial^2u_1}{\partial x_2^2}\right)^2}+\overline{\left(\frac{\partial^2u_2}{\partial x_2^2}\right)^2}+\overline{\left(\frac{\partial^2u_3}{\partial x_2^2}\right)^2}\right] = 8\nu^2\left(\overline{c_1^2}+\overline{c_2^2}+\overline{c_3^2}\right)+\cdots\propto x_2^0. \tag{B.16}$$

Obviously, the molecular diffusion term D_ε balances the destruction term Υ and pressure diffusion term Π_ε in order of x_2^0 near the wall from Eqs. (B.9)∼(B.16). Unfortunately, the different in the coefficient of x_2^0 exists, i.e., $12\nu^2\left(\overline{b_1 d_1}+\overline{b_3 d_3}\right)-4\nu\overline{c_2 b_p}/\rho$. In a calculation, if the pressure diffusion term is modeled in the ε-equation, the coefficient $12\nu^2\left(\overline{b_1 d_1}+\overline{b_3 d_3}\right)$ may balance $4\nu\overline{c_2 b_p}/\rho$ which is the coefficient in first term of Π_ε, and the correct wall-limiting behaviour of ε-equation can be obtained near the wall. In the modeled equation, however, the molecular diffusion term balances the modeled term $-C_{\varepsilon 2} f_\varepsilon \varepsilon^2/k$ in general. Since the wall-limiting behaviour of this modeled term is $2\nu^2\left(\overline{b_1^2}+\overline{b_3^2}\right)/x_2^2$, to satisfy the equation balance, the model function f_ε should be proportional to x_2^2. Consequently, the pressure diffusion term modelling is not only satisfying the wall-limiting behaviour but near-wall correcting for the equation.

B.3 Transport equation for the temperature variance

Transport equation for the temperature variance in Eq. (2.15) is given as follows:

$$\frac{Dk_\theta}{Dt} = D_{k_\theta} + T_{k_\theta} + P_{k_\theta} - \varepsilon_\theta, \tag{B.17}$$

where

$$\begin{aligned}
D_{k_\theta} =& \alpha\frac{\partial^2 k_\theta}{\partial x_j \partial x_j} && \text{: Molecular diffusion,}\\
T_{k_\theta} =& -\frac{\partial\overline{u_j k'_\theta}}{\partial x_j} && \text{: Turbulent diffusion,}\\
P_{k_\theta} =& -\overline{u_j\theta}\frac{\partial\bar{\Theta}}{\partial x_j} && \text{: Production,}\\
\varepsilon_\theta =& \alpha\overline{\frac{\partial\theta}{\partial x_j}\frac{\partial\theta}{\partial x_j}} && \text{: Dissipation,}
\end{aligned}$$

here $k'_\theta = \theta^2/2$.

The wall-limiting behaviour of individual terms are obtained with Eqs. (2.20)∼(2.27).

$$D_{k_\theta} \simeq \alpha\frac{\partial^2 k_\theta}{\partial x_2^2} = \alpha\left(\overline{h_1^2}+2\overline{h_2\theta_w}\right)+6\alpha\left(\overline{h_2\theta_w}+\overline{h_1 h_2}\right)x_2+\cdots\propto x_2^0, \tag{B.18}$$

$$T_{k_\theta} \simeq -\frac{\partial\overline{u_2 k'_\theta}}{\partial x_2} = -\overline{c_2\theta_w}x_2 - 2\left(\overline{c_2 h_1^2}+2\overline{c_2 h_2\theta_w}\right)x_2^3+\cdots\propto\begin{cases}\propto x_2^1 & :\theta_w\neq 0\\ \propto x_2^3 & :\theta_w = 0\end{cases}, \tag{B.19}$$

$$P_{k_\theta} \simeq -\overline{u_2\theta}\frac{\partial\bar{\Theta}}{\partial x_2} = -\overline{c_2\theta_w}H_1x_2^2 - \left(\overline{c_2h_1} - \overline{d_2\theta_w}\right)H_1x_2^3 + \cdots \begin{cases} \propto x_2^2 & : \theta_w \neq 0 \\ \propto x_2^3 & : \theta_w = 0 \end{cases}, \tag{B.20}$$

$$\varepsilon_\theta \simeq \alpha\overline{\frac{\partial\theta}{\partial x_2}\frac{\partial\theta}{\partial x_2}} = \alpha\overline{h_1^2} + 4\alpha\overline{h_1h_2}x_2 + 4\alpha\left[\overline{h_2^2} + (3/2)\overline{h_1h_3}\right]x_2^2 + \cdots \propto x_2^0. \tag{B.21}$$

The molecular diffusion term balances with the dissipation term near the wall in order of x_2^0. However, the coefficient $\alpha\overline{h_1h_2}$ of x_2 becomes 0 for the equation balance with $\theta_w = 0$ as mentioned in Chapter 5.

On the other hand, in case of existing of temperature fluctuation on the wall, there are the following fluctuating temperature gradients.

$$\frac{\partial\theta_w}{\partial x_1}, \quad \frac{\partial\theta_w}{\partial x_3},$$

where these are constant.

In this case, ε_θ is represented near the wall as follows:

$$\varepsilon_\theta = \alpha\overline{\left(\frac{\partial\theta_w}{\partial x_1}\right)^2} + \alpha\overline{\left(\frac{\partial\theta}{\partial x_2}\right)^2} + \alpha\overline{\left(\frac{\partial\theta_w}{\partial x_3}\right)^2}. \tag{B.22}$$

Therefore, the wall-limiting behaviour of ε_θ is expressed exactly in case of $\theta_w \neq 0$ as follows:

$$\varepsilon_\theta = \alpha\overline{\left(\frac{\partial\theta_w}{\partial x_1}\right)^2} + \alpha\overline{\left(\frac{\partial\theta_w}{\partial x_3}\right)^2} + 4\alpha\overline{h_2^2}x_2^2 + \cdots \propto x_2^0. \tag{B.23}$$

B.4 Transport equation for the dissipation rate of temperature variance

Transport equation for he dissipation rate of temperature variance in Eq. (2.16) is given as follows:

$$\frac{D\varepsilon_\theta}{Dt} = D_{\varepsilon_\theta} + T_{\varepsilon_\theta} + P^1_{\varepsilon_\theta} + P^2_{\varepsilon_\theta} + P^3_{\varepsilon_\theta} + P^4_{\varepsilon_\theta} - \Upsilon_{\varepsilon_\theta}, \tag{B.24}$$

where

$$
\begin{aligned}
D_{\varepsilon_\theta} =& \alpha \frac{\partial^2 \varepsilon_\theta}{\partial x_j \partial x_j} && \text{: Molecular diffusion,}\\
T_{\varepsilon_\theta} =& -\frac{\partial \overline{u_j \varepsilon'_\theta}}{\partial x_j} && \text{: Turbulent diffusion,}\\
P^1_{\varepsilon_\theta} =& -2\alpha \overline{\frac{\partial u_j}{\partial x_k}\frac{\partial \theta}{\partial x_k}\frac{\partial \bar{\Theta}}{\partial x_j}} && \text{: Mixed production,}\\
P^2_{\varepsilon_\theta} =& -2\alpha \overline{\frac{\partial \theta}{\partial x_k}\frac{\partial \theta}{\partial x_j}\frac{\partial \bar{U}_j}{\partial x_k}} && \text{: Production by mean velocity gradient,}\\
P^3_{\varepsilon_\theta} =& -2\alpha u_j \overline{\frac{\partial \theta}{\partial x_k}\frac{\partial^2 \bar{\Theta}}{\partial x_j \partial x_k}} && \text{: Gradient production,}\\
P^4_{\varepsilon_\theta} =& -2\alpha \overline{\frac{\partial u_j}{\partial x_k}\frac{\partial \theta}{\partial x_k}\frac{\partial \theta}{\partial x_j}} && \text{: Turbulent production,}\\
\Upsilon_{\varepsilon_\theta} =& 2\alpha^2 \overline{\frac{\partial^2 \theta}{\partial x_k \partial x_j}\frac{\partial^2 \theta}{\partial x_k \partial x_j}} && \text{: Destruction,}
\end{aligned}
$$

here $\varepsilon'_\theta = \alpha(\partial\theta/\partial x_m)(\partial\theta/\partial x_m)$.

Considering the case of non-existing temperature fluctuation on the wall for convenience, the wall-limiting behaviour of individual terms are obtained with Eqs. (2.20)∼(2.27).

$$D_{\varepsilon_\theta} \simeq \alpha \frac{\partial^2 \varepsilon_\theta}{\partial x_2^2} = 8\alpha^2 \left[\overline{h_2^2} + (3/2)\overline{h_1 h_3}\right] + \cdots \propto x_2^0, \tag{B.25}$$

$$T_{\varepsilon_\theta} \simeq -\alpha \frac{\partial \overline{u_2 \varepsilon'_\theta}}{\partial x_2} = -\alpha \overline{c_2 h_1^2} x_2 + \cdots \propto x_2^1, \tag{B.26}$$

$$P^1_{\varepsilon_\theta} \simeq -2\alpha \overline{\frac{\partial u_2}{\partial x_2}\frac{\partial \theta}{\partial x_2}\frac{\partial \bar{\Theta}}{\partial x_2}} = -4\alpha \overline{c_2 h_1} H_1 x_2 + \cdots \propto x_2^1, \tag{B.27}$$

$$P^2_{\varepsilon_\theta} \simeq -2\alpha \overline{\frac{\partial \theta}{\partial x_2}\frac{\partial \theta}{\partial x_2}\frac{\partial \bar{U}_2}{\partial x_2}}, = -4\alpha \overline{h_1^2} C_2 x_2 + \cdots \propto x_2^1, \tag{B.28}$$

$$P^3_{\varepsilon_\theta} \simeq -2\alpha u_2 \overline{\frac{\partial \theta}{\partial x_2}\frac{\partial^2 \bar{\Theta}}{\partial x_2^2}} = -4\alpha \overline{c_2 h_1} H_2 x_2^2 + \cdots \propto x_2^2, \tag{B.29}$$

$$P^4_{\varepsilon_\theta} \simeq -2\alpha \overline{\frac{\partial u_2}{\partial x_2}\frac{\partial \theta}{\partial x_2}\frac{\partial \theta}{\partial x_2}} = -4\alpha \overline{c_2 h_1^2} x_2 + \cdots \propto x_2^1, \tag{B.30}$$

$$\Upsilon_{\varepsilon_\theta} \simeq 2\alpha^2 \overline{\left(\frac{\partial^2 \theta}{\partial x_2^2}\right)^2} = 8\alpha^2 \overline{h_2^2} + \cdots \propto x_2^0. \tag{B.31}$$

For case of existing temperature fluctuation on the wall, the wall-limiting behaviour of in-

dividual terms are given as follows:

$$D_{\varepsilon_\theta} \simeq \alpha \frac{\partial^2 \varepsilon_\theta}{\partial x_2^2} = 8\alpha^2 \overline{h_2^2} + \cdots \propto x_2^0, \tag{B.32}$$

$$T_{\varepsilon_\theta} \simeq -\alpha \frac{\partial \overline{u_2 \varepsilon_\theta'}}{\partial x_2} = -16\alpha \overline{c_2 h_2^2} x_2^3 + \cdots \propto x_2^3, \tag{B.33}$$

$$P^1_{\varepsilon_\theta} \simeq -2\alpha \overline{\frac{\partial u_2}{\partial x_2} \frac{\partial \theta}{\partial x_2}} \frac{\partial \bar{\Theta}}{\partial x_2} = -4\alpha \overline{c_2 h_1} H_1 x_2 + \cdots \propto x_2^1, \tag{B.34}$$

$$\begin{aligned} P^2_{\varepsilon_\theta} \simeq & -2\alpha \left(\overline{\frac{\partial \theta}{\partial x_2} \frac{\partial \theta_w}{\partial x_1}} \frac{\partial \bar{U}_1}{\partial x_2} + \overline{\frac{\partial \theta}{\partial x_2} \frac{\partial \theta}{\partial x_2}} \frac{\partial \bar{U}_2}{\partial x_2} + \overline{\frac{\partial \theta}{\partial x_2} \frac{\partial \theta_w}{\partial x_3}} \frac{\partial \bar{U}_3}{\partial x_2} \right) \\ = & -8\alpha \left(\overline{h_2 \frac{\partial \theta_w}{\partial x_1}} B_1 + \overline{h_2 \frac{\partial \theta_w}{\partial x_3}} B_3 + \overline{h_2^2} C_2 \right) x_2 + \cdots \propto x_2^1, \end{aligned} \tag{B.35}$$

$$P^3_{\varepsilon_\theta} \simeq -2\alpha \overline{u_2 \frac{\partial \theta}{\partial x_2}} \frac{\partial^2 \bar{\Theta}}{\partial x_2^2} = -4\alpha \overline{c_2 h_1} H_2 x_2^2 + \cdots \propto x_2^2, \tag{B.36}$$

$$\begin{aligned} P^4_{\varepsilon_\theta} \simeq & -2\alpha \left(\overline{\frac{\partial u_1}{\partial x_2} \frac{\partial \theta}{\partial x_2} \frac{\partial \theta_w}{\partial x_1}} + \overline{\frac{\partial u_2}{\partial x_2} \frac{\partial \theta}{\partial x_2} \frac{\partial \theta}{\partial x_2}} + \overline{\frac{\partial u_3}{\partial x_2} \frac{\partial \theta}{\partial x_2} \frac{\partial \theta_w}{\partial x_3}} \right) \\ = & -8\alpha \left(\overline{b_1 h_2 \frac{\partial \theta_w}{\partial x_1}} + \overline{b_3 h_2 \frac{\partial \theta_w}{\partial x_3}} \right) x_2 + \cdots \propto x_2^1, \end{aligned} \tag{B.37}$$

$$\Upsilon_{\varepsilon_\theta} \simeq 2\alpha^2 \overline{\left(\frac{\partial^2 \theta}{\partial x_2^2} \right)^2} = 8\alpha^2 \overline{h_2^2} + \cdots \propto x_2^0. \tag{B.38}$$

In both cases, the molecular diffusion balances with the destruction term in order of x_2^0. The coefficient $12\alpha^2 \overline{h_1 h_3}$ in Eq (B.25) becomes 0 for the equation balance. In the modeled equation, however, the molecular diffusion term balances the modeled term $-C_{D1} f_{D1} \varepsilon_\theta^2 / k_\theta - C_{D2} f_{D2} \varepsilon_\theta \varepsilon / k$ in general. The order of these terms is x_2^{-2}. Thus, to balance the equation near the wall, the model functions f_{D1} and f_{D2} should be proportional to x_2^2.

References

Abe, K., Kondoh, T. & Nagano, Y. 1994 A new turbulence model for predicting fluid flow and heat transfer in separating and reattaching flows – I. flow field calculations. *Int. J. Heat Mass Transfer* **37**, 139–151.

Abe, K., Kondoh, T. & Nagano, Y. 1995 A new turbulence model for predicting fluid flow and heat transfer in separating and reattaching flows -II. thermal field calculations. *Int. J. Heat Mass Transfer* **38**, 1467–1481.

Abe, K., Kondoh, T. & Nagano, Y. 1996 A two-equation heat-transfer model reflecting second-moment closures for wall and free turbulent flows. *Int. J. Heat and Fluid Flow* **17**, 228–237.

Abe, K., Kondoh, T. & Nagano, Y. 1997 On Reynolds-stress expressions and near-wall scaling parameters for predicting wall and homogeneous turbulent shear flows. *Int. J. Heat and Fluid Flow* **18**, 266–282.

Antonia, R. A., Danh, H. Q. & Prabhu, A. 1977 Response of a turbulent boundary layer to a step change in surface heat flux. *J. Fluid Mech.* **80**, 153–177.

Apsley, D. D. & Leschziner, M. A. 1998 A new low-Reynolds-number nonlinear two-equation turbulence model for complex flows. *Int. J. Heat and Fluid Flow* **19**, 209–222.

Bell, D. M. & Ferziger, J. H. 1993 Turbulent boundary layer DNS with passive scalars. *Near-Wall Turbulent Flows* (Edited by So, R. M. C., Spezale C. G. & Launder B. E.), pp. 327–336, Elsevier.

Bradshaw, P., Ferriss, D. H. & Atwell, N. P. 1967 Calculation of boundary layer development using the turbulent energy equation. *J. Fluid Mech.* **23**, 31–64.

Browne, L. W. B., & Antonia, R. A. 1981 Calculation of a turbulent boundary layer downstream of a sudden decrease in sarface heat flux or wall temperature. In *Proc. 3rd Symp. on Turbulent Shear Flows*, pp. 10.18–10.22, University of California, Davis.

Cebeci, T. 1973 A model for eddy conductivity and turbulent Prandtl number. *Trans. ASME, J. Heat Transfer* **95**, 227–234.

Cebeci, T., Smith, A. M. O. & Mosinskis, G. 1970 Solution of the incompressible turbulent boundary-layer equations with heat transfer *Trans. ASME, J. Heat Transfer* **92**, 133–143.

Charnay, G., Schon, P., Alcaraz, E., & Mathieu, J. 1979 Thermal characteristics of a turbulent boundary layer with an inversion of wall heat flux. In *Turbulent Shear Flows 1* (Edited by Durst, F. *et al.*), pp. 104–118, Springer.

Craft, T. J., Launder, B. E. & Suga, K. 1997 Prediction of turbulent transitional phenomena with a nonlinear eddy-viscosity model. *Int. J. Heat and Fluid Flow* **18**, 15–28.

Daly, B. J. & Harlow, F. H. 1970 Transport equations in turbulence. *Phys. Fluids* **13**, 2634–2649.

Durbin, P. A. 1991 Near-wall turbulence closure modeling without 'damping functions.' *Theoret. Comput. Fluid Dynamics* **3**, 1–13.

Elghobashi, S. E., & Launder, B. E. 1981 Modeling the dissipation rate of temperature variance in a thermal mixing layer. In *Proc. 3rd Symp. on Turbulent Shear Flows*, pp. 15.13–15.17, University of California, Davis.

Gatski, T. B. & C. G. Speziale 1993 On explicit algebraic stress models for complex turbulent flows. *J. Fluid Mech.* **254**, 59–78.

Gibson, M. M., C. A. Verriopoulos & Y. Nagano 1982 Measurements in the heated turbulent boundary layer on mildly curved surface. *Turbulent Shear Flows 3* (Edited by Bradbury, L. J. S. *et al.*), pp. 80–89, Springer.

Hanjalić, K. 1994 Advanced turbulence closure models: a view of current status and future prospects. *Int. J. Heat and Fluid Flow* **15**, 178–203.

Hanjalić, K. & B. E. Launder 1980 Sensitizing the dissipation equation to irrotational strains. *J. Fluids Engineering* **102**, 34–40.

Hattori, H., Hiramatsu, T., & Nagano, Y. 2002 Non-linear two-equation model taking into account the wall-limiting behavior and redistribution of stress components. *Trans. Japan Soc. Mech. Engrs: Ser. B*, in press.

Hattori, H., Nagano, Y., & Tagawa, M. 1993 Analysis of turbulent heat transfer under various thermal conditions with two-equation models. In *Engineering Turbulence Modelling and Experiments 2* (Edited by Rodi W. & Martelli F.), pp. 43–52, Elsevier

Hattori H. & Nagano, Y. 1993 Calculation of turbulent flows with pressure gradients using a k–ε model. *Trans. Japan Soc. Mech. Engrs: Ser. B* **59**, 1043-1048.

Hattori H. & Nagano, Y. 1995a Calculation of turbulent flows with pressure gradients using a k–ε model. *JSME Int. J.: Ser. B* **38**, 518–524.

Hattori H. & Nagano, Y. 1995b Rigorous modelling of two-equation heat-transfer model using direct simulations (1st report, assessment and reconstruction of dissipation-rate equations for temperature variance). *Trans. Japan Soc. Mech. Engrs: Ser. B* **61**, 1114-1121.

Hattori H. & Nagano, Y. 1995c Rigorous modeling of temperature variance and its dissipation-rate equations using DNS databases. In *Proc. 4th ASME-JSME Thermal Engineering Joint Conf.* **1** pp.401-408, Hawaii, USA.

Hattori, H. & Nagano, Y. 1998, Rigorous formulation of two-equation heat-transfer model of turbulence using direct simulations. *Numerical Heat Transfer: Part B* **33**, 153-180

Hattori, H. & Nagano, Y. 1999 Two-layer turbulence model for heat transfer in wall turbulent shear flows In *Proc. 5th ASME-JSME Thermal Engineering Joint Conf.* AJTE99-6454 p.227, (pp.1–8 in CD-ROM), San Diego, USA.

Hattori, H. & Nagano, Y. 2002 An improved turbulence model for rotating shear flows. *Trans. Japan Soc. Mech. Engrs: Ser. B*, in press.

Hinze, J. O. 1975 *Turbulence*, 2nd ed., McGraw-Hill.

Horiuti, K. 1992 Assessment of two–equation models of turbulent passive–scalar diffusion in channel flow. *J. Fluid Mech.* **238**, 150–433.

Hossain, M. S. & Rodi, W. 1982 A turbulence model for buoyant flows and its application to vertical buoyant jets. In *Turbulent Buoyant Jets* (Edited by Rodi, W.), Pergamon.

Johnston, J. P., Halleen, R. M. & Lezius, D. K. 1972 Effects of spanwise rotation on the structure of two-dimensional fully developed turbulent channel flow. *J. Fluid Mech.* **56** 533–557.

Jones, W. P. & Launder, B. E. 1972 The prediction of laminarization with a two-equation model of turbulence. *Int. J. Heat Mass Transfer* **15**, 301–314.

Jones, W. P. & Launder, B. E. 1973 The calculation of low-Reynolds-number phenomena with a two-equation model of turbulence. *Int. J. Heat Mass Transfer* **16**, 1119–1130.

Kader, B. A. 1981 Temperature and concentration profiles in fully turbulent boundary layers. *Int. J. Heat Mass Transfer* **24**, 1541–1544.

Kasagi N. & Ohtsubo, Y. 1992 Direct numerical simulation of low Prandtl number thermal field in a turbulet channel flow. In *Turbulent Shear Flows 8*, pp. 97-119, Springer.

Kasagi, N., Tomita, Y. & Kuroda, A. 1992 Direct numerical simulation of passive scalar field in a turbulent channel flow. *Trans. ASME, J. Heat Transfer* **114**, 598–606.

Kasagi, N. & Matsunaga, A. 1995 Three-dimensional particle-tracking velocimetry measurement of turbulence statistics and energy budget in a backward-facing step flow. Int. J. Heat Fluid Flow **16** 477–485.

Kawamura H. & Kawashima, N. 1994 A proposal of k–$\widetilde{\varepsilon}$ model with relevance to the near wall turbulence. In *Proc. The Int. Symposium on Turbulence, Heat and Mass Transfer*, pp.I.1.1–I.1.4, Lisbon, Portugal.

Kawamura, Y. & Hada, K. 1992 An evolution of k-$\widetilde{\varepsilon}$ model of wall turbulence. In *Proc. 29th National Heat Transfer Symp. of Japan* p. 380, Osaka.

Kim, J. & Moin, P. 1989 Transport of passive scalars in a turbulent channel flow. *Turbulent Shear Flows 6*, (Edited by André, J. C. *et al.*) pp.85–96, Springer.

Kim, J., Moin, P. & Moser, R. 1987 Turbulence statistics in fully developed channel flow at low Reynolds number. *J. Fluid Mech.* **177**, 133–166.

Klebanoff, P. S. 1955 Characteristics of Turbulence in a Boundary Layer with Zero Pressure Gradient. *NCSA Report* 1247.

Kline, S. J., Cantwell, B. J., & Lilley, G. M. 1981 *The 1980–1981 AFOSR–HTTM–Stanford Conference on Complex Turbulent Flow: Comparison of Computation and Experiment I, II and III*, Thermosciences Division, Mechanical Engineering Department,Stanford University, Stanford, Calif.

Kolmogorov, A. N 1942 The equations of turbulent motion in an incompressible fluid. *Izv. Acad. Sci. USSR Phys.* **6**, 56–58.

Kristoffersen, R. & Andersson, H. 1993 Direct simulations of low-Reynolds-number turbulent flow in a rotating channel. *J. Fluid Mech.* **256**, 163–197.

Kuroda, A., Kasagi, N. & Hirata, K. 1994 Direct numerical simulation of turbulent plane Couette-Poiseuille flow: effect of mean shear rate on the near-wall turbulence structure. In *Turbulent Shear Flows 9* (Edited by Durst *et al.*), pp. 241–257, Springer.

Lamballais, E, Lesieur, M. & Métais, O. 1996 Effects of spanwise rotation on the vorticity stretching in transitional and turbulent channel flow. *Int. J. Heat and Fluid Flow* **17**, 324–332

Launder B. E. & Sharma, B. I. 1974 *Letters in Heat Mass Transfer* **1**, 131–138.

Launder, B. E. 1988 On the computation of convective heat transfer in complex turbulent flows. *Trans. ASME, J. Heat Transfer* **110**, 1112–1128.

Launder, B. E. 1981 Turbulence modeling in the vicinity of a wall. *1980–1981 AFOSR–HTTM–Stanford Conf. Complex Turbulent Flows* **2**, 691–699.

Leschziner, M. A. 1982 *An Introduction and Guide to the Computer Code PASSABLE*, UMIST.

Menter, F. R. 1997 Eddy viscosity transport equation and their relation to the k–ε model. *J. Fluids Engineering* **119**, 876–884.

Moser, R. D., Kim, J. & Mansour, N. N. 1999 Direct numerical simulation of turbulent channel flow up to $Re_\tau = 590$. *Physics Fluids* **11**, 943–945.

Myong, H. K. & Kasagi, N. 1990a A new approach to the improvement of k-ε turbulence model for wall-bounded shear flows. *JSME Int. J.: Ser. B* **33**, 63–72.

Myong, H. K. & Kasagi, N. 1990b Prediction of anisotropy of the near-wall turbulence with an anisotropic low-Reynolds-number k–ε turbulence model. *J. Fluids Engineering* **112**, 521–524.

Nagano, Y. & Kim, C. 1988 A two-equation model for heat transport in wall turbulent shear flows. *ASME J. Heat Transfer* **110**, 583–589.

Nagano, Y. & Hattori, H. 2001a An improved turbulence model for rotating shear flows. In *Proc. 2nd International Symposium on Turbulence and Shear Flow Phenomena* **II**, pp. 199–204, Stockholm, Sweden.

Nagano, Y. & Hattori, H. 2001b An improved turbulence model for rotating shear flows. *Journal of Turbulence*, Institute of Physics, in press.

Nagano, Y., Hattori, H. & Abe, K. 1995 Modeling the turbulent heat and momentum transfer in complex flows under various thermal conditions. In *Proc. Int. Symp. Mathematical Modelling of Turbulent Flows* pp. 79-86, Tokyo.

Nagano, Y., Hattori, H. & Abe, K. 1997 Modeling the turbulent heat and momentum transfer in flows under different thermal conditions. *Fluid Dynamic Research* **20**, 127–142.

Nagano, Y. & Hishida, M. 1985 Production and dissipation of turbulent velocity and temperature fluctuations in fully developed pipe flow In *Proc. 5th Symp. on Turbulent Shear Flows*, pp. 14.19–14.24, Cornell University, Ithaca.

Nagano Y. & Hishida, M. 1987 Improved form of the k–ε model for wall turbulent shear flows. *J. Fluids Engineering* **109**, 156–160.

Nagano, Y., Pei, C. Q. & Hattori, H. 2000 A new low-Reynolds-number one-equation model of turbulence. *Flow, Turbulence and Combustion* **63**, 135–151

Nagano, Y., Sato, H., Hattori H. & Yin, Y. 1993 numerical analysis of turbulent heat transfer in various Prandtl number fluids. In *Proc. 5th Int. Symp. Computational Fluid Dynamics* **2** pp.299–304, Sendai, Japan.

Nagano, Y. & Shimada, M. 1994 Critical assessment and reconstruction of dissipation-rate equations using direct simulations. In *The Recent Developments in Turbulence Research* (Edited by Zhang, Z. S. & Miyake Y.), pp.189–217, Int. Academic Publishers.

Nagano, Y. & Shimada, M. 1995a Rigorous modeling of dissipation-rate equation using direct simulations. *JSME Int. J.: Ser. B* **38**, 51–59

Nagano, Y. & Shimada, M. 1995b Computational modeling and simulation of turbulent flows. In *Computational Fluid Dynamics Review 1995* (Edited by Hafez, M. M. & Oshima, K.), 695–714, Wiley.

Nagano, Y. & Shimada, M. 1996 Development of a two-equation heat transfer model based on direct simulation of turbulent flows with different Prandtl numbers. *Phys. Fluids* **8**, 3379–3402

Nagano, Y., Shimada, M. & Youssef, M. S. 1994 Progress in the development of a two-equation heat transfer model based on dns databases. In *Proc. The Int. Symposium on Turbulence, Heat and Mass Transfer* pp.3.2.1–3.2.6, Lisbon, Portugal.

Nagano, Y. & Tagawa, M. 1990a An improved k–ε model for boundary layer flows. *J. Fluids Engineering* **112**, 33–39.

Nagano, Y. & Tagawa, M. 1990b A structural turbulence model for triple products of velocity and scalar. *J. Fluid Mech.* **215**, 639–657.

Nagano, Y. Tagawa, M.& Tsuji, T. 1991 An improved two-equation heat transfer model for wall turbulent shear flows. In *Proc. ASME/JSME Thermal Engng. Joint Conference* **3**, pp.233–240, Reno, USA.

Nagano, Y. Tagawa, M.& Tsuji, T. 1992 Effect of adverse pressure gradients on mean flows and turbulence statistics in a boundary layer. *Turbulent Shear Flows 8* (Edited by Durst, F. *et al.*), pp. 7–21, Springer.

Nakayama, A. 1995 *PC-Aided Numerical Heat Transfer and Convective Flow*, CRC press.

Nee, V. W. & Kovasznay, L. S. G. 1969 Simple phenomenological theory of turbulent shear flows. *Phys. Fluids* **12**, 473–484.

Nishimura, M. & Kasagi, N. 1996 Direct numerical simulation of combined forced and natural turbulent convection in a rotating plane channel. In *Proc. 3rd KSME–JSME Thermal Engineering Conf.* **3**, pp. 77–82, Kyongju, Korea.

Patankar, S. V. 1980 *Numerical Heat Transfer and Fluid Flow*, McGraw-Hill.

Pei, C. Q., Hattori, H. & Nagano, Y. 1999a A New Low-Reynolds-Number One-Equation Model of Turbulence for Predicting Fluid Flow and Heat Transfer (1st Report: One-Equation Model Taking into Account the Near-Wall Behavior of Turbulence). *Thermal Science & Engineering* **7**, No. 3, 41–47.

Pei, C. Q., Hattori, H. & Nagano, Y. 1999b A New Low-Reynolds-Number One-Equation Model of Turbulence for Predicting Fluid Flow and Heat Transfer (2nd Report: Development of One-Equation Heat Transfer Model of Turbulence). *Thermal Science & Engineering* **7**, No. 5, 31–39.

Pei, C. Q., Hattori, H. & Nagano, Y. 2000 New low-Reynolds-number one-equation heat transfer model of turbulence. In *Proc. 3rd Int. Symposium on Turbulence, Heat Mass Transfer* (Edited by Nagano, Y. *et al.*), pp. 349–356, Aichi Suppan.

Pope, S. B. 1975 A more general effective-viscosity hypothesis. *J. Fluid Mech.* **72**, 331–340.

Prandtl, L. 1925 Über die ausgrebildete Turbulenze. *ZAMM* **5**, 136–139.

Prandtl, L. 1945 Über ein neues Formelsystem der ausgebildete Turbulenz. *Nachr. Akad. Wiss. Göttingen, Math. Phys.* 6–19.

Reynolds, W. C., Kays, W. M. & Kline, S. J. 1958 Heat transfer in the turbulent incompressible boundary layer, iii–arbitrary wall temperature and heat flux. *NASA MEMO*, 12–3–58W.

Rodi, W. 1976 A new algebraic relation for calculating the Reynolds stress. *ZAMM* **56**, 219-221.

Rodi, W. & Mansour, N. N. 1993 Low Reynolds number k–ε modelling with the aid of direct simulation data. *J. Fluid Mech.* **250**, 509–529.

Rodi, W., Mansour N. N. & Michelassi. V. 1993 One-equation near-wall turbulence modeling with the aid of direct simulation data. *J. Fluids Engineering* **115**, 196–205.

Shikazono N. & Kasagi, N. 1996 Second-moment closure for turbulent scalar transport at various Prandtl numbers. *Int. J. Heat Mass Transfer* **39** 2977–2987.

Shima, N. 1993 Prediction of turbulent boundary layers with a second-moment closure: part II – effect of streamline curvature and spanwise rotation. *J. Fluids Engineering* **115**, 64–69.

Shimada M. & Y. Nagano 1996 Advanced two-equation turbulence model for complex flows in engineering. In *Proc. 3rd Int. Symp. Engineering Turbulence Modelling and Measurements*, pp. 111–120.

Shimomura, Y. 1989 A statistically derived two-equation model of turbulent shear flows in rotating system. *J. Phys. Soc. of Japan* **58** 352–355.

Sommer, T. P., So, R. M. C. & Lai, Y. G. 1992 A near-wall two-equation model for turbulent heat fluxes. *Int. J. Heat Mass Transfer* **35**, 3375–3387.

Spalart, P. R. 1986 Numerical study of sink-flow boundary layers. *J. Fluid Mech.* **172**, 307–328.

Spalart, P. R. 1988 Direct simulation of a turbulent boundary layer up to R_θ=1410. *J. Fluid Mech.* **187**, 61–98.

Spalart, P. R. & Allmaras, S. R. 1994 A one-equation turbulence model for aerodynamics flows. *La Recherche Aerospatiale* No. 1, 5–21.

Speziale, C. G., Sarkar, S. & Gatski, T. B. 1997 Modelling the pressure-strain correlation of turbulence: an invariant dynamics system approach. *J. Fluid Mech.* **227** 245–272.

Subramanian C. S. & Antonia, R. A. 1981a Response of a turbulent boundary layer to a sudden decrease in wall heat flux. *J. Heat Mass Transfer* **24** 1641–1647.

Subramanian, C. S., & Antonia R. A. 1981b Effect of Reynolds number on a slightly heated turbulent boundary layer. *J. Fluid Mech.* **176**, 265–281.

Suga, K. & Abe, K. 2000 Nonlinear eddy viscosity modelling for turbulence and heat transfer near wall and shear-free boundaries. Int. J. Heat and Fluid Flow **21**, 37–48.

Taulbee, D. B. 1992 An improved algebraic Reynolds stress model and corresponding nonlinear stress model. *Phys. Fluids A* **4**, 2555–2561.

Verriopoulos, C. A. 1983 Effects of convex surface curvature on heat transfer in turbulent flow, Ph.D. Dissertation, Imperial College.

Vogel, J. C., & Eaton, J. K. 1984 *Report MD-44, Thermosciences Division,* Dept. Mech. Engng., Stanford Univ.

Youssef, M. S., Nagano, Y. & Tagawa, M. 1992 A two-equation heat transfer model for predicting turbulent thermal fields under arbitrary wall thermal conditions. *Int. J. Heat Mass Transfer* **35**, 3095–3104.